

A GRAVITY AND MAGNETIC INTERPRETATION
OF THE BAY ST. GEORGE CARBONIFEROUS
SUBBASIN IN WESTERN NEWFOUNDLAND

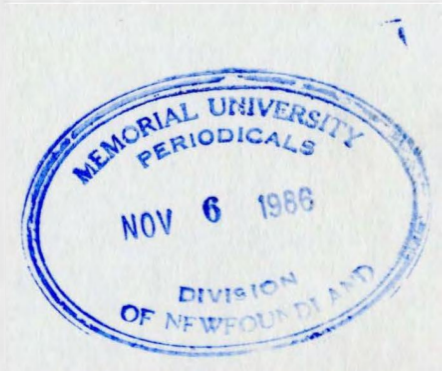
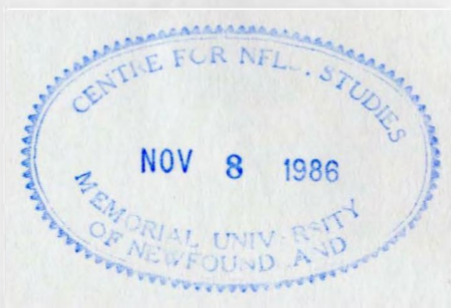
CENTRE FOR NEWFOUNDLAND STUDIES

**TOTAL OF 10 PAGES ONLY
MAY BE XEROXED**

(Without Author's Permission)

SAMUEL THOMAS PEAVY

C37700





National Library
of Canada

Bibliothèque nationale
du Canada

Canadian Theses Service

Services des thèses canadiennes

Ottawa, Canada
K1A 0N4

CANADIAN THESES

THÈSES CANADIENNES

NOTICE

The quality of this microfiche is heavily dependent upon the quality of the original thesis submitted for microfilming. Every effort has been made to ensure the highest quality of reproduction possible.

If pages are missing, contact the university which granted the degree.

Some pages may have indistinct print especially if the original pages were typed with a poor typewriter ribbon or if the university sent us an inferior photocopy.

Previously copyrighted materials (journal articles, published tests, etc.) are not filmed.

Reproduction in full or in part of this film is governed by the Canadian Copyright Act, R.S.C. 1970, c. C-30. Please read the authorization forms which accompany this thesis.

AVIS

La qualité de cette microfiche dépend grandement de la qualité de la thèse soumise au microfilmage. Nous avons tout fait pour assurer une qualité supérieure de reproduction.

S'il manque des pages, veuillez communiquer avec l'université qui a conféré le grade.

La qualité d'impression de certaines pages peut laisser à désirer, surtout si les pages originales ont été dactylographiées à l'aide d'un ruban usé ou si l'université nous a fait parvenir une photocopie de qualité inférieure.

Les documents qui font déjà l'objet d'un droit d'auteur (articles de revue, examens publiés, etc.) ne sont pas microfilmés.

La reproduction, même partielle, de ce microfilm est soumise à la Loi canadienne sur le droit d'auteur, SRC 1970, c. C-30. Veuillez prendre connaissance des formules d'autorisation qui accompagnent cette thèse.

THIS DISSERTATION
HAS BEEN MICROFILMED
EXACTLY AS RECEIVED

LA THÈSE A ÉTÉ
MICROFILMÉE TELLE QUE
NOUS L'AVONS REÇUE

A GRAVITY AND MAGNETIC INTERPRETATION OF THE BAY ST. GEORGE
CARBONIFEROUS SUBBASIN IN WESTERN NEWFOUNDLAND

by
Samuel Thomas Peavy



A thesis submitted to the School of Graduate
Studies in partial fulfillment of the
requirement for the degree of
Master of Science

Department of Earth Sciences
Memorial University of Newfoundland
September 1985

St. John's, Newfoundland

Abstract

Gravity and magnetic data were used to model and interpret the subsurface structure of the Bay St. George Carboniferous Subbasin in western Newfoundland.

A total of 236 gravity stations with an average spacing of 4.0 km were used. Magnetic data were digitized on a 0.8 km grid from existing 1:63360 scale aeromagnetic maps. Regional and residual anomaly maps for a 5th-order polynomial were obtained for both gravity and magnetic maps using a trend analysis program.

Densities and magnetic susceptibilities from 242 samples of evaporites, representative sedimentary rocks, and anorthositic samples of inferred basement type were determined.

Programs for 2-D and 2.5-D gravity inversion, 2.5-D forward gravity modelling, and 3-D gravity and magnetic modelling were written in FORTRAN and tested. These were used to determine the basement topography, and to delineate faults, obtain thickness estimates of the sedimentary infill, and locate possible new evaporite deposits.

Results from the 2.5-D inversion compared favorably to the final 3-D gravity model, showing that the 2.5-D process can be used to estimate basement topography. 3-D magnetic modelling confirmed that the basement shape defined by gravity modelling was correct geometrically.

The results of the modelling were combined with a qualitative interpretation of the gravity and magnetic maps to yield a model of the subsurface geology. Several new faults were located in the subbasin, and several of the old faults were extended. Three possible

new evaporite deposits were also located. The maximum thicknesses of the sediments in the basin were discovered to be ~6 km in the St. Davids Syncline and 4 to 5 km in the Barachois Synclinorium. The throws of the Crabbes Brook and Shoal Point faults were found to be between 0.5 and 3 km, and 4.5 km, respectively.

Table of Contents

Chapter 1: Introduction	1 - 3
Chapter 2: Data Collection and Reduction	4 - 18
2.1 Collection and Reduction of Gravity Data	4
2.2 Collection and Reduction of Magnetic Data	10
2.3 Trend Analysis of Gravity and Magnetic Data	11
Chapter 3: Geology of the Bay St. George Carboniferous Subbasin	19 - 35
3.1 Introduction	19
3.2 Lithology of the Sedimentary Rocks	20
3.2.1 Anguille Group	21
3.2.2 Codroy Group	24
3.2.3 Barachois Group	27
3.3 Structural Geology	28
3.4 Evaporite and Coal Deposits	32
3.5 The Pre-Carboniferous Basement	34
Chapter 4: Physical Properties of the Carboniferous Sedimentary Rocks and the Pre-Carboniferous Basement	36 - 50
4.1 Introduction	36
4.2 Methods Used to Measure Density and Magnetic Susceptibility	37
4.3 Physical Properties of the Sedimentary Samples	41
4.4 Physical Properties of the Pre-Carboniferous Samples	43
Chapter 5: Computer Programming for Gravity and Magnetic Modelling	51 - 107
5.1 Introduction	51
5.2 Two-Dimensional, Least-Squares Gravity Modelling	51
5.3 2.5-D Gravity Modelling and a Comparison to 2-D Modelling	54

5.4	2.5-D Inverse Gravity Program	58
5.5	Testing the 2.5-D Gravity Inversion Program	64
5.6	Three-Dimensional Gravity Modelling	101
5.7	Three-Dimensional Magnetic Modelling	103
Chapter 6:	Interpretation and Results of Gravity and Magnetic Modelling	108 - 139
6.1	Introduction	108
6.2	Qualitative Interpretation of the Gravity and Magnetic Maps	109
6.3	Surface Effects of Possible Basement Lenticular Magnetite Deposits on Gravity and Magnetic Interpretation	111
6.4	Results of the 2.5-D Gravity Inversion	112
6.5	Results of 3-D Gravity and Magnetic Modelling	118
6.6	A Comparison of the 2.5-D Gravity Inversion Model with the 3-D Gravity Model	131
6.7	Summary of Results	133
Chapter 7:	Conclusions	141 - 142
	Acknowledgements	143 - 144
	Bibliography	145 - 149
	List of Appendices	150

v

List of Figures

Figure 1.1	Map of the study area.	2
Figure 2.1	Posting of gravity stations in the study area.	5
Figure 2.2	Bouguer anomaly map.	9
Figure 2.3	Total field, IGRF magnetic data for Bay St. George.	12
Figure 2.4	Reduced magnetics - contour map (no averaging).	13
Figure 2.5	Reduced magnetics - contour map (25 pt. straight averaging)	14
Figure 2.6	Residual gravity after trend analysis - order = 5.	17
Figure 2.7	Residual magnetics after trend analysis - order = 5.	18
Figure 3.1	Geology and location of drill holes and evaporite deposits.	22
Figure 4.1	Indian Head and Steel Mountain density histogram.	44
Figure 4.2	Indian Head and Steel Mountain magnetic susceptibility histogram.	46
Figure 4.3	Plot of χ vs. ρ for the Indian Head and Steel Mountain samples.	49
Figure 4.4	Histogram of frequency of samples in Zones A-I for the basement samples.	50
Figure 5.1	Effects of finite strike-length on gravity profiles.	56
Figure 5.2	Effects of variable width, thickness, and depth of burial on 2.5-D gravity calculations.	57
Figure 5.3	Flowchart for 2.5-D gravity inversion program.	59
Figure 5.4	Polygon for 2.5-D gravity.	61
Figure 5.5	Gravity for various models and true and calculated models.	69

Figure 5.6	Gravity for dipping prisms and inversion models.	77
Figure 5.7	Basement step and basement slope models.	79
Figure 5.8	Basement step vs. basement contact.	81
Figure 5.9	Reverse and normal faults.	83
Figure 5.10	Body buried at various depths and inversion results.	86
Figure 5.11	Modelling results from four irregular polygons.	90
Figure 5.12	Bodies for 2-D vs. 2.5-D inversion comparison.	94
Figure 5.14	Numerical integration for 3-D gravity calculation.	102
Figure 5.15	Observed and calculated magnetic data for the Cayn Sea Mount.	106
Figure 6.1	Profile locations for 2.5-D modelling.	113
Figure 6.2	Posting of inferred sediment thicknesses from 2.5-D modelling.	115
Figure 6.3	Inferred basement topography map from 2.5-D modelling.	116
Figure 6.4	Difference in calculated and observed gravity for model 1 using a -0.18 g/cm^3 density contrast.	119
Figure 6.5	Sedimentary block boundaries for 3-D gravity modelling.	120
Figure 6.6	Calculated gravity for model 1.	123
Figure 6.7	Difference in calculated and observed gravity for model 1.	124
Figure 6.8	3-D gravity model 4.	126
Figure 6.9	Difference in calculated and observed gravity for model 4.	127

Figure 6.10	Calculated magnetic anomalies from model 4.	130
Figure 6.11	Cross-section near Robinsons River showing geology, and 2.5-D and 3-D gravity models.	132
Figure 6.12	Final surface geology map.	136
Figure 6.13	Final basement topography map.	138

List of Tables

4.1	Densities Calculated for Each Sedimentary Unit	42
4.2	Zones of ρ and k for Figure 4.4	48
5.1	Parameters and results for models shown in Figure 5.5.	65
5.2	Parameters and results for dipping prisms:	75
5.3	Parameters and results for a buried body.	75
5.4	2-D vs. 2.5-D inversion depths.	99
5.5	3-D Sphere Test: Gravity.	104
5.6	3-D Sphere Test: Magnetics.	107
6.1	Density Contrasts for 3-D Modelling	121
6.2	Features Labelled in Figures 6.12 and 6.13	135
6.3	Thickness Estimates for the Lithologic Units of the Bay St. George Subbasin	139

Chapter 1: Introduction

The subject of this thesis is the modelling and interpretation of gravity and magnetic anomalies in the north-central portion of the Bay St. George Carboniferous subbasin in Western Newfoundland. The study area is $\sim 2000^2$ km (see Figure 1.1).

The subbasin is located on the southwest coast of the island. Onshore, the basin extends westward from the Long Range Mountains to St. Georges Bay, and from Cape Anguille northward to near Stephenville. The full offshore extent of the subbasin is unknown at present. The Bay St. George subbasin is a part of the Maritimes Basin of Atlantic Canada, and is associated with the Carboniferous Deer Lake and White Bay basins in north-central Newfoundland.

The geology of the subbasin is summarized in a Newfoundland Department of Mines and Energy report (Knight, 1983).

Sedimentary rocks are of terrestrial, lacustrine, and marine origin, and were deposited as a wrench-type basin was formed by right-lateral, strike-slip movements along the Long Range Fault. Economic deposits of evaporites are found in the study area, along with small quantities of coal. The basement rocks are of granitic/anorthositic composition and are assumed to be similar to those found at Indian Head and Steel Mountain.

There are 236 gravity stations with an average station spacing of 4.0 km. The gravity data consists of stations collected by personnel of Memorial University in 1983 augmented by data from the Dominion

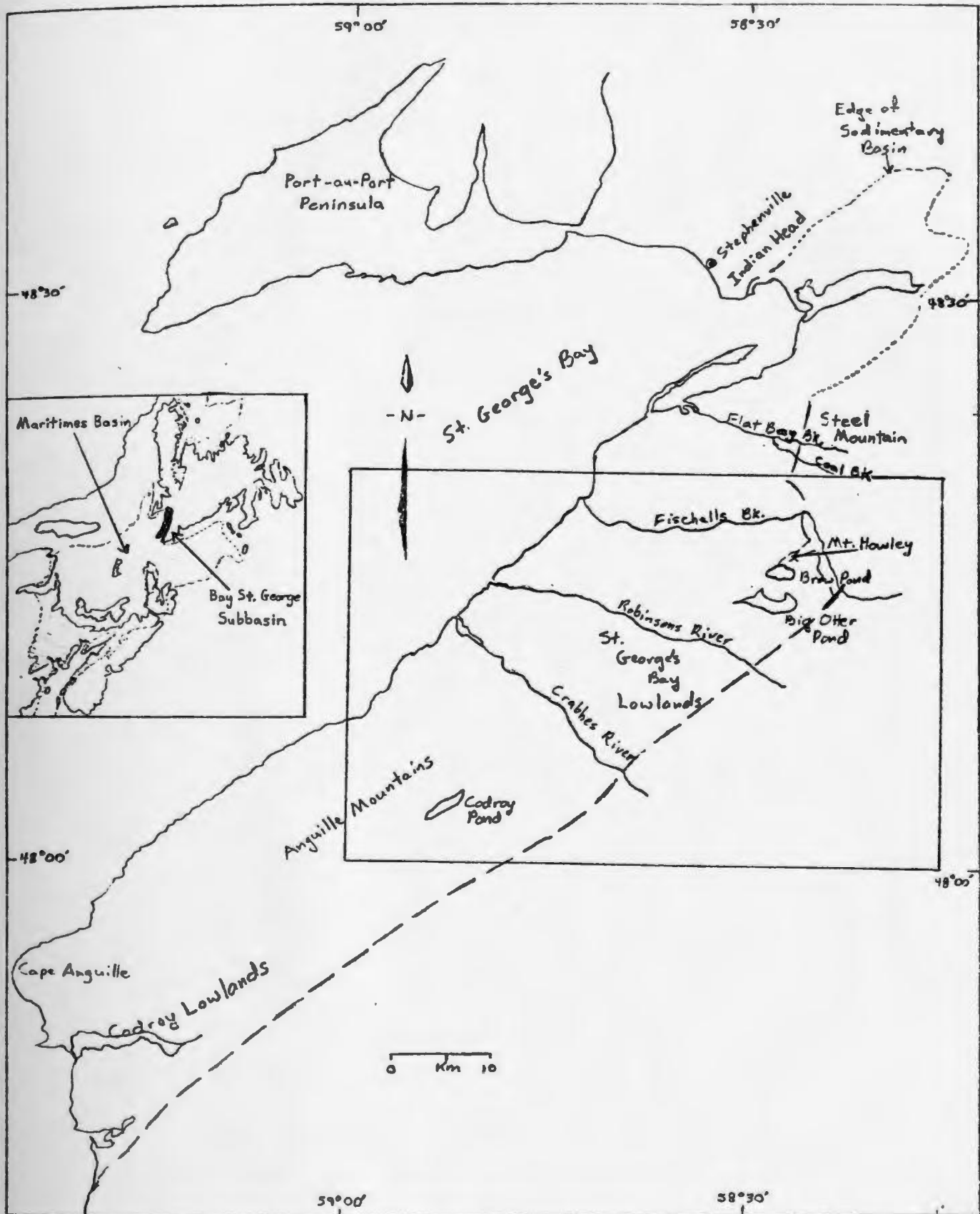


Figure 1.1 Map of the Bay St. George area. Study area is the boxed-in area on the map. The insert is of the Maritimes Basin complex of Atlantic Canada.

Observatory survey of the 1960's (Weaver, 1967) and from Weir's Trans-Canada Highway survey (1971). Magnetic data were obtained by digitizing existing 1:63360 maps of the area on a 0.8 km grid, then removing the IGRF background field to yield a magnetic anomaly map of the study area. Trend analysis was used on both gravity and magnetic data in order to remove the regional trend from the data, leaving the residual anomalies - which are associated with the near surface structure of the area - behind.

In order to constrain the geophysical modelling, 105 representative samples of sedimentary rocks from the subbasin along with 132 samples of anorthosites from Indian Head and Steel Mountain were used for density and magnetic susceptibility measurements. In addition, a few samples of rock salt, gypsum, and anhydrite were also measured.

In order to model the subbasin, several computer programs were written in the FORTRAN language. Along with 3-D forward gravity and magnetic modelling programs, 2.5-D forward and inverse modelling programs were also developed and tested. These were used to determine the topography of the basement-sediment interface, and to delineate faults, estimate the thickness of sedimentary infill in the basin, and locate possible new evaporite deposits.

Finally, an interpretation based on the results of the geophysical modelling of the gravity and magnetic data and the geology map was constructed. This resulted in a model of the subsurface geology of the Bay St. George Carboniferous subbasin.

Chapter 2: Data Collection and Reduction

2.1 Collection and Reduction of Gravity Data

Gravity data were collected by personnel from Memorial University during the summer of 1983 using a LaCoste-Romberg, temperature compensated gravity meter. Elevation data were obtained at each station using Wallace and Tiernan barometric altimeters and sling psychrometers for temperature and humidity control. The stations were occupied with a spacing of 2.5 km along roads in the area, with the exception of the Pasture Road near Robinsons River and the Crabbes River Road, which were occupied at a 1 km spacing. Additional stations off the roads were done using helicopter transportation. The elevations for the survey were tied to the Geodetic Survey of Canada benchmark at the Stephenville Airport. All gravity readings were tied directly to the Earth Physics Branch gravity base also at the airport. In addition to this data, data from the Dominion Observatory survey of the 1960's (Weaver, 1967) and from Weir's Trans-Canada Highway survey (1971) were included to give a total of 236 stations in the study area (see Figure 2.1 and Appendix 1.1).

The 1983 data were reduced to Bouguer anomalies using a computer program for that purpose. The program calculates the observed, theoretical, and Bouguer gravity at each station.

The observed gravity can be calculated using the relation

$$g_{\text{obs}} = g_{\text{base}} + k(R_B - R_S) - D_f \quad (2.1)$$

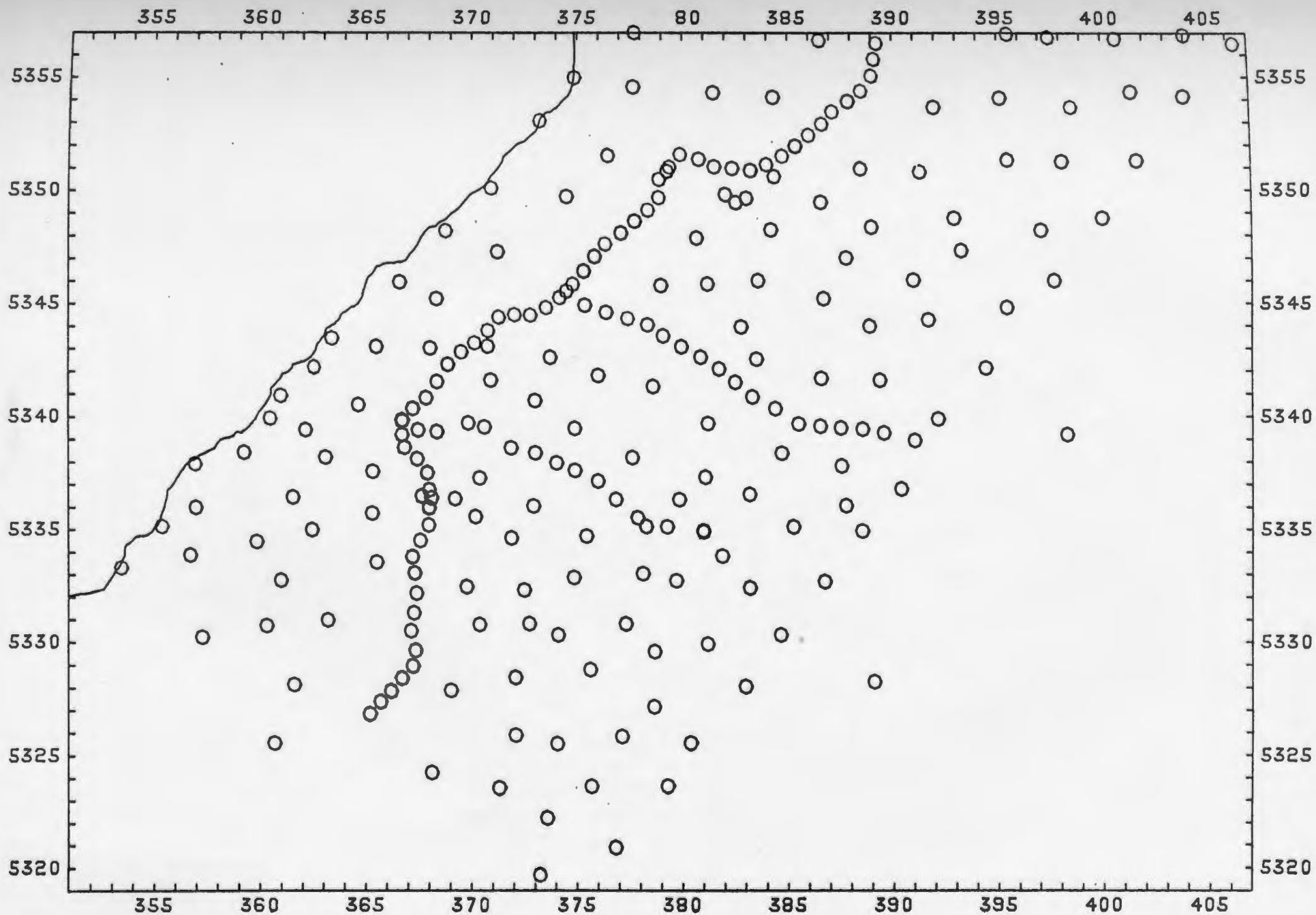


Figure 2.1 Posting of gravity station locations in study area.
 Coordinates of box in kilometers (UTM zone 21).
 (Scale = 1:250000)

where g_{base} is the absolute gravity at the base station in mGal, k is the gravity meter constant in mGal/scale reading, R_B and R_S are the gravity meter reading at the base station and the field station, respectively, and $D_f(t)$ is the gravity meter drift correction. The gravity meter drift is assumed to be a linear function and is calculated from the relation

$$D_f(t) = \frac{\Delta R_B}{\Delta t} \quad (2.2)$$

where $D_f(t)$ is the gravity meter drift correction for a measurement made at time t , ΔR_B is the difference between the starting and closing values of R_B for a particular traverse, Δt is the total time of the traverse, and the last term is the elapsed time since the start of the traverse.

The theoretical gravity is the reference gravity calculated from the 1967 International Gravity Formula (IGF, 1967):

$$g_{\text{the}} = 978031.85 \times (1 + 0.0053024 \times \sin^2(\phi) - 0.00000585 \times \sin^2(2\phi)) \quad (2.3)$$

where ϕ is the latitude in degrees and g_{the} is the theoretical gravity in milligals.

In order to obtain the Bouguer anomaly at each station, the observed gravity has to be corrected for free air and Bouguer effects. The free air effect is caused by the distance the station is away from the center of the Earth, or, since the gravity values are referenced to sea level, its elevation, and can be calculated by the simple relation (Telford, et.al., 1976)

$$g_{FA} = \frac{g_0 \times h}{R} \quad (2.4a)$$

where g_0 is the gravitational acceleration at sea level, h is the elevation of the station with respect to the Earth's center, and R is the radius of the Earth.

The Bouguer effect is due to the mass of material between the station and sea level. It can be removed by using the equation (Telford, et.al., 1976)

$$g_{BOUG} = 2\pi G \rho_c h \quad (2.4b)$$

where G is the universal gravitational constant, h is the elevation, and ρ_c is the Bouguer density or the density of the material between the station and sea level, usually taken to be the average crustal density of 2.67 g/cm^3 .

These two corrections can be combined quite simply to give the equation for Bouguer anomalies (Nettleton, 1976)

$$g_B = g_{obs} - g_{the} + 0.06 \times E + 0.0078 \times H \quad (2.5)$$

where E is the elevation of the station in feet and H is the instrument height above the ground surface in inches. The elevations are in units of feet because the barometric altimeters measure them in feet. The third term ($0.06 \times E$) is a combined elevation factor that takes both the free air and Bouguer effects into account. The last term is a free air correction for the space between the instrument and the ground.

The other data from Weaver (1967) and Weir (1971) were computed originally using a different datum than the 1983 Memorial data. These

were reduced to the same datum by using the equation (Anonymous)

$$g_{\text{new}} = g_{\text{old}} - 0.95 - 13.6 \times \sin^2(\phi) + 0.05 \times \phi \quad (2.6)$$

where g_{old} is the anomaly under the old Potsdam system, g_{new} is the anomaly under the new IGSN71 system, and ϕ is the latitude of the station in degrees. The old system was established by making worldwide gravity measurements relative to the value determined at Potsdam, Germany by pendulum measurements in 1906. This value was found to be too large by 14 mGal, and in 1971 the new system was implemented by making adjustments to the gravity values at stations worldwide (Nettleton, 1976). The correction is approximately, -6.2 mGal for stations in the study area.

The final reduced Bouguer anomaly map is shown in Figure 2.2, with the coastline added for reference. The elevations determined are accurate to ± 2 m and the station locations (scaled from 1:50000 maps) are accurate to ± 50 m, resulting in an uncertainty of ± 0.5 mGal. No terrain corrections were applied to the data. For almost all of the stations in the area, the terrain correction would amount to less than 0.5 mGal. For seven stations (7) near the Long Range Mountains, terrain corrections of as much as 15 mGal are possible due to rapid elevation changes on the order of 300 m, however, for only four of these stations was the terrain effect greater than 5 mGal. These were not applied because of the small number of stations, and the fact that these stations are at the edges of the study area, and are not as important to the modelling process as stations in the central portions of the area.

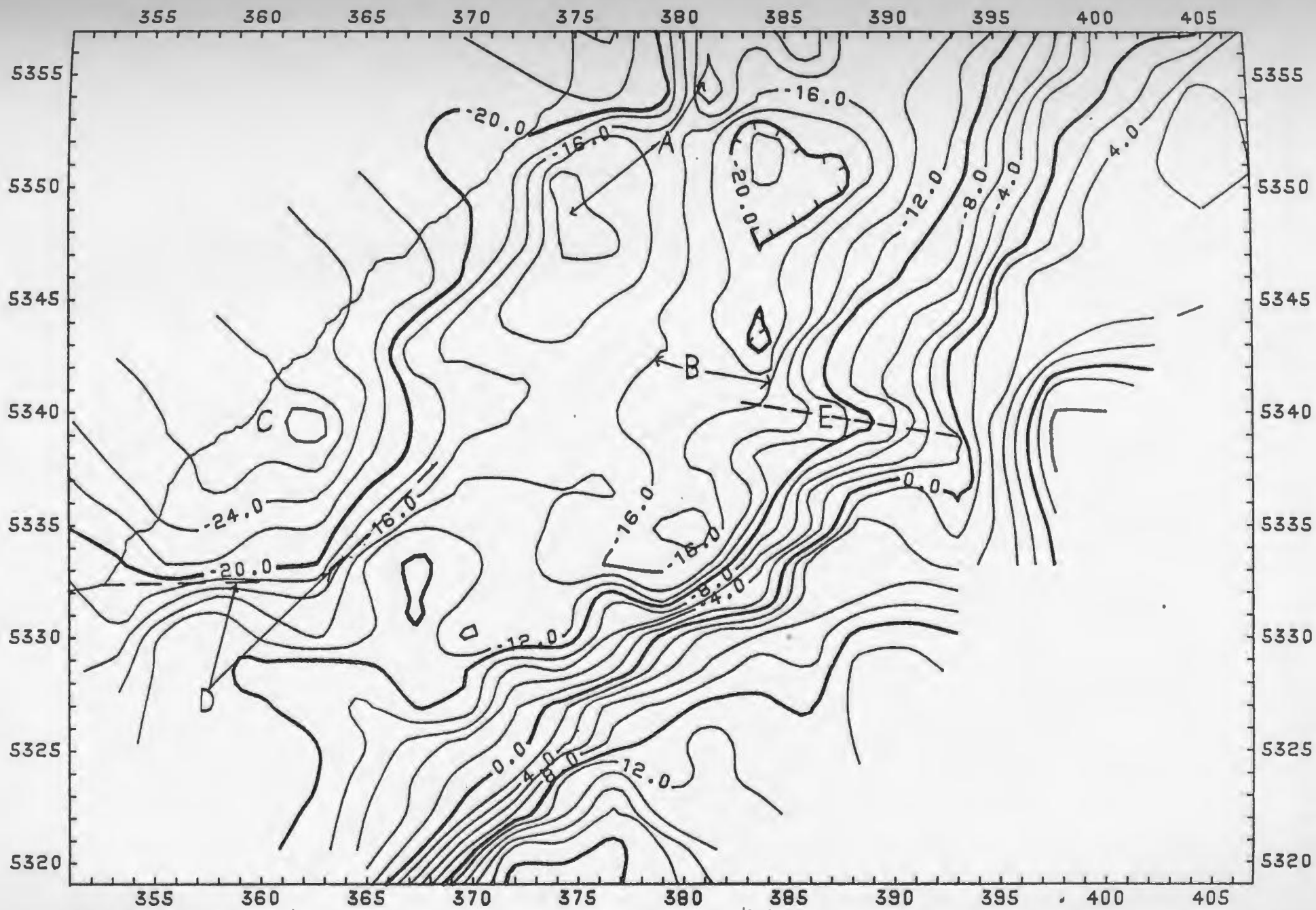


Figure 2.2 Bouguer anomaly map. Contour interval = 2 mGal.
 Letters referred to in Chapter 6. (scale = 1:250000)

2.2 Collection and Reduction of Magnetic Data

Magnetic data were digitized from 1:63360 scale total field aeromagnetic maps published by the Geological Survey of Canada (GSC, 1968, a-d). These maps were based on data collected along east-west flight lines by flux-gate magnetometers. The lines were separated horizontally by 800 m and flown at an altitude of 300 m. These maps were digitized using a 0.5 inch spacing in both latitude and longitude, making the distance between grid-points equal to 0.8 km.

The first step in aeromagnetic data processing is the removal of the IGRF (International Geomagnetic Reference Field) background field from the data. However, the maps used to obtain the data were produced at an arbitrary magnetic reference level, so they don't match with standard total field maps. In order to make the data consistent with other maps in the area and therefore useful for future work, the original data was converted into standard total field values by matching the edges of the 'old' maps to the adjacent edges of the standard maps surrounding the area. In this manner a correlation between the arbitrary reference and the standard total field magnetic values could be made. This was done for four different map pairs, and a plot of the 'old' field values vs. their standard counterparts was drawn and a straight line could be traced through the data points for each map pair. A standard linear regression program was used to obtain a slope and intercept for each data set. Three out of the four sets of data from the map pairs had almost the same slope and intercept values. These values were averaged to obtain an empirical conversion equation:

$$M_{STD_i} = 0.913 \times M_{o_i} + 53457$$

where M_{STD_i} and M_{o_i} are the standard and 'old' values for the magnetic field at a station i , respectively. The resulting total field, IGRF corrected map of the study area is shown in Figure 2.3.

After the IGRF corrected field was established for the magnetic data, the IGRF background field was removed using a modified version of a program originally written by Miller and Weig (1982). Values for the background field were interpolated from corner point values in the IAGA Bulletin 29 (1971) for each point in the grid. These values were subtracted from the IGRF corrected values at the grid-points to give the reduced magnetic anomaly map shown in Figure 2.4. A 25 point averaging process was then applied to the reduced magnetic data (see Figure 2.5). The averaging process calculated the average value of a 5 X 5 block of data points and placed that straight averaged value at the central point of the block. The averaging was done for two reasons: 1) the filtered grid-point spacing of 4 km is consistent with the average gravity station spacing in the area; and 2) the averaging removes short-wavelength, high amplitude anomalies which are due to small, localized features that are of minimal interest in the geophysical modelling of the Subbasin.

2.3 Trend Analysis of Gravity and Magnetic Data

A trend analysis program based on the equations of Whitten (1973) was written by T.E. Jaidley of Memorial. The trend analysis is done by fitting a polynomial of the form

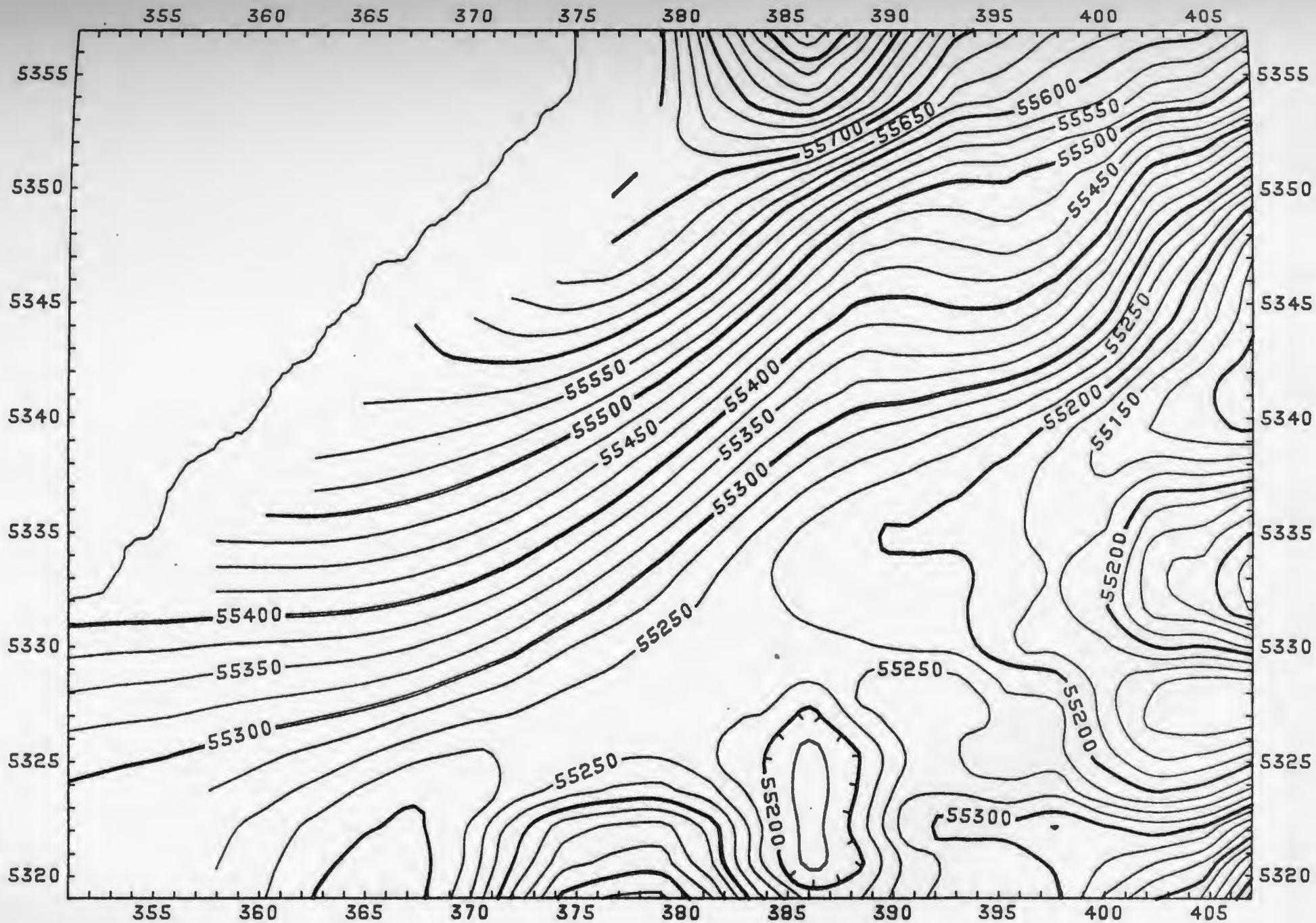


Figure 2.3 Total field, IGRF corrected magnetic map of the study area.
Contour interval = 25 nT. (scale = 1:250000)

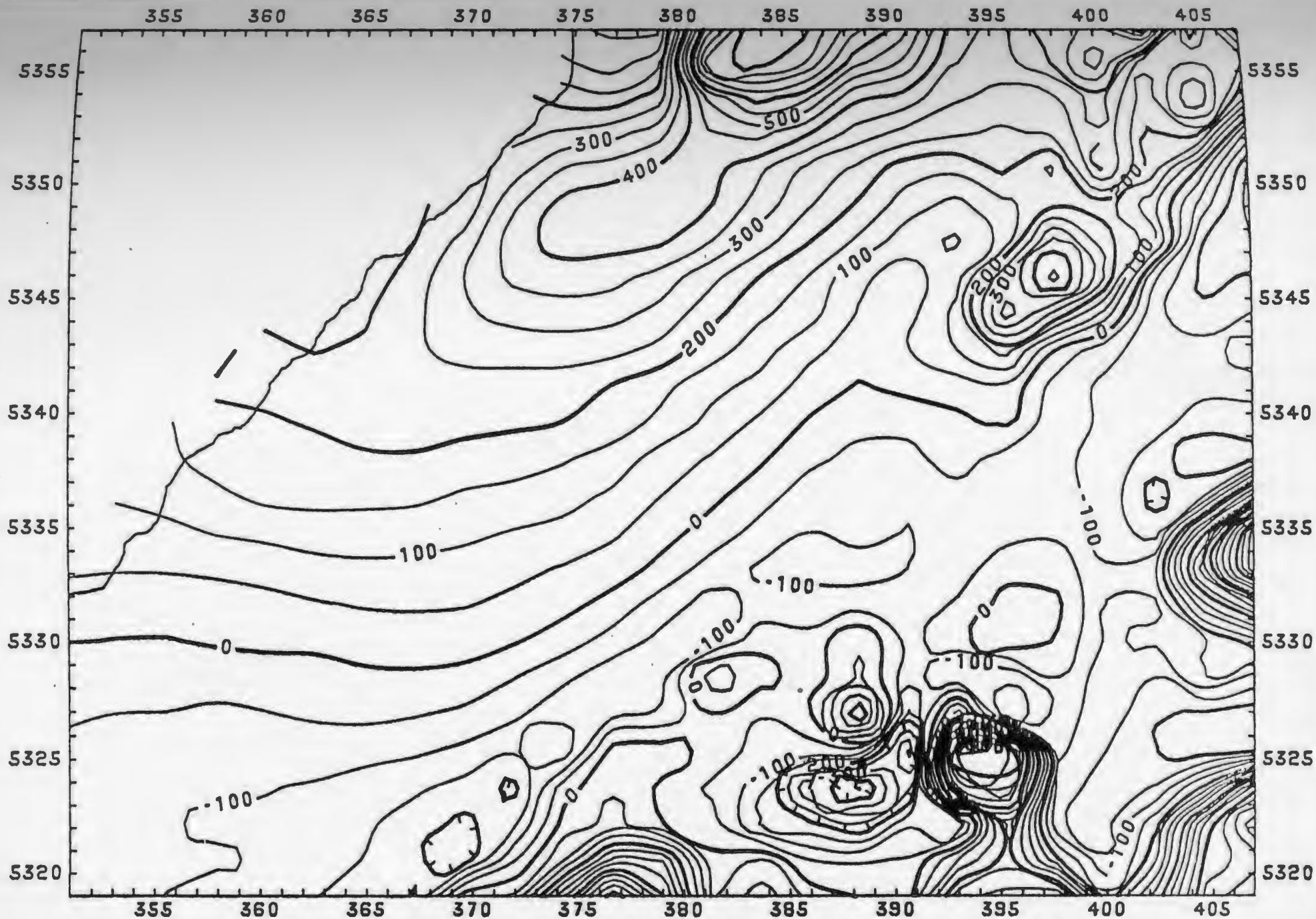


Figure 2.4 Contour map of reduced magnetics (no averaging).
Contour interval = 50 nT. (scale = 1:250000)

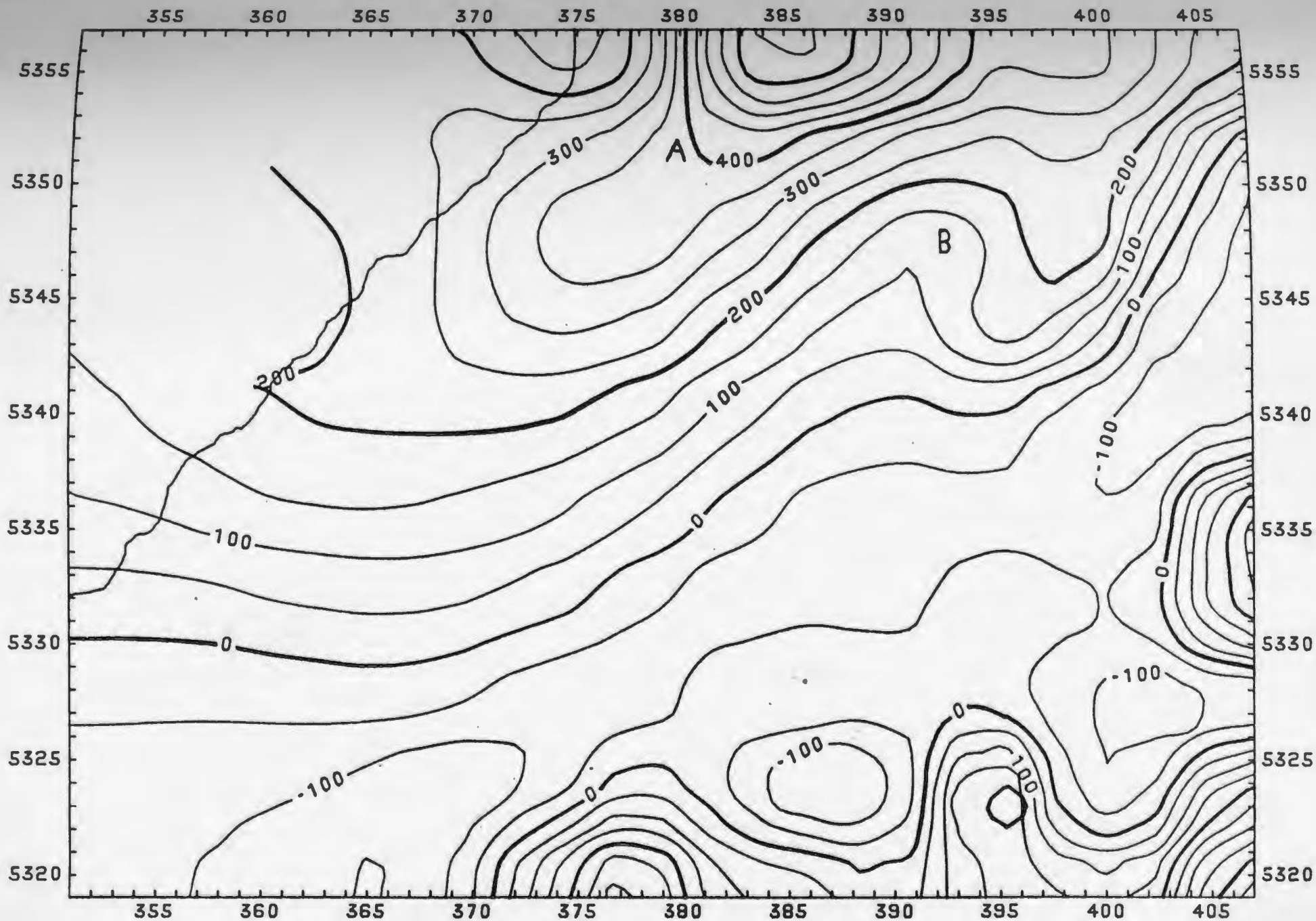


Figure 2.5 Contour map of reduced magnetics (25-point averaging).
 Letters referred to in Chapter 6. Contour interval = 50 nT.
 (scale = 1:250000)

$$A_i(x,y) = \sum_{k=0}^n \sum_{j=0}^{n-k} a_{kj} x^k y^j \quad (2.8)$$

to the data via a least-squares technique. In Equation 2.6, A_i is the calculated regional trend, n is the order of the polynomial being fitted to the data, and a_{kj} is the coefficient to be determined by least-squares. The solution may be written in matrix notation as (Miller, 1970)

$$(s_{ml}) = \left(\sum_{i=1}^N x^{k+m} y^{l+j} \right)^{-1} \left(\sum_{i=1}^N A_i x^k y^j \right) \quad (2.9)$$

where

$$k = 0, 1, \dots, n$$

$$j = 0, 1, \dots, n-k$$

$$m = 0, 1, \dots, n$$

$$l = 0, 1, \dots, n-m$$

and N is the number of data points. The result of an application of this type of filter to gravity or magnetic data is a regional trend which is inferred to be caused by deep heterogeneities in the Earth's crust. This is removed by subtracting the regional from the original anomaly at each point, or

$$\Delta A_i = A_{O_i} - A_{C_i}$$

where ΔA_i is the residual anomaly at a station i , and A_{O_i} and A_{C_i} are the original and regional anomalies, respectively. After the removal

of the regional trend, the residual map should represent the local, geologically correlatable features in the subsurface (Nettleton, 1976).

Contour plots were made for trend analyses of both the reduced gravity and magnetic fields. Polynomial orders 1 through 6 were used in both cases. An analysis of these plots showed that the 5th order trends had the best fit to the original gravity and magnetic data, therefore they were used as the regional trend for both gravity and magnetics. The regional fields were subtracted from the original reduced data to obtain residual anomaly maps for gravity (Figure 2.6) and magnetics (Figure 2.7). Major features of these maps (lettering on Figures 6.6 and 6.7) will be discussed in Section 6.2.

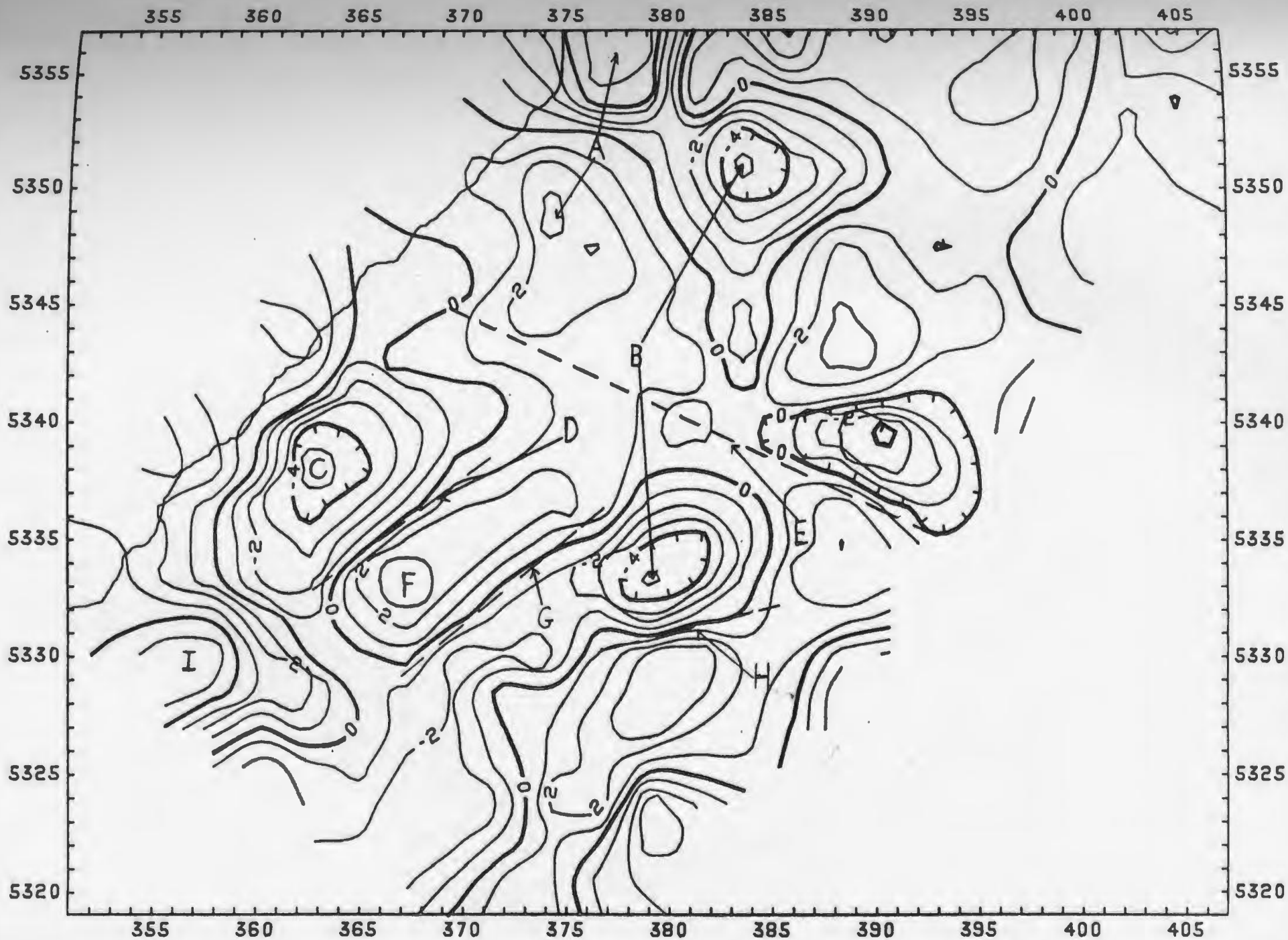


Figure 2.6 Residual gravity after trend analysis -- order = 5.
 Letters referred to in Chapter 6. Contour interval = 1 mGal.
 (scale = 1:250000)

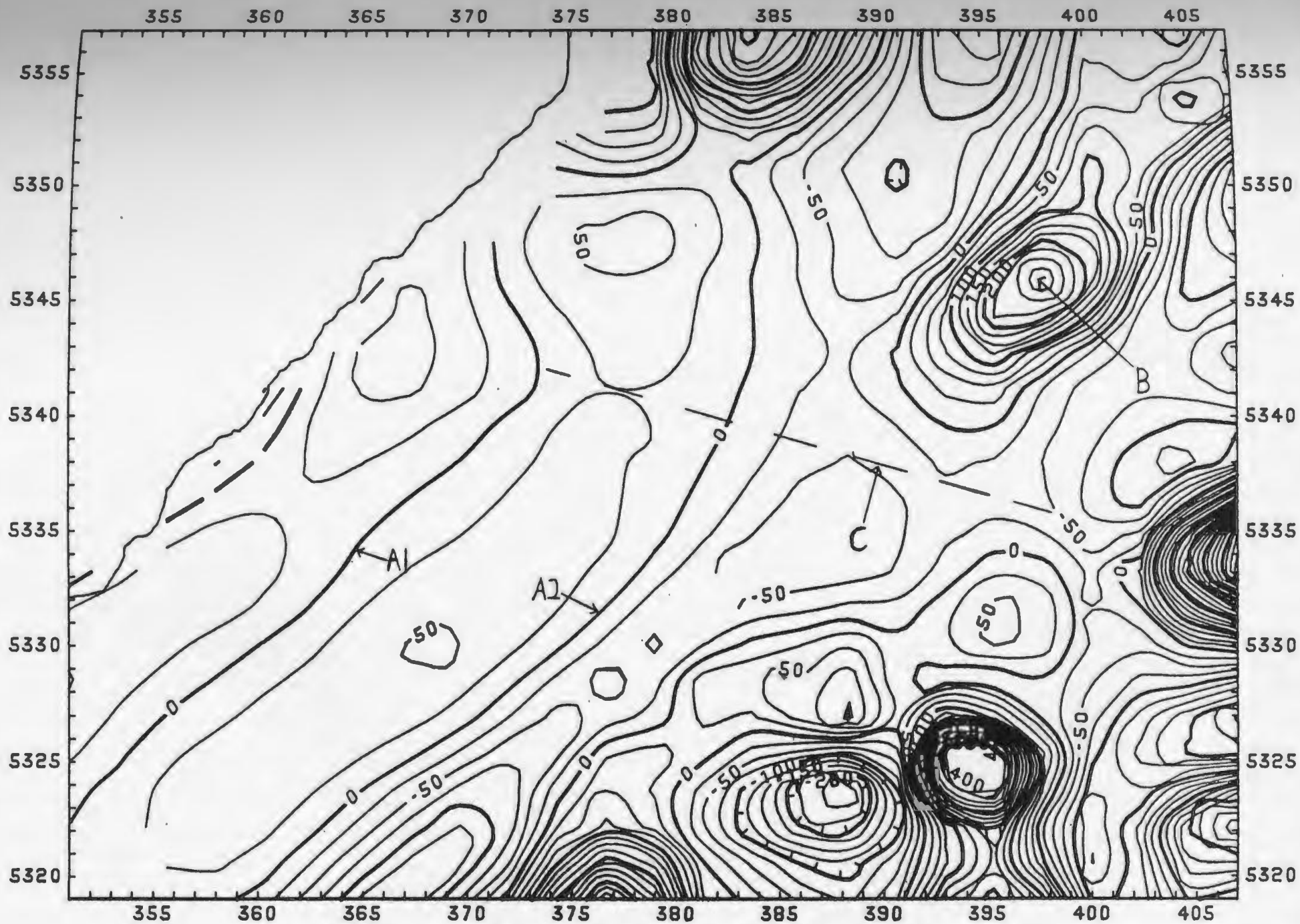


Figure 2.7 Residual magnetics after trend analysis - order = 5.
 Letters referred to in Chapter 6. Contour interval = 25 nT.
 (scale = 1:250000)

Chapter 3: Geology of the Bay St. George Carboniferous Subbasin

3.1: Introduction

This chapter on the geology of the Bay St. George Carboniferous Subbasin is based largely on Knight's report (1983), which provides a detailed description of the stratigraphy and an analysis of the tectonic setting, depositional environments, structural history, and mineral potential of the area.

The Bay St. George Carboniferous Subbasin is a part of the Maritimes Basin complex of Atlantic Canada (Knight, 1983). It is located on the west coast of the island of Newfoundland between Cape Anguille and Stephenville (see Figure 1.1).

The Subbasin was formed by Late Devonian right-lateral, strike-slip movements along the Long Range Fault. An analysis of the major structural elements shows a pattern of synthetic and antithetic faults and folds fitting into the wrench-fault basin hypothesis.

The sediments were deposited in a 45-60 million year period from the Upper-Devonian (Famennian) to Lower Pennsylvanian (Westphalian-B). The environment changed during deposition from a non-marine fluvial and lacustrine environment (Anguille Group), to a marine/non-marine, arid evaporitic environment (Codroy Group), to a floodplain and backswamp humid climate (Barachois Group). The overall thickness of deposits may have been as great as 10 km, with the present fill being 6 km (Knight, 1983).

Major deposits of salt and gypsum have been found in the northern part of the Subbasin within the Codroy Group. Deposits of coal have

been found in Barachois sediments. However, the coal deposits have proven uneconomic thus far.

The Pre-Carboniferous basement is inferred to be of an anorthositic-granitic character that closely resembles the Indian Head and Steel Mountain complexes, which outcrop in the northern area of the Subbasin (see Section 3.5).

3.2. Lithology of the Sedimentary Rocks

The sedimentary rocks of the Bay St. George Subbasin are divided into 3 groups by Knight (1983):

- 1) the Anguille Group (map units 2-5 in Figure 3.1); consisting of non-marine, lacustrine, fluvial-deltaic, and fluvialite rocks of Late Famennian to Tournaisian age (350-335 my);
- 2) the Codroy Group (map units 6-8 in Figure 3.1); consisting mostly of fluvialite redbeds, but including marine siliciclastics, carbonates, and evaporites of middle to upper Visean age (335-323 my); and
- 3) the Barachois Group (map unit 11 in Figure 3.1), consisting of fluvial and coal-bearing strata of Namurian to Westphalian-B age (323-300 my).

Each group will be subdivided into its component formations, and these in turn will be described with regard to general lithology, thickness,

and environment of deposition. Particular attention will be paid to major lithologic components of the northern part of the Subbasin.

3.2.1 Anguille Group

The Anguille Group is subdivided into four formations. In order of ascendancy, these are the Kennels Brook Formation, the Snakes Bight Formation, the Friars Cove Formation, and the Spout Falls Formation (Knight, 1983).

The Kennels Brook Formation (Unit 2 in Figure 3.1) consists of gray-green and red sandstones and pebbly sandstones, red siltstones, interbedded gray and brown siltstones and mudstones with gray limestones at the top. These sediments are fluvial and were deposited by braided streams and meandering rivers. The thickness of the Kennels Brook Formation is ~3200 m, but it is only 714 m on the crest of the Anguille Anticlinorium (Figure 3.1).

The Snakes Bight Formation (Unit 3 in Figure 3.1) includes basal deposits of shales and sandstones, followed upward by thick, bedded gray sandstone, black shale and siliceous shale units, with minor gray siltstone, dolomite, sandy limestone and quartz and dolomitic conglomerate. These were deposited in a narrow, northeasterly trending, deep lake ~30 km long (called Snakes Bight Lake). The thickness of the formation ranges from 785 m northwest of the Snakes Bight Fault to ~1000 m southeast of the Snakes Bight Fault (see Figure 3.1).

The Friars Cove Formation (Unit 4 in Figure 3.1) consists of a basal gray sandstone and conglomerate member, with gray-black

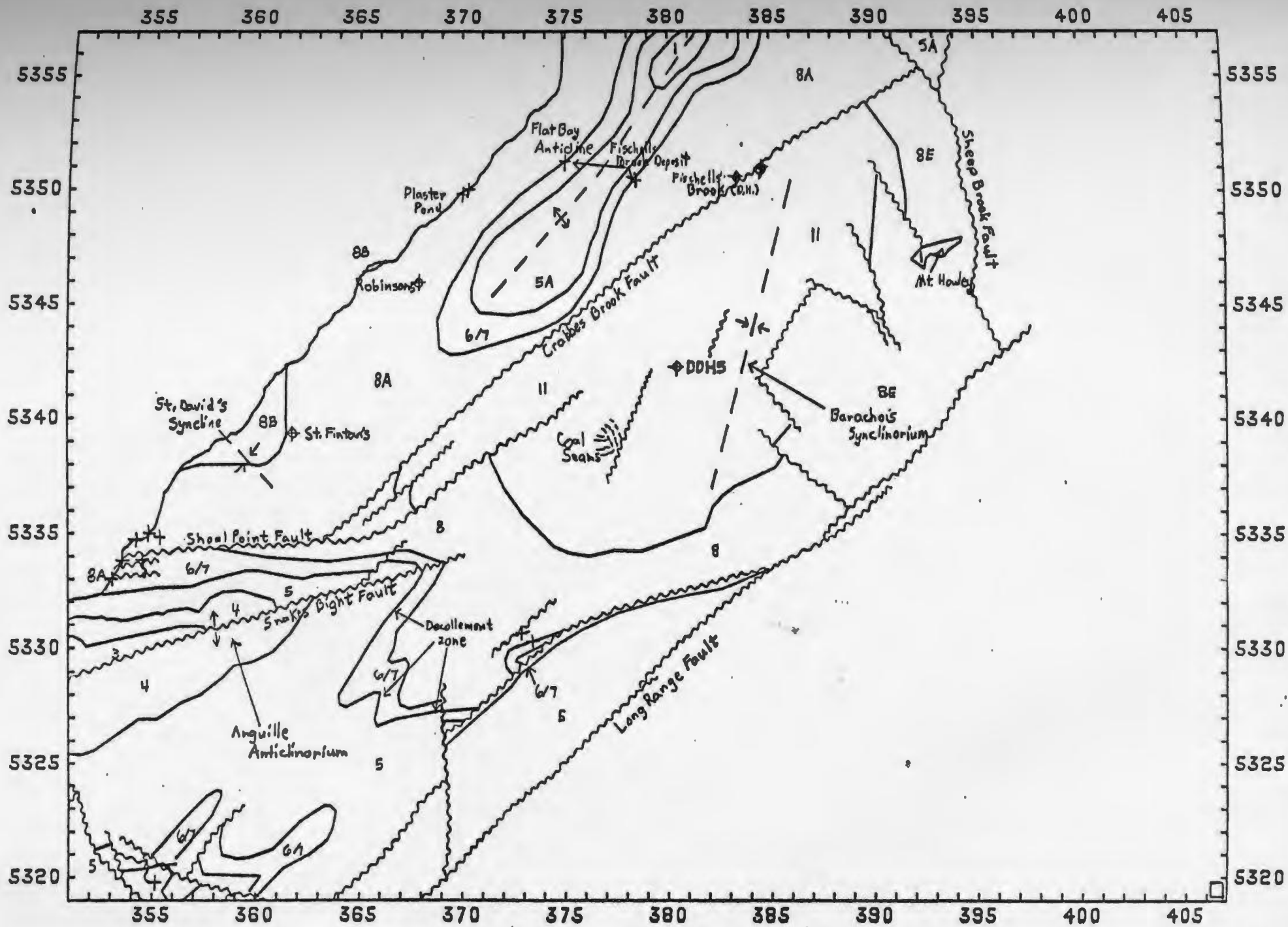


Figure 3.1 Geology and location of drill holes and evaporite deposits.

Legend for Figure 3.1

Symbol	Description
	Fault
	Geologic Contact
	Anticline
	Syncline
	Drill Hole
	Gypsum/Anhydrite
1	Pre-Carboniferous Basement
2	Kennels Brook Formation
3	Snakes Bight Formation
4	Friars Cove Formation
5	Spout Falls Formation
5A	Fischells Conglomerate
6	Ship Cove Formation
7	Codroy Road Formation
8	Robinsons River Formation (undivided)
8A	Jeffreys Village Member
8B	Highlands Member
8E	Brow Pond Lentil
11	Undivided Barachois Group

sandstones, siltstones, and mudstones, local redbeds and dolomitic limestones and dolostones. These sediments represent the final fill of the Snakes Bight Lake, and therefore represent a fluvial-deltaic, shallow lacustrine setting. The average thickness of the Friars Cove Formation is about 500m, but it thickens to as much as 1300 m in the northeast Anguille Mountains (Figure 1.1).

The Spout Falls Formation (Unit 5 of Figure 3.1) forms a northeastward thickening prism consisting of sandstone with minor siltstone in the south, and minor conglomerate in the central Subbasin. Farther north, the Spout Falls Formation is replaced by the Fischells Conglomerate (Unit 5a in Figure 3.1). The environment of deposition was a sandy and fluvial system that prograded southward over the Friars Cove Formation. The Spout Falls Formation is 780 m thick northeast of the Snakes Bight Fault, but thickens to 2250 m west of Codroy Pond (southern part of Figure 1.1). The Fischells Conglomerate has a thickness of 100-150 m in the Flat Bay anticline and >200 m near Coal Brook (Figure 3.1).

In conclusion, the Anguille Group consists of a sequence of non-marine fluvial and lacustrine strata laid down in a generally narrow, tectonically active basin. The overall thickness of the Anguille Group in the study area varies between 200 m in the north to 4000 m in the southern end.

3.2.2 The Codroy Group

The Codroy Group is subdivided into four formations. These are the Ship Cove Formation, the Codroy Road Formation, the Robinsons

River Formation, and the Woody Cape Formation (Knight, 1983). Of these, only the first three are present in the study area.

The Ship Cove Formation (Unit 6 in Figure 3.1) consists mainly of limestone with some siltstone, shale and sandstone. These sediments were deposited following marine flooding in quiet, relatively deep (20-50 m) water. The formation is only 18-20 m thick.

The Codroy Road Formation (Unit 7 in Figure 3.1) consists mostly of siltstones and mudstones, with some dolomites and gypsum and anhydrite occurrences. The environment of deposition of the Codroy Road Formation was mainly an intertidal flat in the south and extreme north; while in the central area, the sediments were deposited in a narrow, hypersaline lagoon. The thicknesses are small, ranging from ~120 m at Ship Cove to 145 m at Fischells Brook. The main features of this formation are the decollement it formed when it overrode the Ship Cove Formation at the northern terminus of the Anguille Anticline (see Section 3.2.1), and the gypsum and anhydrite deposits -- some of which are substantial (Knight, 1983; see Section 3.4 and Figure 3.1).

The Robinsons River Formation (Unit 8 in Figure 3.1) has been subdivided into five members: the Jeffreys Village Member, the Highlands Member, the Mollichignick Member, the Overfalls Brook Member, and the Brow Pond Lentil (Knight, 1983). These combine to give an overall initial thickness of 5-6 km for the Robinsons River Formation. However, the Mollichignick and Overfalls Brook Members can be ignored, since they occur mostly in the Codroy Lowlands to the south of the study area.

The Jeffreys Village Member (Unit 8a of Figure 3.1) consists predominantly of red siltstones and sandstones, with some conglomerate, limestones, shale and major evaporite deposits (see

Section 3.4 and Figure 3.1). The thickness of the Jeffreys Village Member is 1400 m, but it may be as thick as 2000-2100 m southwest of the Flat Bay anticline.

The Highlands Member (Unit 8b of Figure 3.1) is predominantly thick red sandstone with some gray and yellow sandstone. There are also two units of possible marine origin consisting of limestone and gray to white sandstone and shale. The thickness of the Highlands Member has been measured to be 884 m along the coast south of Crabbes River.

The Brow Pond Lentil (Unit 8e of Figure 3.1) consists entirely of pink and red, pebbly and cobbly arkosic grits and sandstone. The thickness of this unit is unknown.

In the St. George's Bay Lowlands (Figure 1.1), the paleoclimate was an arid to semiarid, hot climate. The various members were deposited in a sequence of four stages:

- 1) progradation of fine, red, alluvial sediments from the southeast and the retreat of the sea into the northeast part of the Subbasin;
- 2) widespread expansion of shallow evaporite conditions in the study area, leading to the salt sequences and limestones;
- 3) thick, non-marine redbeds with thin marine sediments intercalated, showing a series of marine transgression/regression cycles with regressions becoming dominant in the upper sequences; and

- 4) for the Highlands Member only: axial area blanketed by red alluvium from the northeast deposited by meandering rivers.

In conclusion, the Codroy Group was deposited during a period of marine transgression/regression episodes caused by tectonic activity within the Subbasin. This activity caused subsidence, accounting for the great thickness of the Robinsons River Formation and the evaporite deposits of the lower Jeffreys Village Member.

3.2.3 The Barachois Group

The Barachois Group has been divided into only two units -- the Searston Formation (in the far south of the Subbasin) and the Undivided Barachois Group (Unit 11 in Figure 3.1), assumed to consist of both the Searston Formation and the "coal measures" (Knight, 1983). The Barachois Group is composed of green-gray to red sandstone, pebbly sandstone, red siltstone with dark gray to black shales and mudstones, and coal seams (discussed further in Section 3.4). The environment of deposition was that of meandering river channels with adjacent flood plains and backswamps. The overall thickness of the Barachois Group is 1500-1600 m in the study area, thinning to the north.

3.3 Structural Geology

The Bay St. George Subbasin contains several types of structures. Among these are (a) northeasterly trending folds, (b) thrust faults and decollement zones, (c) northeasterly trending faults, (d) northwesterly trending faults, and (e) east trending faults. All of these occur in the area of study (Figure 3.1).

There are three major northeasterly trending folds in the area. These are the Flat Bay Anticline, the Barachois Synclorium, and the Anguille Anticlinorium (Knight, 1983). Also, there is a northwesterly trending, minor syncline known as St. David's Syncline.

The Flat Bay Anticline is a doubly-plunging, anticlinal fold with an orientation of 037° T. Away from the fold axis, the overlying strata dip as much as 80° locally, but dips of 50° are more common. At the core of the anticline is a basement outcrop, overlain unconformably by sediments of the Anguille and Codroy Groups.

To the east of the Flat Bay Anticline is the Barachois Synclorium, a doubly-plunging, open syncline oriented 027° T. Dips in the synclorium are moderate ($\sim 40^{\circ}$), but steepen near fault contacts. The sedimentary infill of the syncline is composed of rocks of the Barachois, Codroy, Anguille Groups.

In the southern end of the study area is the northern closure of the Anguille Anticlinorium. This anticline is cut by the Snakes Bight Fault (discussed later), which lies along or near the hinge of the anticline. Both turn from an initial orientation of $\sim 030^{\circ}$ to $\sim 070^{\circ}$ at the northern terminus. The Anguille Anticlinorium is covered by sediments of the Anguille Group.

St. David's Syncline is a northwesterly trending syncline with dips in the range of 40° - 50° and a plunge of 30° - 39° . This syncline is at right angles to the other regional-scale folds. This configuration probably results from its position between the Flat Bay and Anguille anticlines. St. David's syncline is covered at the surface by sediments of the Highlands and Jeffreys Village Members of the Robinsons River Formation (Mid-Upper Visean).

A decollement zone is developed at the base of the Codroy Road Formation (Codroy Group) in the southern end of the study area (Figure 3.1). This formation of fine siliciclastics and evaporites overlies the more competent limestones and dolostones of the Ship Cove Formation. The decollement is evidenced by a zone of shattered and sheared rocks (Knight, 1983). This zone is up to 6 m thick and directly overlies the Ship Cove Formation. The decollement was probably caused by the Codroy Road Formation sliding over the Ship Cove Formation during an episode of upright, harmonic folding.

There are many high angle faults in the study area. Only ones of significance to the overall structure of the Subbasin will be discussed here.

Of the northeasterly trending faults, by far the most important is the Long Range Fault (Figure 3.1). This fault forms the southeastern boundary of the Subbasin and is a strike-slip fault oriented from 041° to 052° . Vertical movement on the fault was on the order of 10 km. (Knight, 1983). This movement was necessary to accommodate the load of Carboniferous sediments deposited to the west. Evidence for vertical

movements is based on bedding attitudes adjacent to the fault surface, which dip steeply away from the fault, and on locally overturned or folded beds.

The Snakes Bight Fault transects the Anguille Anticlinorium in the southern part of the study area and is oriented $\sim 070^{\circ}$ T (Knight, 1983). A right-lateral displacement of 10 km along the fault is evidenced by the displacement of beds of the Anguille Group (Figure 3.1).

The Crabbes Brook Fault is oriented at 037° and intersects the Barachois Synclinorium at an angle of 25° (Figure 3.1). A downthrow of several thousand meters occurred to the southeast of the fault, and right-lateral, strike-slip movement is likely also.

The only major northwesterly trending fault in the study area is the Sheep Brook Fault in the northeastern part of the study area (Figure 3.1). The fault trends northward in the northern part bordering the Fischells Conglomerate (Anguille Group), then it turns southeast until it reaches the Long Range fault.

A major easterly trending fault, called the Shoal Point Fault, occurs just north of the Anguille Mountains (Figure 3.1). This is a vertical fault with a downthrow to the north. The inland extent of the fault is unknown, although Knight (1983) shows it to intersect the Crabbes Brook Fault. It is possible, however, that it continues eastward, truncating the Snakes Bight Fault and eventually reaching the Long Range Fault.

The structural evolution of the Subbasin is interpreted to be the result of right-lateral slip along the major northeasterly trending faults, creating a wrench-fault basin as described by Wilcox, et al.

(1973) (Knight, 1983). The main evidence in favor of right-lateral wrench movements is the en echelon arrangement of fold axes oblique to the Long Range and Snakes Bight faults. It is also supported by the interpretation of northeasterly and northwesterly trending faults as synthetic-antithetic conjugate faults (Knight, 1983). Vertical movements probably affected the development of the Subbasin later. These movements are evidenced by bedding attitudes, folds and local slickensliding within the Long Range fault zone, and northeasterly and easterly trending faults showing large vertical displacements (Knight, 1983).

The geometry of the fold and fault system is in agreement with the Wilcox model. The angle of intersection of the northeasterly trending fold axes with the main wrench faults (the Long Range and Snakes Bight faults), the orientation of both the northeasterly and northwesterly trending faults, and the intersection angle of these faults with each other and the Long Range and Snakes Bight faults are all in accord with the wrench model.

The progression of deformation and local variations from the strike-slip model were caused by: (a) the presence of a crystalline basement from Robinsons River northwards acted as a buttress and prevented the development of the more complex structures of the southern subbasin; (b) the presence of incompetent rock units in the Anguille and Codroy Groups promoted folding as a mechanism to accommodate shortening; and (c) the presence of a thickening sandstone sequence in the northern Anguille Mountains caused the formation of consistently open folds in that area.

Knight has concluded that the Bay St. George Subbasin was created by right-lateral wrench faulting along the Long Range Fault. This occurred in the Late Devonian. Deposition followed and continued until the Mid-Pennsylvanian. The sediments were folded and faulted various times during the 45-60 million year history of deposition, resulting in such major features as the Anguille Anticlinorium, the Snakes Bight Fault, and the Barachois Synclinatorium. Finally, a major deformation episode occurred, corresponding to the Variscan Orogeny.

3.4 Evaporite and Coal Deposits

Evaporite deposits are found in the Codroy Group throughout the Bay St. George Subbasin. They are the result of various marine transgression/regression episodes during the deposition of the Codroy Group. The evaporites are gypsum, anhydrite, celestite (very minor) and sodium and potassium salts (Knight, 1983). Coal deposits are found in the Barachois Group and are the result of backswamp environment during deposition.

There are several large, economic deposits of gypsum and anhydrite in the northern area of the Subbasin (Knight, 1983). Within the study area, only 2 major gypsum deposits occur. One is at Fischells Brook, with a total of 10 million tonnes; and the other is at Plaster Pond, (Figure 3.1) with a total of 0.5 million tonnes (Figure 3.1). Both of these deposits are within the Codroy Road Formation. Smaller deposits occur in the upper Codroy Road Formation and the Jeffreys Village Member of the Robinsons River Formation (Figure 3.1).

Halite and potash deposits occur in the Jeffreys Village Member.

(Knight, 1983). Three drill holes have found substantial deposits of salt and potash at St. Fintan's, Robinsons, and Fischells Brook (Figure 3.1).

The St. Fintan's and Robinsons deposits occur in the lower Jeffreys Village Member at ~235 m depth, and have various potassium-rich horizons throughout each salt section. The St. Fintan's deposit is 120 m thick, of which the lower 70 m is poor in salt. The Robinsons deposit has two horizons of salt (104 m and 54 m thick), separated by 100 m of anhydrite and halite-bearing mudstones and thin halite beds (Knight, 1983).

The Fischells Brook deposit could be in both the Jeffreys Village Member and Codroy Road Formation, although the drill hole only found sediments from the Jeffreys Village Member. The drill hole penetrated 390 m of salt without reaching the bottom. The potassium-rich zone occurs at the top of the salt and is ~6 m thick. Bouguer gravity anomalies suggest that the salt body may be a cylindrical plug, with a maximum thickness of 1.2 km, and a maximum radius of 1 km (Knight, 1983). This equals a volume of 3500 million cubic meters of salt. However, increased occurrence of gypsum and anhydrite were noted with increasing drill hole depth, meaning that this estimate could be high.

Coal deposits occur exclusively in the Barachois Group (Figure 3.2) and are, in general, very minor (Knight, 1983). A maximum thickness of 1.5-4 m has been reported for the Jukes Seam along Barachois Brook. Other seams are much thinner. A recent drill hole ('DDH5' in Figure 3.1) intersected a few seams of only 10-20 cm thickness, suggesting that the coal seams pinch out away from the main exposure area along Barachois Brook.

In conclusion, there are substantial deposits of gypsum and salt in the study area, with thicknesses of > 390 m for the salt and 300 m for the gypsum deposits. All occur in units of the lower Codroy Group. Coal deposits occur in several localities in Barachois Group sediments of the study area. These coal seams are relatively thin and are not economically significant at this time.

3.5 The Pre-Carboniferous Basement

Not much is known about the Pre-Carboniferous basement rocks of the Bay St. George Subbasin. These rocks occur below Anguille Group sediments and outcrop in only two areas: the core of the Flat Bay Anticline and Mount Howley (Figure 3.1).

The basement in the northern Subbasin is believed to be from the Humber tectonostratigraphic zone of the Newfoundland Appalachians (Williams, 1978). The Humber Zone is composed of: a) Precambrian gneisses, probable Grenvillian granites and anorthosites, and Cambrian diabase dikes; b) Cambro-Ordovician clastic and carbonate rocks; c) transported sedimentary, volcanic, and ophiolitic rocks of the Humber Arm Allocthon; d) greenschist-grade metasedimentary rocks; and e) Late Silurian-Devonian redbeds.

The basement outcrops of Steel Mountain and Indian Head, located just to the east and west of the north part of the Subbasin, respectively, indicate that only rock type (a) is present in the area (Heyl and Ronan, 1954, Baird, 1954). Therefore, for the purposes of this study, the basement is assumed to be anorthositic-granitic in nature and Grenvillian in age (Murthy and Rao, 1976). Of major note

in these complexes are lenses of magnetite found near both localities (Heyl and Ronan, 1954, Baird 1954), which could cause problems in the gravity and magnetic interpretation. The implication of these basement rocks for the interpretation of the gravity and magnetic fields is discussed in Chapter 6.

Chapter 4: Physical Properties of the Carboniferous Sedimentary
Rocks and the Pre-Carboniferous Basement

4.1 Introduction

In potential field modelling, ambiguity in the solution is always a problem (Skeels, 1947, Al-Chalabi, 1971, Jackson, 1972) which arises from the fact that no unique mathematical solution exists for any set of potential data. While an infinity of solutions are possible, the most geologically probable models can be obtained by a sensible application of geologic and physical constraints to the model parameters. Among the more important constraining parameters are density and magnetic susceptibility. If the density and magnetic susceptibility of a particular body in the model can be assumed as known, a much better estimate of the thickness and extent of this body can be made from the data.

In order to constrain the geophysical model for the Bay St. George Subbasin, densities and magnetic susceptibilities were obtained for both the sedimentary rocks within the Subbasin and the inferred Pre-Carboniferous basement.

A weighted density of $2.54 \pm 0.09 \text{ g/cm}^3$ has been determined for the sedimentary rocks on the basis of the measurements. Measurements also indicate that the magnetic susceptibility of the sediments is negligible.

For the basement rocks an average density of $2.72 \pm 0.35 \text{ g/cm}^3$ was determined. Magnetic susceptibility measurements indicate that the

two different basement types - Indian Head and Steel Mountain - can be separated by their magnetic signature since the Steel Mountain samples have a significantly different magnetic susceptibility than Indian Head samples.

4.2 Methods used to measure density and magnetic susceptibility

Density and magnetic susceptibility measurements of samples from the Bay St George Subbasin were made. 105 samples of sedimentary rocks and 132 samples of the Indian Head and Steel Mountain complexes were analysed.

Densities for all samples were determined using a triple-beam balance. The samples were weighed by attaching them to a length of monofilament fishing-line tied to the bottom of the weighing pan. The scale was then balanced to remove the effect of the mass of the line. The weight in air was recorded first, then the sample was submerged in a bucket of water and weighed again. The difference between these two weights divided by the density of water gives the volume of the sample in cubic centimeters (cm³), and the 'in situ' density can easily be determined from the relationship

$$\rho_a = \frac{\rho_w \times M_a}{M_a - M_w} \quad (4.1)$$

where:

- ρ = density of the sample in g/cm,
- ρ_w = density of water in g/cm ,
- M_a = mass of the sample weighed in air in grams (g), and
- M_w = volume of the sample in cm .

The density of water was assumed to be 1.000 g/cm³. Using this value adds an error of only 0.4 % to the density measurement for the range between 5°C and 30°C (CRC, 1969), which is small compared to weighing error of 0.03 g (+1.0 %) in the density determinations.

Special problems were encountered in measuring the density of the evaporite samples. Since the samples would have dissolved when submerged in water, a different liquid had to be used. It was decided that it would be safest to use 98 mole-percent methanol instead of water in order to determine the 'in-situ' density. The density of methanol was determined by two different methods. The first, hydrometer measurements, gave a density of 0.795 ± 0.002 g/cm³. The second method used a 100 ml graduated cylinder. The cylinder was weighed without and then with 100 ml of methanol in it. The mass of the methanol was then divided by its volume (100 ml), to give a density of 0.79 ± 0.02 g/cm³. These values are close to the accepted value of 0.79855 g/cm³ at 15°C (CRC, 1962). Measurements were then conducted on the evaporites as for the other samples. Calculations were made using equation 4.1, with ρ_w replaced by the measured density of the methanol.

Magnetic susceptibility values for the sedimentary samples were determined using the Scintrex Digital Magnetic Susceptibility Meter (Model SM-5). The meter uses a high-permeability, 'C'-shaped core wrapped with wire and encased in a rectangular nylon head as a sensor. The sensor measures the difference in reluctance of the magnetic path with and without a sample. It then calculates the magnetic susceptibility, which can be read from an LED display on the instruments base. Values for susceptibility between $100-99,000 \times 10^{-6} \pm 5\%$ cgs units can be measured using this instrument (SM-5 Users Manual, 1980). The SM-5 is suitable for measuring hand samples, but is not very good for measuring small samples. Because the basement samples are small cores, a different method had to be used on them.

Magnetic susceptibility values for the basement samples were measured using an AC susceptibility bridge constructed by R. Patzold (1972). The bridge measures the susceptibility of drilled cores 2.22 cm in diameter. The basement samples were originally used in paleomagnetic research and were cut into 2.22 cm diameter cores for this purpose, therefore they were ideally suited for use with the AC bridge. The bridge uses a set of Helmholtz coils and an oscillator to create an AC field in the sample. The net emf output, which is measured by a set of pick-up coils, is due to induced magnetization -- which is a measure of the magnetic susceptibility. Since there is a linear relationship between output voltage and susceptibility, the susceptibility of a sample can be determined using the following equation:

$$k = (V_1 - V_0) \frac{S}{10} C_f + h_f \quad (4.2)$$

where:

k = magnetic susceptibility in cgs units,

V_1 = output voltage in mV,

V_0 = 'zero' voltage in mV,

S = sensitivity or gain factor,

C_f = calibration constant in cgs/mV, and

h_f = height correction factor in cgs units.

The output voltage (V_1) is read for each sample from a digital voltmeter. The 'zero' voltage (V_0) is determined by changing the phase of the oscillator by 90° and then 'balancing' the bridge until a minimum reading is obtained on the voltmeter. The sensitivity (S) is determined by the gain setting, with the bridge being calibrated for a gain of 10 (hence, the division of S by 10 in equation 4.2). The calibration constant (C_f) is determined by placing a current-carrying coil in the apparatus. When a small current is applied, the coil has an effective susceptibility (k_e) of 2.36×10^{-6} cgs units. The output voltage obtained when this coil is used is then divided into k_e to give the calibration constant. The height correction factor (h_f) is needed because the samples are not of a constant height, and therefore not of a constant volume. These factors were taken from a graph prepared by R. Patzold (1972, p. 25). Errors in susceptibility measurements using the bridge range from 3 % to 10 % (R. Patzold, 1972, p. 28). However, since susceptibilities in the range of 10×10^{-6} are negligible in magnetic modelling, the error is closer to 5 %.

4.3 Physical Properties of the Sedimentary Samples

Density and magnetic susceptibility measurements were done using representative samples of sedimentary rocks collected by I. Knight and C. C. K. Fong between 1973 and 1975 in the Bay St. George Subbasin and obtained from the Mines & Energy core storage building in Torbay, and on samples from a drill hole drilled by Longyear in 1983 for Memorial University. (For the location of the drill hole (DDH-5), see Figure 3.1.) Also, samples of halite, gypsum, and anhydrite from the Bay St. George Subbasin provided by the Mineral Development Division of Mines & Energy and I. Knight were measured.

Each sample was identified with respect to group, formation and/or member, and general lithology. Once the data was collected, a systematic evaluation of the density of each rock unit was performed. For the Anguille and Codroy Groups, the percent composition by general lithology for each formation and/or member was obtained from Knight (1983). For the Barachois Group, a lithology log of the rocks from the Longyear drill hole (DDH-5) was used to obtain the percent constituency of each rock type (S. Solomon, 1984). Then the overall density of each member or formation was calculated by weighting the average density obtained for each rock type within the unit by its percent composition. In this manner, densities were obtained for each rock unit. An estimate of the overall density of each group was obtained by using the thickness of each formation (from Chapter 3) as a weighting factor for the density. Table 4.1 shows the resulting densities for each formation and group, along with the standard deviation of the samples from each unit.

Table 4.1: Densities calculated for each sedimentary unit
 Density values are mean standard deviation
 (# = number of samples)

Group	Geologic Unit Formation	Member	Map unit	#	Density(g/cm)
Anguille	Kennels Brook	---	2	2	2.58 0.11
"	Snakes Bight	---	3	2	2.67 0.10
"	Friars Cove	---	4	6	2.67 0.04
"	Spout Falls	---	5	4	2.59 0.04
"	Fischells Cong.	---	5a	2	2.32 0.03
Anguille (average).....					2.63 0.06
Codroy	Ship Cove	---	6	2	2.72 0.03
"	Codroy Road	---	7	6	2.48 0.14
"	Robinsons River	Jeffreys Village	8a	11	2.40 0.09
"	"	Highlands	8b	7	2.53 0.13
"	"	Brow Pond Lentil	8e	3	2.58 0.03
Codroy (average).....					2.47 0.09
Barachois	Searston	---	9	5	2.51 0.08
"	Upper Series	---	10	33	2.56 0.08
Barachois (average).....					2.54 0.08
Evporites	anhydrite	---	---	2	2.97 0.03
"	gypsum	---	---	2	2.28 0.03
"	salt	---	---	2	2.18 0.03

As expected, the more deeply buried Anguille Group had the highest density ($2.63 \pm 0.06 \text{ g/cm}^3$) of the three groups. The Codroy Group had the lowest density ($2.47 \pm 0.09 \text{ g/cm}^3$) due to a low value for the relatively thick Robinsons River Formation. The evaporite samples had measured densities of $2.18 \pm 0.03 \text{ g/cm}^3$ for the salt, $2.28 \pm 0.03 \text{ g/cm}^3$ for the gypsum, and $2.97 \pm 0.03 \text{ g/cm}^3$ for the anhydrite. The weighted average density of the sediments in the area of the Barachois Synclorium was calculated to be $2.54 \pm 0.09 \text{ g/cm}^3$.

Magnetic susceptibility measurements of the sedimentary rocks were also done. However, since the values of susceptibility were less than 100×10^{-6} cgs units, the Scintrex SM-5 meter could not measure a value. Therefore, the effective magnetic susceptibility of the sedimentary section is assumed to be negligible for the purpose of magnetic modelling. The AC susceptibility bridge was not used because the samples were not 2.22 cm diameter cores.

4.4 Physical Properties of the Pre-Carboniferous Samples

Density and magnetic susceptibility measurements were done on anorthositic samples from the Indian Head and Steel Mountain complexes collected by G. S. Murthy in 1974. The complexes, as mentioned earlier in Chapter 3, are Grenvillian gneisses and igneous intrusives of anorthositic-granitic character (Murthy and Rao, 1976).

The average density of the 89 Indian Head samples was $2.68 \pm 0.07 \text{ g/cm}^3$. These samples were very regular, with only 16 % falling outside the range of 2.60 to 2.75 g/cm^3 (see Figure 4.1).

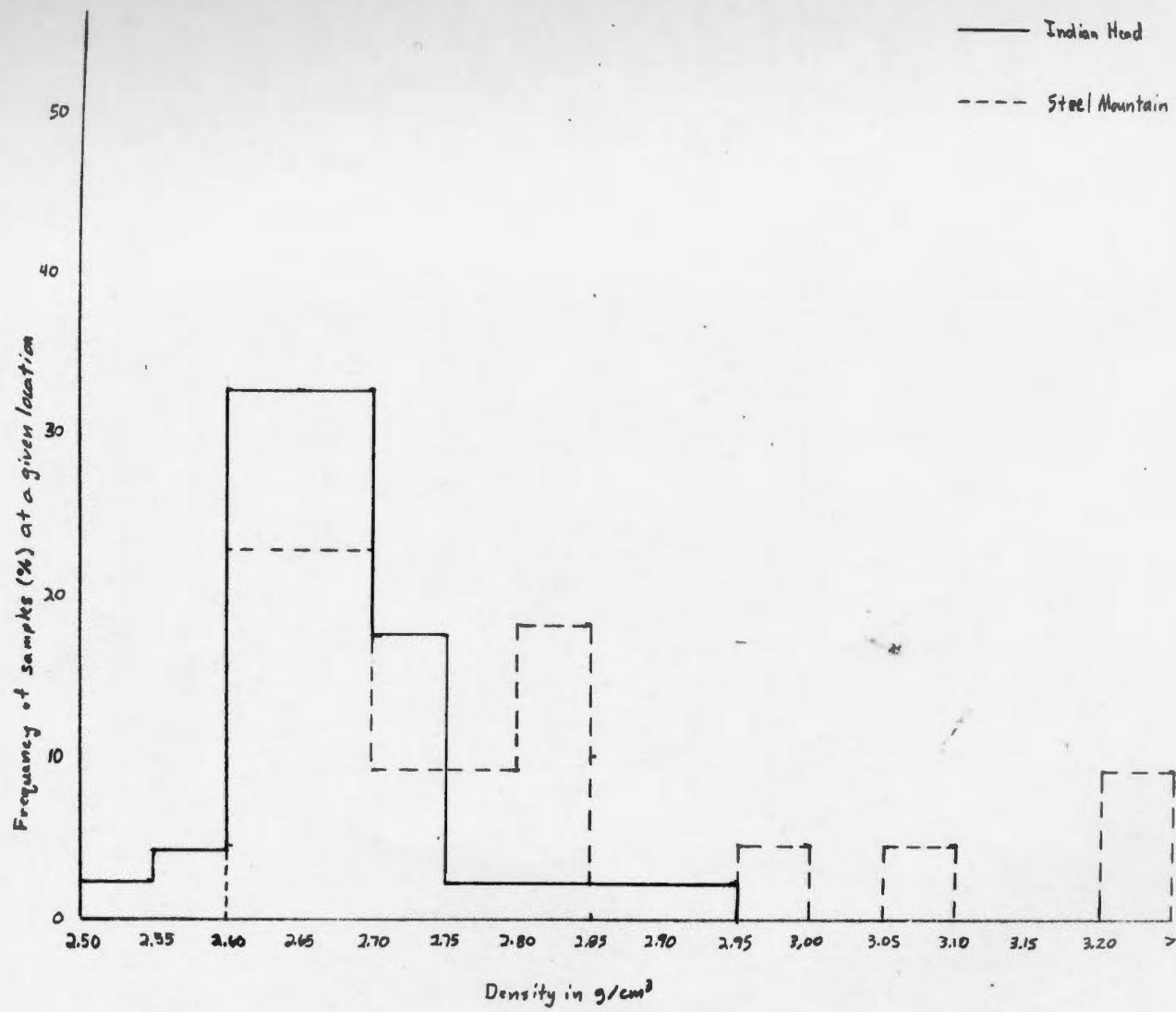


Figure 4.1 Histogram of frequency of densities for Indian Head and Steel Mountain samples.

The average density of the 43 Steel Mountain samples was 2.83 ± 0.34 g/cm³. The high standard deviation of the Steel Mountain samples results from some unusually high-density samples, with values up to 4.27 g/cm³ recorded. These samples have an unusually high magnetite content, and could be related to lenses of magnetite that occur in the area (Baird, 1954). The range of Steel Mountain density values is from 2.60 to 4.27 g/cm³, with only 55 % lying within the range of 2.60 to 2.75 g/cm³. The rest of the samples have densities greater than 2.75 g/cm³. The average density of the inferred basement is 2.72 ± 0.36 g/cm³, giving a density contrast of -0.18 g/cm³ with the sedimentary section.

Susceptibility measurements of the Indian Head samples show that 80 % lie in the range of $0-100 \times 10^{-6}$ cgs units (Figure 4.2) -- i.e. 80 % of the Indian Head samples lie in the range of the sedimentary section and are therefore of negligible susceptibility. The maximum observed magnetic susceptibility for these samples was 1836×10^{-6} cgs units.

Steel Mountain magnetic susceptibility measurements showed much more scatter (Figure 4.2), with a range of $5-6000 \times 10^{-6}$ cgs units. For three of the samples, the susceptibility values were too high to be measured by the bridge, and one sample had to be cut into a disk only 0.56 cm thick before a value of 7668×10^{-6} cgs units could be obtained. Only 36 % of the Steel Mountain samples have susceptibilities less than 100×10^{-6} cgs units, while 23 % of the samples are greater than 5000×10^{-6} cgs units (Figure 4.2).

The density and magnetic susceptibility histograms show the distinct difference between the Indian Head and Steel Mountain samples, even though the lithologies of the samples are similar. Figure 4.3 is a plot of density versus susceptibility for all the

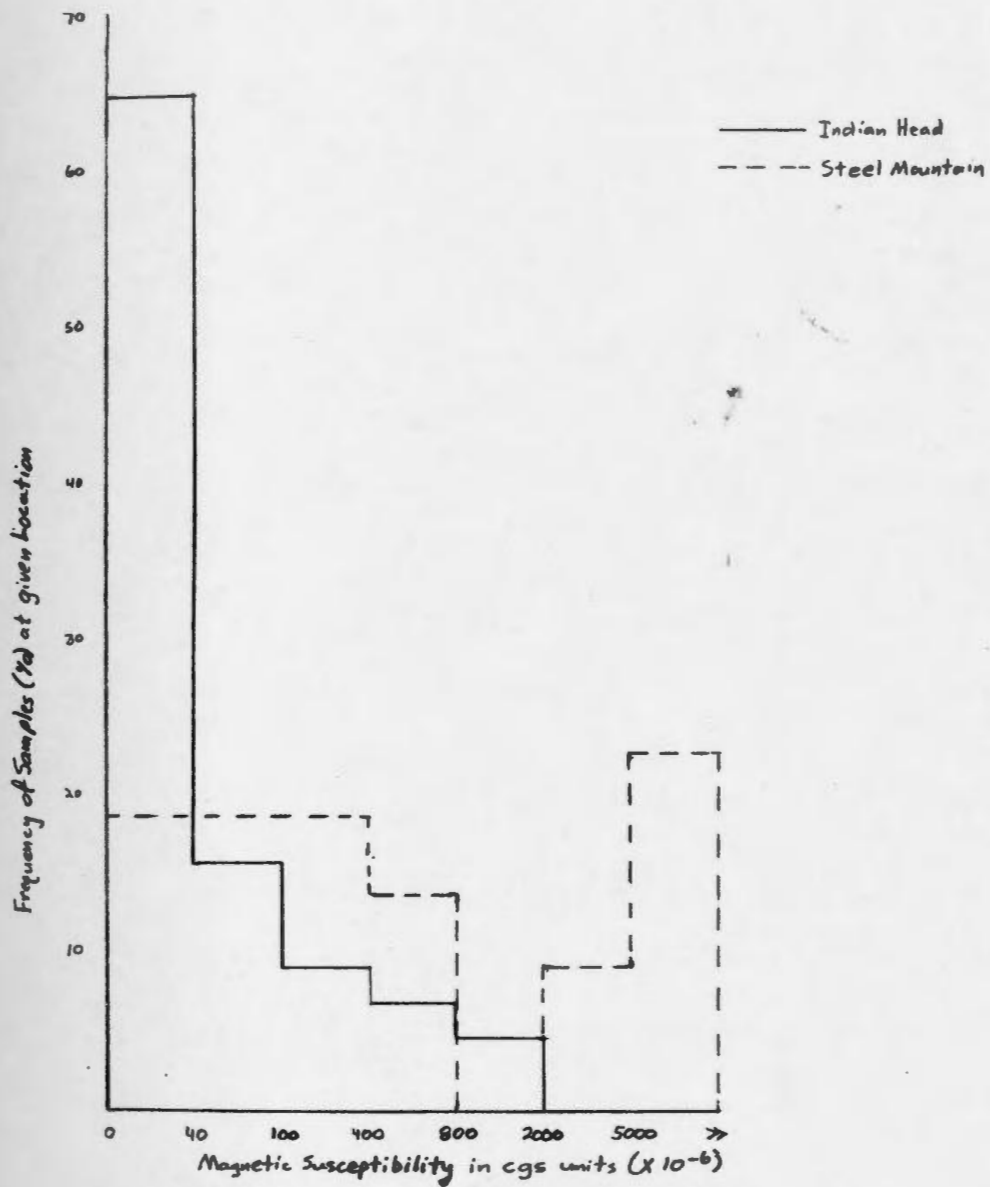


Figure 4.2 Histogram of frequency of magnetic susceptibilities for Indian Head and Steel Mountain samples.

samples. The Indian Head samples are generally grouped toward the left-half (low susceptibility end) of the graph and are all below the 3.00 g/cm^3 line. The Steel Mountain samples, however, are spread out over the entire graph.

If the graph is divided into zones ranging from 'low' to 'high' density and susceptibility (see Table 4.6), a histogram of the percent total number of samples versus zone can be drawn (Figure 4.4), showing that the Indian Head samples are skewed towards the low susceptibility end (zones A-C) and that the Steel Mountain samples are shifted towards the higher susceptibility end (zones G-I). From this, it can be concluded that the Steel Mountain samples are of a higher susceptibility than samples of similar lithology from Indian Head. Assuming that the Bay St. George Subbasin is underlain by basement of both the Indian Head and Steel Mountain types, areas of higher magnetic anomaly are very likely to be underlain by Steel Mountain basement type. Hence, these basement types can be separated and delineated in a magnetic modelling process. Density values could not be used to separate the two basement types because the standard deviation of the Steel Mountain samples is so high that the two density values - those of Steel Mountain and Indian Head - are statistically equal.

Table 4.2: Zones of ρ vs. k for Figure 4.4
 All densities in g/cm. All magnetic susceptibilities in cgs units $\times 10$
 (IH = Indian Head, SM = Steel Mountain)

Zone	Range in Density		Range in Magnetic Susceptibility	Number of Samples		
				IH	SM	Total
A		2.66	k 100	20	4	24
B	2.56	2.74	k 100	14	3	17
C		2.74	k 100	2	1	3
D		2.66	100 k 700	1	0	1
E	2.66	2.74	100 k 700	5	3	8
F		2.74	100 k 700	0	2	2
G		2.66	k 700	0	1	1
H	2.66	2.74	k 700	1	1	2
I		2.74	k 700	2	7	9

○ - Indian Head
 ▲ - Steel Mountain

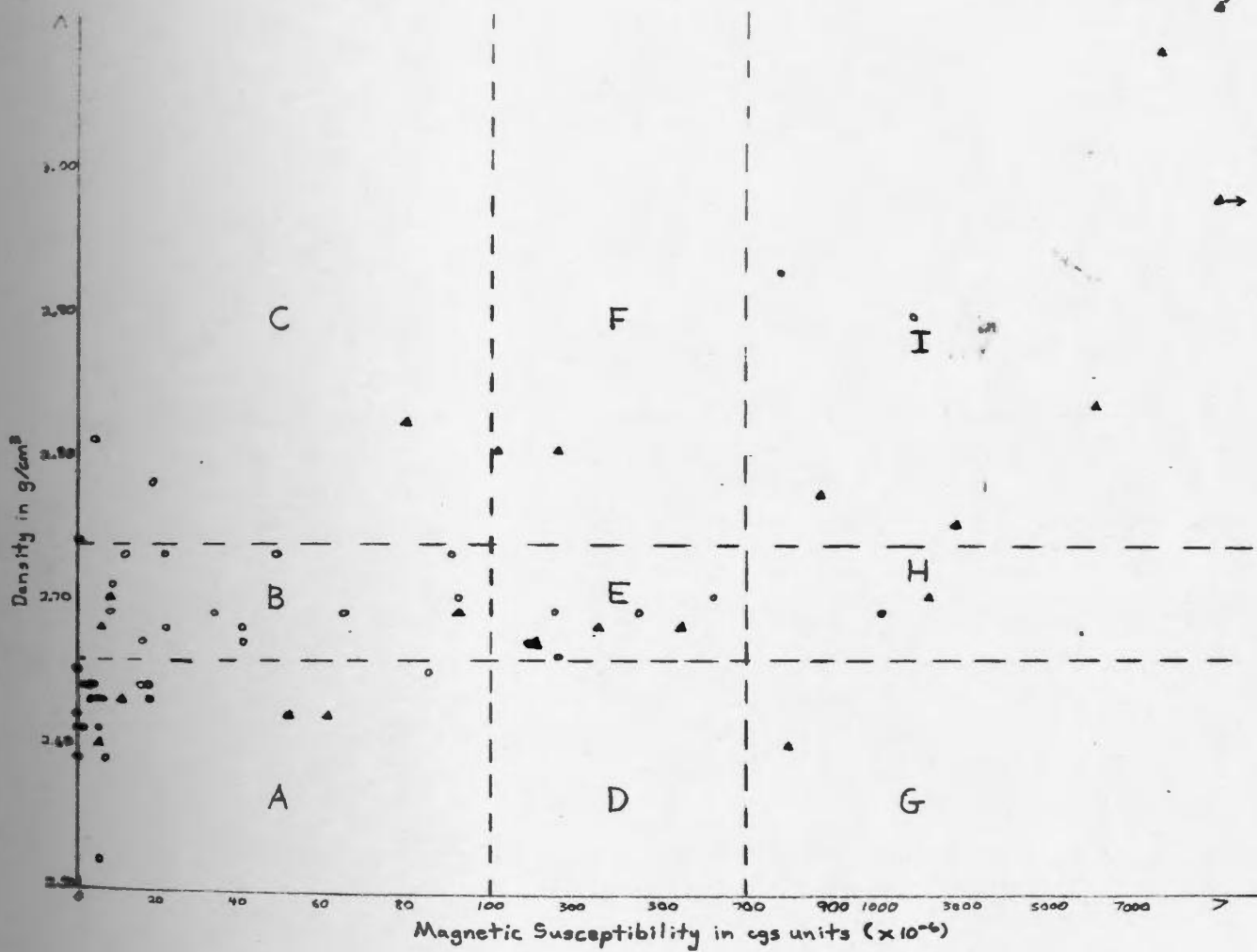


Figure 4.3 Plot of ρ vs. k for the Indian Head and Steel Mountain samples.

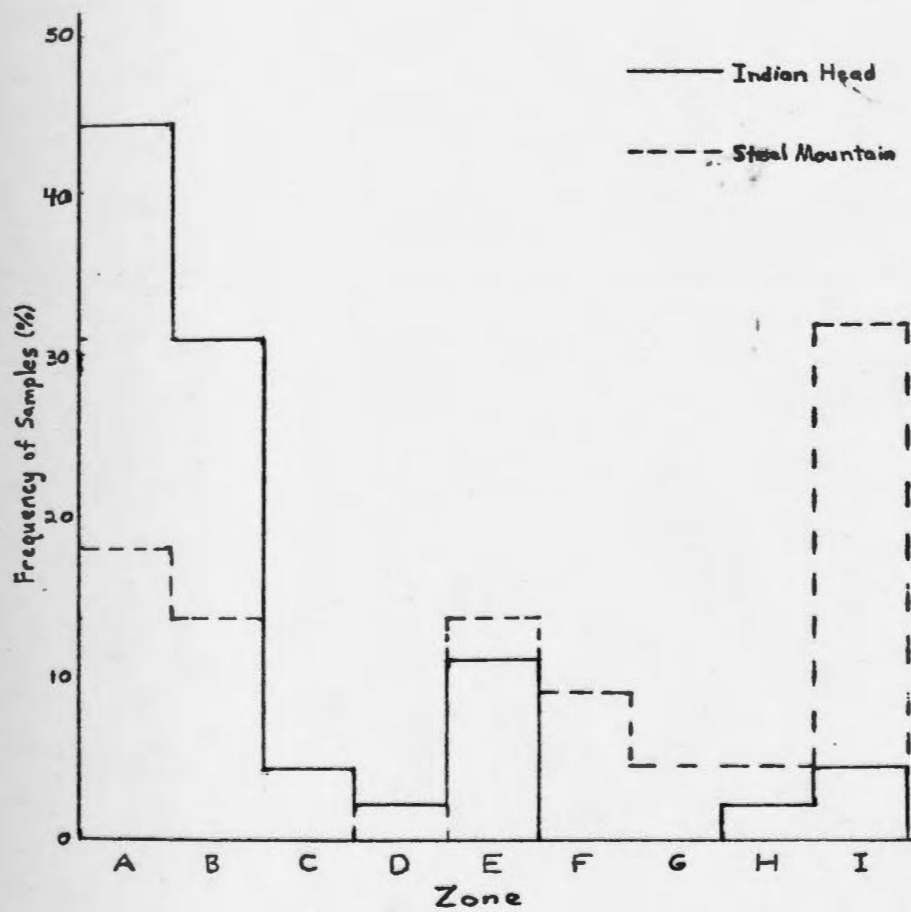


Figure 4.4 Histogram of frequency of samples in Zones A-I (Table 4.2) for the basement samples. Percentages based on number of samples in each zone per each of Indian Head and Steel Mountain rocks.

Chapter 5: Computer Programming for Gravity and Magnetic Modelling

5.1 Introduction

This chapter discusses the programming used to perform the gravity and magnetic modelling of the Bay St. George Carboniferous Subbasin. The gravity modelling consists of a 2.5-D inversion procedure and 3-D forward modelling method. The 2.5-D inversion is a new least-squares procedure based on the ideas of Bott (1960) and the formulation of Rasmussen and Pedersen (1979). This procedure was tested extensively and it was found to give good results for several simple and complex models. However, it was discovered that dissimilar situations could give nearly identical inverse models because the gravity anomalies were nearly identical in shape and amplitude. A three-dimensional modelling program based on Talwani and Ewing (1961) was written and tested. A 3-D magnetics modelling program based on Talwani (1965) was also written and tested.

5.2 Two-Dimensional, Least-Squares Gravity Modelling

Geophysical inversion involves the estimation of the parameters of an Earth model from a set of observations. In particular, gravity modelling requires the use of gravity anomalies in order to determine the dimensions and/or density of a model. When compared with forward modelling, gravity inversion has the advantage of being relatively

fast compared with the trial and error process of forward modelling. The main problem with the inverse techniques is a lack of control by the interpreter over the final solution which often leads to models which are not geologically feasible. The use of constraints based on geological or other geophysical evidence is a useful method of controlling the inverse solution. However, even the constraints do not eliminate the problem of nonuniqueness which is inherent in all mathematical solutions to potential field problems.

There are many types of gravity inversion techniques which can be applied to an anomaly to obtain a model. Perhaps the simplest to understand and apply is the least-squares technique. Least-squares techniques search for a minimum of the following equation

(Marquardt, 1963):

$$e = \sum_{i=1}^N (y_{oi} - y_{ci})^2 \quad (5.1)$$

where e is the sum of the squares of the difference between the observed (y_{oi}) and the calculated (y_{ci}) values at all points N . Equation 5.1 is evaluated after each iteration until the minimum is found. For the gravity case, N is the number of stations, y_{oi} is the observed gravity at the i^{th} station, and y_{ci} is the calculated gravity at that same station. y_c is a function of the model parameters and the equations or kernels used to determine the anomaly at a given location. The model parameters, which include coordinates of body

corners and density, are adjusted at each iteration until a global minimum to Equation 5.1 is found and a "best-fit" model is produced. This procedure has been applied to the direct inversion of gravity anomalies by many authors, the first being M.H.P. Bott in 1960.

Bott used equally-spaced (digitized) gravity anomalies to determine the geometry of a sedimentary basin. The technique calculated the thickness of two-dimensional rectangular blocks of a single density contrast beneath each gravity station along a profile, with the width of each block equal to the station spacing; i.e. the blocks were all the same width and centered below each station, and each block being of the same density contrast. The initial thickness of each block was determined by the relation (Bott, 1960)

$$\Delta t = \frac{g_{\text{obs}}}{41.9 \times \Delta \rho} \quad (5.2a)$$

where t is the calculated thickness in km, g_{obs} is the observed gravity at each station in mGal, $\Delta \rho$ is the density contrast in g/cm^3 , and the number 41.9 represents the product $2\pi GS$, where G is the universal gravitational constant, and S is scaling factor which takes care of discrepancies in units. The change in thickness of the each block was calculated using the infinite slab formula (Bott, 1960)

$$\Delta t = \frac{\Delta g}{41.9 \times \Delta \rho} \quad (5.2b)$$

where Δg is the residual gravity (calculated - observed), and the other factors are identical to those in Equation 5.2a. Each block

was adjusted by its respective change in thickness, then the contribution of all the blocks was calculated at each station. A residual was then determined, and the process continued until a minimum sum of squared residuals was found.

Bott's technique, although simplistic, proved to be effective in estimating the depth and shape of sedimentary basins. Other authors (Corbato, 1965, Qureshi and Mula, 1971, and Al-Chalabi, 1971b) have improved Bott's basic technique by using: (a) undigitized data, and (b) 2-D bodies of polygonal cross-section that more closely approximate geologic bodies. However, there are problems with Bott's technique. Aside from the usual problems of gravity inversion, the use of the 2-D approximation could add appreciable error. Since the 2-D methods assume an infinite strike-length perpendicular to the anomaly profile, bodies calculated for areas with relatively short strike-lengths could be too shallow. If finite strike-length were taken into account through the use of end-corrections to the 2-D approximation, much better estimates of thickness and morphology could be made from the gravity anomalies.

5.3 2.5-D Gravity Modelling and a Comparison to 2-D Modelling

In 1979, Rasmussen and Pedersen developed an equation by which end-corrections could be calculated for 2-D gravity models, thus creating the 2.5-D gravity method. The method is called "2.5-D" because the strike-length of the body is finite while the basic 2-D,

polygonal shape is maintained along strike. The end corrections 'subtract' the effects of the mass contained within the 2-D polygon outside the given strike-length, thereby correcting the calculated gravity along the profile.

In order to illustrate the effect of finite strike-length on the calculated gravity at a point along a profile, a computer program based on the Rasmussen and Pedersen (1979) formulation was written in the FORTRAN language (see Appendix 2.1 for a program listing). The gravity anomaly along a profile for various strike-lengths was calculated. Figure 5.1 is a plot of the results for a rectangular block 3 km wide, 1.5 km thick, with the top buried at a 2 km depth and having a density contrast of $+0.10 \text{ g/cm}^3$. For each different strike-length, the body was symmetric, i.e. the total strike-length of the body was evenly divided on each side perpendicular to the profile. For comparison, a 2-D profile calculated by equations from Grant and West (1965) for a block with the same dimensions but having infinite strike length is also shown. Only for strike-lengths >7.5 times the width of the body is the maximum 2-D anomaly within 5 % of the 2.5-D anomaly, showing that the 2-D approximation would not have been valid for shorter strike-lengths. However, is width the most important factor to consider when deciding between 2-D and 2.5-D modelling techniques?

A comparison of the effect on the 2.5-D gravity calculation of variable thickness, width, and depth of burial of bodies was conducted. Figure 5.2 is a plot of percent of the maximum, 2-D anomaly calculated for that block versus the changing lengths of the variables. Two conclusions can be drawn from these results: (1) that

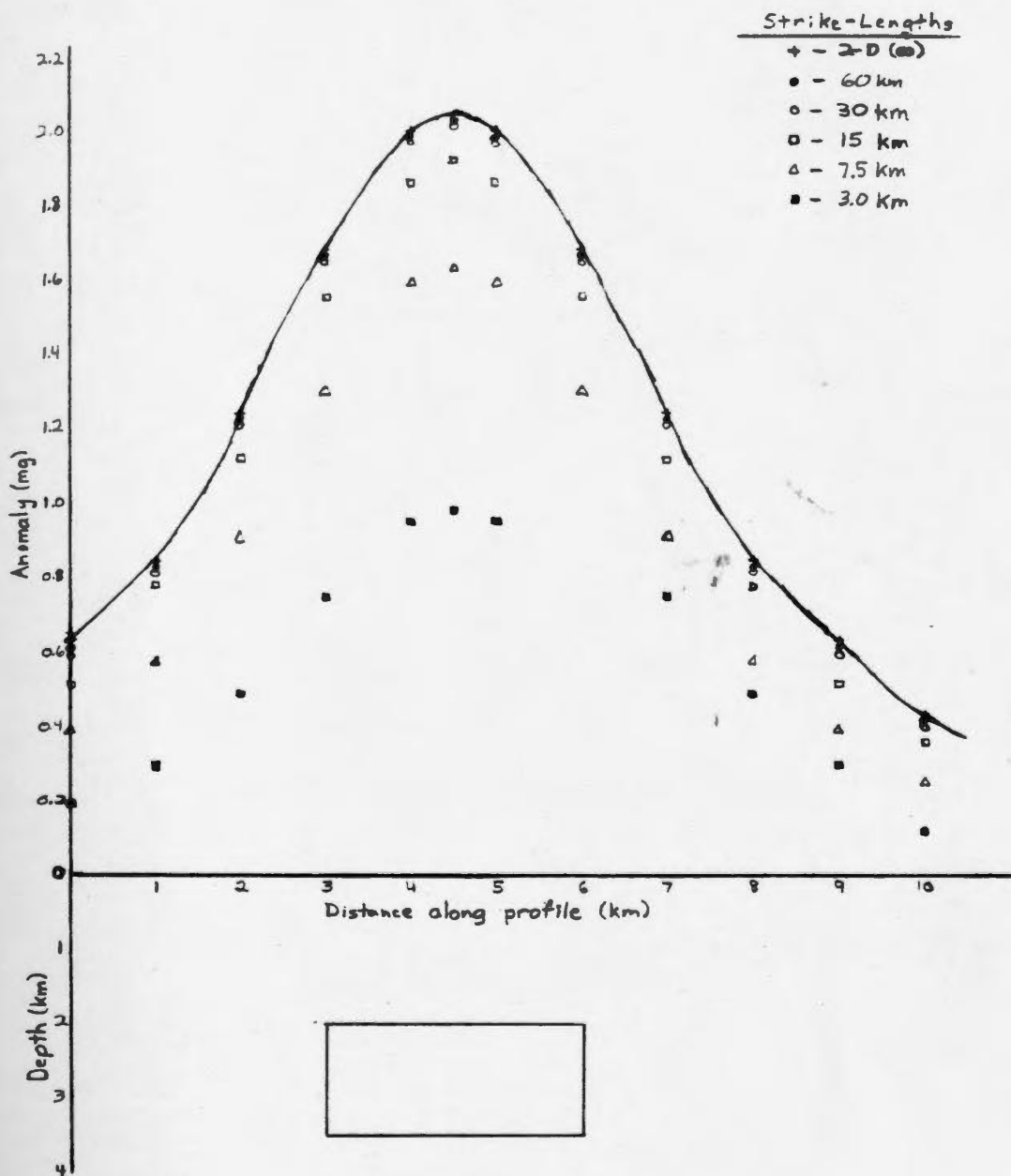


Figure 5.1 Effects of finite strike-length on gravity profiles.

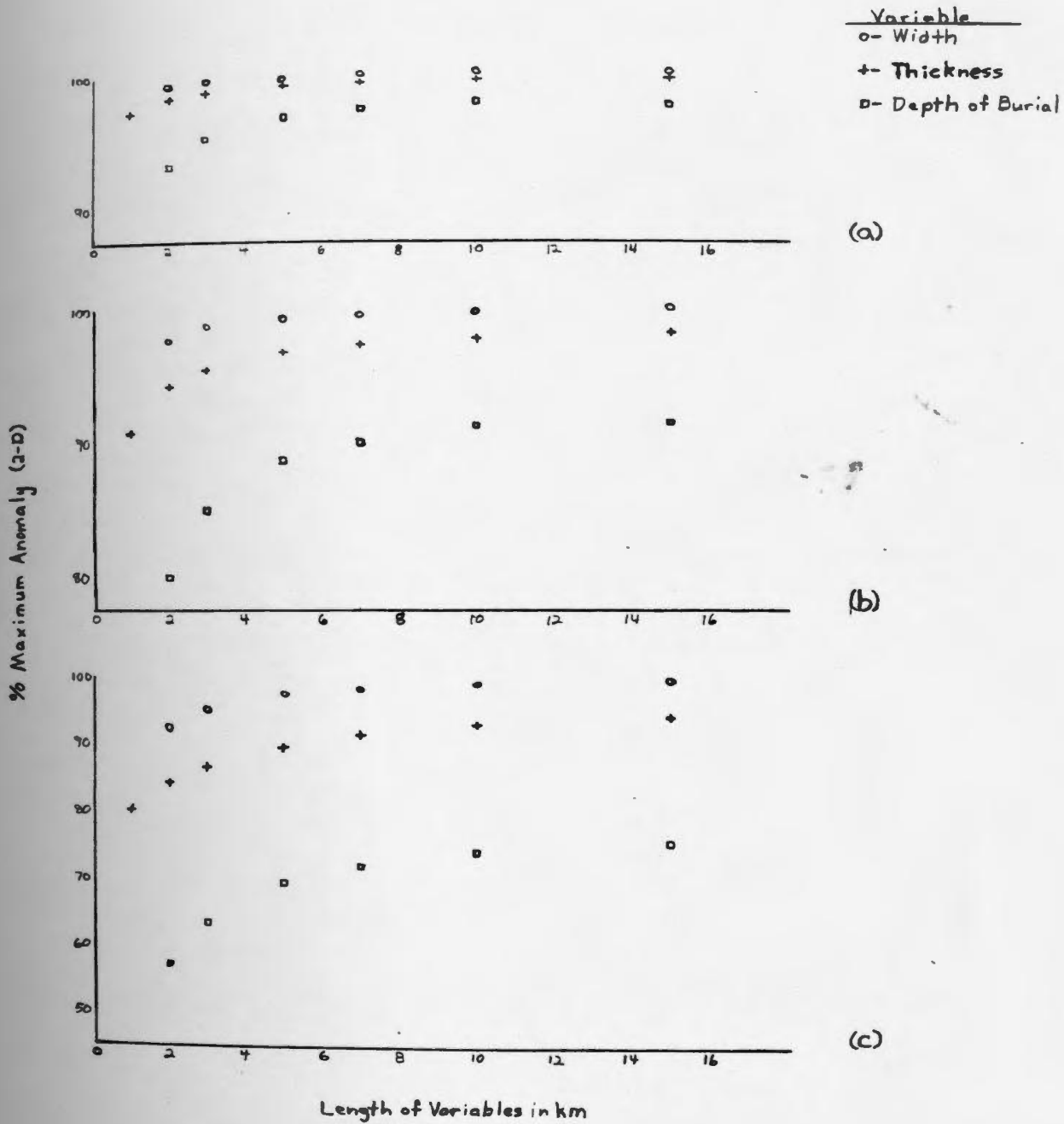


Figure 5.2 Effects of variable width, thickness, and depth of burial on 2.5-D gravity calculations for the strike-lengths that are (a) 10 times, (b) 5 times, and (c) 2.5 times the length of the variable (width, thickness, or depth of burial).

all three variables are less important when their lengths are greater; and (2) while all three variables are affected by finite strike-length, the depth of burial appears to be the most sensitive. Telford, et.al. (1976, p.66) suggest that a body is two-dimensional when the strike-length is twenty (20) times all other dimensions. Based on Figure 5.2, if the strike-length is ten (10) times the largest dimension, the 2-D approximation is within 10 % of the actual gravity value. Therefore, any depth estimates using a 2-D gravity inversion process on data meeting the '10 X' criteria will have a 10 % or less error associated with them. For data where the strike-length is less than 10 times the largest body dimension, the errors will be larger.

5.4 2.5-D Inverse Gravity Program

A 2.5-D gravity inversion program was written based on the equations of Rasmussen and Pedersen (1979) (see Appendix 2.2 for a program listing). A flowchart for the program is shown in Figure 5.3. The program reads in gravity data along a profile and parameters for an inversion, and calculates the single density contrast model that fits the observed data within an error σ_{res} (variable SIGMA in the program) is a number chosen such that the mean of the residuals is close to zero and the standard deviation of the residuals is ≤ 0.5 mgal - the error in the gravity observations. Iterations of the program continue until the value of the sum of the squared residuals (of Equation 5.1)

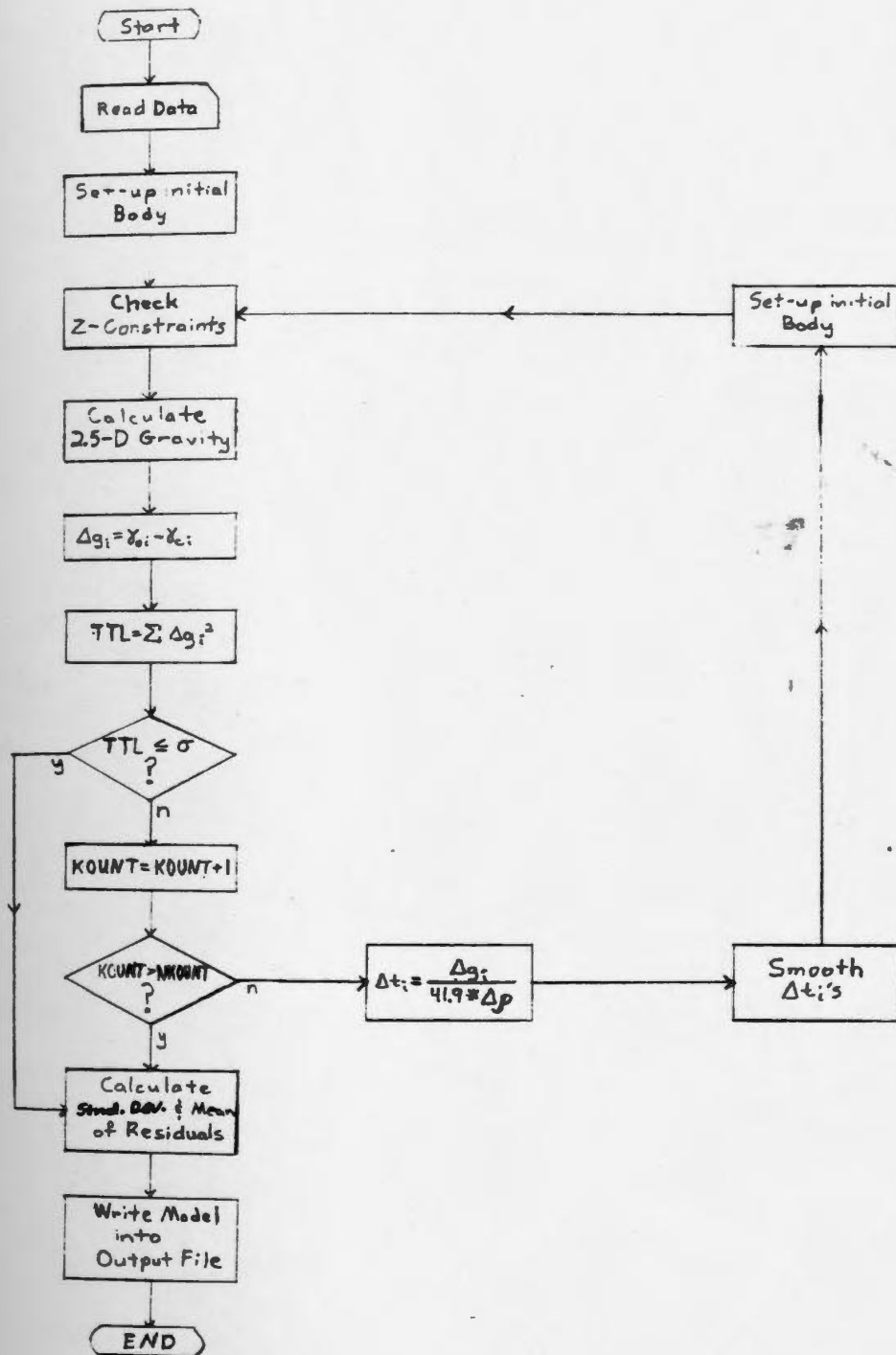


Figure 5.3 Flowchart for 2.5-D gravity inversion program.

is less than σ , or when the number of iterations is greater than a specified maximum number of iterations (NKOUNT in the program). These conditions can be expressed mathematically as

$$\sigma \geq \epsilon, \text{ and} \quad (5.3a)$$

$$k_i > k_{\max} \quad (5.3b)$$

If condition 5.3b is reached before 5.3a, the values of ϵ (which were stored in a data file) are analyzed to see if a minimum had been reached that was greater than σ , or if no minimum had been reached. If a minimum was reached, the value of σ is set equal to the minimum and the program is run again to produce the best fit model. If no minimum was reached, then the best fit maximum number of iterations is increased to a sufficient number for condition 5.3a to be met. An initial model is obtained by calculating a thickness based on the infinite slab formula (Equation 5.2) for the body at each gravity station, with Δg being equal to the observed gravity for this initial model. The body is then numbered clockwise starting at the top, left-hand corner to give a body with polygonal cross-section (Figure 5.4). The gravity effect of the body is then calculated at each station location using the Rasmussen and Pedersen equations.

The z-coordinates of the model are adjusted after each iteration using the infinite slab formula (Equation 5.2) with the value of the residual, Δg , defined as

$$\Delta g = \gamma_{oi} - \gamma_{ci} \quad (5.4)$$

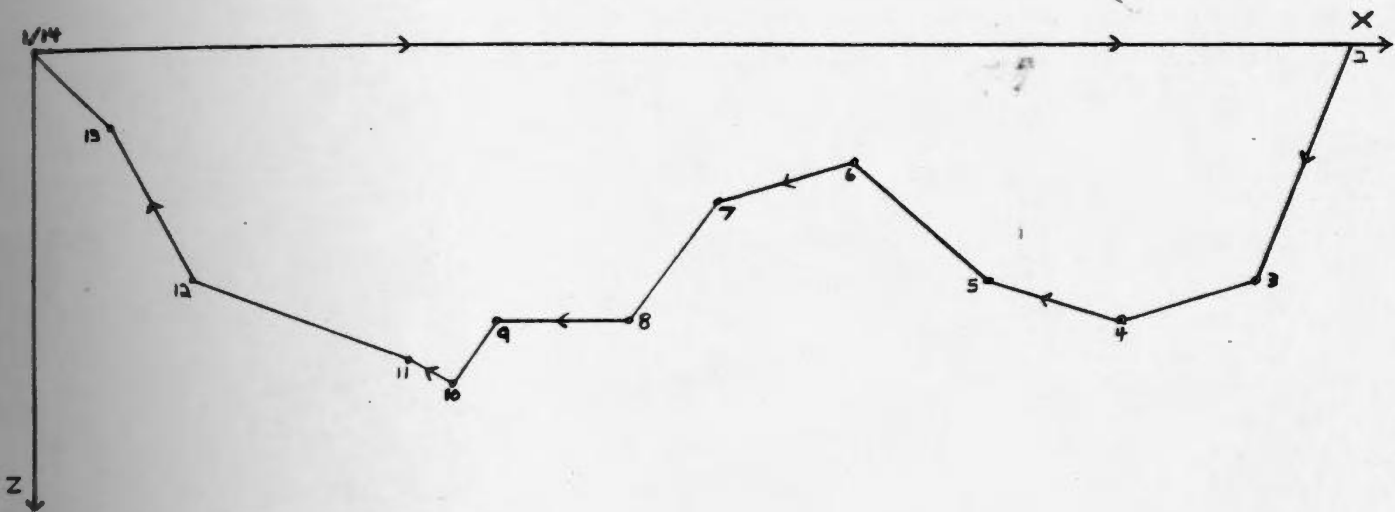


Figure 5.4 Polygon for 2.5-D gravity, showing the clockwise numbering system.

where γ_{oi} is the observed gravity at station i , γ_{ci} is the calculated gravity at station i , and N is the number of stations. The changes in thickness obtained from Equation 5.2 are 'smoothed' by a bell curve of the form

$$\omega = \cos^2 \phi / 2.0 \quad (5.5)$$

centered at each station location, with w being the calculated weight at a location away from the center of the bell curve, and

$$\phi = \pi / 2 \times (\Delta x / \text{WIDTH}) \quad (5.6)$$

where Δx is the distance from the center point to the weighted point and WIDTH is the half-width of the bell curve. The value of WIDTH was set at 5 km after testing showed that this value gave good convergence without deforming the larger features determined by the inversion. The calculated weight, w , is then multiplied by the Δt of the center point to give the contribution of the central Δt at the weighted point (Δt_{21}). The Δt_{21} 's are summed at each point and then the sum is added to the original thickness change at that point. This total is the adjusted thickness change (Δta) at that point. The Δta 's are then added to the previous thickness at each station to give the new thickness for the next iteration.

The purpose of the smoothing is to distribute the contribution of the depth below each gravity station among the neighboring depth points. The calculated gravity at each station is calculated from the entire body, but mass near the observation point has more effect than mass farther away. Since this mass affects the calculated

gravity it also affects the residual gravity (Δg), and therefore, by Equation 5.2, the thickness adjustment. Distributing the calculated change in thickness (Δt) at any one station over the neighboring stations is a way of considering the contribution of neighboring mass to the calculated gravity when evaluating Δt .

The new body attained after smoothing is used for the next iteration and the process is continued until either condition 5.3a or condition 5.3b are met, in which case the data and the calculated model are written into a data file and the standard deviation and the mean of the residuals are calculated. If the standard deviation and mean are unsatisfactory (Miller, 1977), a new σ is chosen and the program is run again.

Another feature of the program not discussed above is the ability to apply constraints to the z-coordinates calculated by the program. At each data point, the z-coordinate may be: (a) allowed to evolve without constraints, (b) constrained to lie within a certain depth range, or (c) constrained to a particular depth. Whole bodies may also be constrained to lie below a certain depth level. The constraints would be applied in the case of geological, drill hole, or other geophysical knowledge about the area of study.

The advantages and disadvantages of this modelling process will be discussed in the next section.

5.5 Testing the 2.5-D Gravity Inversion Program

Tests were conducted to check the accuracy of solutions derived by the 2.5-D gravity inversion program for different shaped bodies. These shapes ranged from simple, rectangular blocks to complex basement topography. Data for the tests were generated using the 2.5-D forward modelling program. This data was then inverted and the resulting model was compared to the original model. In all cases, the bodies were symmetric, i.e. the strike-lengths on either side of the x-axis were equal. Additional tests (not shown here) give similar results for asymmetric bodies. In addition, a comparison of the 2.5-D inversion program to a similar 2-D program was undertaken to show the effect of finite strike-lengths on the inversion process.

Figure 5.5 shows the results for four different simple bodies. The important parameters for each body, including strike-length, density contrast, and depth of burial, plus the results of the 2.5-D inversion are summarized in Table 5.1. In each case, the strike-length and density of each body were assumed known for the inversion.

A comparison of either models 5.5a and 5.5b, or models 5.5c and 5.5d, shows the importance of having as many data points as possible over the body. In both cases, the greater number of data points over the body make models 5.5b and 5.5d fit the original models better than their counterparts (5.5a and 5.5c). Note that 5.5d doesn't fit its original model as well as 5.5b fits its original model. This can be attributed to the relative narrowness of the gravity anomaly of the

Table 5.1: Parameters and results for models shown in Figure 5.5.
 All distances are in kilometers. Density contrast in g/cm^3 .

Body	Density Contrast	Width	Thickness	Depth of Burial	Strike-length		Number of Iterations	Mean	Variance	Calculated Thickness (Center of body)
1	+0.10	10	2	0	100	2.81	2	0.048	0.466	1.92
"	"	"	"	"	"	4.40	2	0.207	0.269	1.93
2	+0.15	2	3	0	30	1.98	32	0.000	0.141	2.62
"	"	"	"	"	"	2.95	23	0.069	0.159	2.99
3	-0.15	20	5	0	30	6.57	46	-0.032	0.468	4.33
"	"	"	"	"	"	6.96	39	-0.040	0.495	4.36
4	-0.15	20	5	0	30	6.89	11	0.015	0.492	4.85
"	"	"	"	"	"	4.83	20	-0.028	0.483	5.00

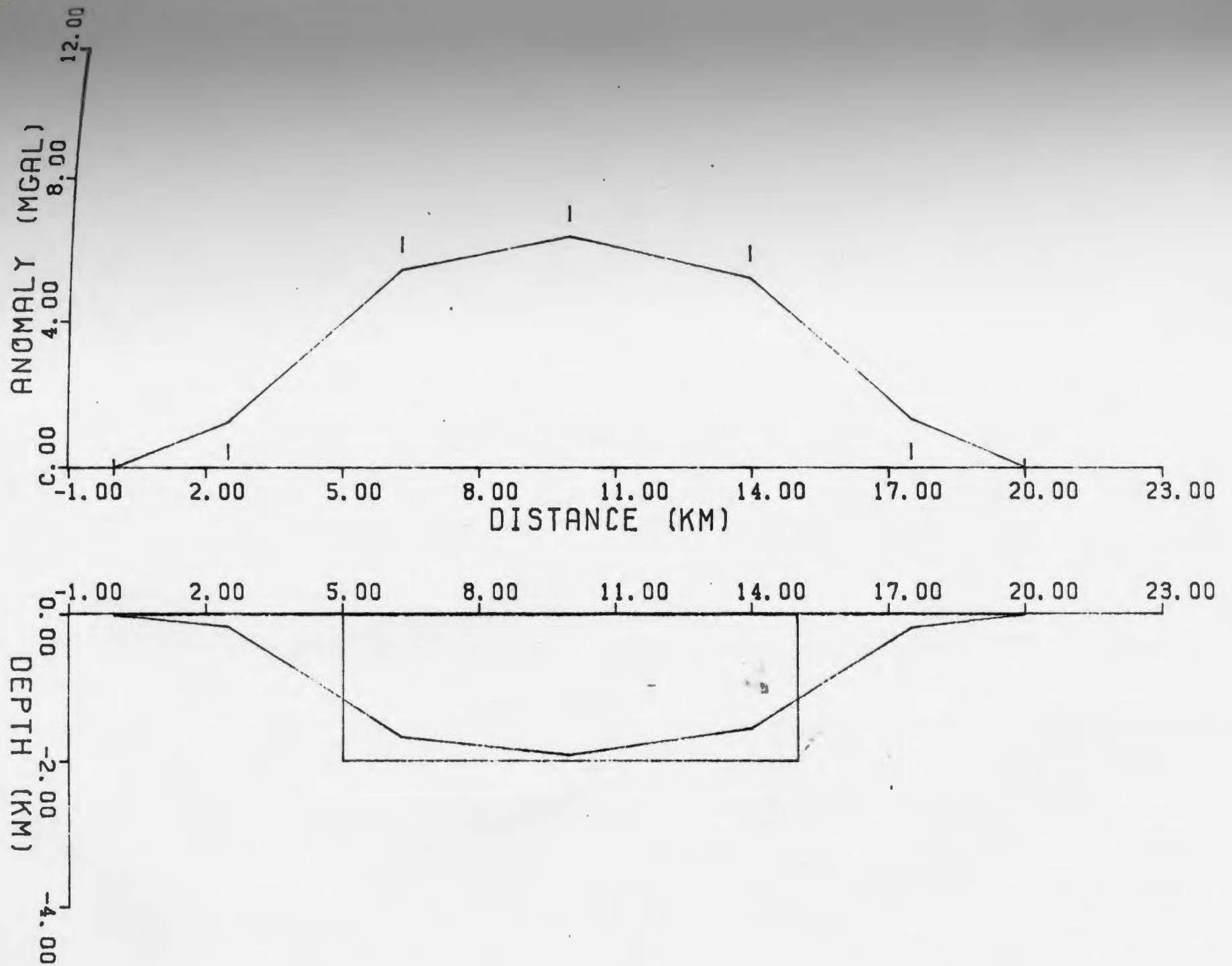


Figure 5.5a True and calculated models and gravity fit for a wide block (Body #1 with 3 stations over body)

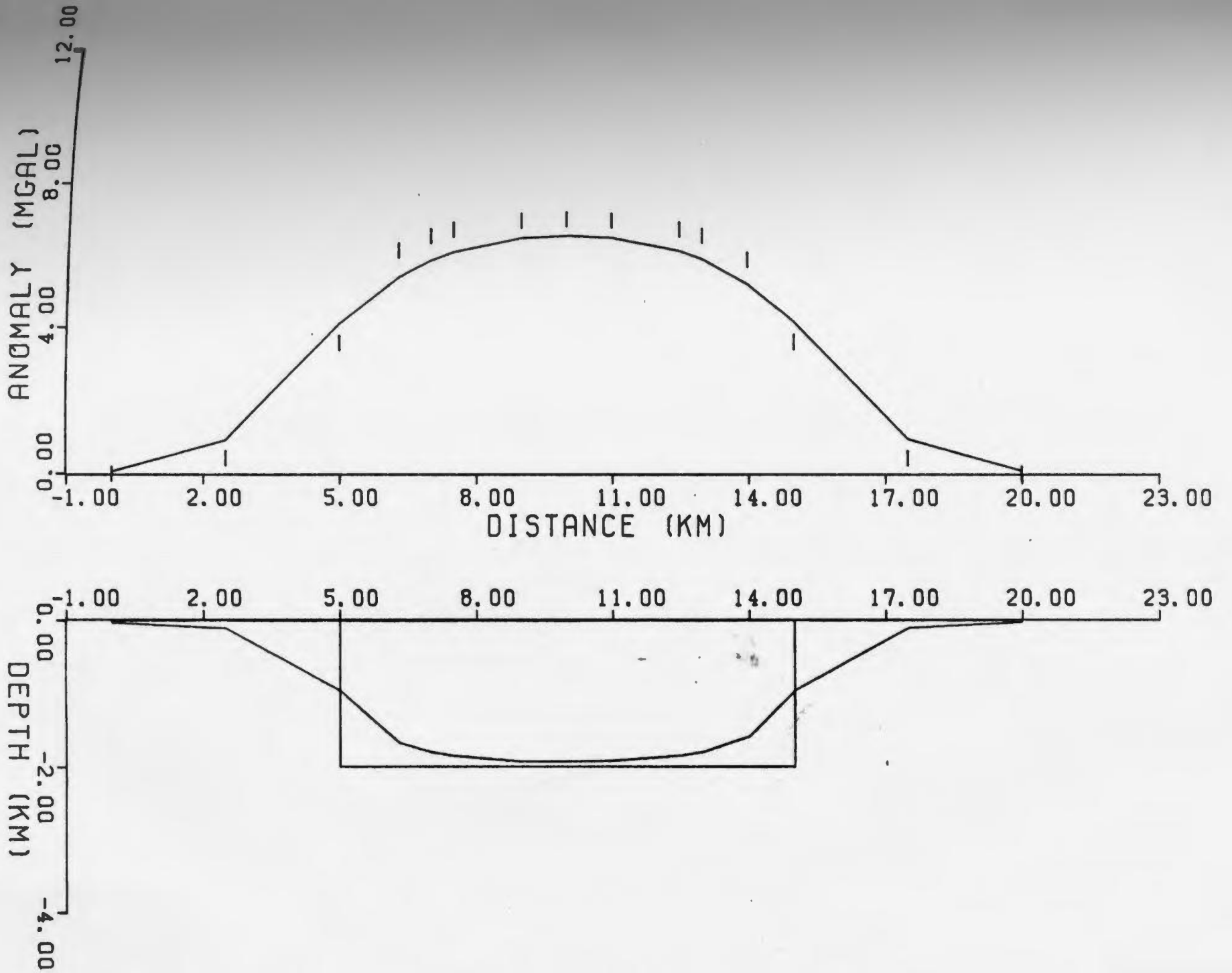


Figure 5.5b True and calculated models and gravity fit for a wide block (Body #1 with 11 stations over body).

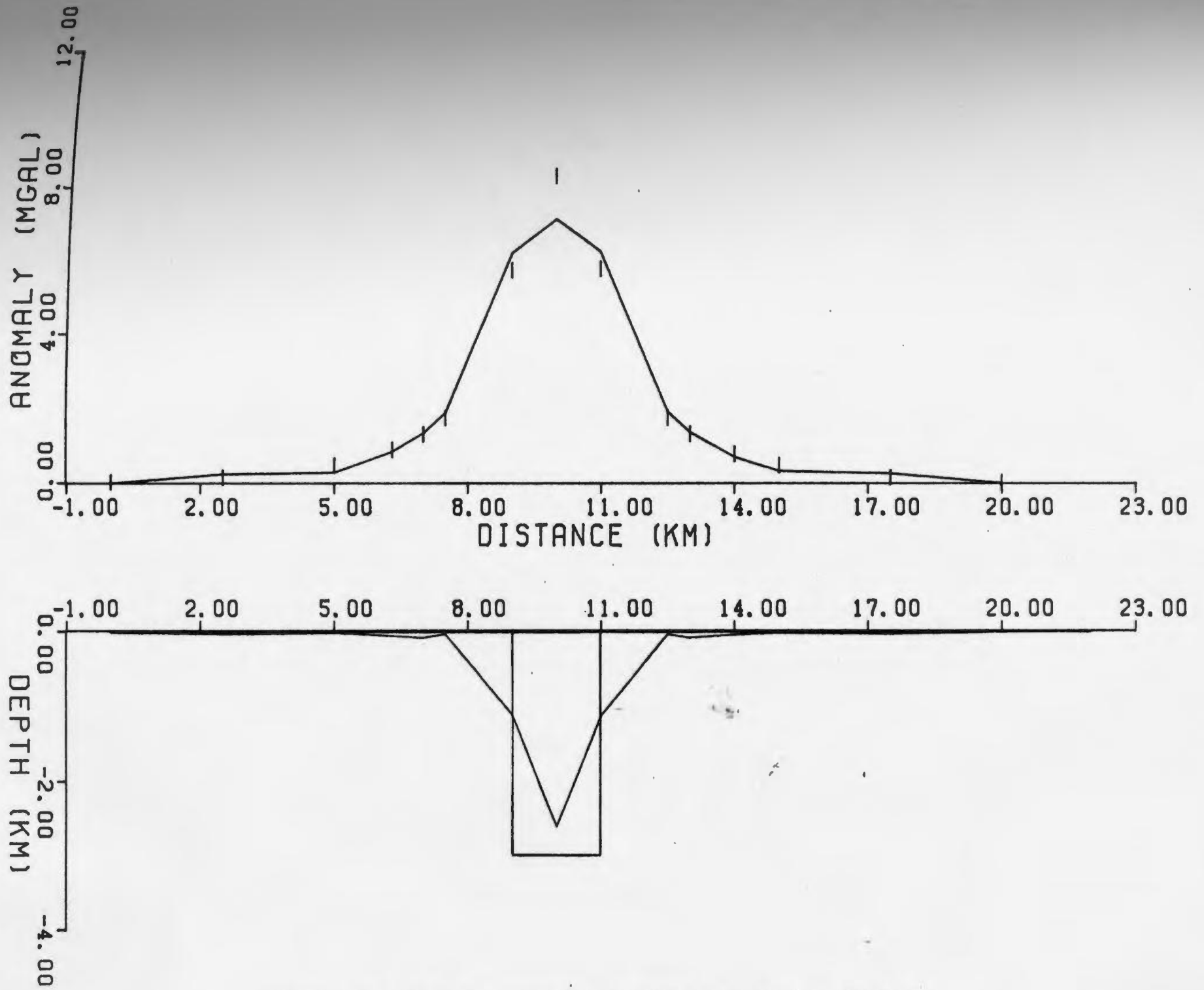


Figure 5.5c True and calculated models and gravity fit for a narrow block (Body #2 with 3 stations over body).

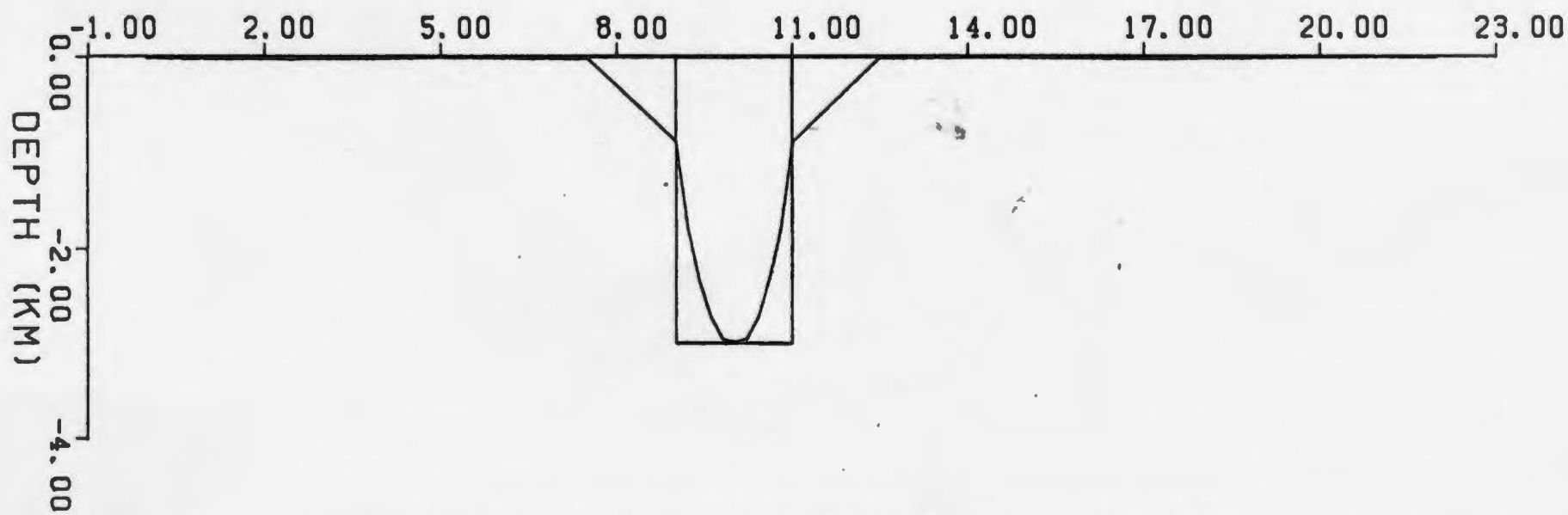
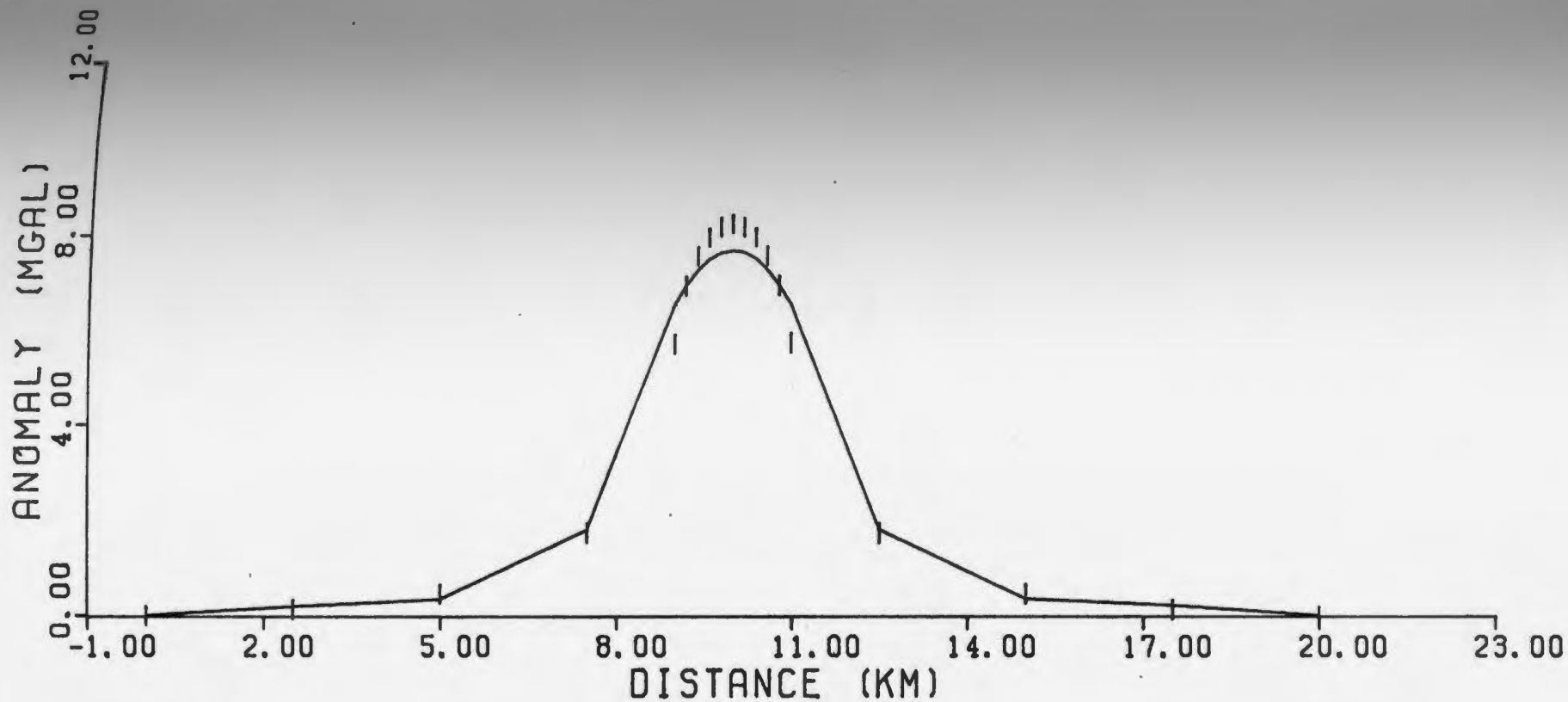


Figure 5.5d True and calculated models and gravity fit for a narrow block (Body #2 with 10 stations over body).

second body, as the inverse procedure has difficulty fitting a model to high amplitude, narrow wavelength anomalies. Much better results are obtained for wider bodies because there is more 'room' to place mass by increasing the depth of the body.

Models 5.5a and 5.5f illustrate the problem of side-lobes. These side-lobes are created at the edge of the gravity model to help compensate for a sudden 'lack of mass' just off the edges of the profile. Since the body is assumed to lie within the confines of the profile, bodies which start and end on the edges of a profile often cause large side-lobes. Note that inverted model 5.5f fits better on the right side than model 5.5e. The reason for the improvement was an extension of the second x-coordinate of the inverted body by 5 km, illustrating how seemingly minor changes can greatly affect the resulting model. An adjustment of this type shouldn't be done unless there is geologic or geophysical evidence to support the adjustment.

Bodies which start and/or end beyond the edges of the gravity profile also cause side-lobes, although these are very small when compared to those mentioned previously. Figures 5.5g and 5.5h show the substantial difference between the side-lobes of a body whose edges are at the edges of the profile (5.5g), and those of a body whose edges are outside the edges of the profile (5.5h).

The only way to eliminate or reduce the magnitude of the side-lobes is to extend the profile off both edges of the body so that the body is contained within the profile limits. This not only reduces or eliminates the side-lobes, it also provides a larger data set over the area and a better model.

The next tests were conducted using dipping prisms for the original bodies. Table 5.2 shows the parameters and results of the

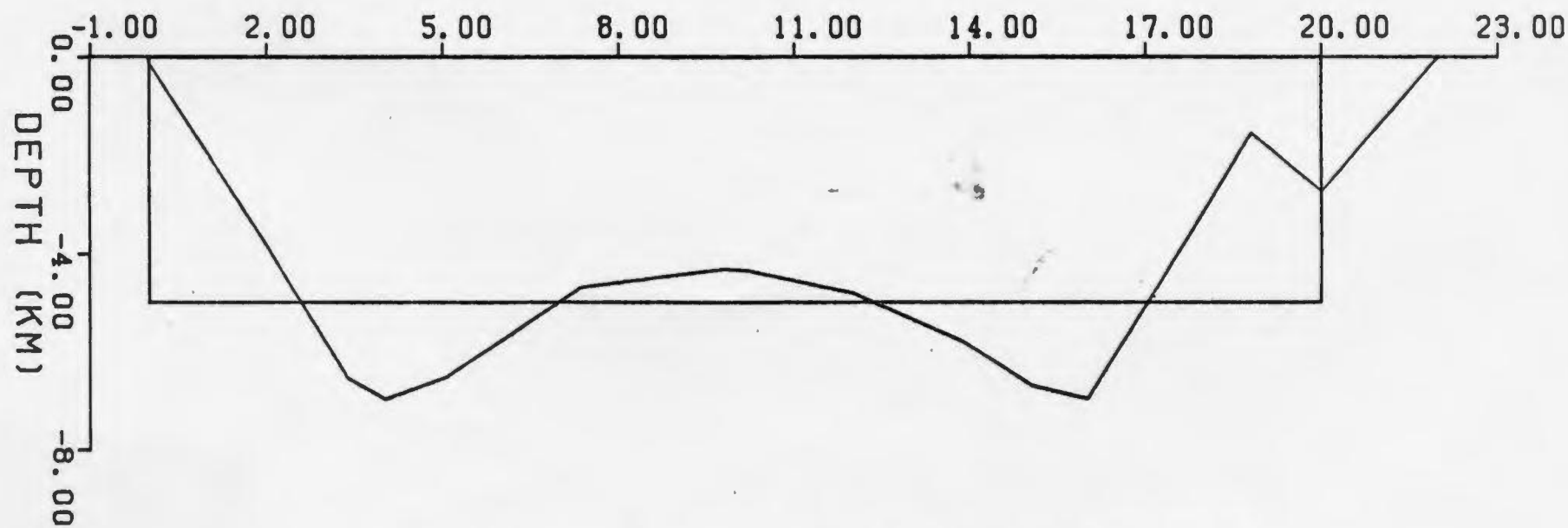
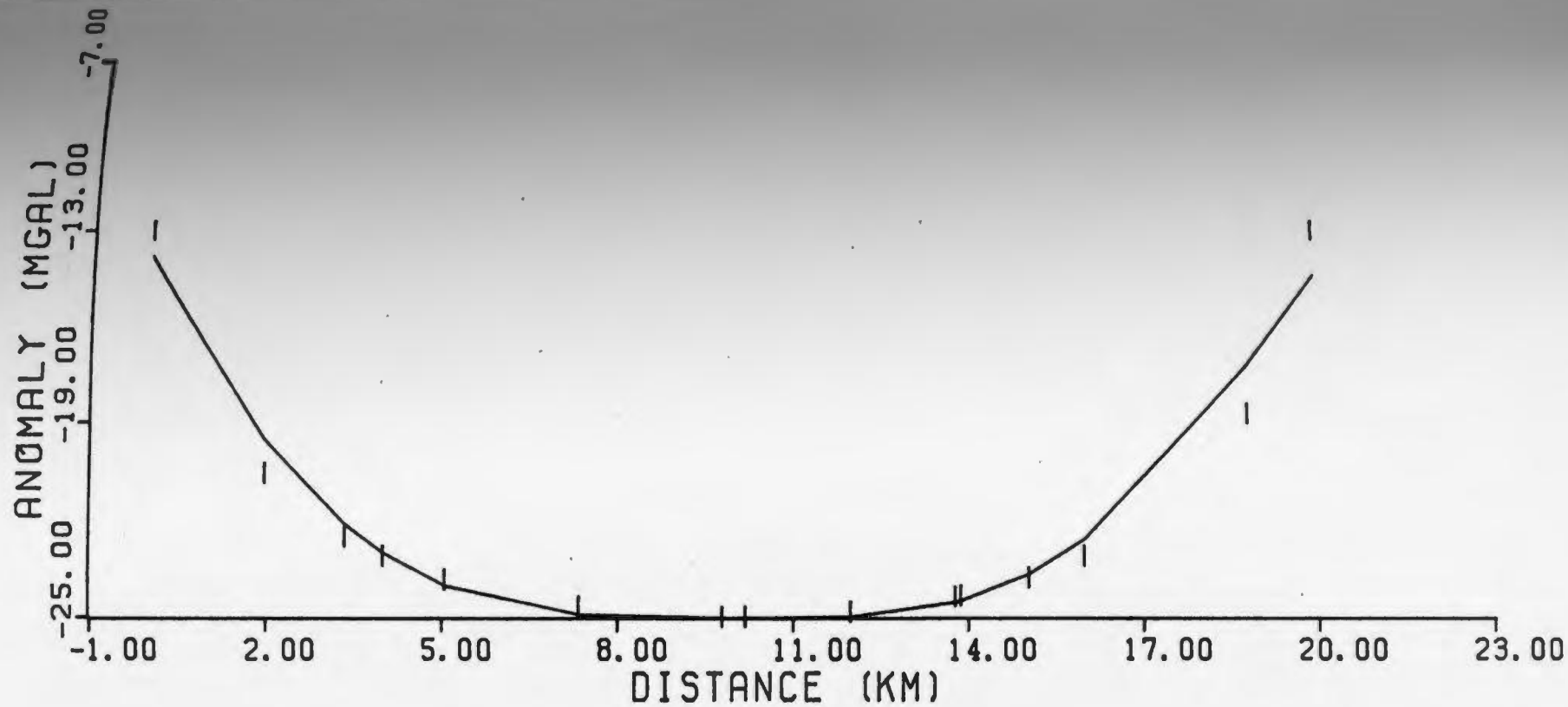


Figure 5.5e True and calculated models and gravity fit for a 20 km wide block (Body # 3).

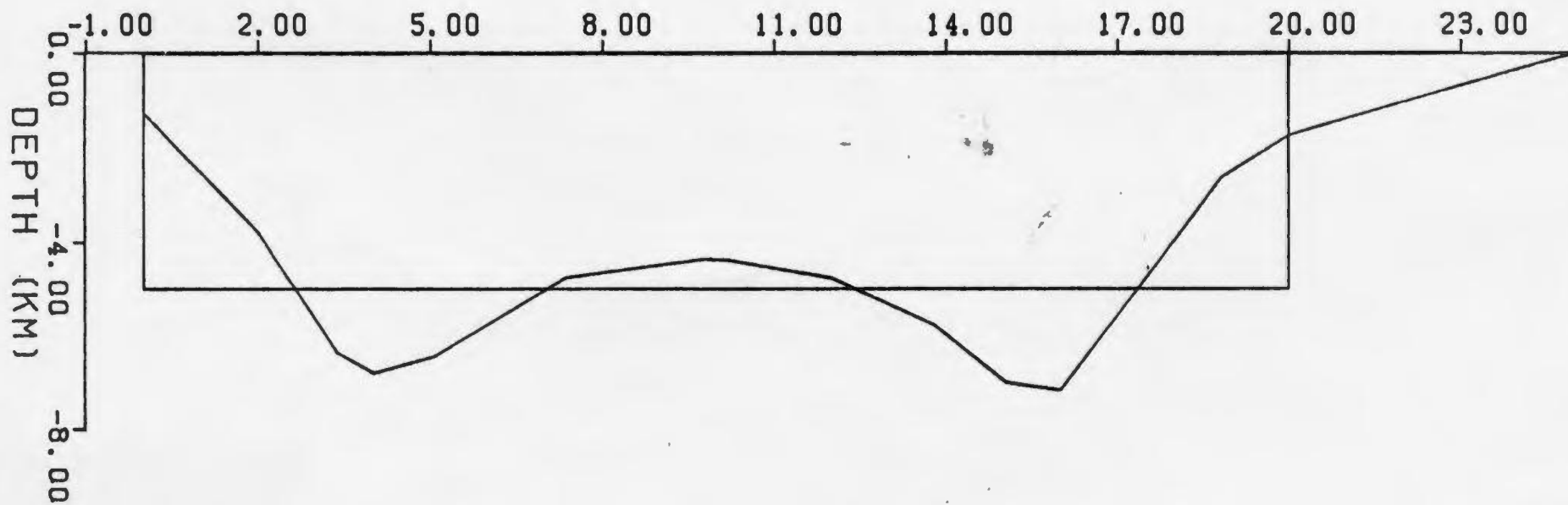
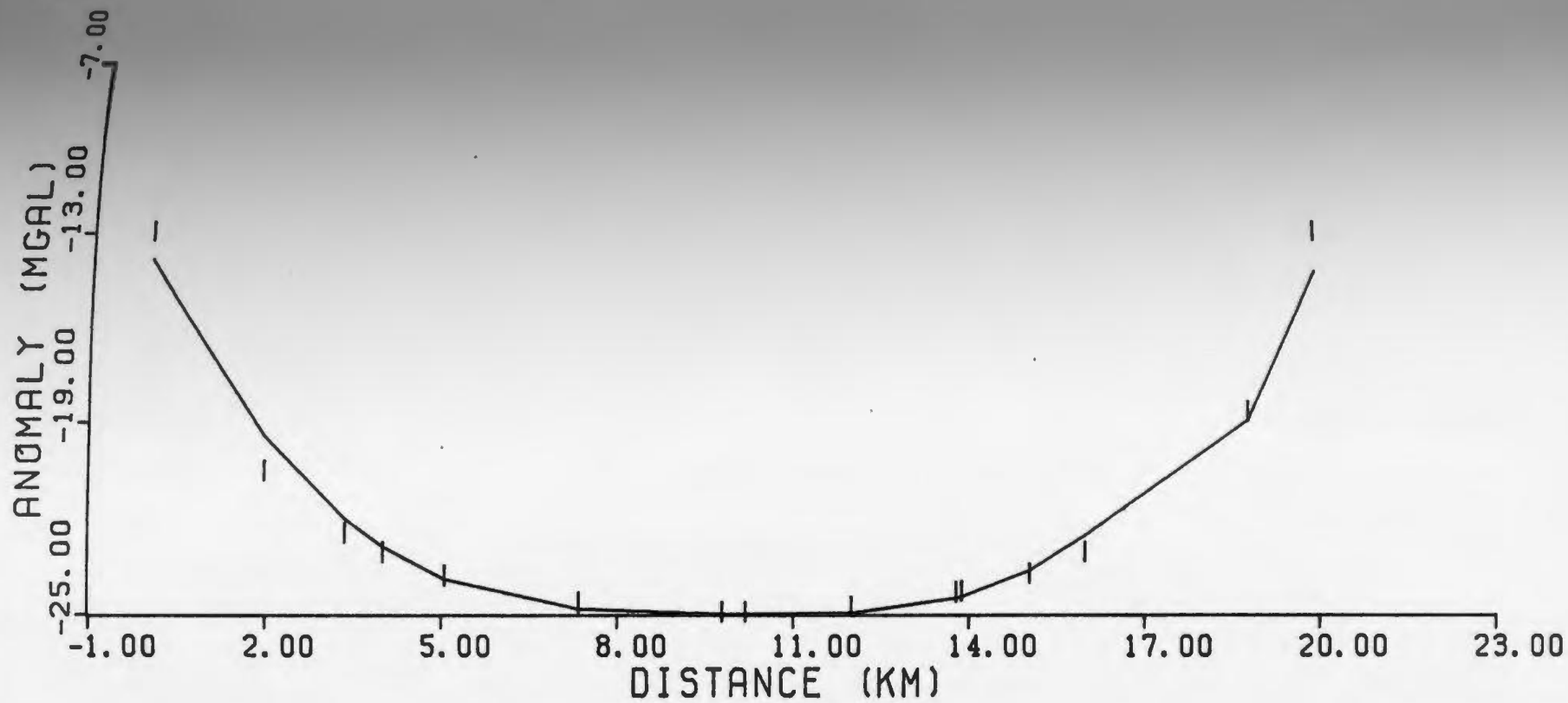


Figure 5.5f True and calculated models and gravity fit for a 20 km wide block (Body # 3):

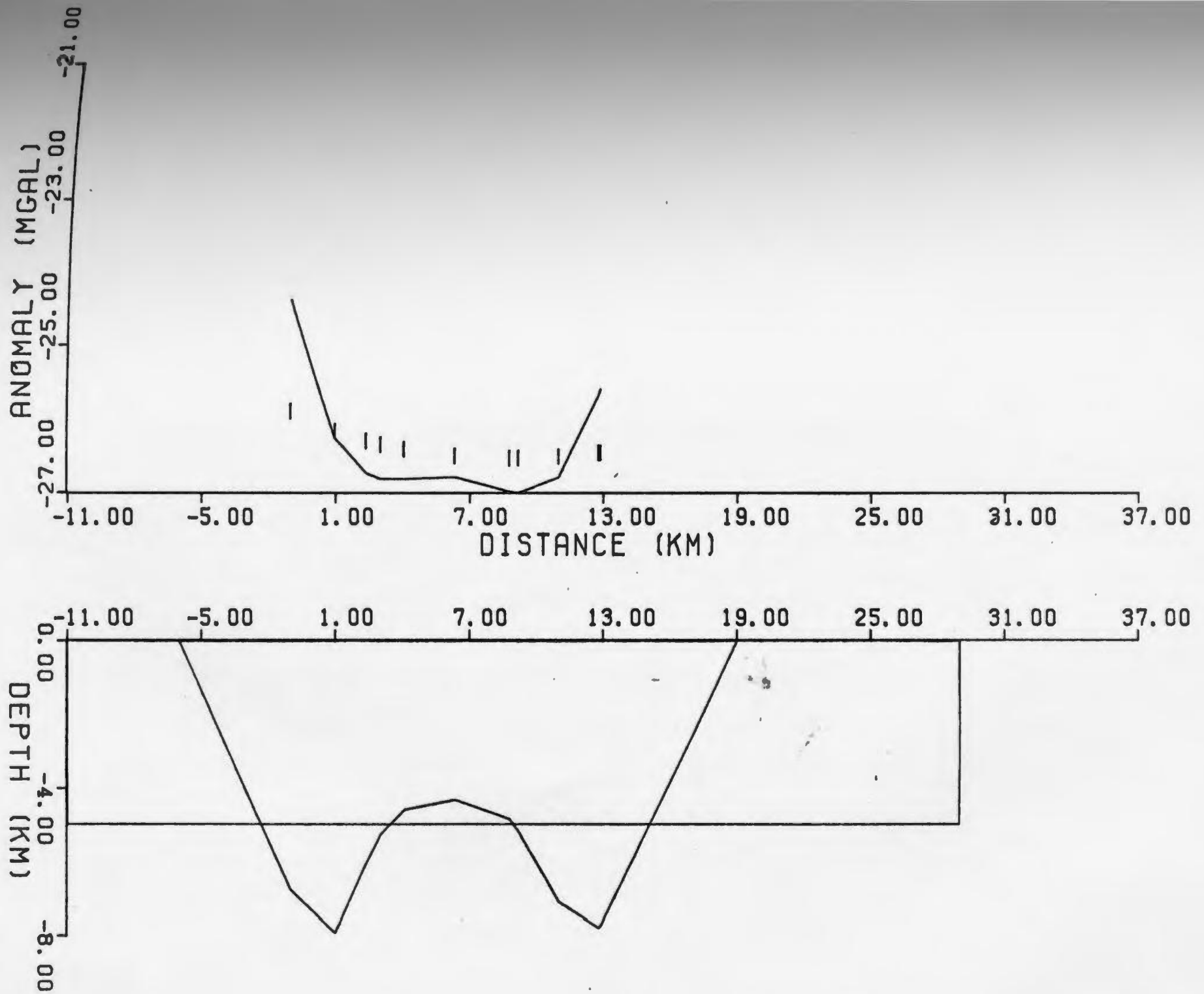


Figure 5.5g True and calculated models and gravity fit for a

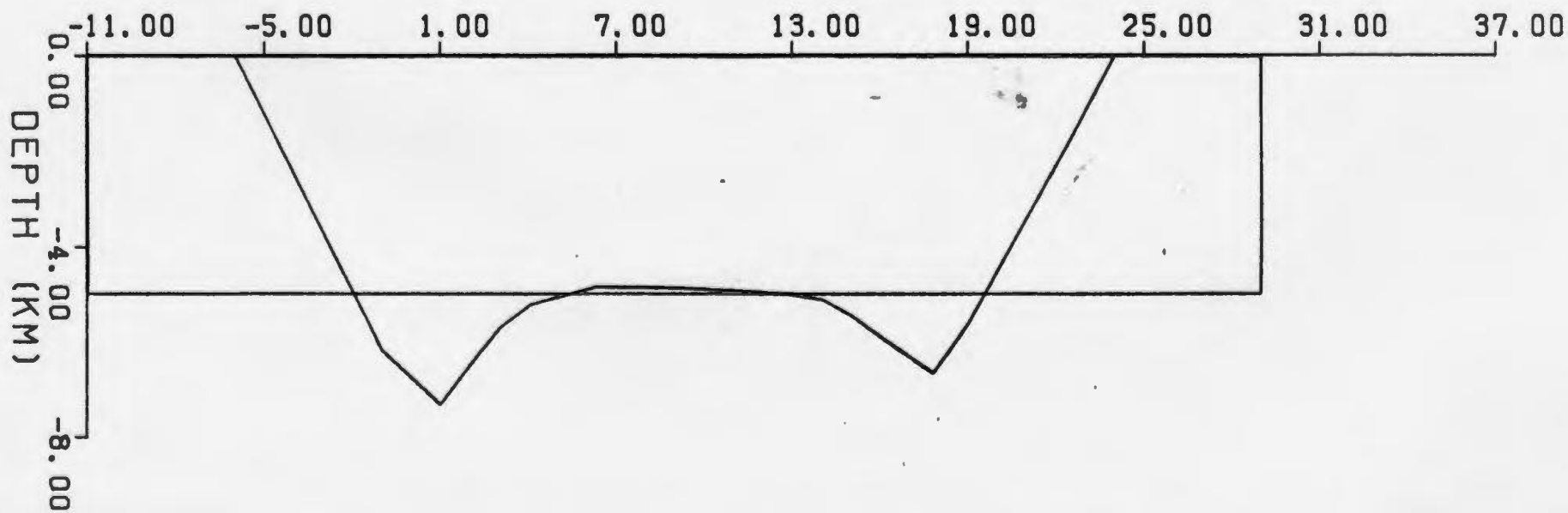
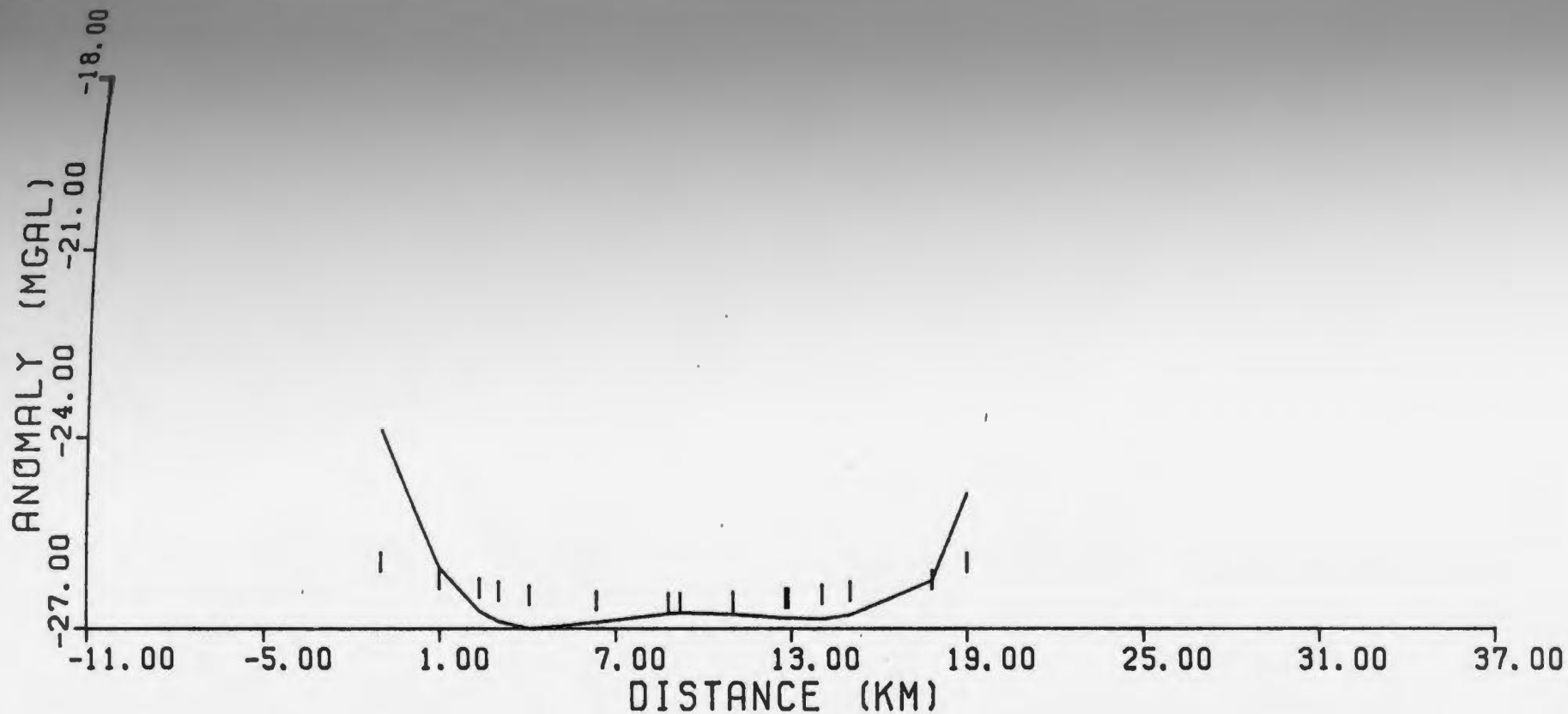


Figure 5.5h True and calculated models and gravity fit for a 40 km wide block (Body # 3).

Table 5.2: Parameters and results for dipping prisms₃. All distances are in kilometers. All densities in g/cm³.

Body	Density Contrast	Thickness	Depth of Burial	Dip	Strike-Length		Number of Iterations	Mean	Variance	Calculated Thickness (Maximum)
A	+0.30	3	0	37	10	4.99	60	-0.073	0.288	3.62
B	"	"	"	"	"	4.99	30	-0.043	0.292	3.14

Table 5.3: Parameters and results for a buried₃ body. All distances are in kilometers. Density in g/cm³.

Density Contrast	Thickness	Depth of Burial	Strike-length	Width		Number of Iterations	Mean	Variance	Calculated Thickness (Center of Body)
+0.75	0.8	0.50	5	10	3.76	4	0.015	0.221	0.50
"	"	1.00	"	"	4.30	7	-0.096	0.243	0.79
"	"	1.50	"	"	7.87	10	-0.210	0.416	1.02
"	"	2.00	"	"	11.90	22	-0.467	0.469	1.45

inversion. For dips in opposite directions, the shape of the bodies were not well defined (Figure 5.6), but the depth estimates were satisfactory. Also, while a dip angle cannot be determined from the inverted model, the asymmetry of these models gives the direction of dip, with the model's 'peak' skewed to the up-dip side.

Several simple geologic models were tested next. The first model considered was the basement step or vertical fault model. Figure 5.7a shows the anomaly and inverted model for a basement step model with a vertical throw of 3.5 km. The calculated depths to the upper and lower basement are in very good agreement with the original model. The resulting model for the basement step was compared to a sloping basement model. Figure 5.7b shows the inverted slope model. The depth estimates of the lower basement and slope match the original model. A comparison of the two resulting models shows that they are distinguishable by the 2.5-D gravity inversion procedure. However, distinguishability is not always attainable from the inversion procedure. Figure 5.8 shows that basement step and basement contact models could generate very similar anomalies, making it impossible for the inversion program to distinguish between the models, i.e. a basement contact may be mistakenly interpreted as a normal fault or sloping basement. Magnetic anomalies of the same area may help define the correct model. A similar situation may occur for normal and reversed faults of equal, but opposite, dips and equal throws. Figure 5.9 illustrates this problem well, as the inverted models are indistinguishable.

A test to determine how well the inversion procedure could define a buried body was conducted. As before, the strike-length and density contrast were assumed known. The depth of burial was varied and the

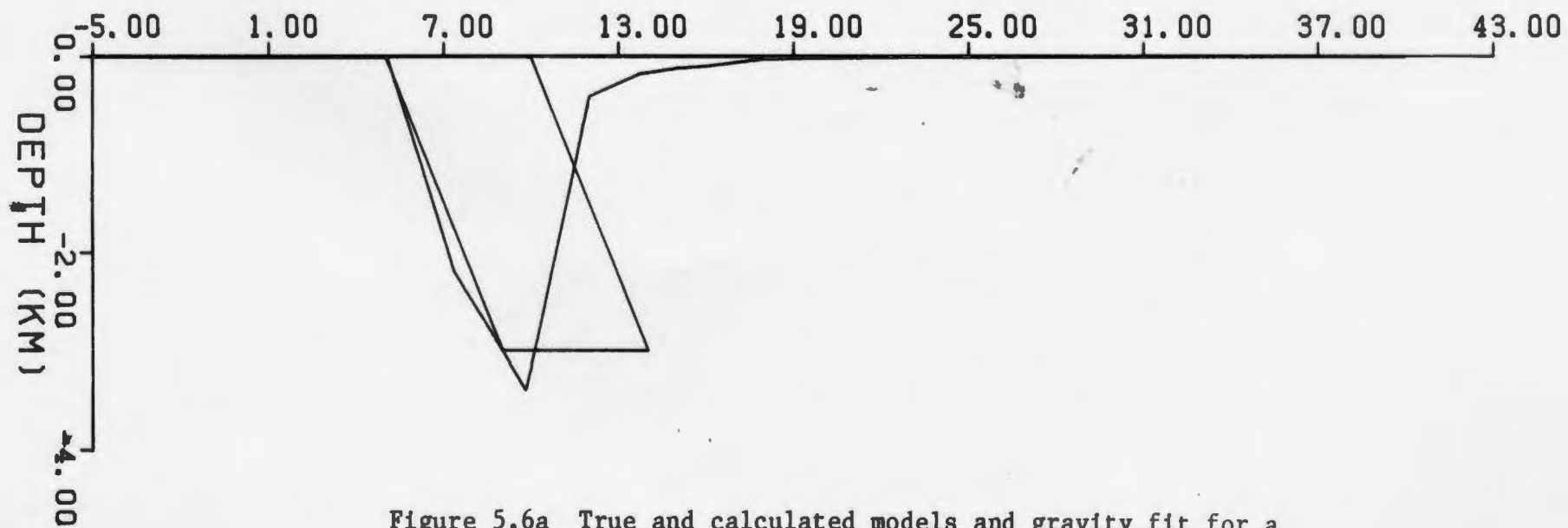
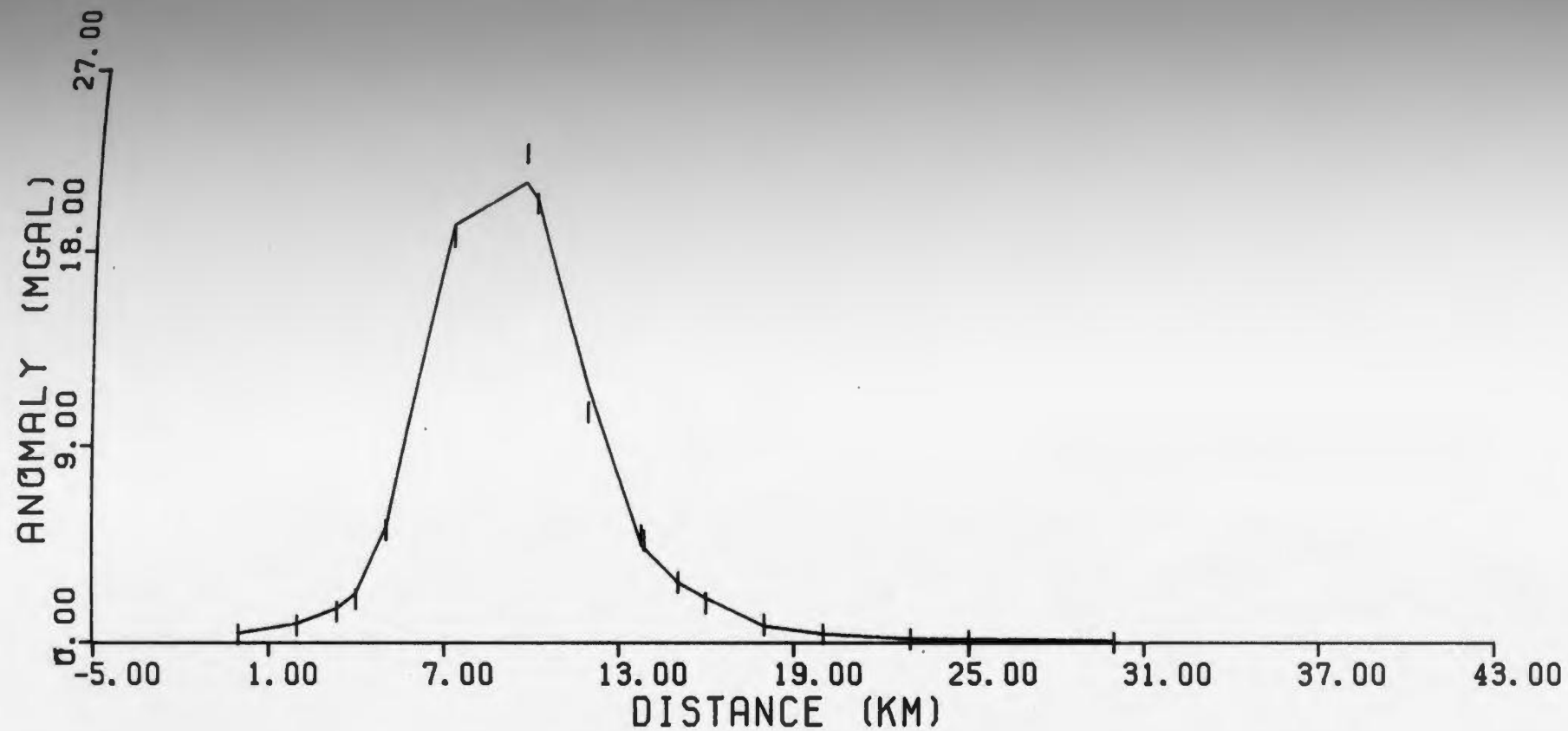


Figure 5.6a True and calculated models and gravity fit for a right-dipping prism.

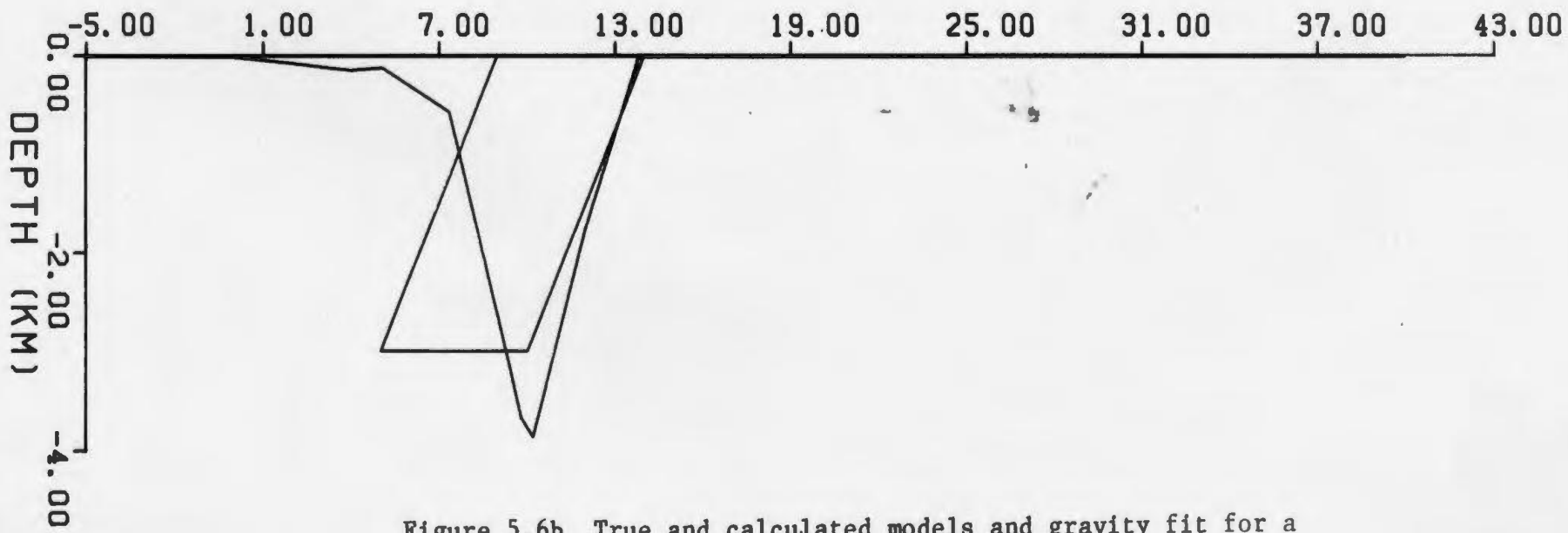
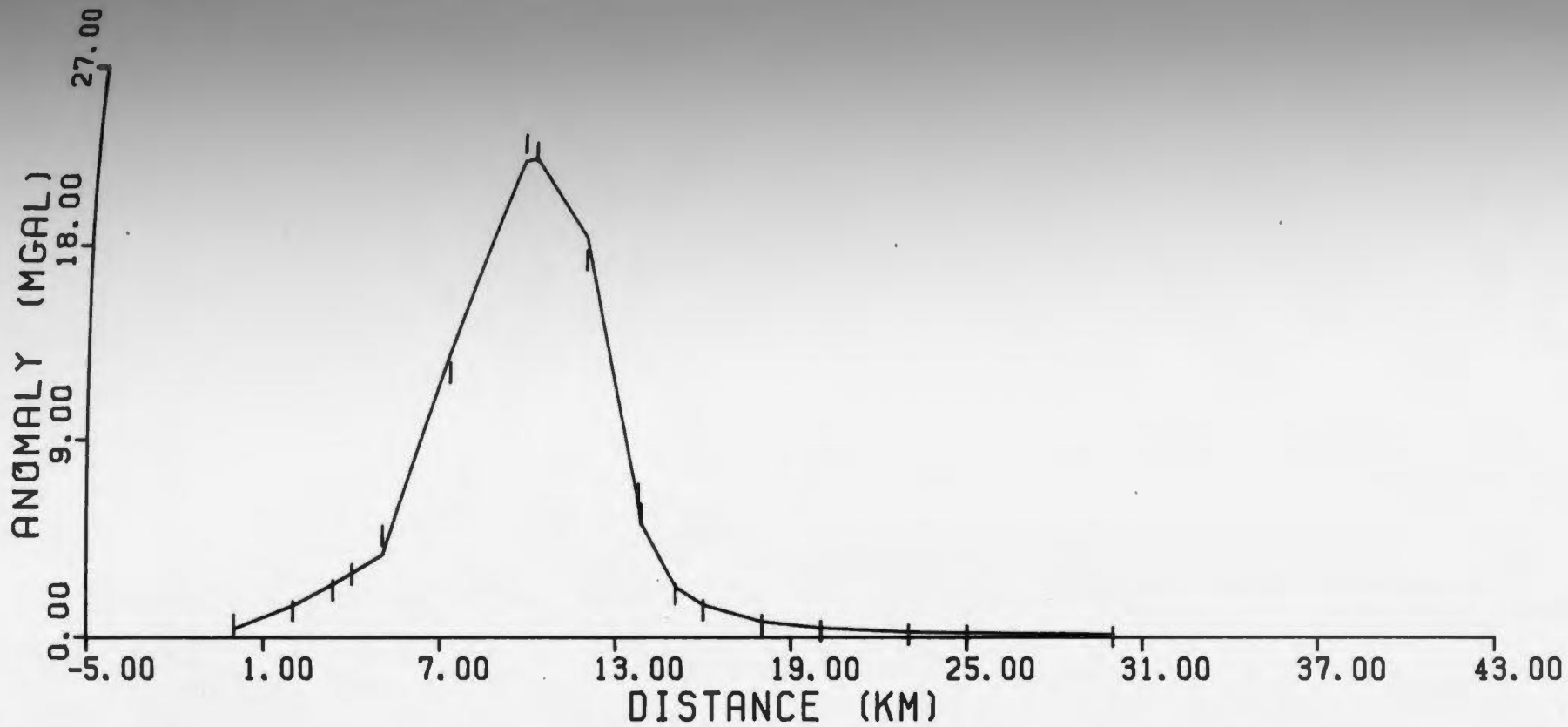


Figure 5.6b True and calculated models and gravity fit for a left-dipping prism.

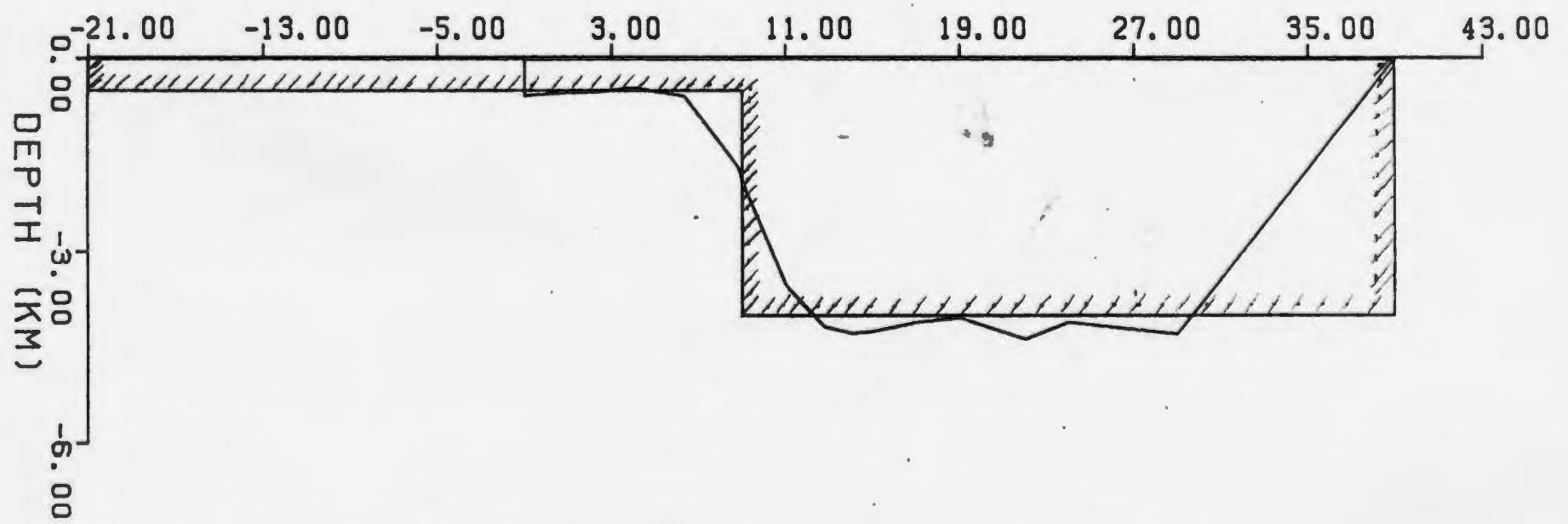
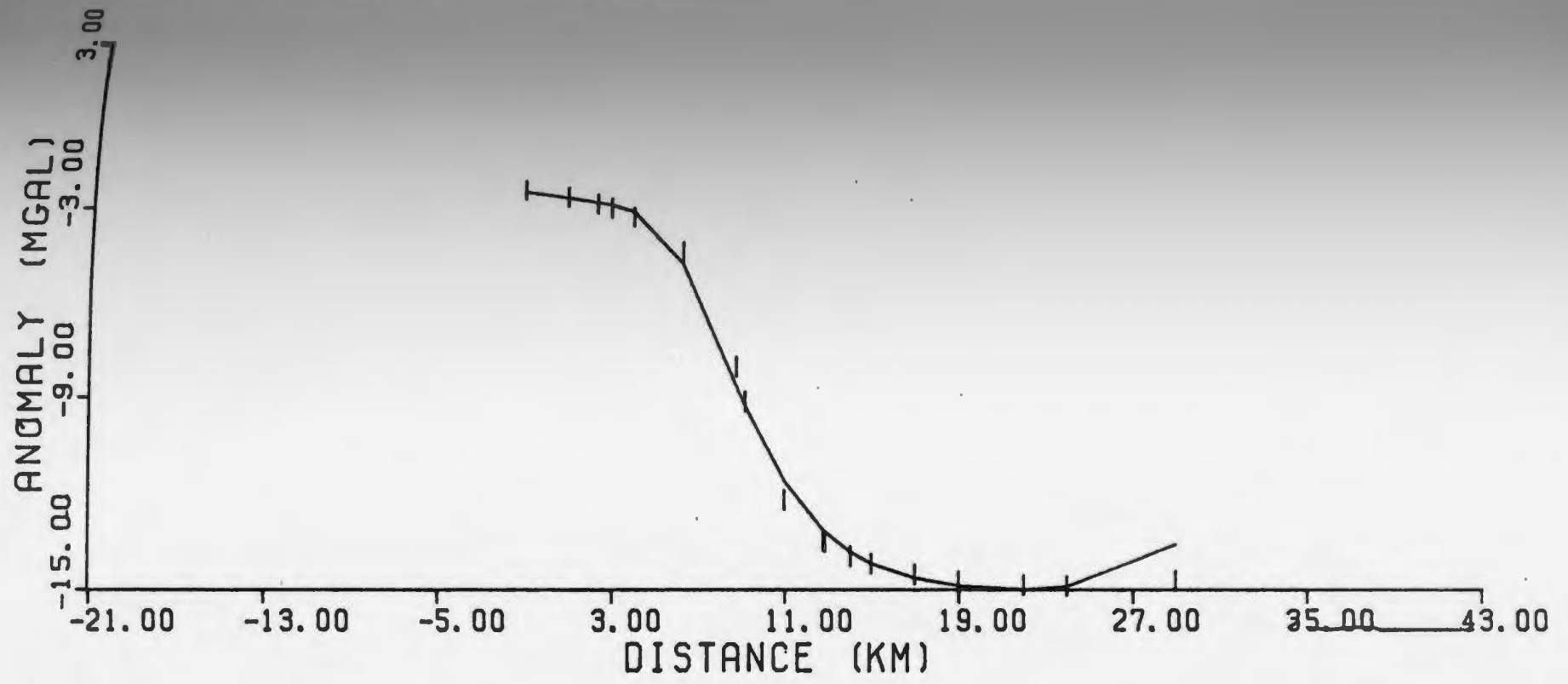


Figure 5.7a True and calculated models and gravity fit for a basement step. Hatched body is the true model.

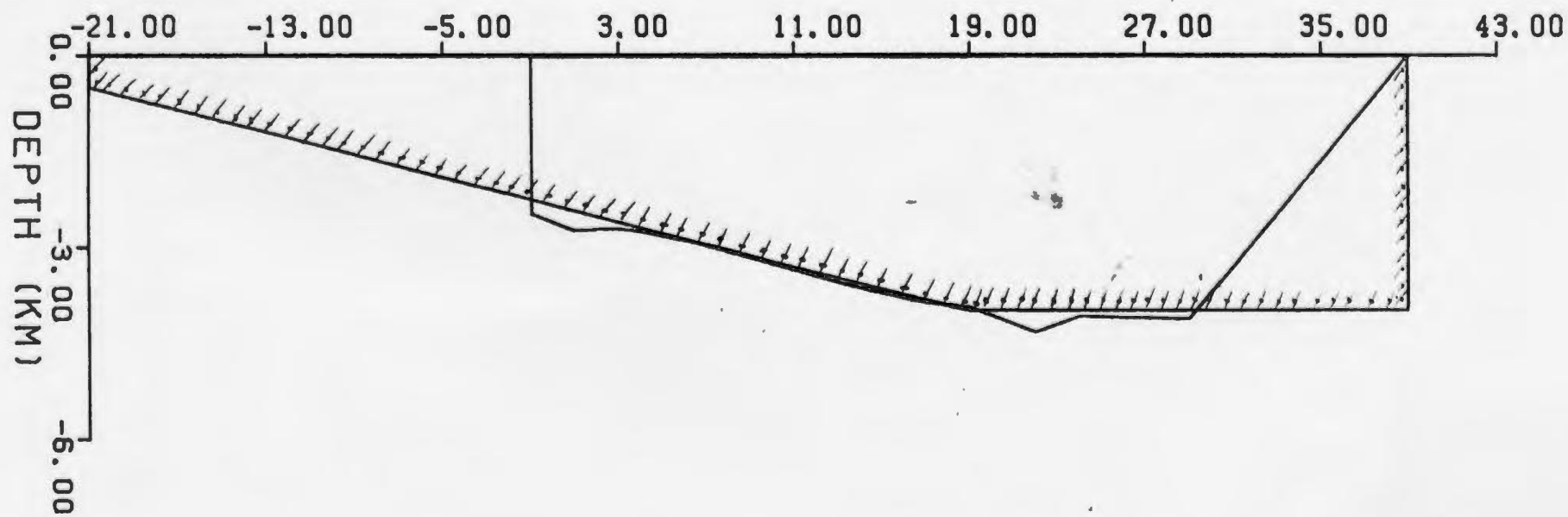
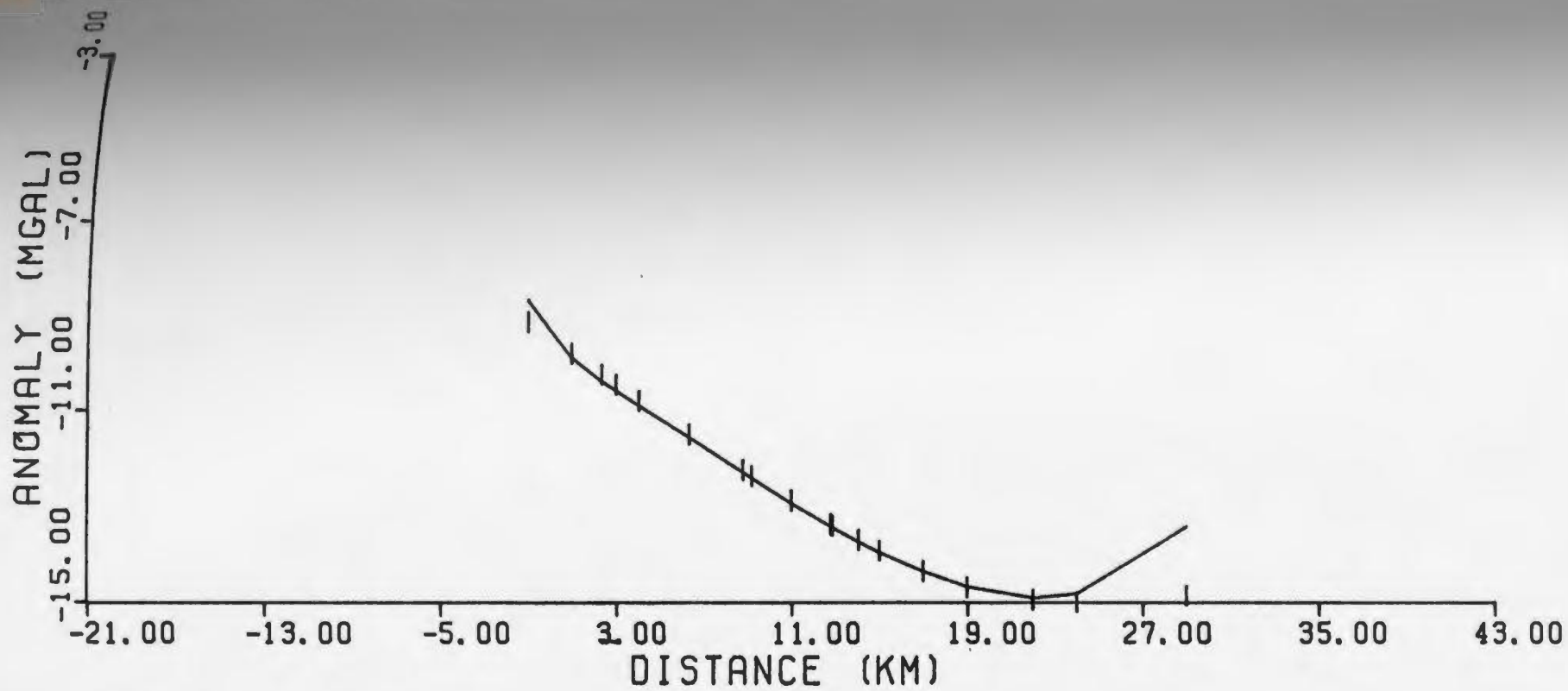


Figure 5.7b True and calculated models and gravity fit for a basement slope. Hatchured body is the true model.

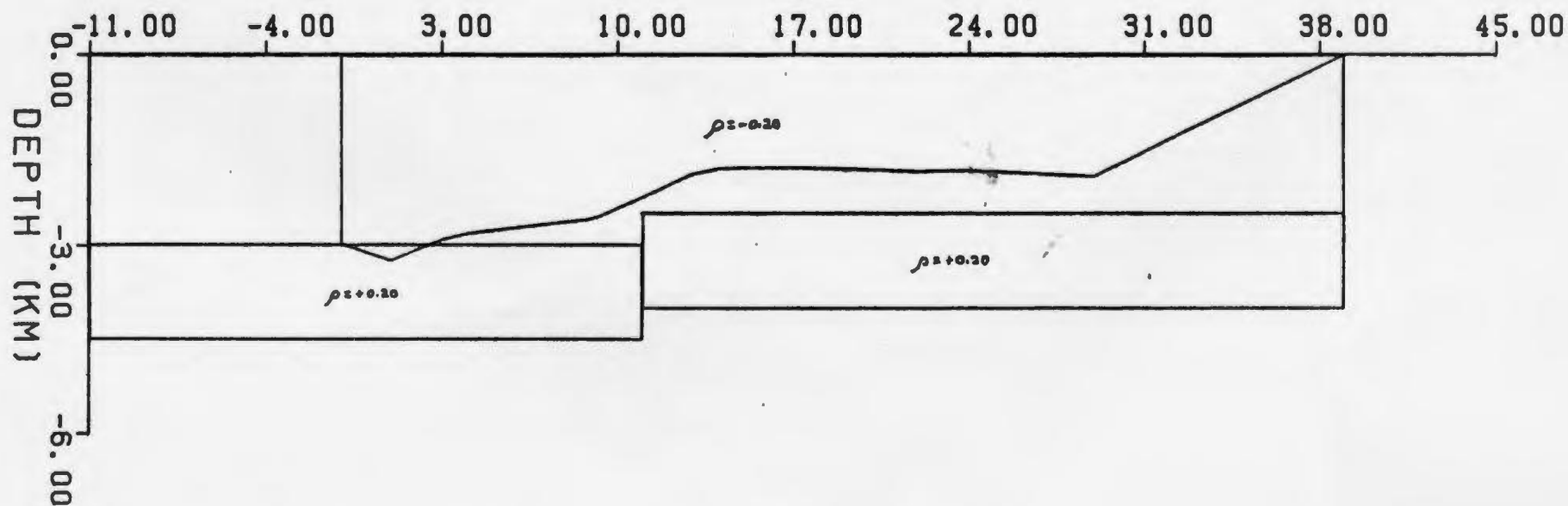
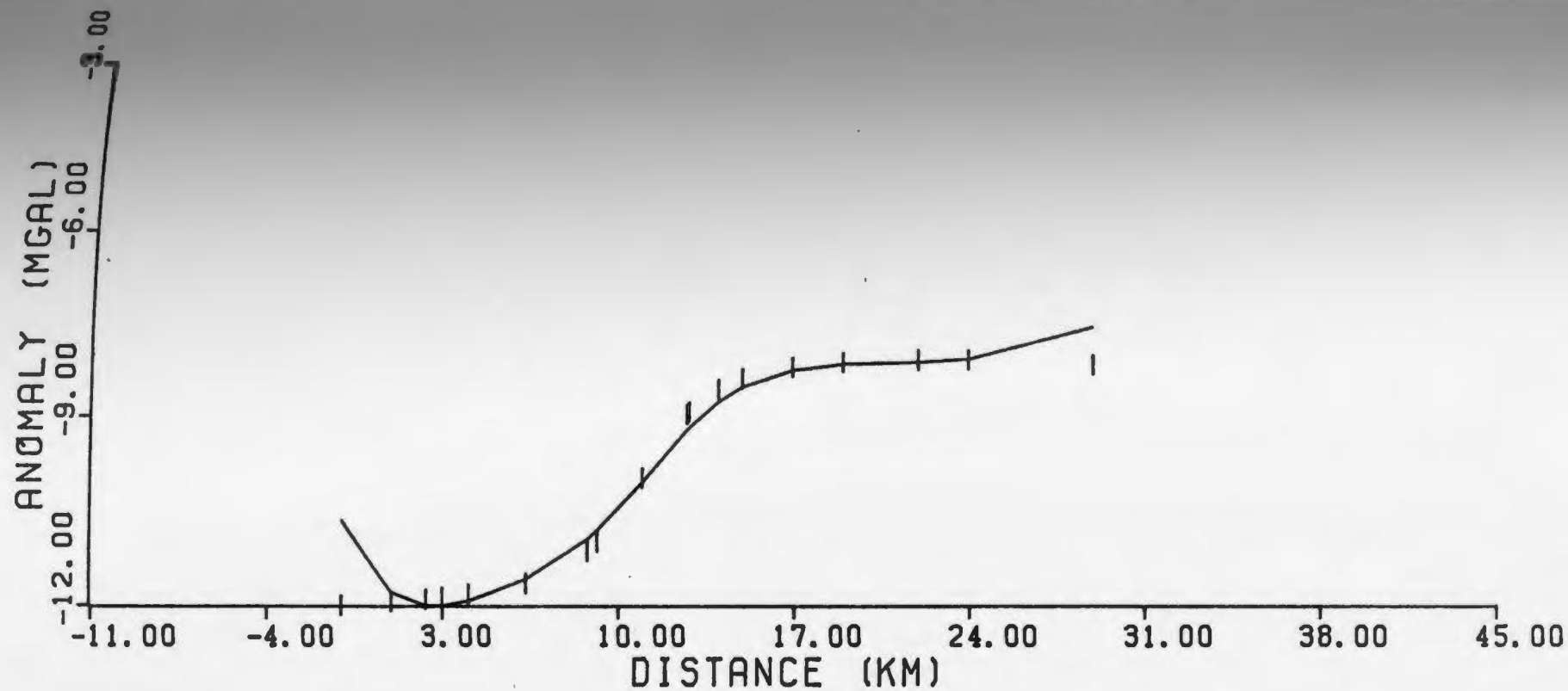


Figure 5.8a True and calculated models and gravity fit for a basement step

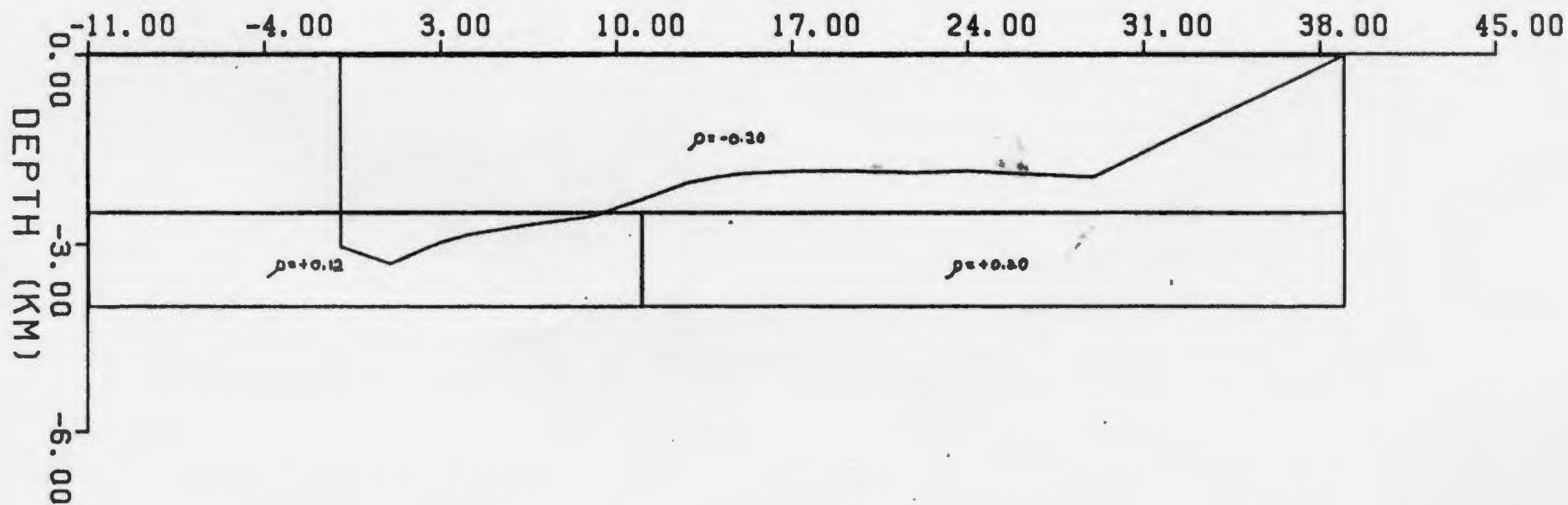
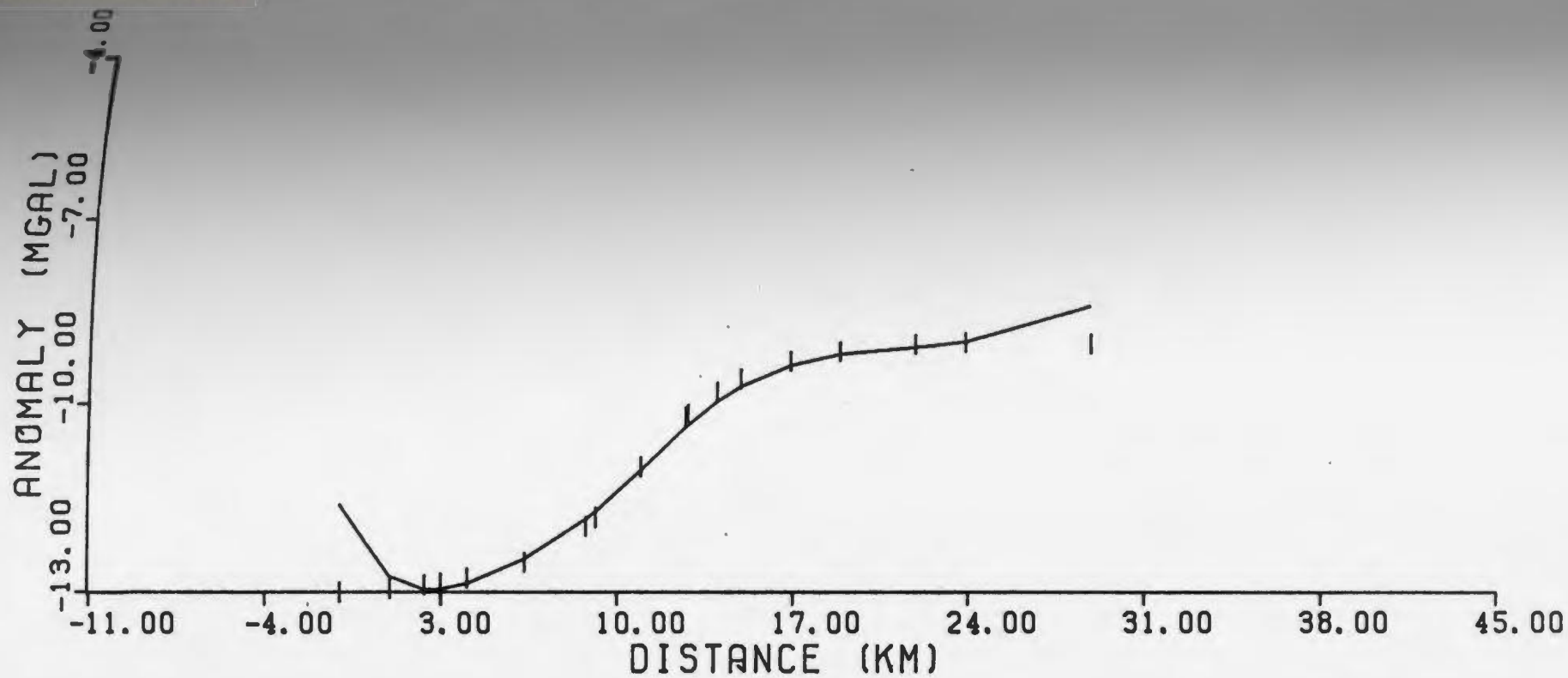


Figure 5.8b True and calculated models and gravity fit for a basement contact.

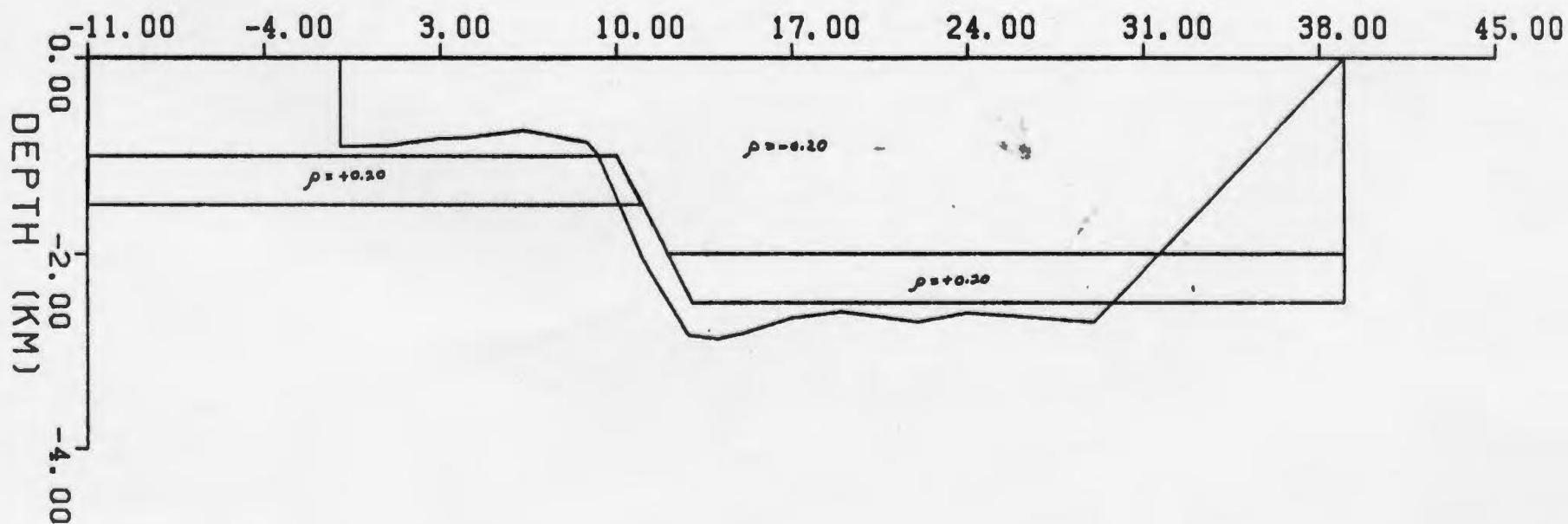
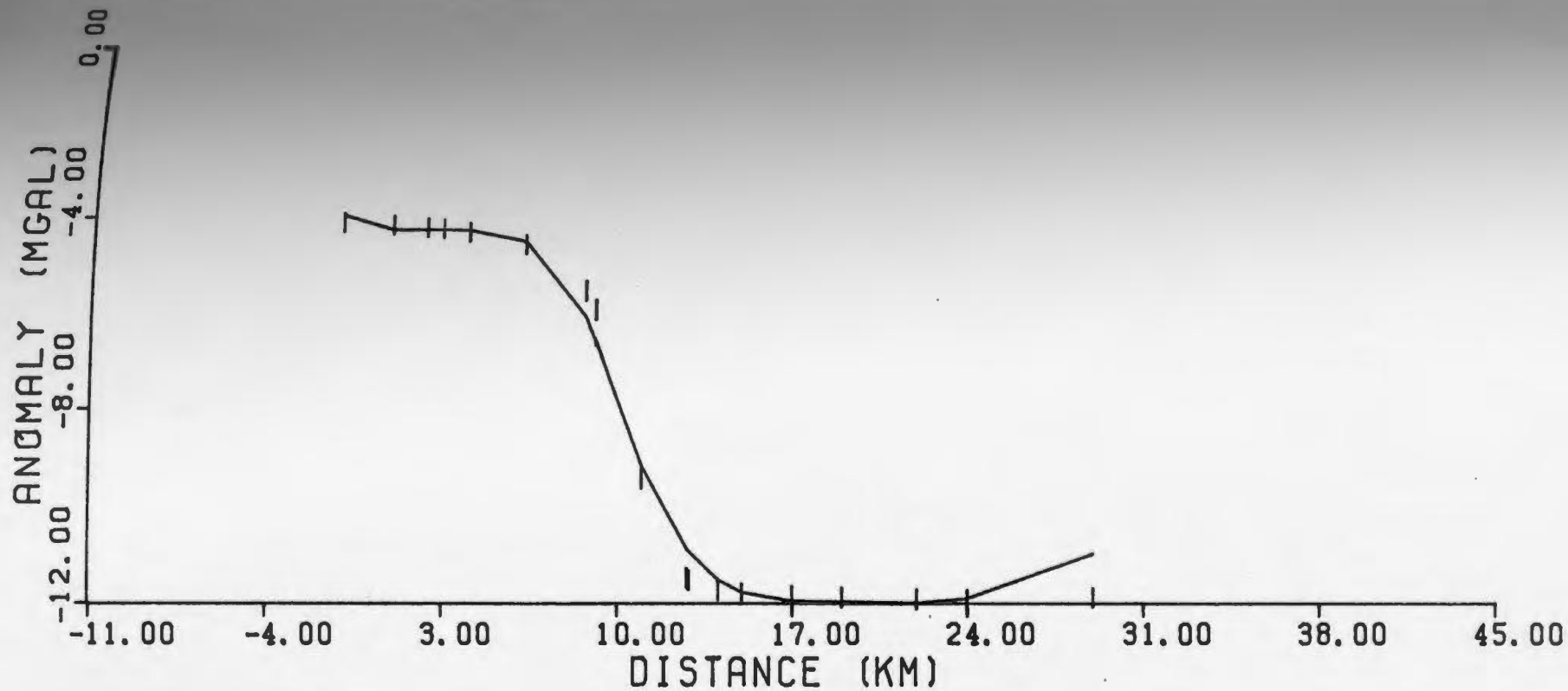


Figure 5.9a True and calculated models and gravity fit for a normal fault.

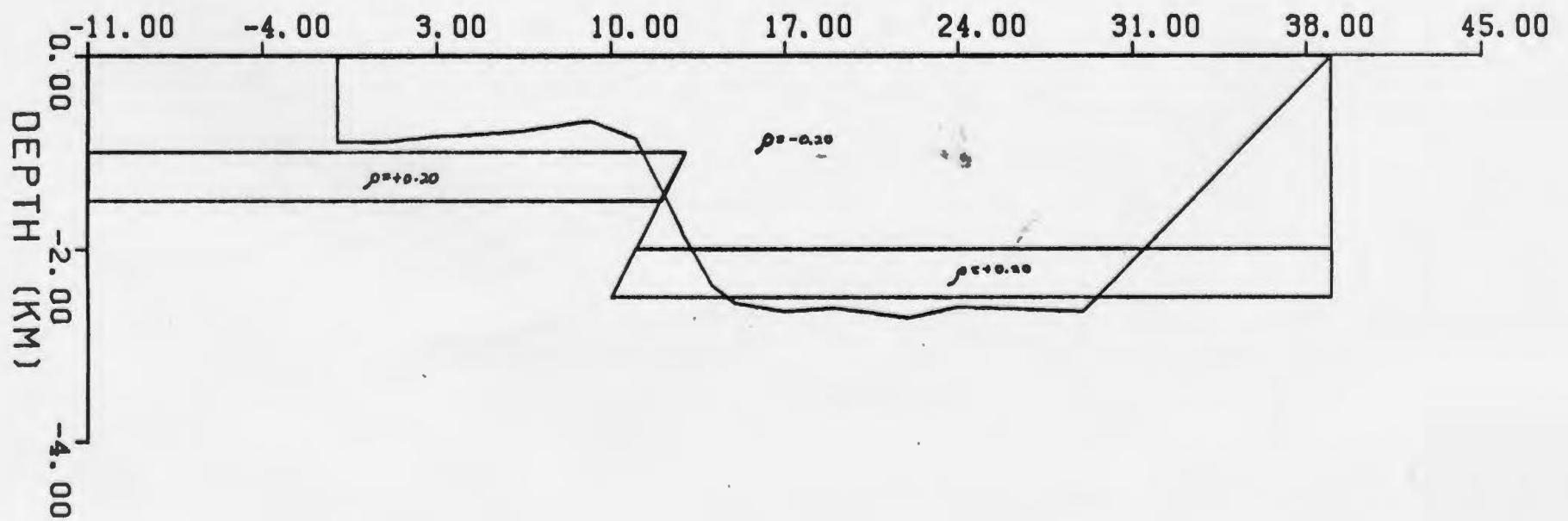
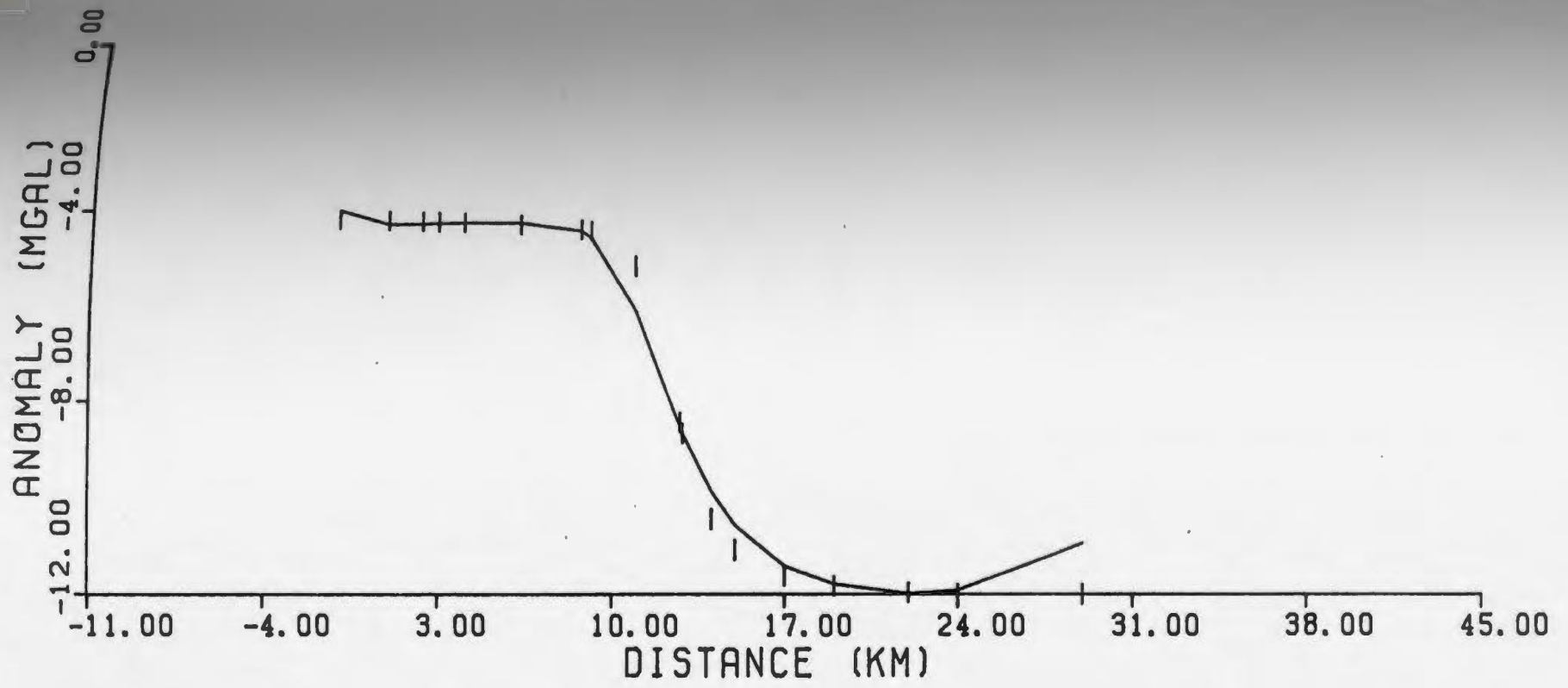


Figure 5.9b True and calculated models and gravity fit for a reverse fault.

results are listed in Table 5.3 and illustrated in Figure 5.10. All of the inverted models were the proper shape, however, the deeper bodies were thicker, as more mass was necessary to fit the anomaly.

As a final test of the 2.5-D inverse program, four irregular polygons were used. The calculated and 'observed' anomalies, and the true and calculated models are shown in Figure 5.11, a-d. The fit was good for all four models, although some of the finer details can't be seen in the calculated models. These small features could possibly be detected if more data points were included in the profile over these features.

From the above tests, it can be concluded that the developed 2.5-D gravity inversion procedure is a viable one. Several important conclusions about the procedure resulted from the testing. These are:

- 1) Use as many data points as possible along the profile;
- 2) Small width anomalies are difficult to invert properly;
- 3) Side-lobes at the edges of the inverted model can be eliminated or reduced if the edges of the gravity profile are totally outside the body edges; and
- 4) Unlike situations giving anomalies of similar magnitude and shape will produce nearly the same model, as shown above with basement step and basement contact models.

A 2-D gravity inversion program similar to the 2.5-D procedure was written in order to test the effects of finite strike-length on the

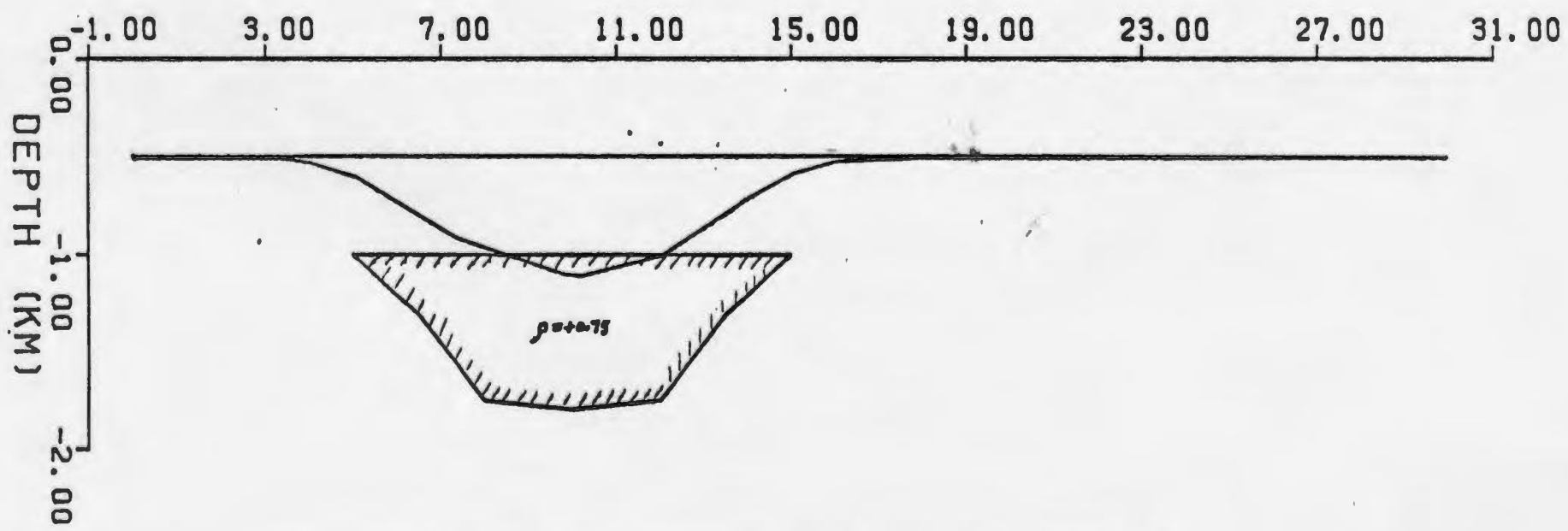
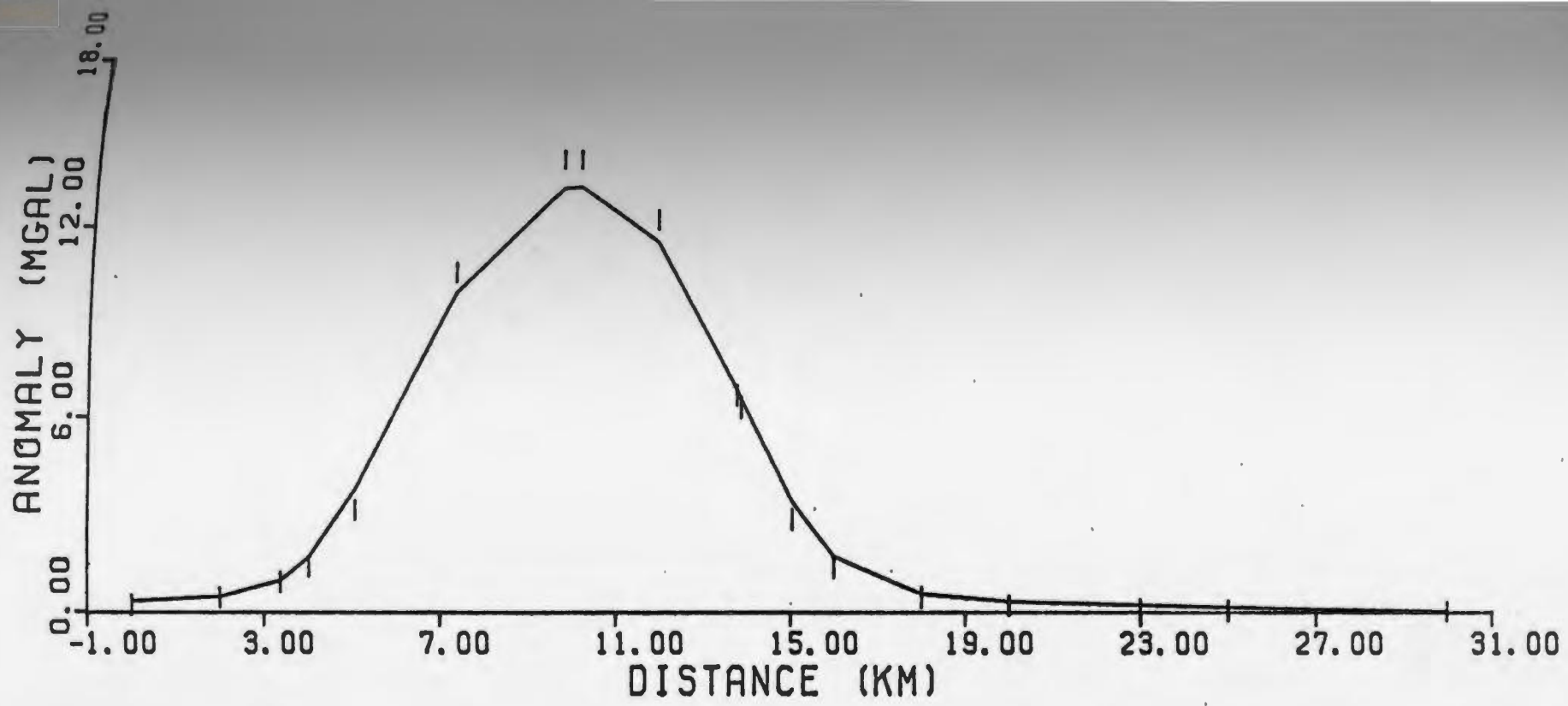


Figure 5.10a True and calculated models and gravity fit for a body buried at 1 km (zdepth = 0.5 km). Hatched body is the true model.

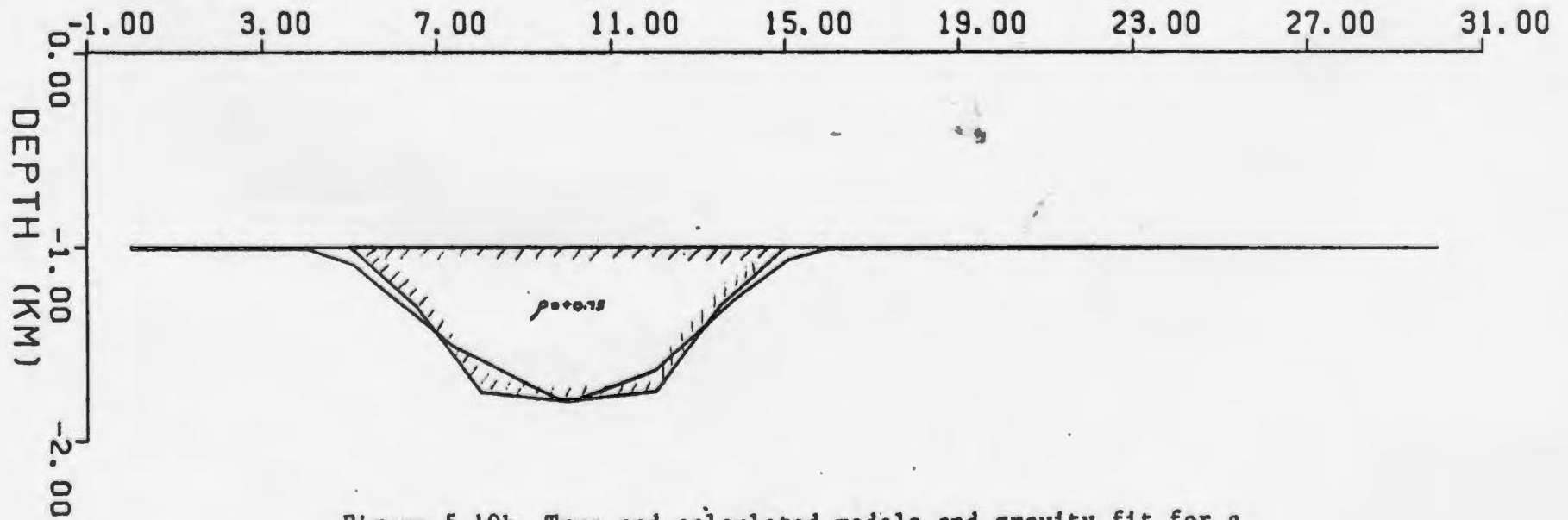
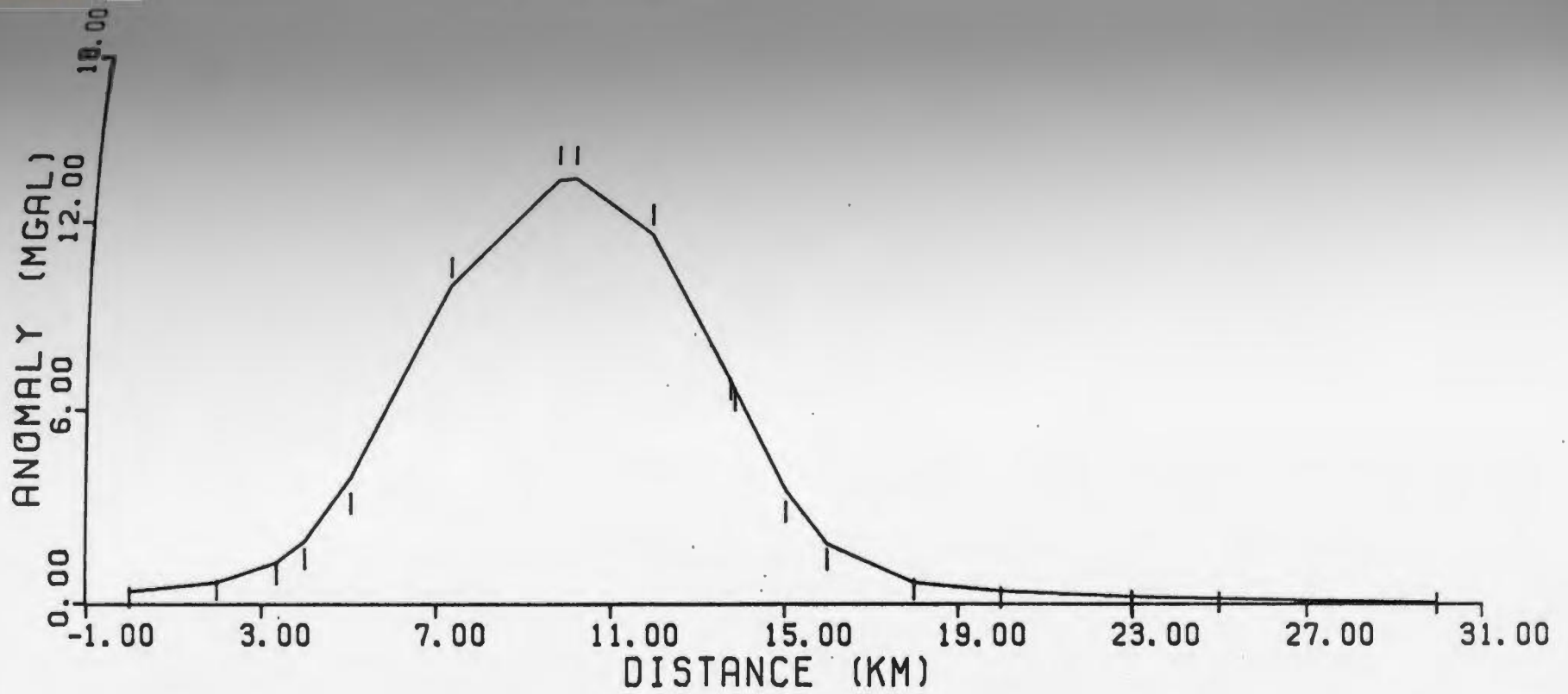


Figure 5.10b True and calculated models and gravity fit for a body buried at 1 km (zdepth = 1.0 km). Hatchured body is the true model.

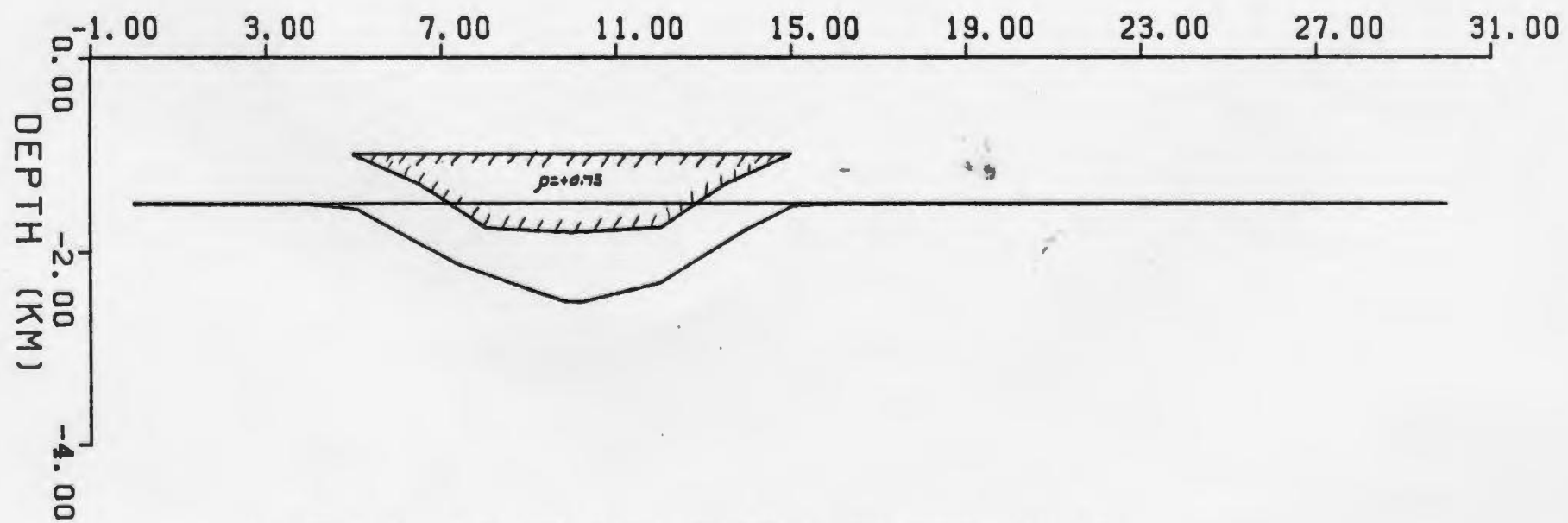
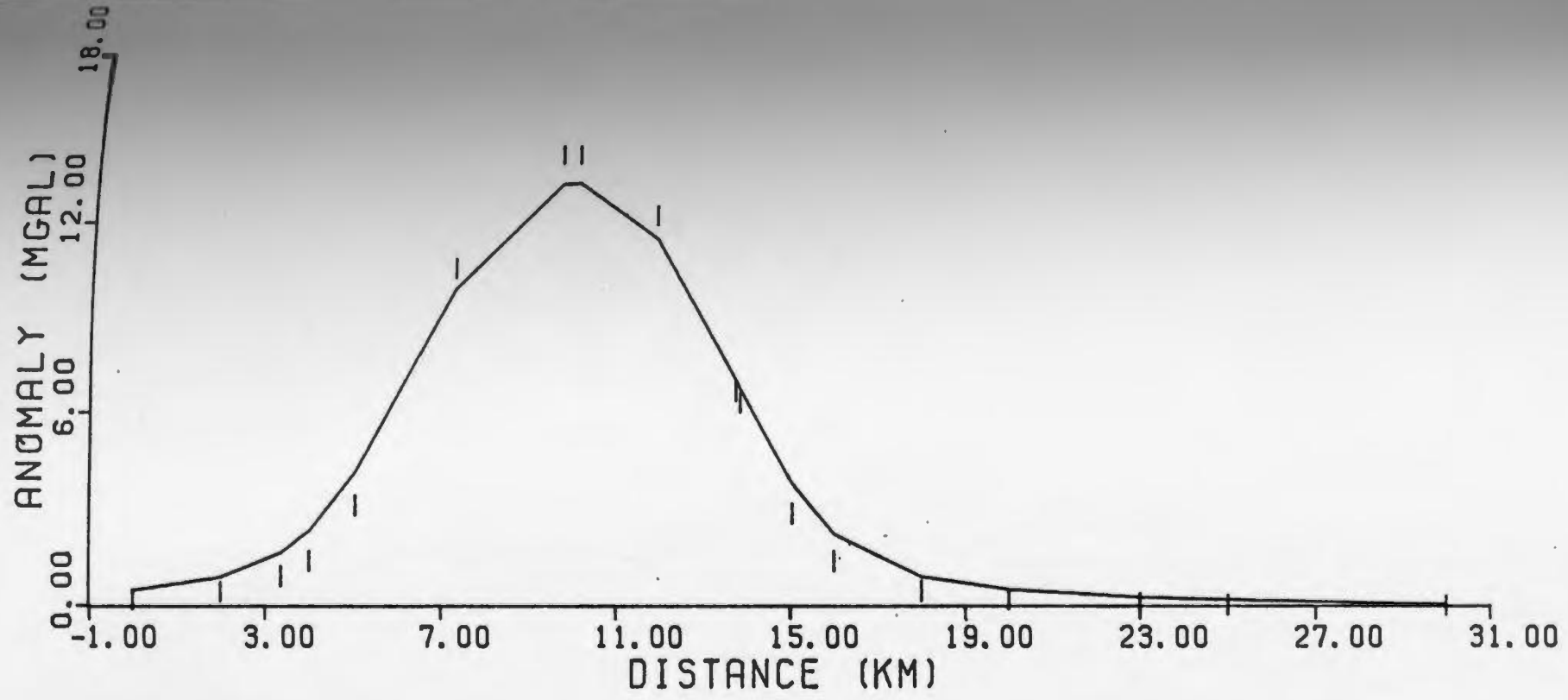


Figure 5.10c True and calculated models and gravity fit for a body buried at 1 km (zdepth = 1.5 km). Hatchured body is the true model.

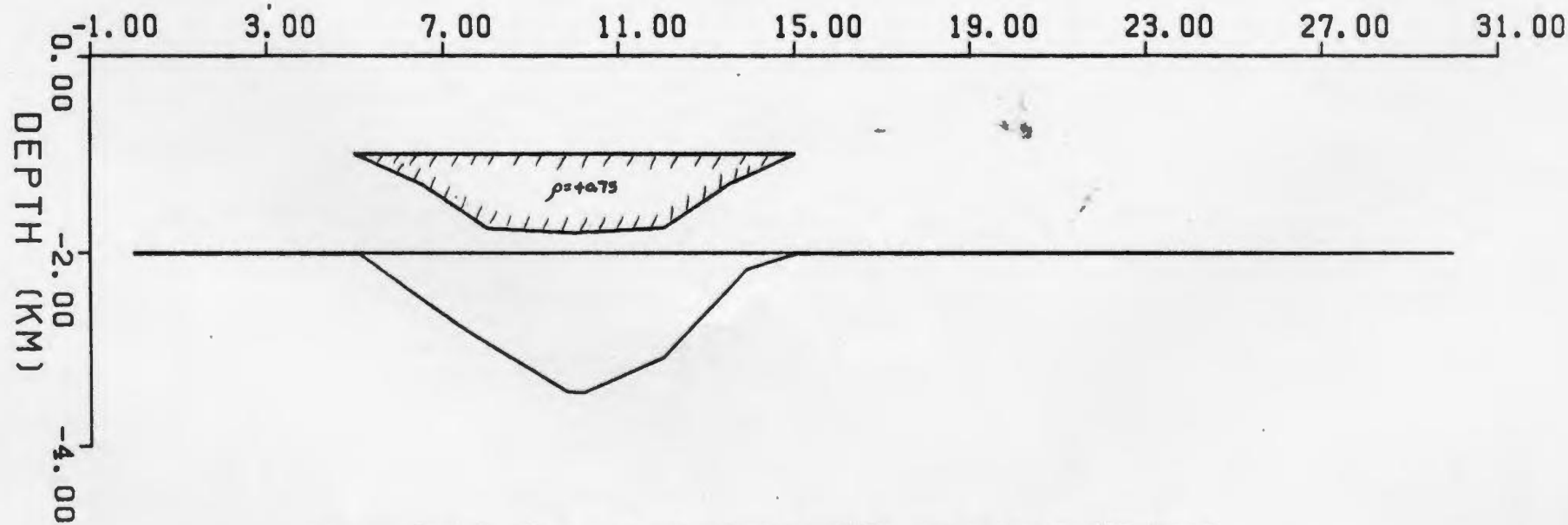
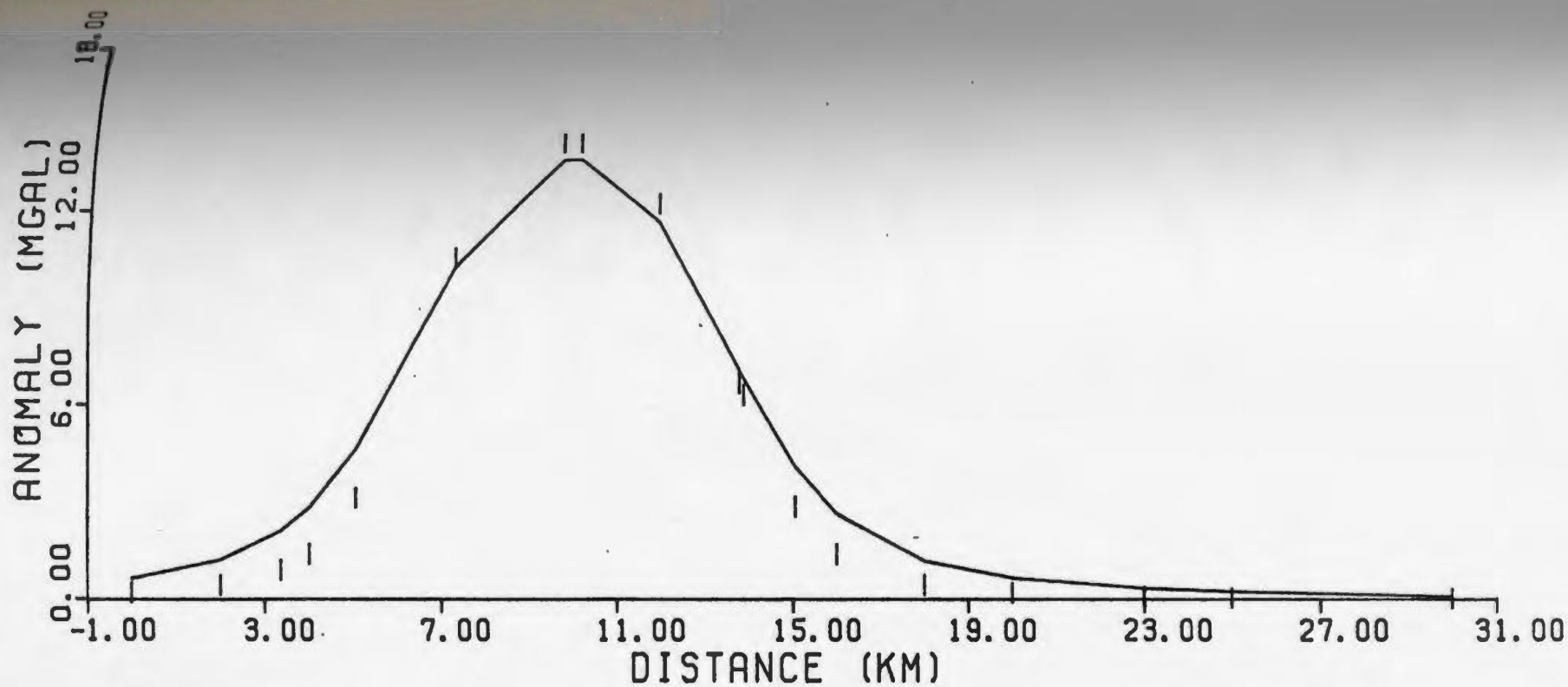


Figure 5.10d True and calculated models and gravity fit for a body buried at 1 km (zdepth = 2.0 km). Hatched body is the true model.

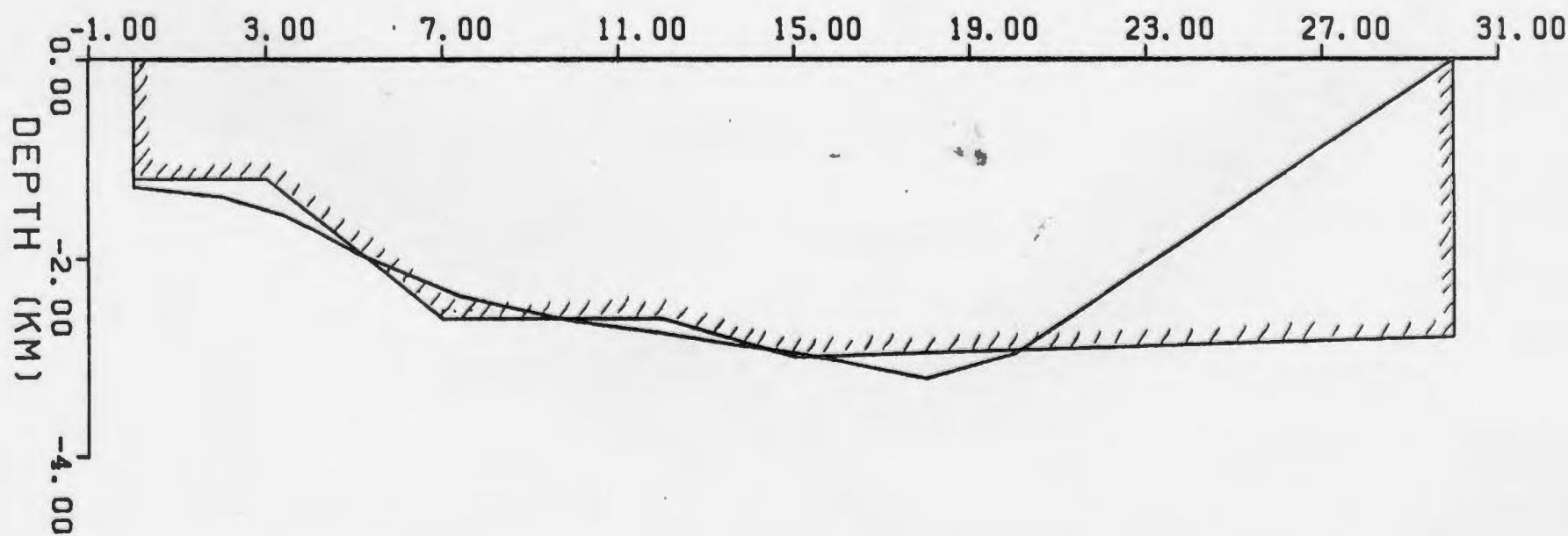
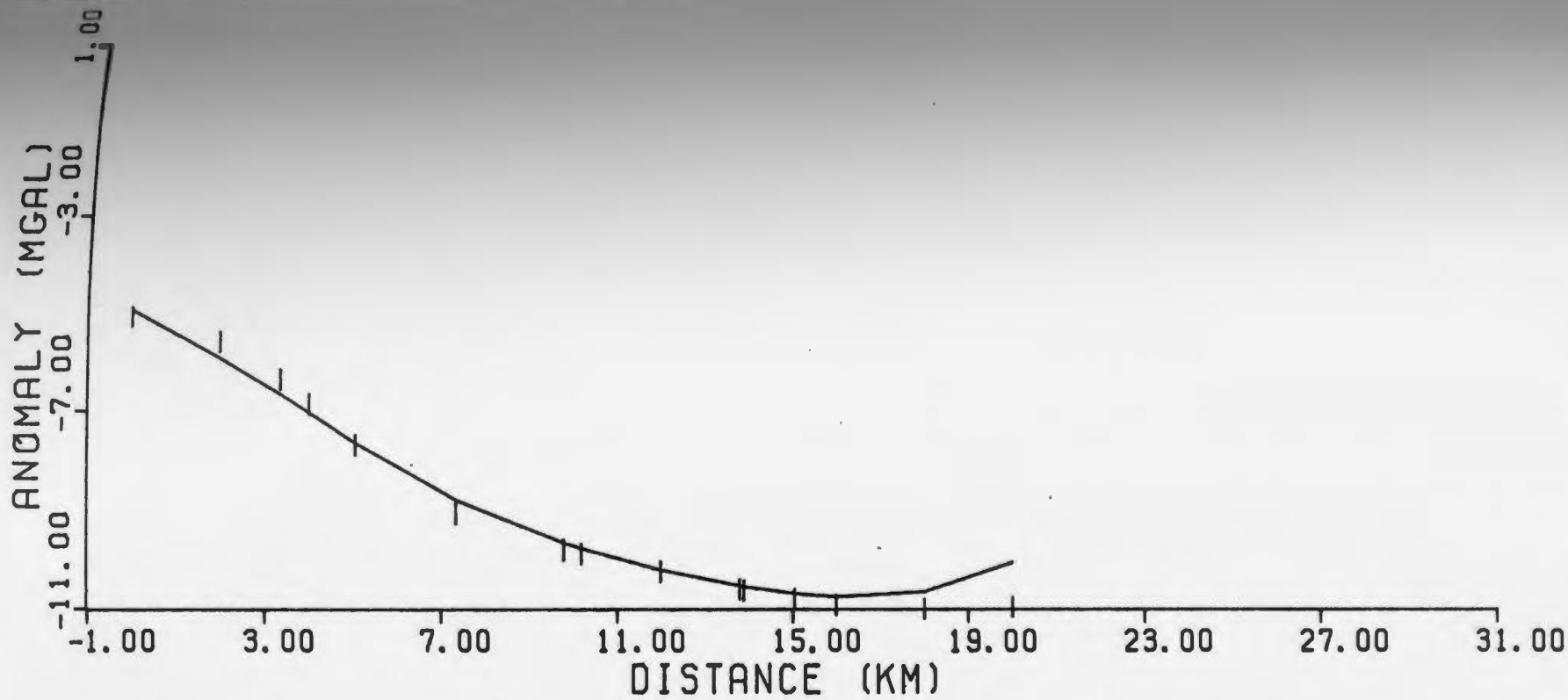


Figure 5.11a True and calculated models and gravity fit for an irregular polygon. Hatched body is the true model.

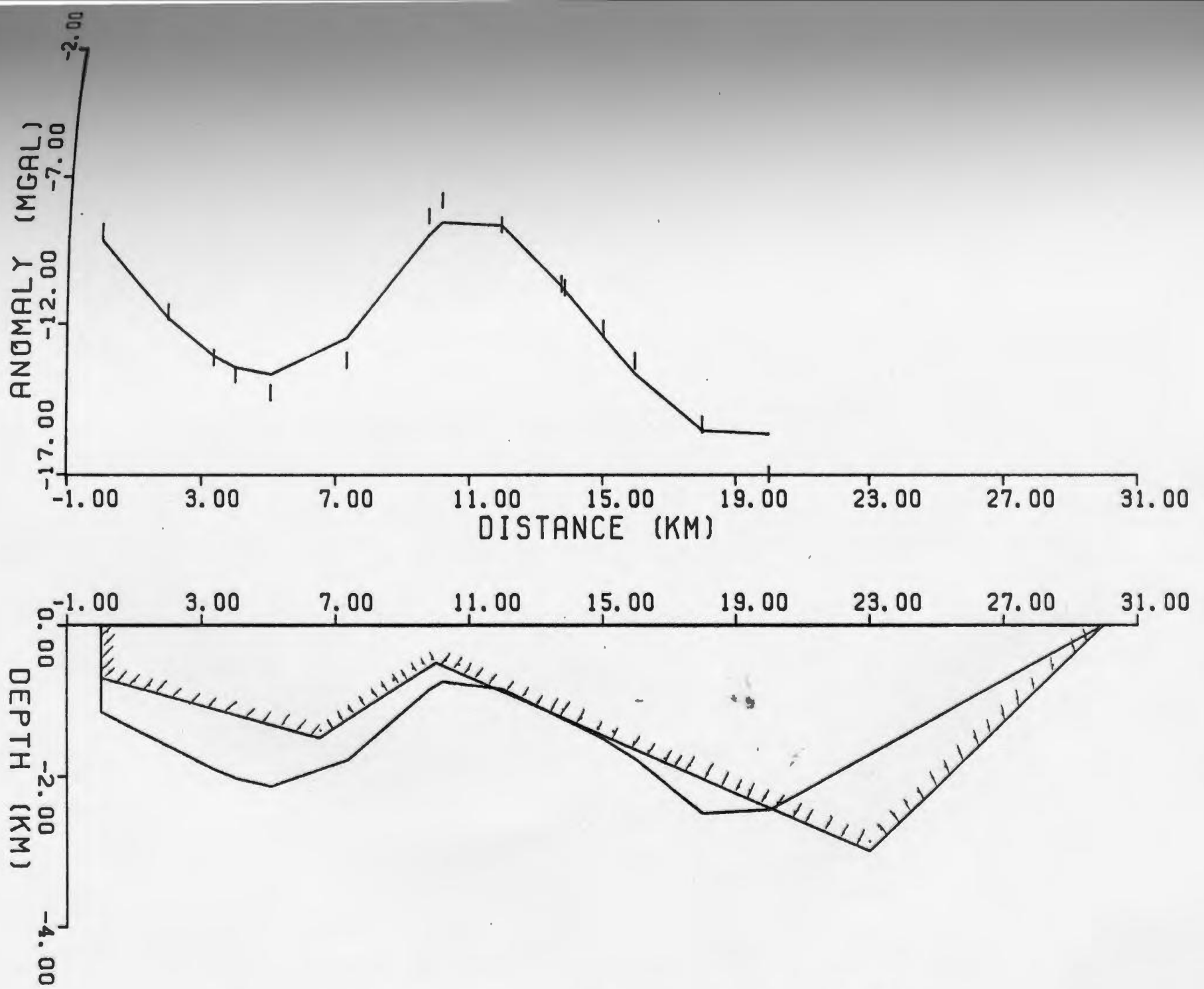


Figure 5.11b True and calculated models and gravity fit for an irregular polygon. Hatched body is the true model.

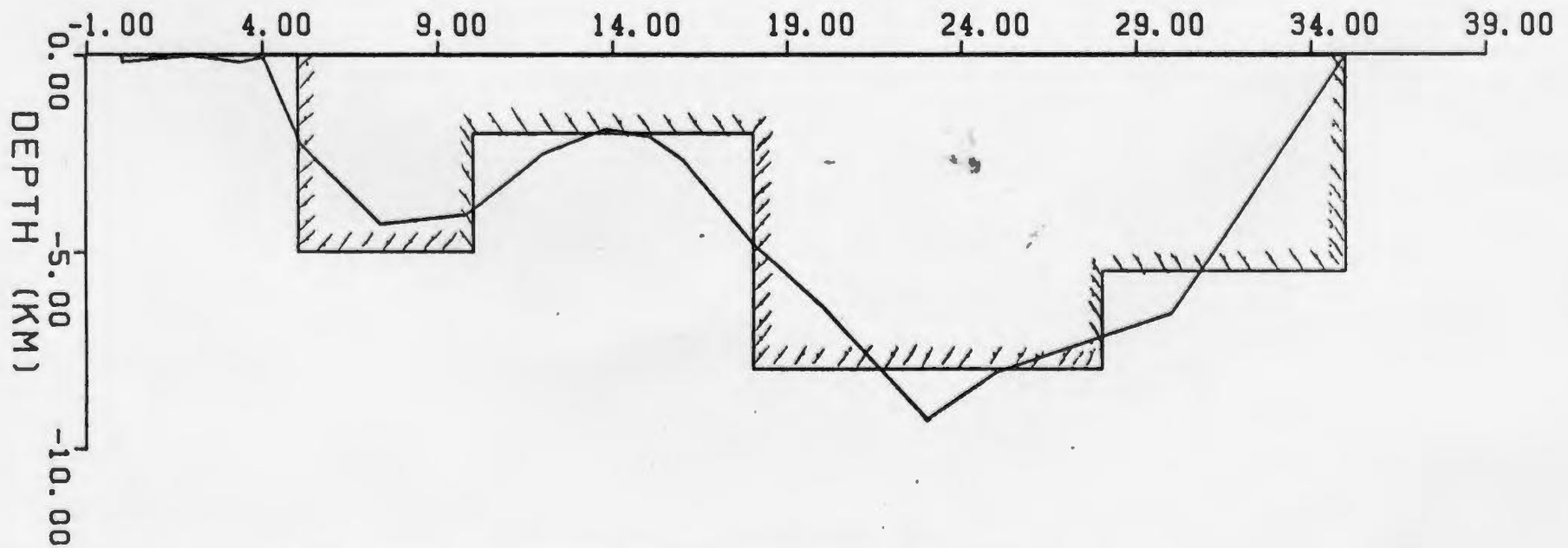
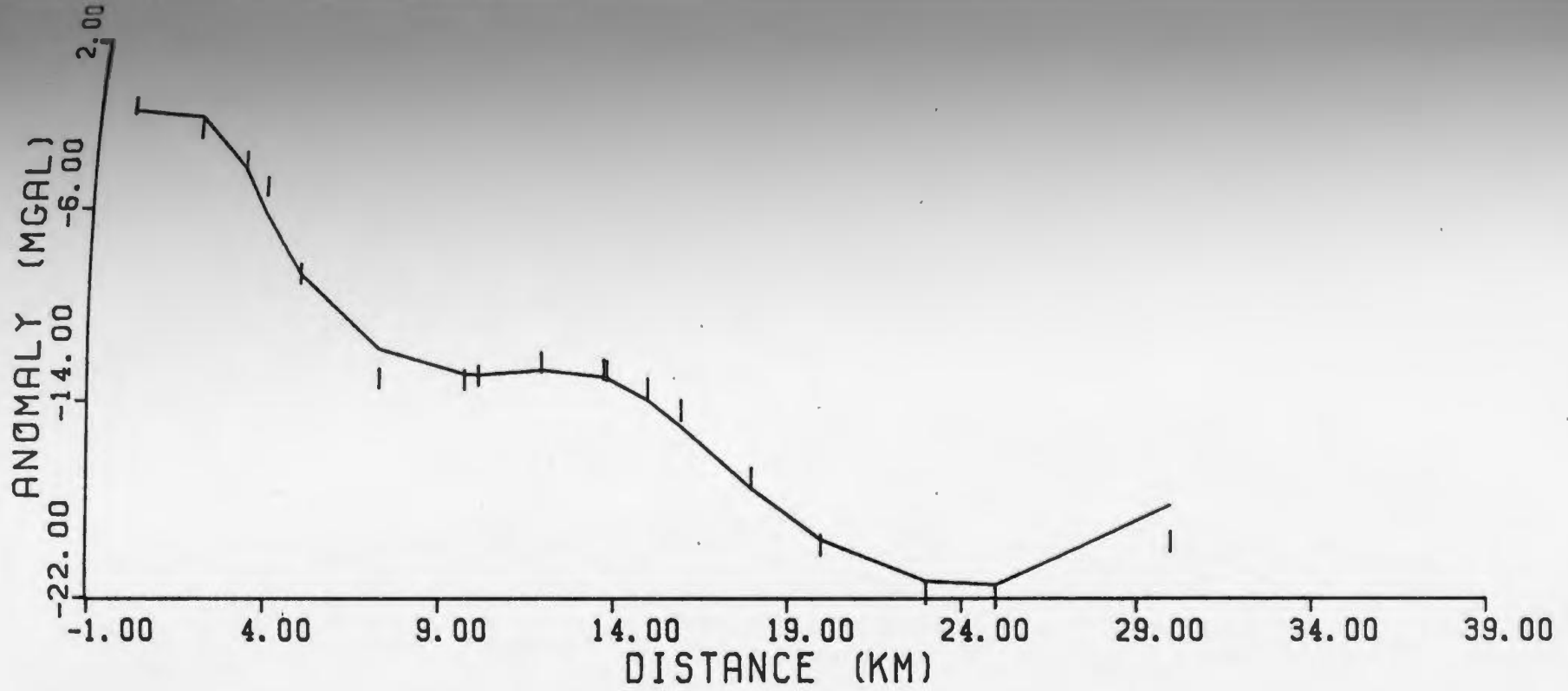


Figure 5.11c True and calculated models and gravity fit for an irregular polygon. Hatched body is the true model.

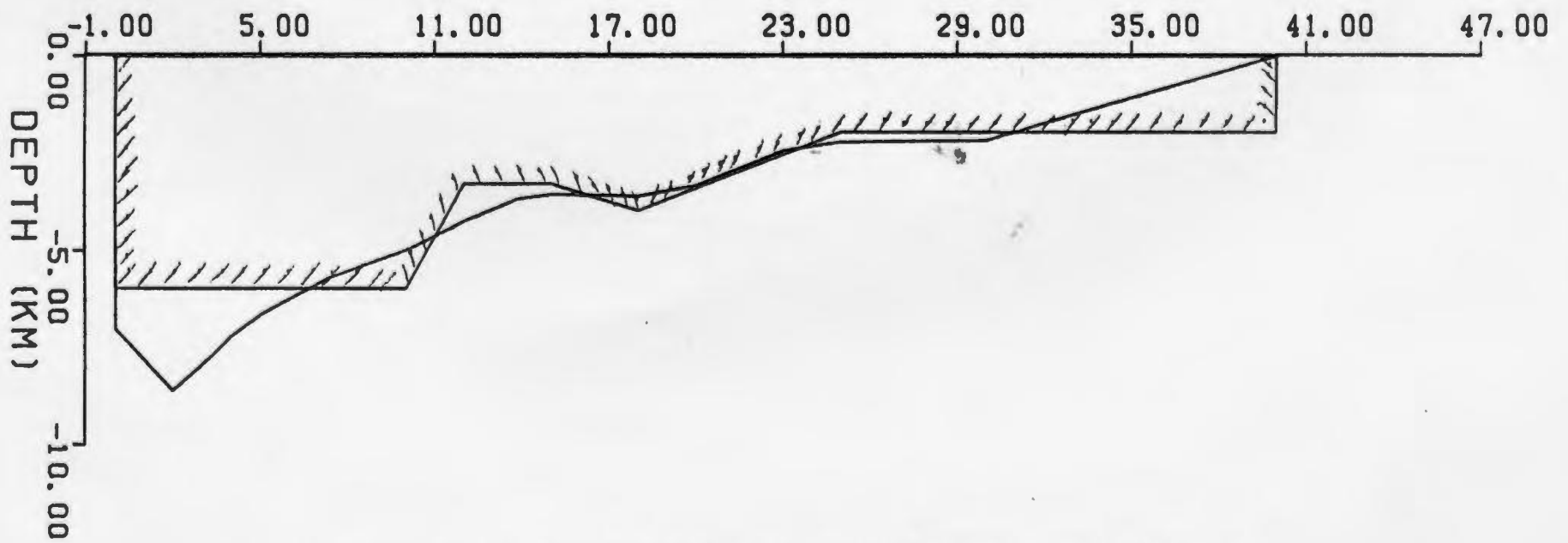
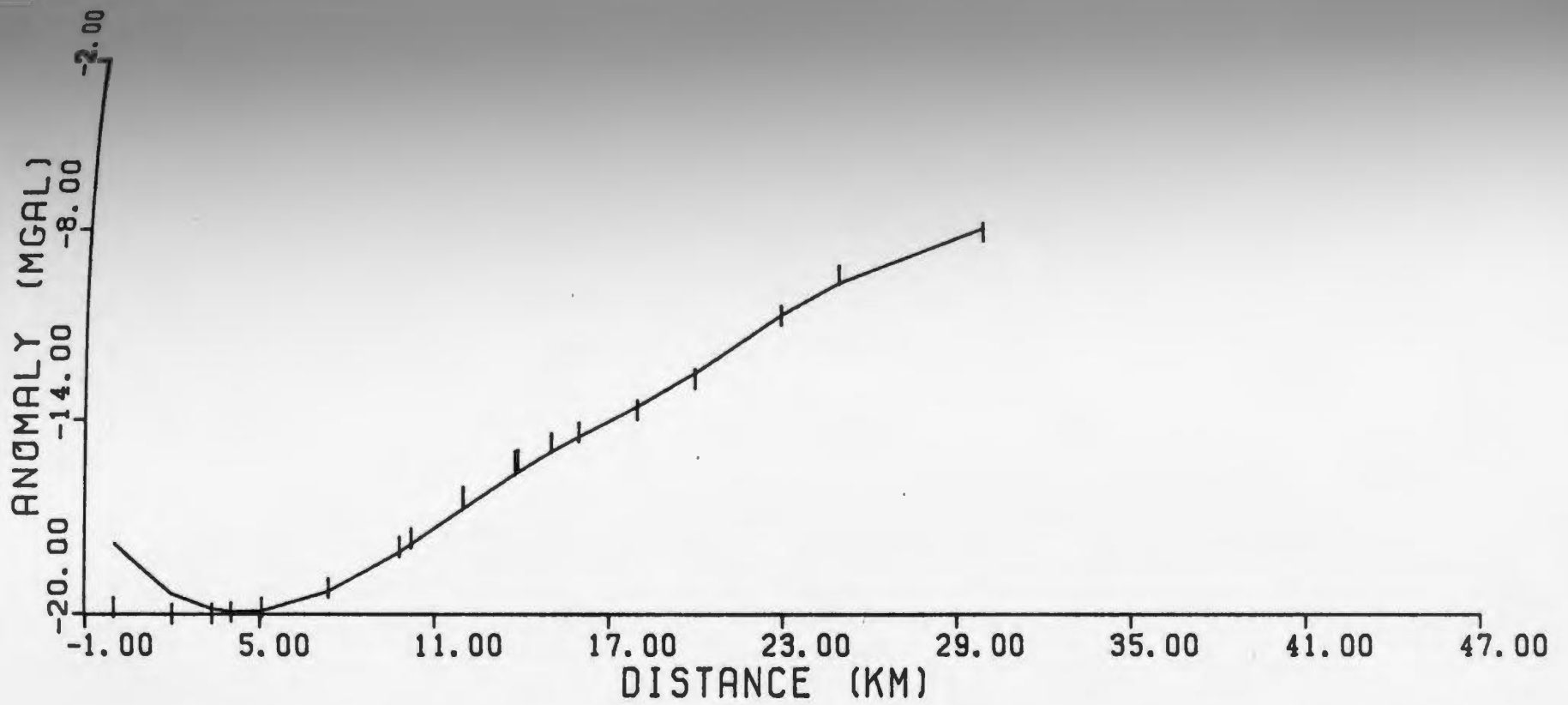


Figure 5.11d True and calculated models and gravity fit for an irregular polygon. Hatched body is the true model.

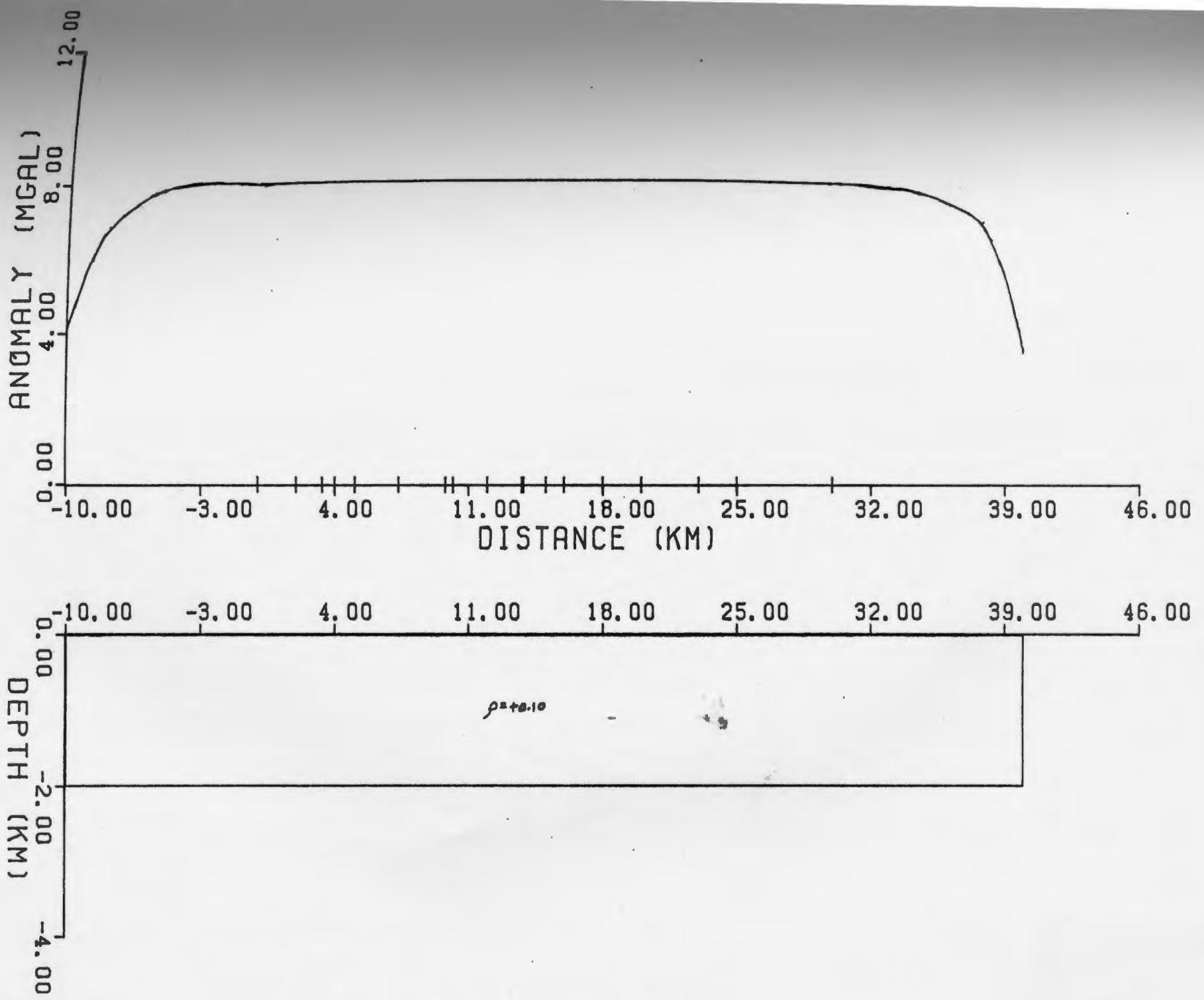


Figure 5.12a Gravity and wide block model.

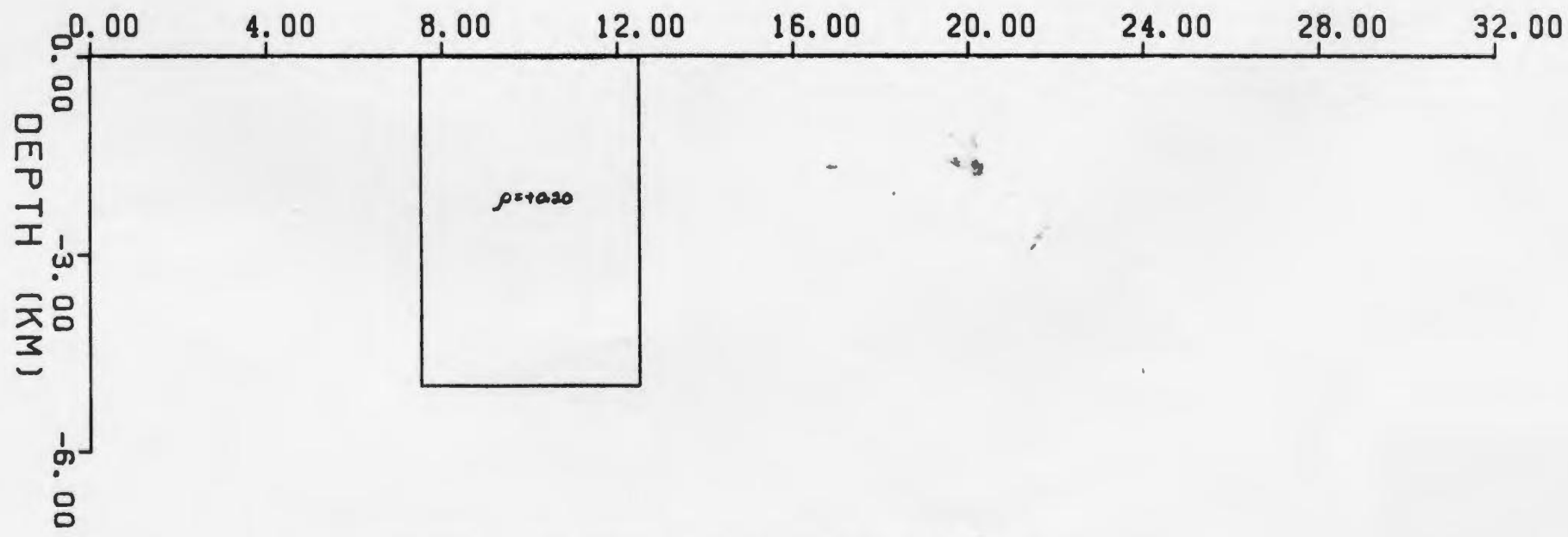
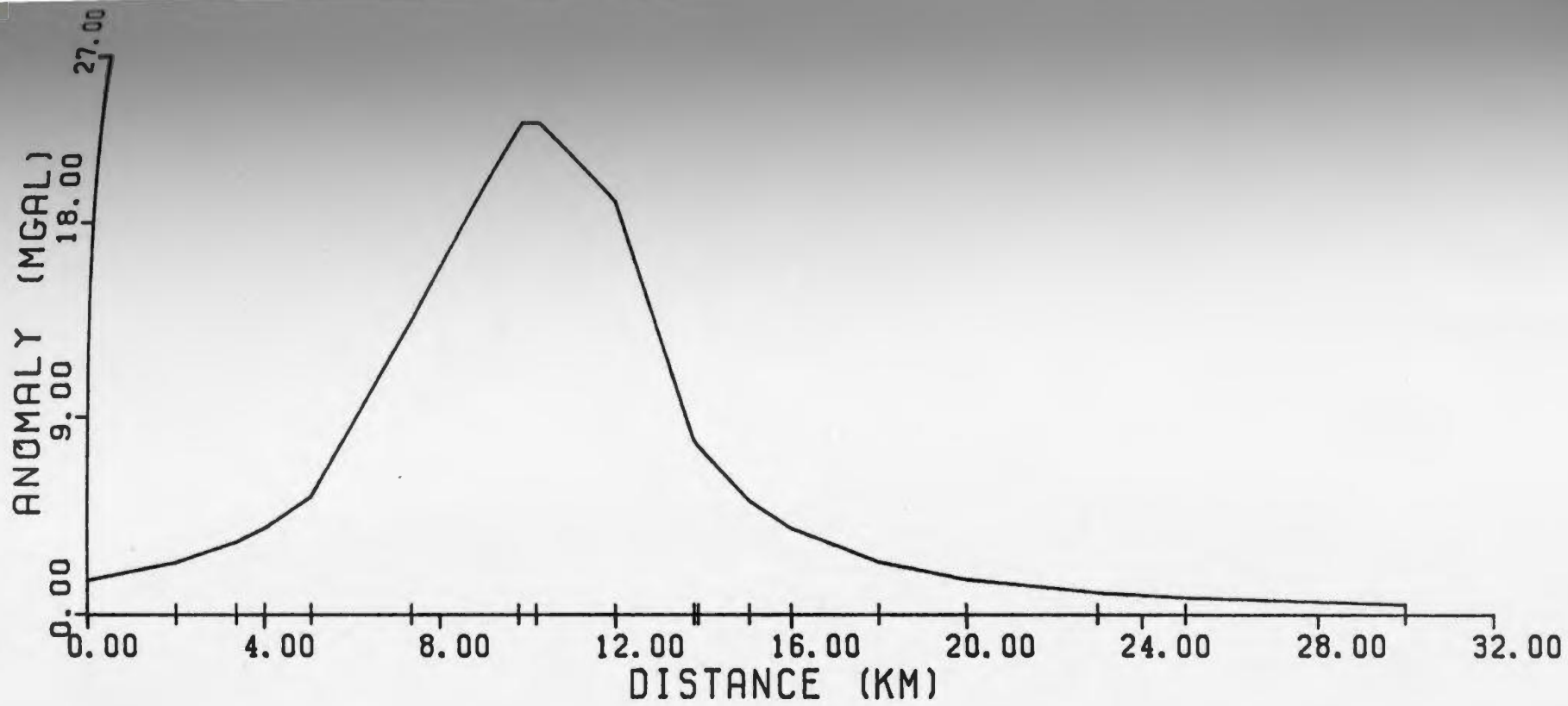


Figure 5.12b Gravity and narrow block model.

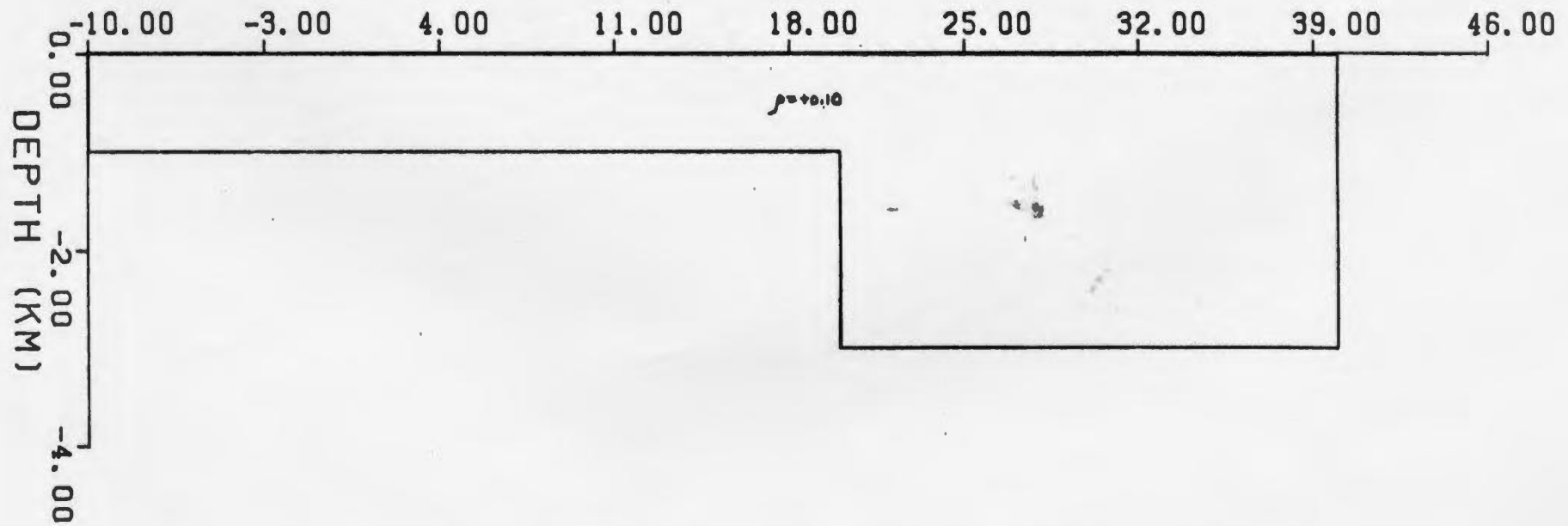
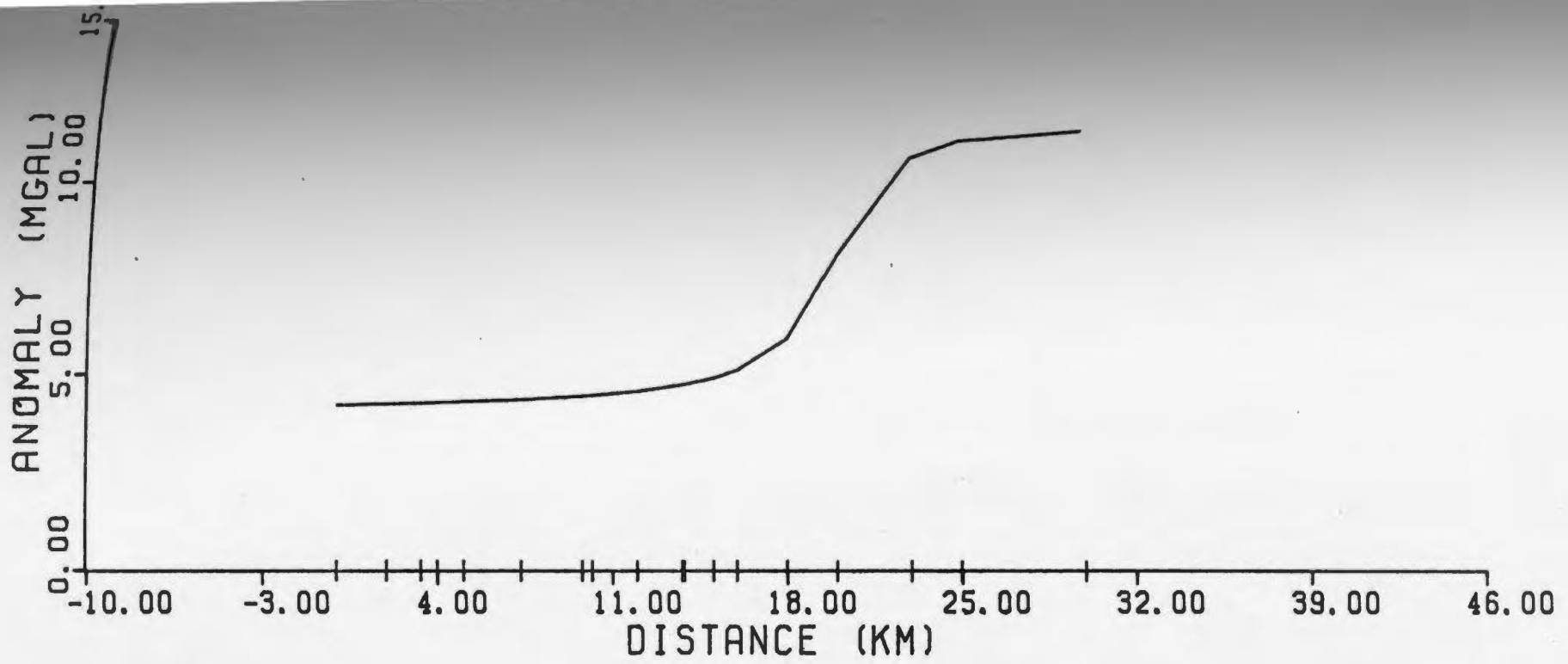


Figure 5.12c Gravity and basement step model.

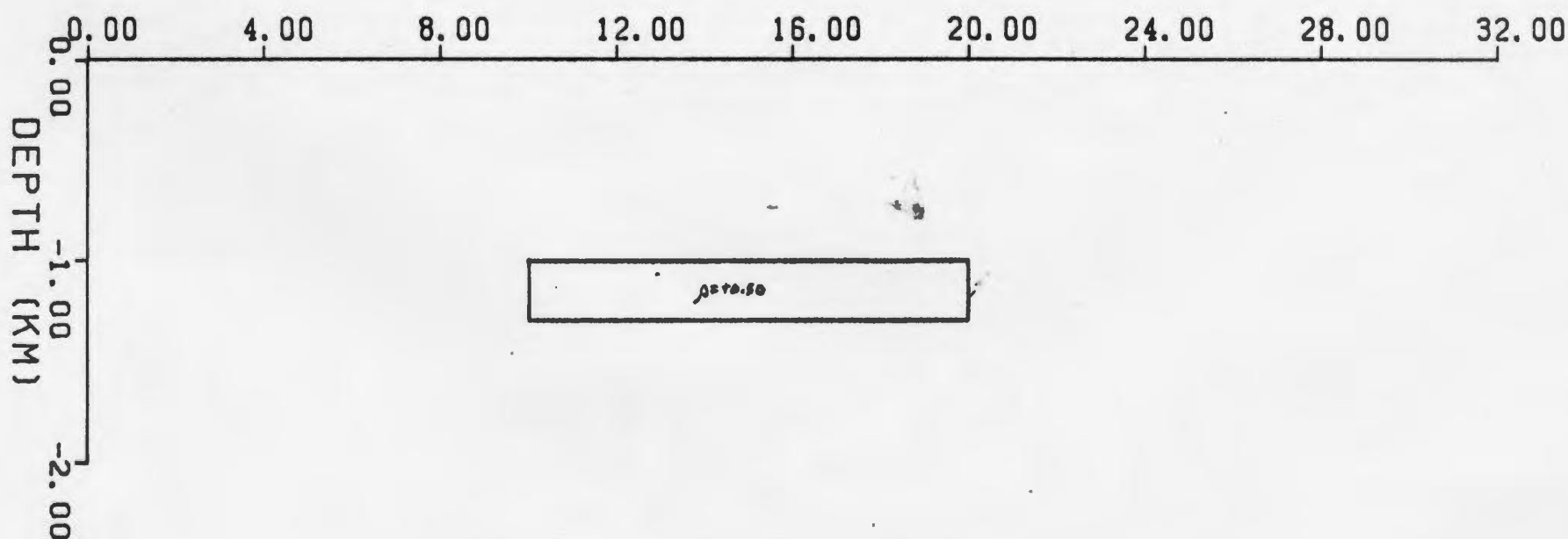
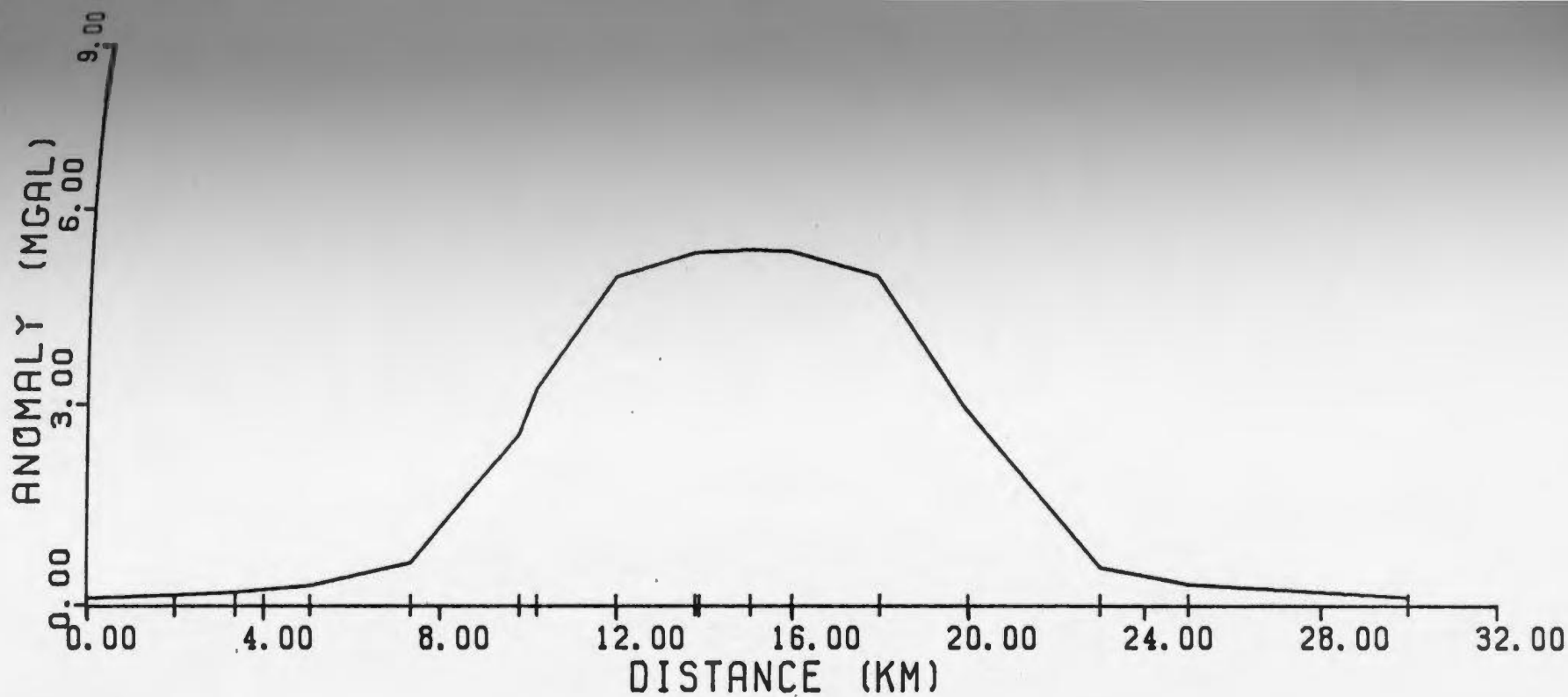


Figure 5.12d Gravity and buried body model.

inversion process (see Appendix 2.3 for a program listing). Four bodies were chosen for the inversion: a wide block, a narrow block, a basement step, and a buried block (see Figure 5.12). In all cases the density contrast and the depth of burial were assumed known. For the 2.5-D inverse, the strike-length was also known. Table 5.4 summarize the results of the testing. The testing consisted of generating gravity profiles for the bodies using the 2.5-D forward modelling program and the various strike-lengths, then inverting the profiles using both the 2-D and 2.5-D inversion programs. In Table 5.4 the last column, giving the calculated thickness at the center of the body, illustrates that the decrease in strike-length and the accompanying reduction in the amplitude of the anomaly caused the 2-D inverted models to become successively shallower for successively shorter strike-lengths. The 2.5-D inverse, however, produced models of the correct depth extent for all strike-lengths. It can be concluded from this test, that 2-D inversion is only valid for long strike-lengths, where the results were nearly identical to the 2.5-D results.

In conclusion, the 2.5-D gravity inversion program works very well if two of the more important parameters - density and strike-length - are well determined or known. Even if a range of densities and/or strike-lengths were used, the resulting set of possible solutions would do much to constrain the models derived from any forward modelling procedure. A proper determination of the depth of burial was found to be important when inverting the gravity anomaly due to a buried body.

Table 5.4: 2-D vs. 2.5-D inversion depths. All distances in kilometers.
 All densities in g/cm . (NA = not applicable)
 Body A is a wide block. Body B is a narrow block. Body C is
 a basement step. Body D is a buried body.

Body	Which Inversion	Density Contrast	Width	Thickness	Depth of Burial	Strike-length	Number of Iterations	Mean	Variance	Calculated Thickness (Center of body)	
A	2.5-D	+0.10	50	2	0	300	0.80	4	0.046	0.045	2.02
"	2-D	"	"	"	"	NA	0.80	4	0.046	0.045	2.02
"	2.5-D	"	"	"	"	100	0.64	5	0.029	0.037	2.02
"	2-D	"	"	"	"	NA	0.79	4	0.046	0.044	2.01
"	2.5-D	"	"	"	"	25	0.69	5	0.038	0.039	2.01
"	2-D	"	"	"	"	NA	0.74	4	0.043	0.041	1.95
"	2.5-D	"	"	"	"	5	0.70	7	0.075	0.035	1.99
"	2-D	"	"	"	"	NA	0.54	3	0.055	0.028	1.57
B	2.5-D	+0.20	5	5	0	300	8.99	76	-0.129	0.511	7.08
"	2-D	"	"	"	"	NA	8.88	77	-0.130	0.504	7.11
"	2.5-D	"	"	"	"	100	8.99	76	-0.130	0.511	7.08
"	2-D	"	"	"	"	NA	8.93	76	-0.138	0.505	7.08
"	2.5-D	"	"	"	"	25	8.90	76	-0.128	0.506	7.08
"	2-D	"	"	"	"	NA	8.89	71	-0.215	0.474	6.82
"	2.5-D	"	"	"	"	5	8.90	48	-0.108	0.511	5.73
"	2-D	"	"	"	"	NA	8.81	14	-0.186	0.482	3.41

Table 5.4: 2-D vs. 2.5-D inversion depths. All distances in kilometers.
 All densities in g/cm³. (NA = not applicable)
 Body A is a wide block. Body B is a narrow block. Body C is
 a basement step. Body D is a buried body.

Body	Which Inversion	Density Contrast	Width	Thickness	Depth of Burial	Strike-length	Number of Iterations	Mean	Variance	Calculated Thickness (Center of body)	
C	2.5-D	+0.10	50	1/3	0	300	3.20	3	0.071	0.183	1.03/2.99
"	2-D	"	"	"	"	NA	3.20	3	0.071	0.183	1.03/2.99
"	2.5-D	"	"	"	"	100	3.22	3	0.073	0.184	1.03/2.99
"	2-D	"	"	"	"	NA	3.18	3	0.070	0.182	1.02/2.99
"	2.5-D	"	"	"	"	25	3.44	3	0.099	0.192	1.01/2.96
"	2-D	"	"	"	"	NA	4.93	2	0.096	0.280	0.99/2.78
"	2.5-D	"	"	"	"	5	3.93	4	0.179	0.197	0.99/2.62
"	2-D	"	"	"	"	NA	3.85	1	0.130	0.208	0.88/1.79
D	2.5-D	+0.50	10	0.3	1.0	300	2.68	2	0.032	0.157	0.29
"	2-D	"	"	"	"	NA	2.69	2	0.032	0.157	0.29
"	2.5-D	"	"	"	"	100	2.70	2	0.032	0.158	0.29
"	2-D	"	"	"	"	NA	2.70	2	0.030	0.158	0.29
"	2.5-D	"	"	"	"	25	2.76	2	0.046	0.160	0.29
"	2-D	"	"	"	"	NA	2.73	2	0.019	0.160	0.28
"	2.5-D	"	"	"	"	5	2.27	3	0.075	0.128	0.28
"	2-D	"	"	"	"	NA	2.51	2	-0.036	0.146	0.23

5.6 Three-Dimensional Gravity Modelling

A 3-D gravity modelling program based on the formulation of Talwani and Ewing (1961) was written by M. Talwani in 1965. This original program was modified so that multiple body, 3-D gravity modelling could be done on the VAX11/780 computer at Memorial University. The Talwani and Ewing formulation uses a series of contours in the x-y plane at different depths to describe a body. This method was chosen because it can describe bodies of arbitrary shape, making it more suitable to the description of the subsurface geology of the Bay St. George Subbasin, and it is compatible with the 3-D magnetics program described in Section 5.7.

The program performs an analytic integration in the x-y plane around each polygonal laminae describing the contours of the body at depth z_1 to get a value V_1 , which is the gravity contribution due to laminae l . Once the analytic integration for each contour is complete, a numerical integration in z is performed by interpolating parabolas on a V_1-z_1 plane as shown in Figure 5.13 (Talwani, 1965a). The parabolas are interpolated with three points defining each parabola. The areas between these parabolas and the z-axis give the value of the integral. In areas between two V_1 's that have segments of 2 parabolas through them, the arithmetic mean of the areas between each segment and the z-axis is taken as the integral value. The final summation of all areas between all parabolic segments and the z-axis gives the value of the anomaly.

The input data for the program consists of the x-y coordinates of each gravity station and the value of the anomaly at each station, followed by the lamina coordinates, depths, and densities of each

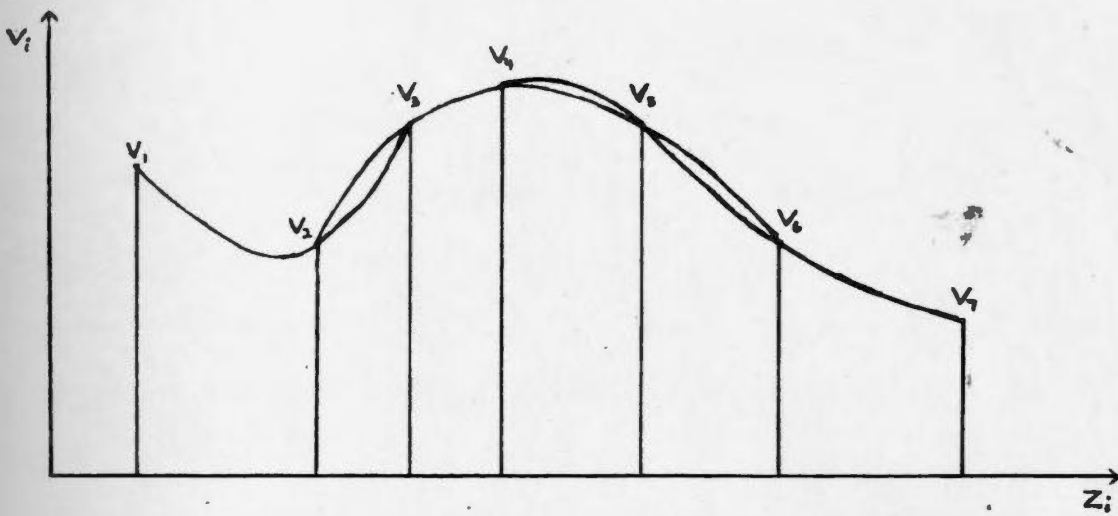


Figure 5.13 Graphical representation of the numerical integration for 3-D gravity calculations.

body. All anomalies are in milligals, all distances in kilometers, and all densities in g/cm^3 . The output file contains the x-y coordinates of each gravity station and the observed, calculated and residual gravity. An analysis of the output can be used to alter the model until a sufficient fit between the calculated and observed anomalies is obtained.

Test data for the Caryn Mount were provided in Talwani (1965a), along with output from his 3-D program. These data were used in the modified program and the results are identical to Talwani's to the 4th decimal place. Another test was performed using a sphere described by contours at 0.5 km intervals. The results, shown in Table 5.5, matched theoretical values to within 2%. From the results of these tests it was concluded that the 3-D gravity modelling program was working and could be used to interpret data from the Bay St. George Subbasin.

5.7 Three-Dimensional Magnetic Modelling

A 3-D magnetic modelling program was written based on the formulation of Talwani (1965b) (see Appendix 2.5 for a program listing). This magnetic method is similar in procedure to the 3-D gravity program described previously, and as the bodies are described in the same manner, going from a 3-D gravity to a 3-D magnetic model is a simple procedure. The program calculates the vertical and horizontal field components, and the total field at each observation point for all bodies being used.

Table 5.5 Sphere test results for 3-D gravity program.

x	Theoretical Value	Calculated Value	Difference	%
-10.0	0.074	0.073	0.001	1.35
-5.0	0.423	0.415	0.008	1.81
-4.0	0.670	0.660	0.011	1.64
-3.0	1.098	1.080	0.018	1.64
-2.0	1.788	1.758	0.030	1.68
-1.0	2.655	2.602	0.053	1.99
0.0	3.104	3.045	0.059	1.90
1.0	2.655	2.601	0.054	2.00
2.0	1.788	1.756	0.032	1.79
3.0	1.098	1.078	0.020	1.82
4.0	0.670	0.659	0.012	1.79
5.0	0.423	0.415	0.008	1.81
10.0	0.074	0.073	0.001	1.35

The input data for the program consists of the total field strength at that part of the Earth's surface, the declination and inclination of the Earth's magnetic field in that area, the x-y coordinates and observed anomaly at each station location, and the coordinates and magnetic susceptibilities of the laminae for each body. All anomaly values are in nanoteslas, all distances in kilometers, and all susceptibilities are in cgs units. The output file contains the x-y coordinates of each observation point, along with the observed, calculated, and residual total field magnetic anomalies. As in the gravity case, the 3-D model can be adjusted based on the output from the magnetics program until an acceptable fit to the observed data is obtained.

Test data from the Caryn Sea Mount was provided in Talwani (1965b). This data was used to test the 3-D magnetics modelling program. Figure 5.14 shows the observed and calculated fields for the Caryn Sea Mount for a total field intensity of 53,800 nanoteslas, a declination of 14° W, and an inclination of 69.2° as suggested by Talwani.

Another test was done using a sphere of radius 2 km with contours 0.5 km apart. Table 5.6 shows the theoretical and calculated values for a sphere with $D = 0^{\circ}$, $I = 45^{\circ}$, and $F = 50,000$ nT. These results are quite close, and it was concluded that the 3-D magnetic program worked and could be used to help interpret the Bay St. George Subbasin. This result is not as close as the 3-D gravity result of the previous section because the 3-D magnetic modelling program is more sensitive than the gravity program, i.e. the approximation of the sphere was not close enough and more laminae would have improved the results.

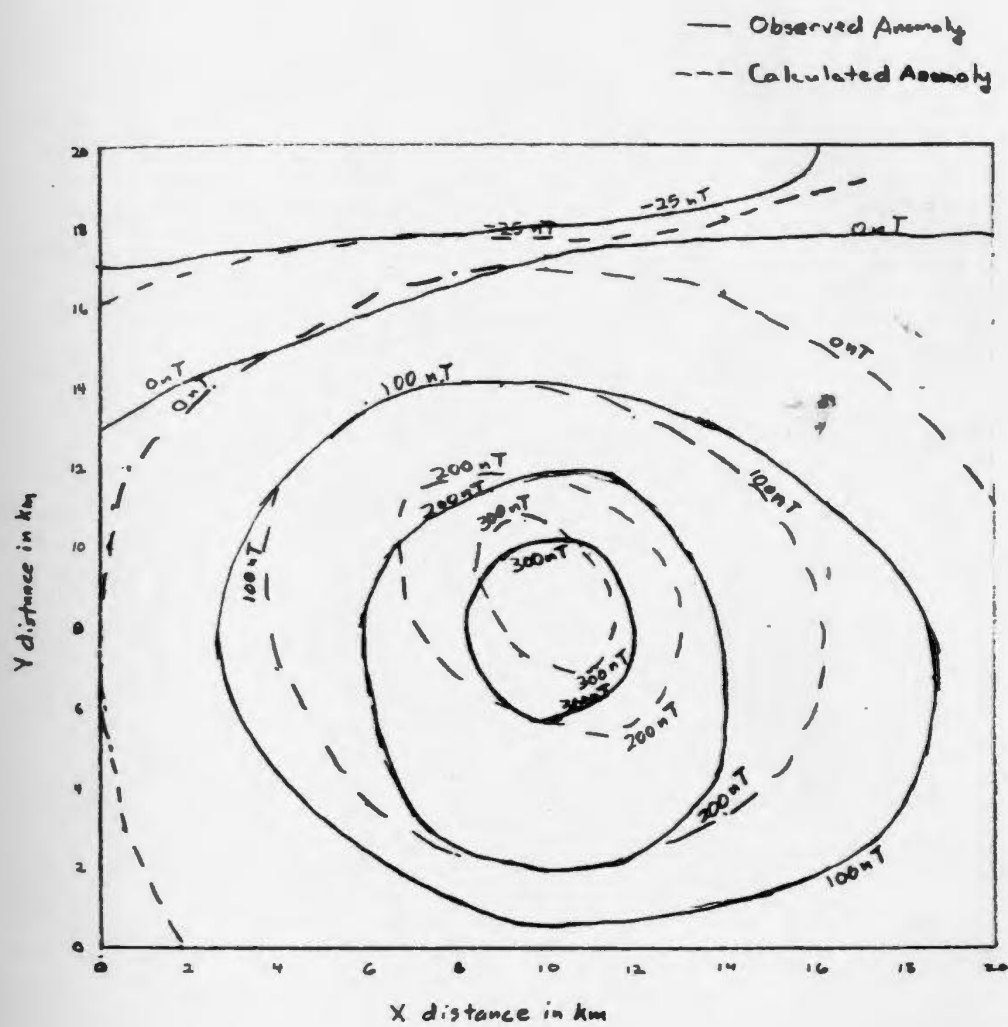


Figure 5.14 Observed and calculated magnetic anomalies for the Caryn Sea Mount.

Table 5.6: Sphere test results for 3-D magnetics program.
Values are total field anomalies.

x	Theoretical Value	Calculated Value	Difference	%
-10.0	-0.95	-0.86	-0.09	-9.58
-5.0	-2.27	-2.50	0.23	10.13
-4.0	-25.06	-27.03	1.97	7.86
-3.0	-43.64	-45.78	2.14	4.90
-2.0	-62.89	-65.15	2.26	3.59
-1.0	-42.15	-44.20	2.05	4.86
0.0	61.71	63.89	2.18	3.54
1.0	147.53	151.03	4.50	3.05
2.0	133.98	138.01	4.03	3.01
3.0	87.27	89.80	2.53	2.90
4.0	51.72	53.83	2.11	4.08
5.0	30.65	32.44	1.79	5.84
10.0	3.88	3.60	-0.28	-7.22

Chapter 6: Interpretation and Results of Gravity and Magnetic Modelling

6.1 Introduction

This chapter discusses the results of the gravity and magnetic modelling and gives a geophysical interpretation of the data. A qualitative interpretation of the original data and the residual maps (see Section 2.3) was done first in order to delineate faults and determine the subsurface extent of the various anticlinal and synclinal features in the study area. Next, a study of the surface effects of possible buried magnetite lenses was done to determine their significance in 3-D modelling.

The 2.5-D gravity inversion program discussed in Section 5.4 was used on profiles across the subbasin in order to determine the basement topography and the thickness of the sediments. The resulting 2.5-D model was used as an initial model for 3-D modelling. Once a good fit between the calculated and observed gravity was attained, a magnetic model was done on to check the validity of the 3-D gravity model. Finally, an interpretation of the model results was undertaken and compared with the geology according to Knight (1983).

6.2 Qualitative interpretation of the gravity and magnetic maps

Before the actual modelling took place, a qualitative interpretation of the gravity and magnetic maps was undertaken. This determined the subsurface extent to the various anticlines and synclines in the area, and delineated faults. The gravity and magnetic maps discussed in this section can be found in Chapter 2.

In the Bouguer anomaly map (Figure 2.2), five major features of the study area can be easily discerned: The Flat Bay Anticline, the Barachois Synclorium, the St. Davids Syncline, the Shoal Point Fault, and the Long Range Fault (see Chapter 3 for a complete discussion of the geologic terms used here). The Flat Bay Anticline is indicated by the relative gravity high in the north-central map area ('A' in Figure 2.2). The Barachois Synclorium is outlined by the -16 mGal contour line ('B' in Figure 2.2). St. Davids Syncline is indicated by the deep low near the coast ('C' in Figure 2.2). The Shoal Point Fault can be roughly traced by a line parallel to the contours at 'D' in Figure 2.2. The tightly bunched contour lines in the eastern part of the study area locate the Long Range Fault.

At location 'E' in Figure 2.2, there is a bowing of the contour lines, indicative of a fault that isn't shown on the geology map. The Crabbes Brook Fault appears to have little expression on the Bouguer anomaly map. This is probably due to its close proximity to the Flat Bay Anticline and the Barachois Synclorium, and these strong high and low gravity features may mask the expression of the Crabbes Brook Fault.

The 5th-order residual gravity map, obtained via trend analysis as described in Section 2.3, is shown in Figure 2.6 and elucidates the conclusions reached from Figure 2.2. The letters 'A' through 'E' represent the same structures on both maps. The fault at 'E' is better delineated on the residual map, and appears to be continuous across the entire basin. An apparent basement high at 'F' appears to be bounded by the Shoal Point Fault ('D') and another fault (G), both trending northeast. Another fault is delineated at 'H' on the residual map and is approximately at the position of a fault on the geology map (Figure 3.1). Finally, the high at 'I' is the Anguille Anticline.

The 25-point averaged aeromagnetic map of the study area (Figure 2.5) reveals only two features: the Flat Bay Anticline and Mt. Howley. The Flat Bay Anticline is outlined by the high region around 'A' in Figure 2.5, and Mt. Howley appears as a kink in the northeasterly trending contour lines at 'B'. The basin area is shown clearly as an area of smoothly varying contour lines trending approximately southwest-northeast. Faults within the basin, for example the Crabbes Brook Fault, have little apparent magnetic expression, suggesting that these faults may not extend into the magnetic basement.

The 5th-order residual magnetic anomaly map obtained by trend analysis (see Section 2.3) and shown in Figure 2.7 shows other features not seen in Figure 2.5. One unusual feature is the relative high located between the two zero level contours ('A1' and 'A2' in Figure 2.7). This region doesn't correlate well with either the geology or gravity maps, and could indicate a zone of higher magnetic susceptibility in the basement. The other high region, at 'B', is

caused by sources just outside the subbasin. The subbasin can be seen as the negative area to the west, including the positive area between 'A1' and 'A2'. An apparent fault at 'C' (Figure 2.7) matches the location of the assumed fault marked 'E' in both Figures 2.2 and 2.6.

6.3 Surface effects of possible basement lenticular magnetite deposits on gravity and magnetic interpretation

As mentioned in Chapter 3, there are lenticular magnetite deposits located at Indian Head and Steel Mountain (Heyl and Ronan, 1954, Baird, 1954). An analysis of the strikes and dips given for the lenses in both areas indicate a strike of $N70^{\circ}W$ and an approximate dip of $25^{\circ} NE$.

In order to test the gravity and magnetic effect of magnetite lenses, a lens 200 m long, 50 m wide, and 10 m thick representing the largest probable lens that would be found in the basement, was modelled. (Heyl and Ronan, 1954, Baird, 1954). For both the gravity and magnetic tests, the lens was buried at six depths ranging from 0.0-0.5 km and the respective effect calculated.

For the gravity test a density of 5.12 g/cm^3 (Telford, et.al., 1976, p. 28) was used, giving a density contrast of 2.40 g/cm^3 with the basement. The maximum effect was only 0.45 mGal, which is less than the uncertainty in the gravity observations. Therefore, it was assumed that magnetite lenses of comparable size in the basement would show no surficial gravity effects.

For the magnetics test, a magnetic susceptibility of 0.50 cgs units was used (Telford, et.al., 1976, p. 121). The maximum effect was at the 0.0 km depth and was ~ 82000 nT. However, this effect diminished rapidly with depth, so that at 200 m the effect was only 95 nT, indicating that the effect of the lens would only be noticeable if it were very close to the surface. Therefore, as with the gravity case, the magnetic effects of magnetite lenses in the basement would be minimal, and can be ignored in the modelling procedure.

6.4 Results of the 2.5-D gravity inversion

The 2.5-D gravity inversion program described in Section 5.4 was used to obtain an initial thickness estimate of the sedimentary section and to determine the relative basement topography in the study area. A series of gravity profiles across the area were inverted by the program (see Figure 6.1). The profiles were generated by using a transection program on the data, and all stations within 1 km of each profile line were included. There were 16 profiles across the geologic strike (numbered 1-14, 1S, and 2S in Figure 6.1) and four profiles along the geologic strike (numbered 1B-4B in Figure 6.1). A total of 143 different stations were used in all the profiles.

For each profile, a model was calculated using a density contrast of -0.18 g/cm^3 between the sediments and basement as calculated in Section 4.4. Since this density contrast is negative, stations with positive anomalies were removed from the profiles leaving 65 % of the original 236 stations. Also, a strike-length for each body in the Y direction had to be assigned. For the 16 profiles across the geologic

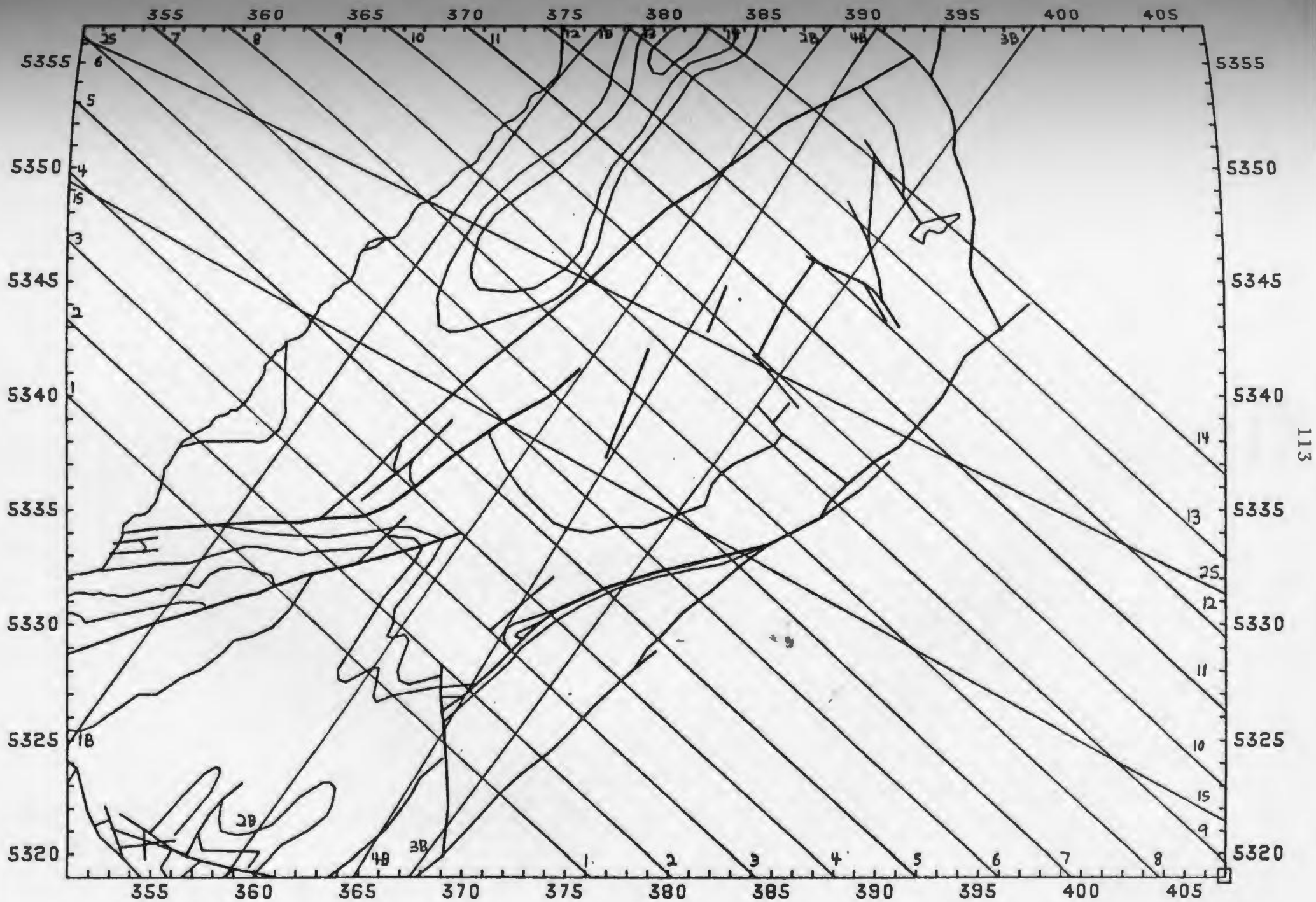


Figure 6.1 Profile locations for 2.5-D modelling. Faults are the darker lines. (scale = 1:250000)

strike, an overall strike-length of 60 km was used. The other profiles used a 30 km strike-length. These two strike-lengths were measured from the center of the study area, therefore all the calculated models are asymmetric. The strike-lengths were estimated by using a geology map. Appendix 3.1 lists the Y strike-lengths, the sum of the squares of the difference between the calculated and observed gravity (ϵ), the number of iterations, the mean, and the standard deviation of each resulting model. Plots of the models are shown in Appendix 3.2. The calculated thickness of sediments at each station was plotted (Figure 6.2), with the depth estimates of stations that were shared between profiles being averaged. The depth estimates at the shared stations were within 0.5 km of each other in most cases, with only a few areas having cross-over differences of greater than 1.0 km. After the removal of the effects of the known salt and gypsum deposits (Section 3.4) and a proposed salt diapir at 'D', a contour plot of the inferred basement topography was drawn (Figure 6.3). The removal of the evaporite bodies' effects was done by smoothing the contours near the deposits by ignoring the deep apparent sediment thicknesses associated with these deposits and contouring the rest of the points.

In Figure 6.3, large features, such as the Flat Bay Anticline and the Barachois Synclinorium, are easily identified (see Figure 3.1). St. Davids Syncline is evidenced by the 8 km sediment thickness near the coast. Other sediment thicknesses, marked 'A', 'B', and 'C' in Figure 6.3, are not readily apparent from the surface geologic expression. 'A' is an apparent basement rise which could be a northeastern extension of the Anguille Anticline. The basement low at 'B' could be partly, but not entirely, explained by the Fischells Brook salt diapir. The other feature, a basement low at 'C', has no apparent surficial

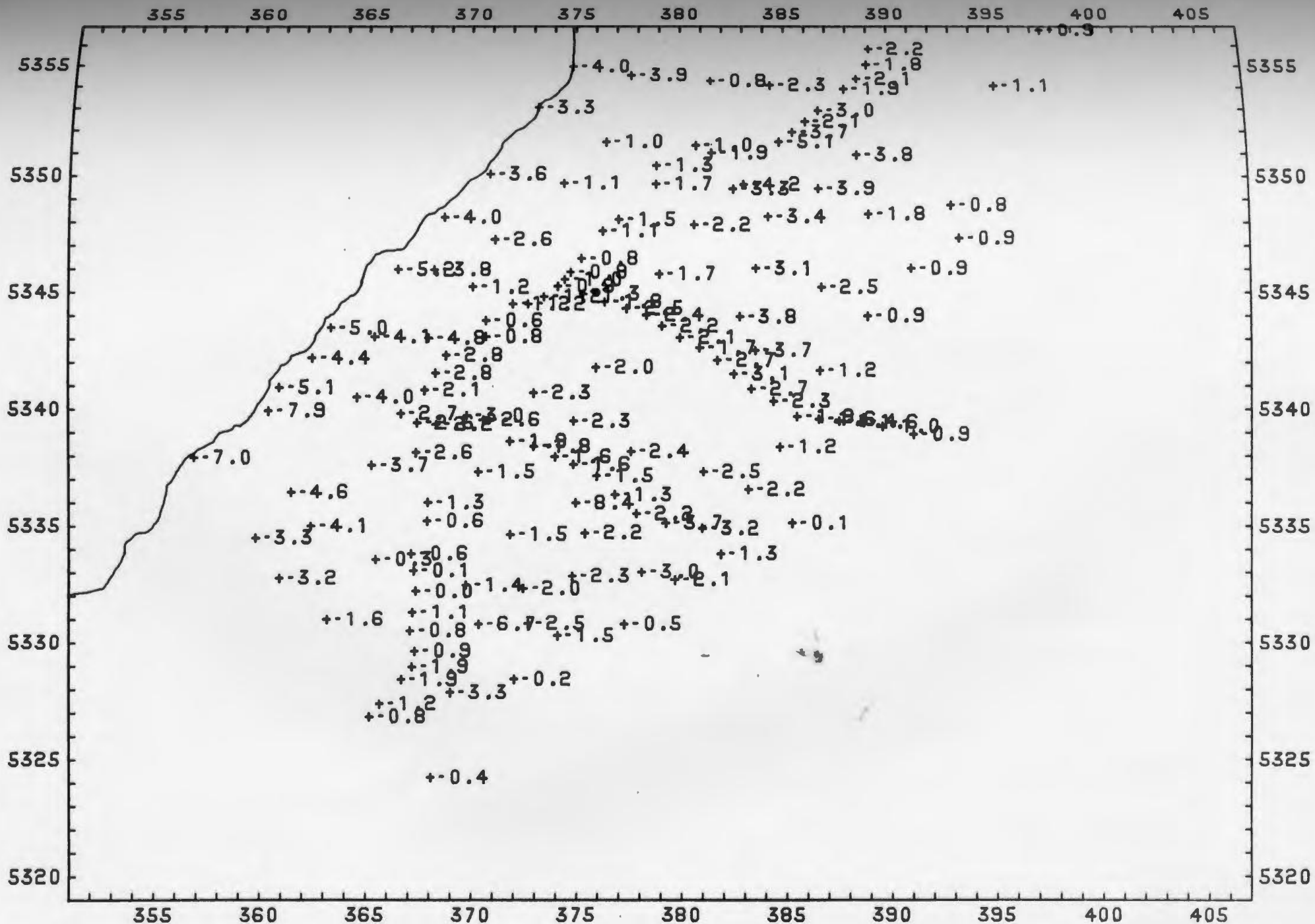


Figure 6.2 Posting of inferred sediment thicknesses from 2.5-D modelling. (scale = 1:250000)

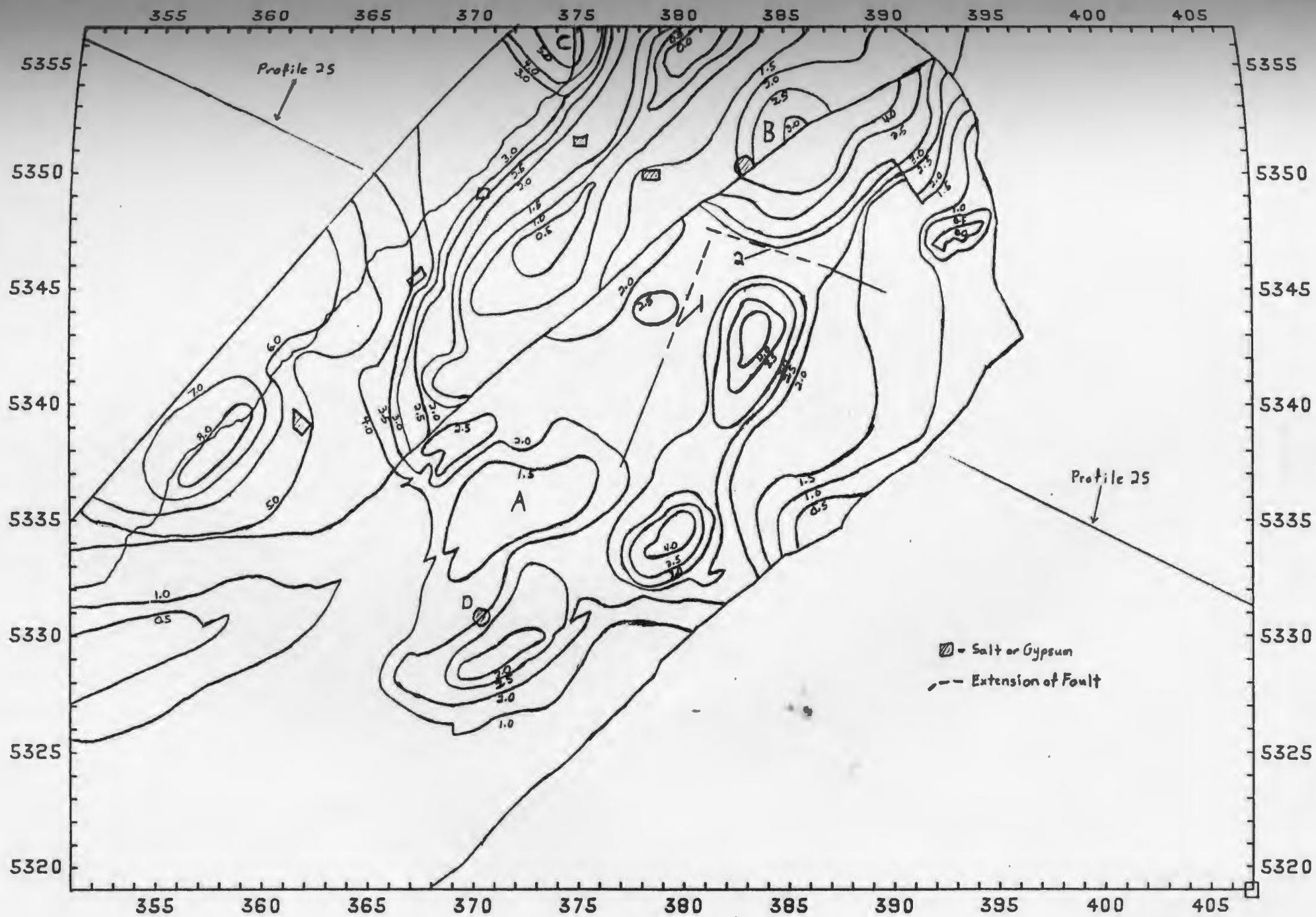


Figure 6.3 Inferred basement topography map from 2.5-D modelling. Contours = depth in km. scale = 1:250000)

relationship. However, two minor faults, marked '1' and '2', can be extended as shown in Figure 6.3, and thus become major faults within the Barachois Group area.

According to the 2.5-D model, the Crabbes Brook Fault has an apparent downthrow to the west of 1.5-2.0 km at the northern end, reduced to 0.5 km near the Anguille Anticline. The Shoal Point Fault (see Figure 6.3) has an apparent downthrow to the north of 4.0 km. The Barachois Synclinorium is well defined by a series of north-northwesterly trending basement lows with an average depth of 4 km. The Flat Bay Anticline is easily seen just to the west (Figure 6.3). The average thickness of the sediments in the Brow Pond area is 1.5 km (Figures 1.1 and 6.3). The thickness of the Anguille strata in the southern part of the study is not well defined due to a scarcity of data points in the area.

In conclusion, the 2.5-D inversion program gave an estimate of the basement topography, sediment thickness, and fault and salt deposit locations. Features 'A', 'B', and 'D' appear to be real structures, as there are possible geologic explanations for them. 'C', however, is at the edge of Profile 12, and may be only a invention of the modelling. The fault identified on both the gravity and magnetic maps ('E' in Section 6.2) was not seen because the profiles were roughly parallel to it, and the along strike profiles didn't have a set of data points near enough to it. Most other features identified on the maps did appear in the 2.5-D model.

6.5 Results of 3-D gravity and magnetic modelling

After the 2.5-D inversion model was completed, it was digitized and used as an initial model for the 3-D gravity modelling program (described in Section 5.6). Since the determination of sediment thickness was the foremost consideration, it was decided that only bodies representing the sedimentary section would be used, with all sedimentary block densities being compared to the basement density of 2.72 g/cm^3 as defined in Section 4.4. The measured density of the basement is therefore assumed to be approximately equal to the mean regional density. Since all density contrasts were negative, the stations with positive Bouguer anomalies were eliminated, leaving 204 out of the original 236 gravity stations. All the eliminated stations were either outside or close to the edge of the sedimentary area, and therefore contribute little to the modelling process.

As a first test of the validity of the 2.5-D model, a 3-D model was done using a single sedimentary body with a density contrast of -0.18 g/cm^3 - the same as that used in the 2.5-D modelling above. The results were good, with 64% of the gravity differences being $\leq 4.0 \text{ mGal}$ and $41\% \leq 2.0 \text{ mGal}$. Out of 204 stations, only 20 had differences $> 5 \text{ mGal}$. Since the effect of salt bodies was ignored, the correspondence between the calculated and observed gravity values is excellent (see Figure 6.4).

The area was next divided into seven different sedimentary bodies and a series of salt and gypsum deposits based upon the geology discussed in Chapter 3. The boundaries of the sedimentary blocks, shown in Figure 6.5, are based on surface geologic contacts between

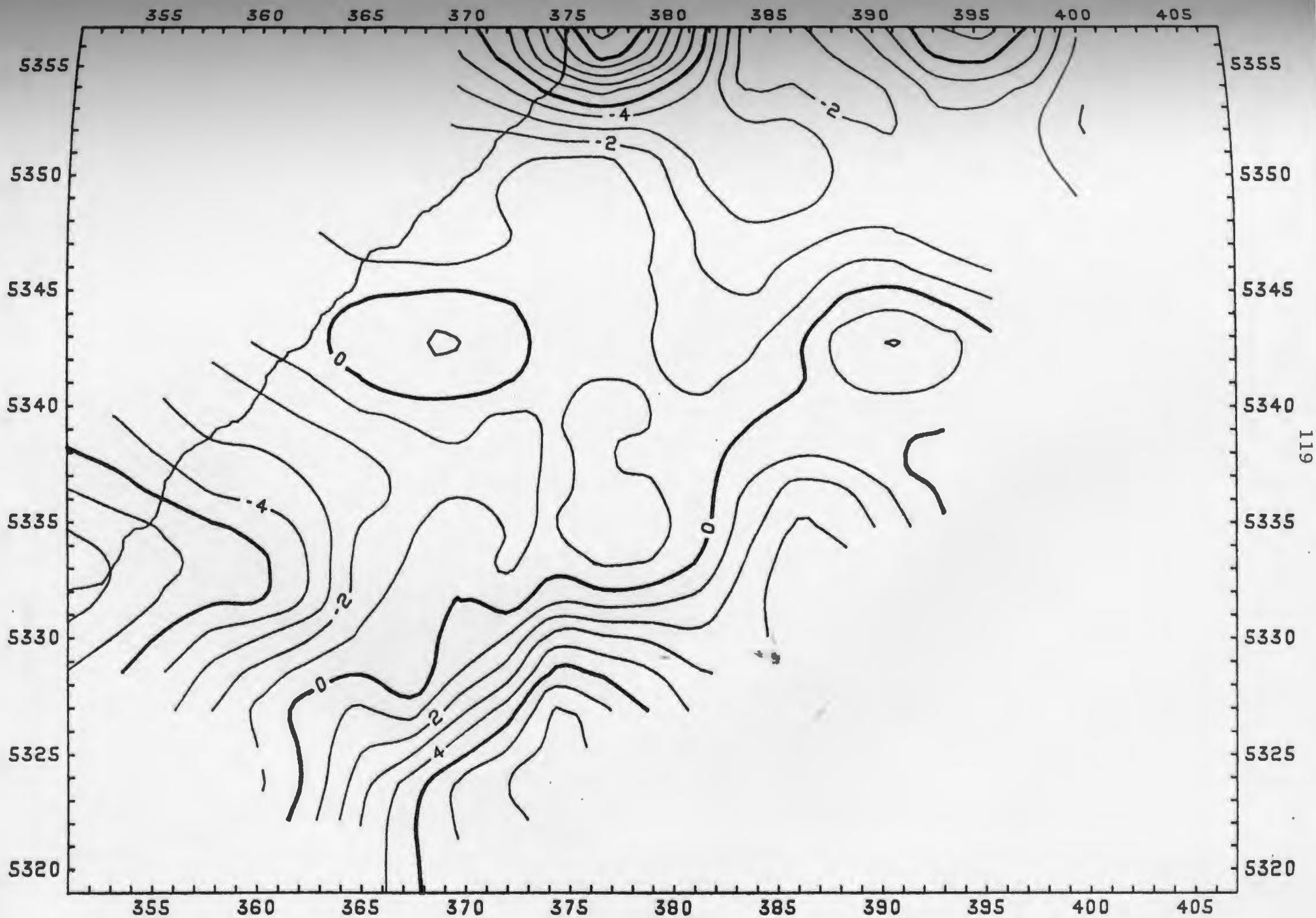


Figure 6.4 Difference in calculated and observed gravity for model 1 using a -0.18 g/cm^3 density contrast. Contour interval = 1 mGal. (scale = 1.250000)

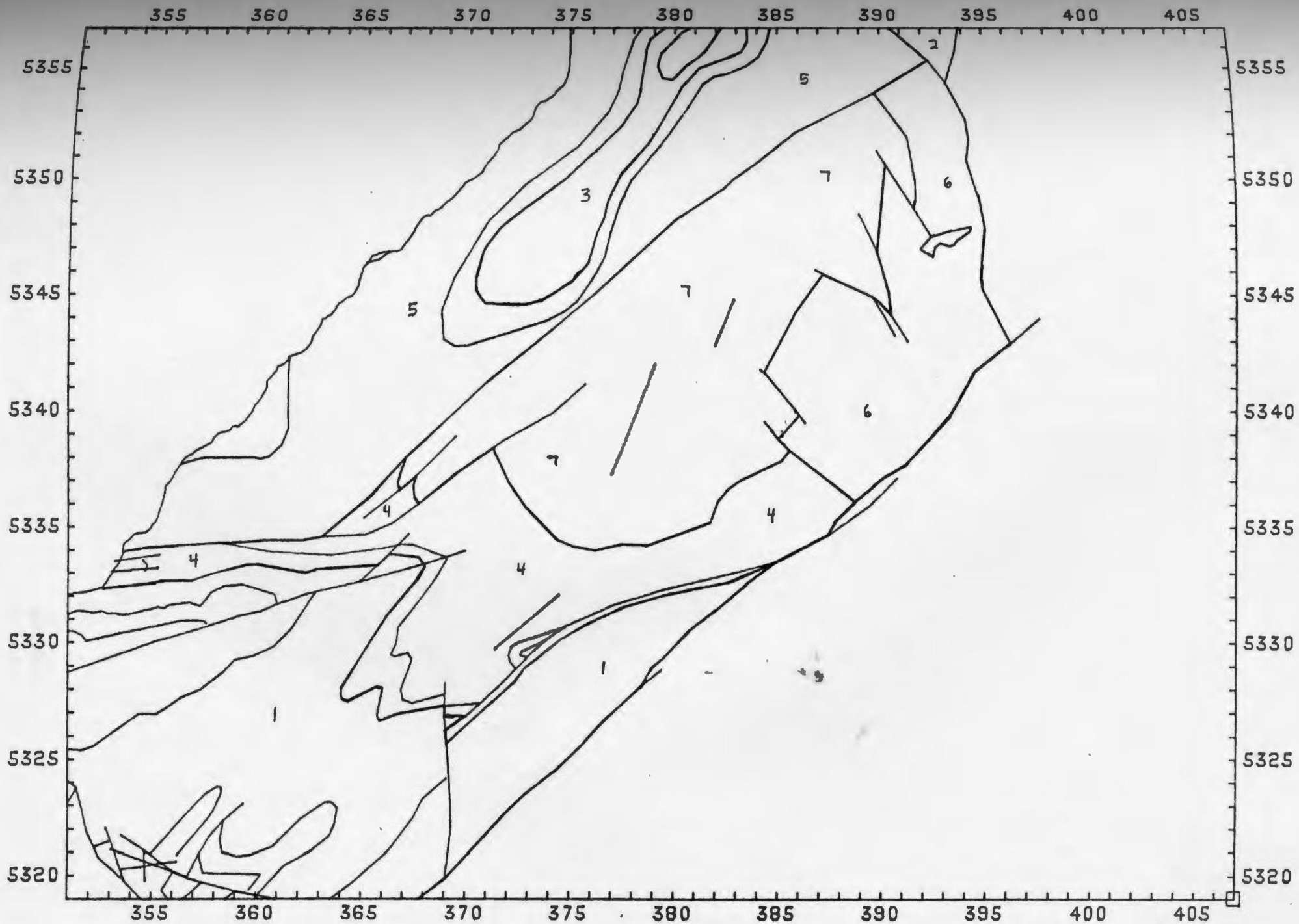


Figure 6.5 Sedimentary block boundaries used in 3-D gravity modelling. (scale = 1:250000)

Table 6.1: Density contrasts for 3-D modelling.
Numbers identify bodies shown in Figure 6.5.

Body	Density Contrast (g/cm^3)
Gypsum deposits	-0.44
St. Fintans Salt	-0.35
Robinsons Salt	-0.21
Fischells Salt	-0.44
Suspected Salt	-0.18
Anguille Group (1)	-0.09
Fischells Conglomerate (2 & 3) (Sheep Brook and Flat Bay Anticline)	-0.40
Robinsons River Formation (4)	-0.25
Jeffreys Village Member (5)	-0.25
Brow Pond Lentil (6)	-0.14
Barachois Group (7)	-0.23

the various lithologies. Density contrasts for each body resulted from a weighted averaging of the densities of the differing lithologies which made up each individual body. The averaging was done as described in Section 4.3, with the total thickness being based on the results from the 2.5-D inversion and not on the geologic estimates. A summary of these density contrasts can be found in Table 6.1, along with the assumed density contrasts of the various salt and gypsum deposits.

The calculated gravity based on the model taken from the 2.5-D model is shown in Figure 6.6, and the difference in gravity between the calculated and observed fields (observed-calculated) is shown in Figure 6.7. From the difference map, it is obvious that the Barachois Block should be thickened somewhat and the Jeffreys Village Block should be thinned. Also, it became apparent that the stations marked 'a'-'d' were either a) bad data points, or b) new salt or gypsum deposits. The first two points, 'a' and 'b', exhibit very local and incongruous anomalies. In these cases the anomaly was centered at that point and the effect was not witnessed at any of the adjacent points. In fact, these anomalies were so different from those around them that it seemed certain that they were bad data points, and therefore were eliminated. Points 'c' and 'd', however, exhibit effects on surrounding points, leading to the conclusion that the associated anomalies are real, and therefore these were considered to be probable salt or gypsum deposits. It was decided that since they do produce a fairly large effect, that they are likely salt deposits, because it was discovered during the running of the first model that the gypsum deposits used made virtually no difference to

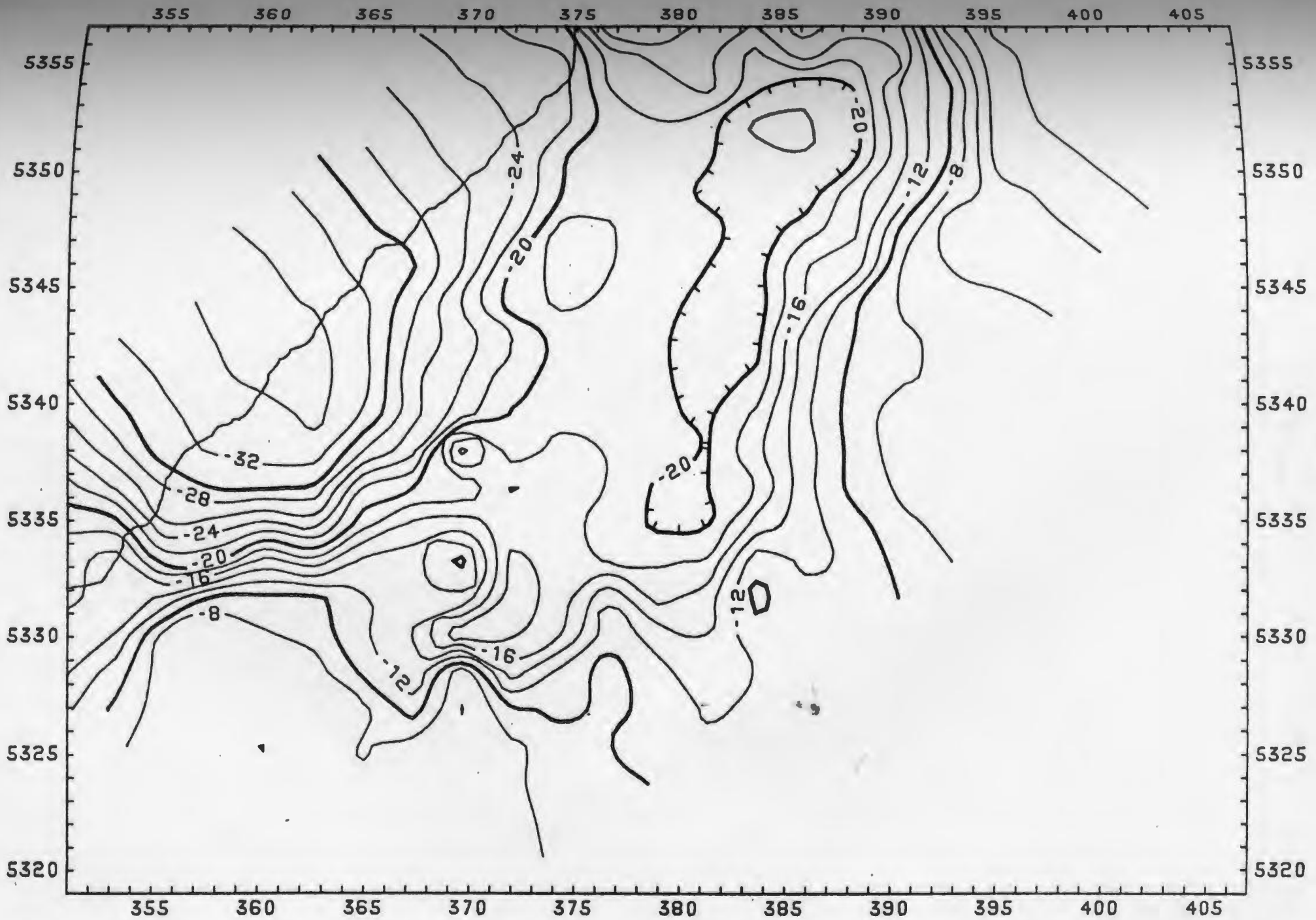


Figure 6.6 Calculated gravity for model 1. Contour interval = 2 mGal.
(scale =1:250000)

the model, as the maximum anomaly was 0.23 mGal. The use of salt deposits at these points effectively eliminated the differences in calculated and observed gravity in those areas. Finally, major revisions in the Anguille area were necessary as expected because of the lack of control from the 2.5-D model.

Adjustments were made to the first gravity model by using the infinite slab formula (Equation 5.2) to calculate a change in the thickness based on the difference in calculated and observed gravity at all the stations used in the modelling. In this manner, new depths to basement were calculated, then plotted and contoured, resulting in a new model. Successive adjustments to the results of additional models led to the final model - model 4 (Figure 6.8).

Figure 6.9 shows the gravity difference map for model 4. The agreement is good with the exception of the area near the St. Davids Syncline, and near the new salt deposit at 'A' in Figure 6.9. An additional 200 m of salt at 'A' would correct the corresponding gravity difference. The St. Davids Syncline sediments still need to be from 0.5-1.0 km thinner. Otherwise, all differences are < 4 mGal, with most (71%) being < 2 mGal.

The faults delineated by 2.5-D modelling are still present in model 4, but another major fault ('B' in Figure 6.8) is necessary to explain the 'break' in the Barachois Synclinorium at this point. This is in the same location one would infer from the magnetics and residual gravity maps (Section 6.2). The basement high at 'C' is probably a buried extension of the Anguille Anticline as postulated earlier, but it could also be the result of block faulting. The relative basement low at 'D' (Figure 6.8) is a northward extension of the Barachois Synclinorium on the upthrown side of the Crabbes Brook Fault.

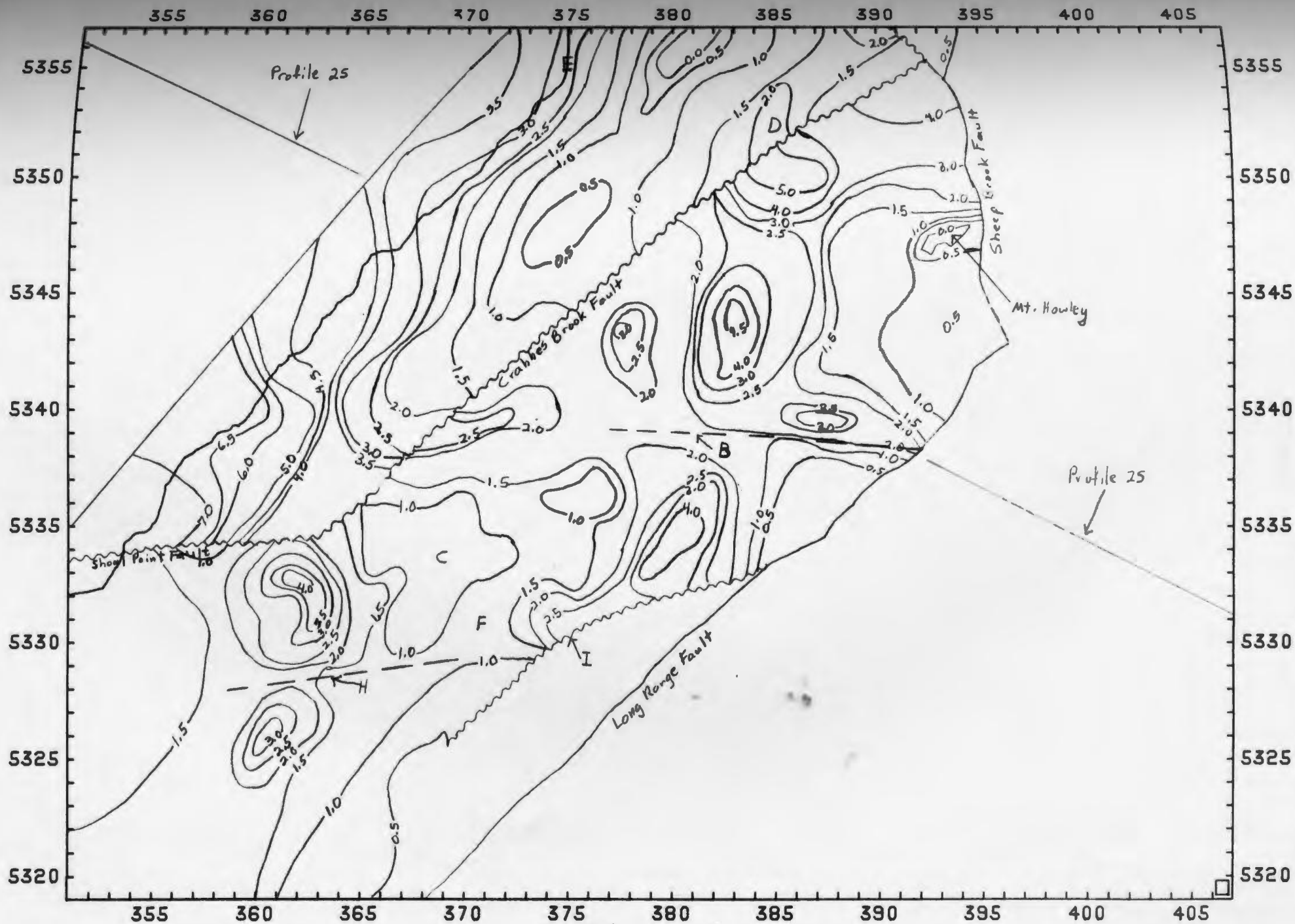


Figure 6.8 Model 4 for 3-D gravity calculation. Contours = depth in km.
(scale = 1:250000)

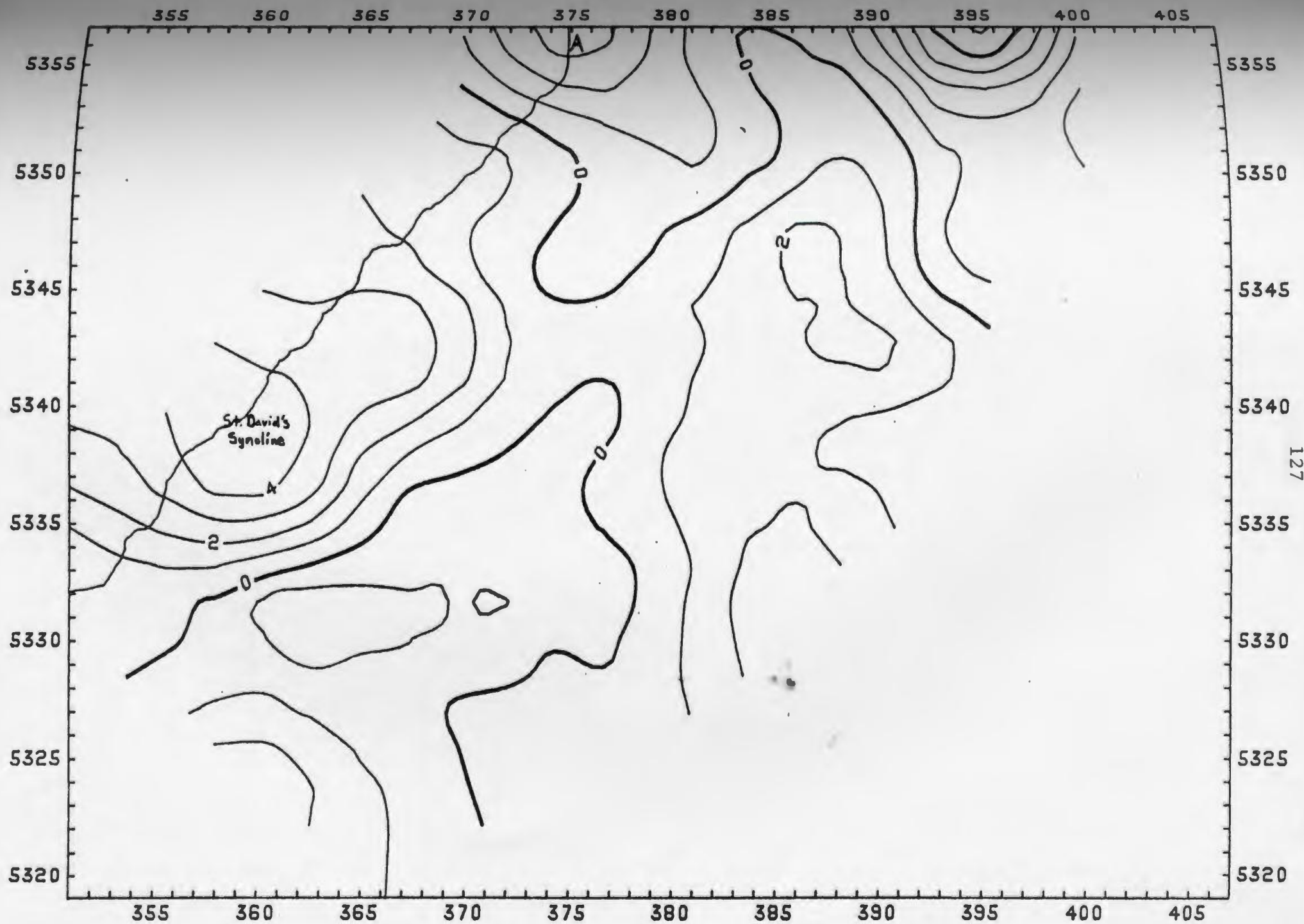


Figure 6.9 Difference in calculated and observed gravity for model 4. Contour interval = 1 mGal. (scale = 1:250000)

low at 'D' (Figure 6.8) is a northward extension of the Barachois Synclinorium on the upthrown side of the Crabbes Brook Fault.

The Crabbes Brook Fault has a downthrow of 3 km to the east at the northern end, changing to 0.5-1.5 km in the southern end. The Shoal Point Fault has a downthrow of ~4.5 km to the north.

Barachois Synclinorium sediments have thicknesses ranging from 4.0-5.0 km, with the thickness increasing to the north. Sediments in the St. Davids Syncline are 6.0 km thick. Sediments in the Brow Pond area have an approximate thickness of 1.5 km, with a maximum of 4.0 km ~5 km north of Mt. Howley.

The Anguille area is still not well defined; although there is some evidence for a new fault ('H' in Figure 6.8). An additional result of the 3-D modelling was a fault marked 'I' on Figure 6.8. There is a major downfaulting of up to 3 km to the north of this fault. The calculated thickness of sediments to the south of this fault was only 100-500 m. Other Anguille sediments were found to be from 3.5-4.0 km thick, with an average of 1.5 km overall.

The three postulated salt deposits ('E', 'F', and 'G' in Figure 6.8) explained the differences between calculated and observed values in those areas well. 'E' is postulated as being similar to the Robinsons or St. Fintans salt deposits (see Section 3.4), and is ~0.6 km in thickness. 'F' and 'G' are salt diapirs with thicknesses of 0.75 km and 0.4 km, respectively, and diameters of ~1.0 km, making them similar to the Fishells Brook deposit. The Fishells Brook deposit had a final thickness of 1.0 km and a diameter of 1 km. The other two known salt deposits - the St. Fintans and Robinsons deposits - were left throughout the modelling at 0.3 km thicknesses.

After model 4 was accepted as the gravity model, a basement block based on the gravity model was used in the 3-D magnetic modelling program (see Section 5.7 for details on the program). This was used mainly to check the validity of the gravity modelling by seeing if the correct shape of magnetic expression was obtained. More detailed modelling wasn't undertaken because the thickness of the magnetic basement was not an important consideration.

The resulting magnetic anomaly plot (Figure 6.10) agrees with the original magnetic map (Figure 2.4) in regards to shape, especially west of the Crabbes Brook Fault. The location of the magnetic high ('A' in Figure 6.10) appears to be shifted on this map with respect to the 25-point averaged aeromagnetic map (Figure 2.5). A logical explanation can be found if the original, unaveraged aeromagnetic map is examined. Figure 2.4 shows the total field aeromagnetic map before averaging. Note the double magnetic peak in the area in question. When the averaging was done, the location of the data points made the magnetic high plot towards the more easterly magnetic peak. Thus the model satisfies the original unaveraged data well.

The easterly magnetic peak mentioned above is caused by a large change in magnetic susceptibility in the basement; a lens of magnetite, or a basement rise in the area. An examination of the Bouguer gravity anomaly map in the area rules out a basement rise if a constant density is used. The lens of magnetite is also ruled out by studies done in Section 6.2, as the depth to basement from gravity is 1.0 km in that area. It can therefore be concluded that a change in susceptibility corresponding with measured susceptibilities (see Section 4.4) has caused this easterly peak.

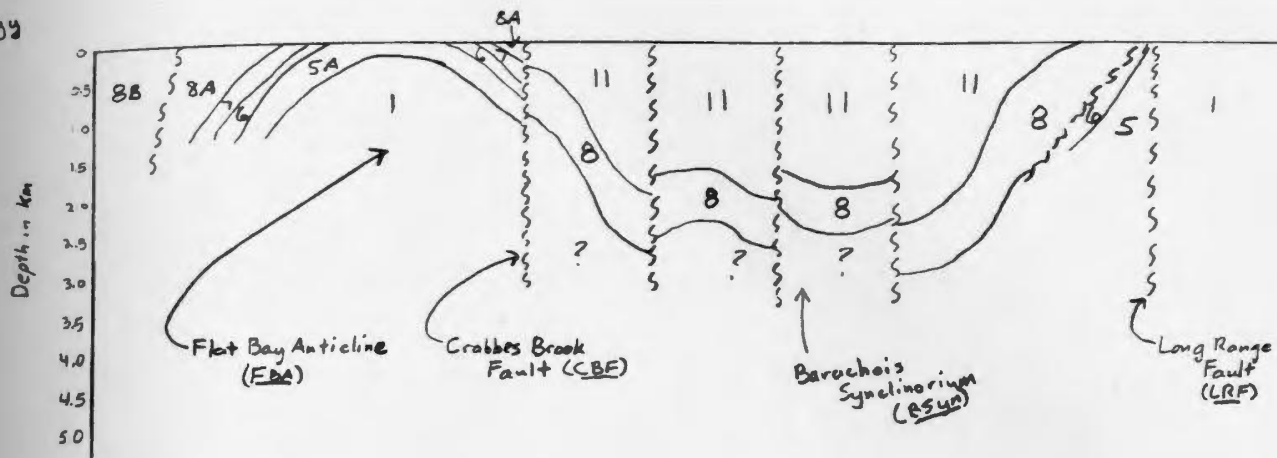
In the rest of the study area, the data fits well, with the exception of Mt. Howley, which has a much higher calculated expression than on the observed data. From Chapter 4, it would seem that a good explanation would be that the basement is not of a single magnetic susceptibility, but of several. The magnetic susceptibility that was used, 0.001 cgs units, was a median susceptibility from all measurements done. From the results of the magnetic model, it would appear that at least 3 bodies of different magnetic susceptibilities are needed to explain the observed field totally. However, as the present model fit the shape of the original field well, it was decided that this model was acceptable as a demonstration that the shape deduced for the basement surface from the gravity data was consistent geometrically with the magnetic field data.

6.6 A comparison of the 2.5-D gravity inversion model with the 3-D forward gravity model.

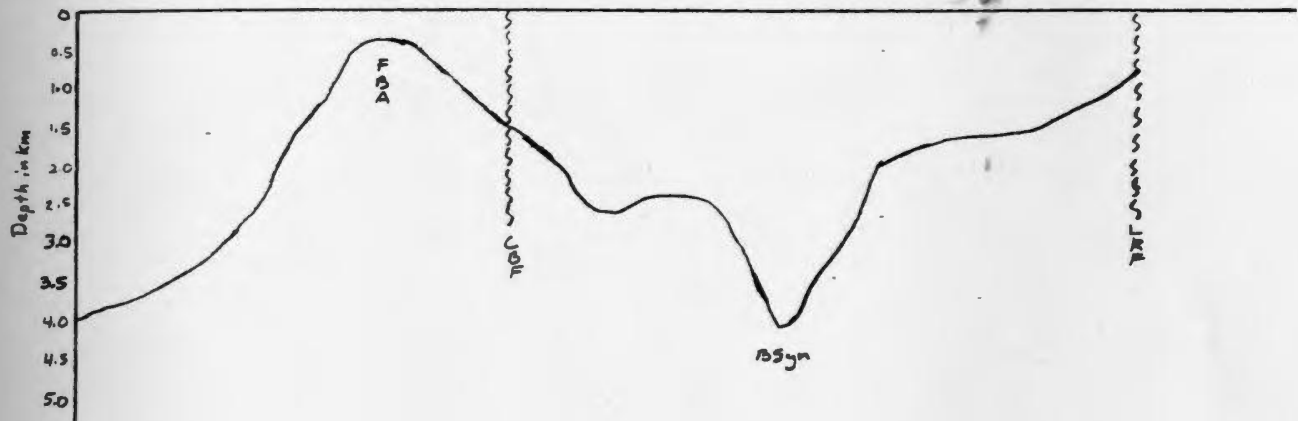
A comparison of Figures 6.3 and 6.8 shows a great similarity between the 2.5-D model and the final 3-D model. The locations of the basement highs and lows did not change appreciably, only the depths were adjusted. Sediment thickness calculations for the 2.5-D model, particularly in the Barachois area, compare very favorably with the 3-D results.

Figure 6.11 shows a cross-section running near Robinsons River, which is located at almost the center of the study area (Profile '2S').

Geology



2.5-D Model



3-D Model

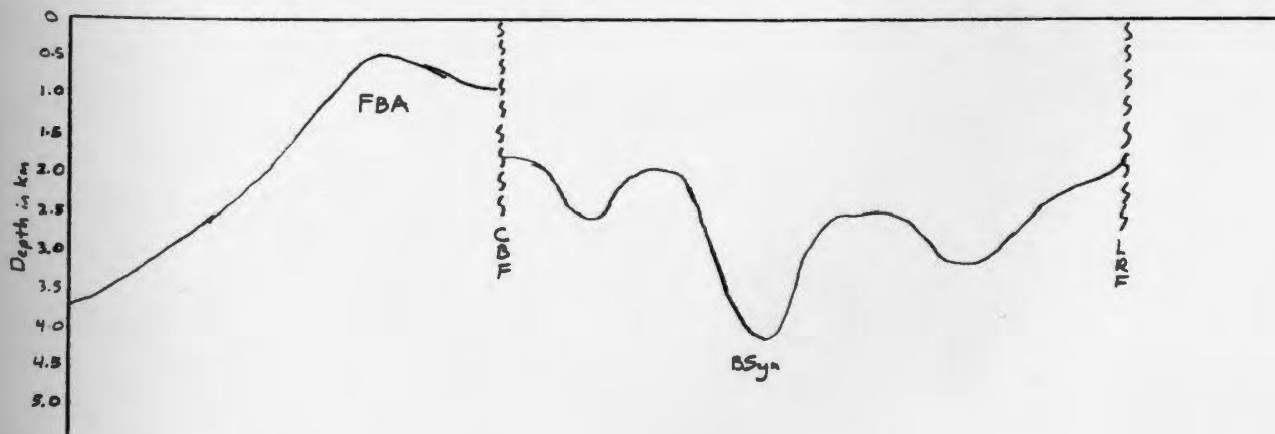


Figure 6.11 Cross-section near Robinsons River showing geology, and 2.5-D and 3-D gravity models.

The figure shows the 2.5-D and 3-D models derived by the modelling process, and the geologic model from Knight (1983). The 2.5-D model is a result of the inversion of profile 2S (the gravity fit can be seen in Appendix 3.2p). The 3-D model also fits the observed gravity well, although there is a difference of 2 mGal in the Barachois area (see Figure 6.9). Both models are fairly consistent with the geologic cross-section, especially the 3-D model.

The marked similarity between the 2.5-D and 3-D models is especially encouraging when the modelling time difference is considered. The 2.5-D model was put together in less than 2 days. Average CPU time per profile was only 6 seconds, or a grand total of 72 minutes CPU for the whole model of 20 profiles. In comparison, the 3-D basin model took a month to perfect, due to the massive amounts of digitizing necessary for the many depth contours for each body. Average CPU time per run was close to 3 minutes.

The similarity of the final 3-D model to the original 2.5-D model occurs because good geologic and density controls were used in determining the 2.5-D model. Therefore, the 2.5-D modelling program results in a quick yet accurate picture of the basement-sediment interface and an estimate of the sediment thicknesses in a basin.

6.7 Summary of results

The gravity modelling of the subbasin has resulted in an model of the basement topography and a delineation of the subsurface extent of major geologic features. Figure 6.12 is a surface geology map based

on the results of the modelling and Figure 6.13 is a basement topography plot based on the 3-D modelling with the major subsurface features labelled. In Table 6.2, a summary of the features shown on Figures 6.12 and 6.13 is presented. As a result of the modelling, several 'new' faults were mapped, and the throws of the Crabbes Brook and Shoal Point faults were determined. Three salt deposits were also postulated to exist based on the gravity modelling. These appear to be significant, particularly the two diapirs in the Crabbes Brook area ('S1' and 'S2' in Figure 6.12). The one postulated near the coast ('S3') could be a very large gypsum deposit instead of salt. If so, it could be economic, as its extent would have to be greater than the salt body that was used because of a lower density contrast (0.10 g/cm^3 or less from Section 4.3).

By far the most significant result of the combined 2.5 and 3-D modelling was the determination of the subsurface topography of the basement-sediment interface. The extent and thickness of sediments in the Barachois Synclinorium and St. Davids Syncline were determined, as were several other features that can't be delineated from an examination of the geology. Also, it is now possible to give an approximation of the thicknesses of the various sedimentary sequences in the study area. The only area that was not well defined was the Anguille Group in the southern part of the study area, and this was due entirely to a scarcity of gravity stations in the area.

Table 6.3 is a list of the geologic units, along with a thickness estimate based on the modelling and the geologic estimates from Knight (1983). The thickness estimates from the modelling were done using a method similar to that for determining densities described

Table 6.2: Features labelled in Figures 6.12 and 6.13.

Feature	Description
A	Fischells Salt
B	Robinsons Salt
C	St. Pintans Salt
S1	New salt diapir, 0.75 km thick.
S2	New salt diapir, 0.40 km thick.
S3	New salt deposit, 0.6 km thick.
D	New fault in Barachois area trending $\sim 100^{\circ}T$
E	New fault in Barachois area trending $\sim 020^{\circ}T$
F	New fault in Barachois area trending $\sim 115^{\circ}T$
G	New fault near Anguille Anticlinorium trending $\sim 080^{\circ}T$
H	Fault trending from $050^{\circ}-070^{\circ}T$ marking southern terminus of Barachois Synclinorium
I ₁ -I ₄	Lows associated with Barachois Synclinorium
J ₁ , J ₂	Highs associated with Flat Bay Anticline
K	St. David's Syncline
L ₁ , L ₂	Northward extension of Anguille Anticlinorium

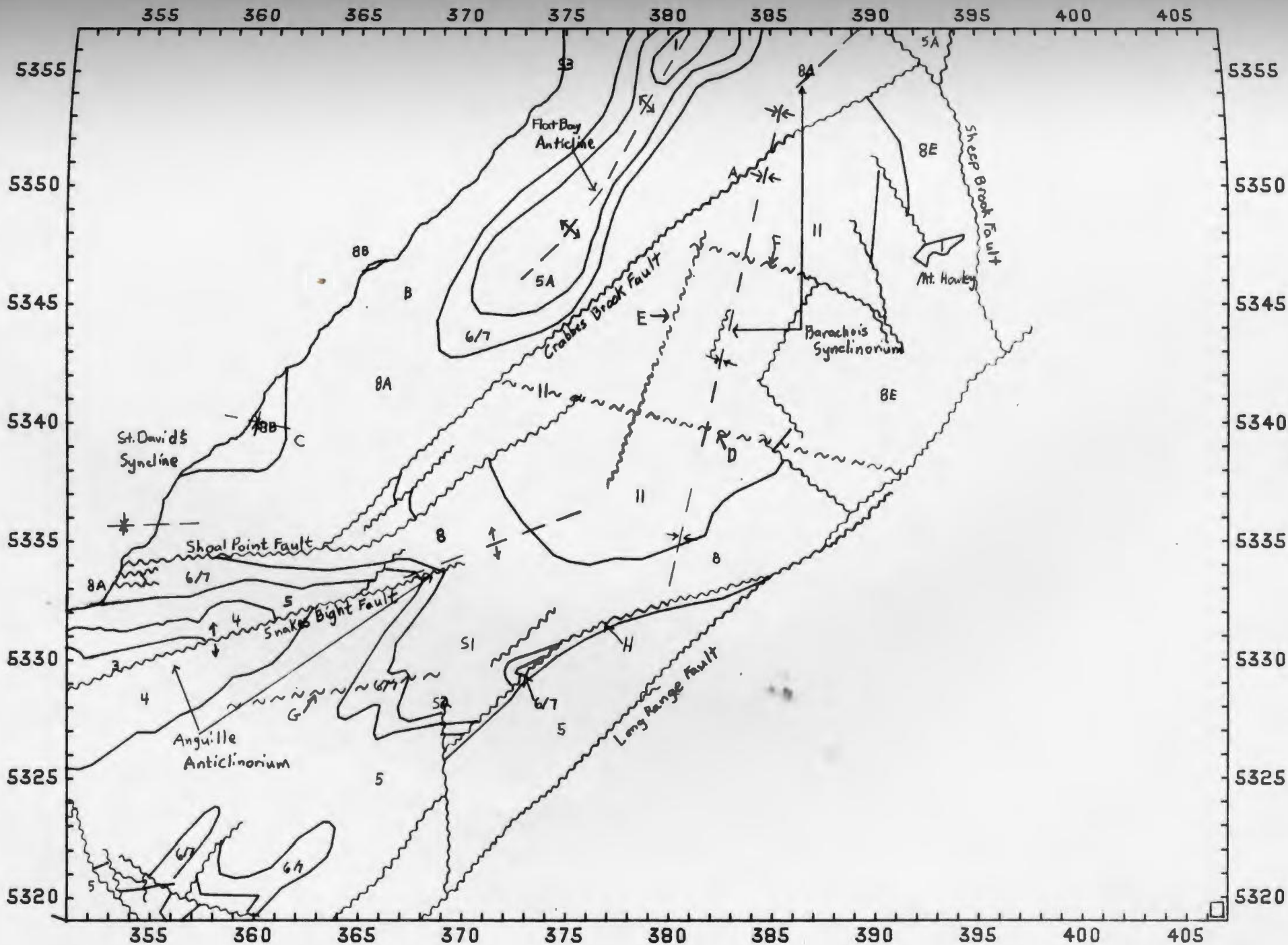


Figure 6.12 Final surface geology map based on the results of model 4.

Legend for Figure 6.12

Symbol	Description
	Fault
	Geologic Contact
	Anticline
	Syncline
D, F, G, etc.	Feature Discussed in Text
1	Pre-Carboniferous Basement
2	Kennels Brook Formation
3	Snakes Bight Formation
4	Friars Cove Formation
5	Spout Falls Formation
5A	Fischells Conglomerate
6	Ship Cove Formation
7	Codroy Road Formation
8	Robinsons River Formation (undivided)
8A	Jeffreys Village Member
8B	Highlands Member
8E	Brow Pond Lentil
11	Undivided Barachois Group

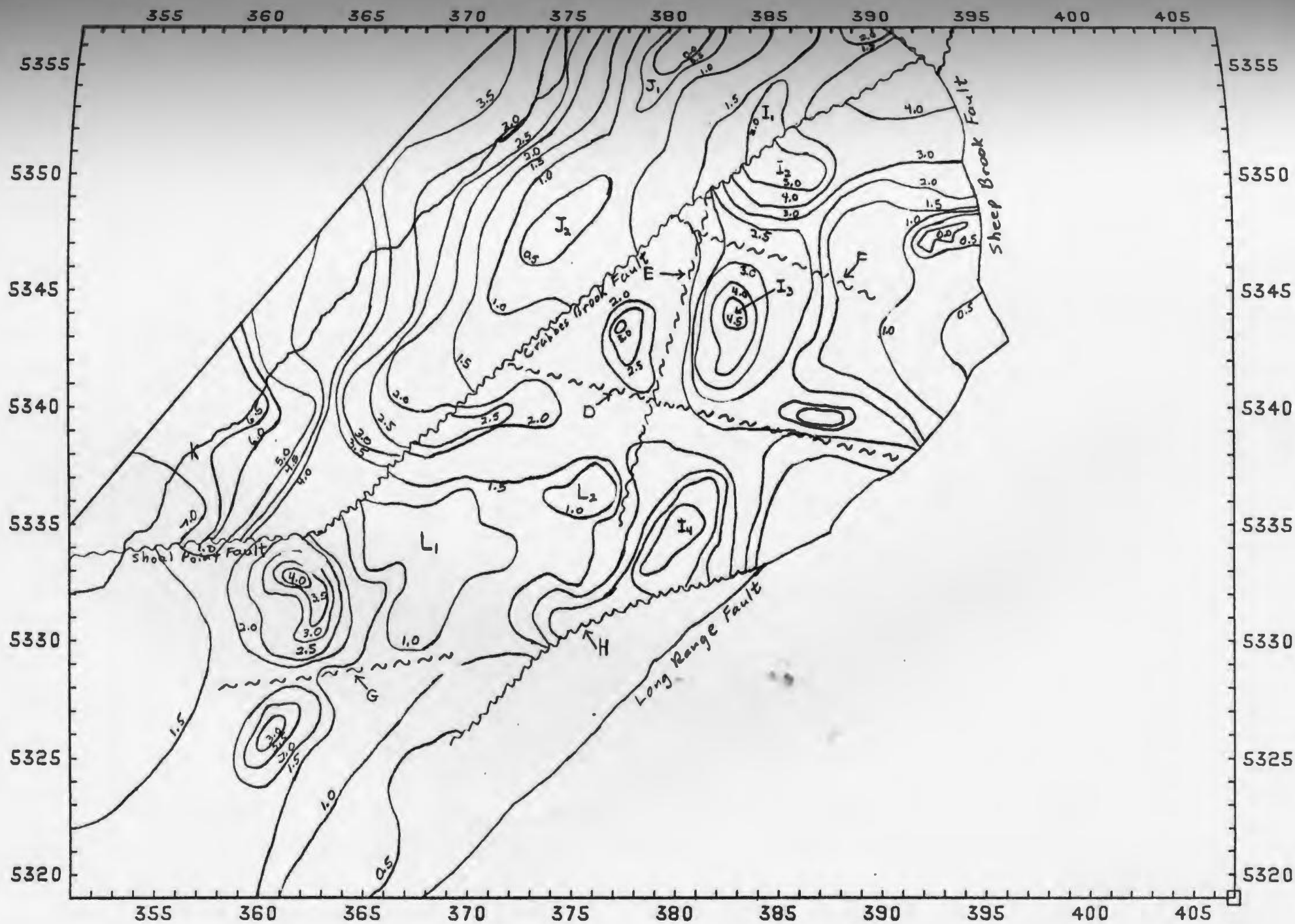


Figure 6.13 Final basement topography map based on the results of model 4. Contours = depth in km. Faults are inferred faults shown in Figure 6.12. (scale = 1:250000)

Table 6.3 Thickness estimates for the lithologic units of the Bay St. George Carboniferous Subbasin.

Map reference	Formation/ Member	Thickness from Knight (1983)	Thickness from modelling
2	Kennels Brook Fm.	3200 m, 714 m in the crest of the Anguille Anticline.	?, certainly <2000 m in the study area.
3	Snakes Bight Fm.	1000 m SE of the Snakes Bight Fault.	1000 m SE of Snakes Bight fault.
4	Friars Cove Fm.	500 - 3000 m in the NE Anguille Mountains	700 m.
5	Spout Falls Fm.	780 m NE of Snakes Bight Fault/ 2250 m W. of Codroy Pond.	1000 m/ ? (no data).
5a	Fischells Cong.	50 - 200 m.	500 m.
6	Ship Cove Fm.	18 - 20 m.	no more than 100 m.
7	Codroy Road Fm.	125 - 140 m.	no more than 300 m.
8a	Jeffreys Village Mem.	1400 m/2000 - 2100 m SW of the Flat Bay Anticline	1200 m/ 2000 m SW of the Flat Bay Anticline
8b	Highlands Mem.	884 m near the coast.	1000 m.
8e	Brow Pond Lentil	?	1000 - 2000 m.
11	Barachois Group	1500 - 1600 m.	1200 m.

in section 4.3. The process was worked in reverse to determine individual thicknesses from an overall thickness through the use of the percent compositions of each member of every geologic Group represented in the area. The results shown in Table 6.3 show that the gravity model is in agreement with the geologic estimates of depth of burial.

Finally, a magnetic model was done and an acceptable geometric shape was obtained in the calculated magnetic expression, showing that the model derived from gravity modelling was of the correct shape.

Chapter 7: Conclusions

The Bay St. George Carboniferous subbasin in Western Newfoundland was studied through the use of gravity and magnetic data collected there. These data were processed and Bouguer and aeromagnetic total field anomaly maps were generated. These maps were then reduced to residual anomaly maps by removing a regional trend from them via trend analysis. These maps were examined qualitatively to determine the locations of major geologic features.

The geology of the subbasin was examined next. Knight's report (1983) gave the sedimentary geology of the subbasin. The geology of the basement was determined by an examination of rocks from the Indian Head and Steel Mountain outcrops just outside of the study area. It was decided that the basement was of similar character to these outcrops.

The physical properties of the basement and sedimentary rocks were determined and used in the computer modelling of the subbasin. The densities determined were $2.54 \pm 0.09 \text{ g/cm}^3$ and $2.72 \pm 0.35 \text{ g/cm}^3$ for the sediments and basement, respectively, and the magnetic susceptibilities were negligible in the case of the sediments and $\sim 1000 \times 10^{-6}$ cgs units for the basement samples.

As a result of the gravity modelling, the basement topography was determined, along with the delineation of major faults, new evaporite deposits, and sediment thickness estimates. A comparison of Figures 3.1 and 6.12 shows that the gravity model confirms the surface geology from Knight (1983) to a large extent, with only a few differences and most of them being from features with no surface expression. The final

geophysical model was determined using the combined gravity, magnetic, and geologic signature of the region.

The value of the 2.5-D inversion program was also confirmed, as the model derived by it was nearly identical geometrically to the final 3-D model. Also, the time saved by using the 2.5-D inversion process makes it very practical. However, it must be stressed that good density and geologic control and a fairly large number of gravity stations in an area are essential to a good estimate of the basement topography. The good results obtained here are a result of good control over the above factors.

Knight's model of the structural evolution of the Bay St. George Carboniferous Subbasin was supported to a large extent by the modelling results. The orientation of the 'new' faults are consistent with the structural conclusions reached by Knight (see Section 3.3), as they can be interpreted as synthetic-antithetic conjugate faults also. In addition, the orientation of the major fold axes were not altered by the modelling, further supporting Knight's conclusions. In other words, nothing was evidenced by the modelling to change the basic interpretation on the basin as a wrench-fault system.

The basic understanding of the subsurface geology gained through the gravity and magnetic modelling will hopefully be useful in other studies, in particular the onshore-offshore gravity and magnetic correlations and the seismic studies being done at this time in the Subbasin.

Acknowledgements

The author would like to thank the following persons and organizations for assistance in this project:

Dr. H.G. Miller, my supervisor, for his patience, helpfulness, and friendship during the course of my work.

Drs. J.A. Wright, G. Quinlan, E.R. Deutsch, J.B. Merriam, and J.P. Hodych of the Geophysics group in the Department of Earth Sciences for their helpful discussions on geophysics.

Dr. I. Knight of the Department of Mines and Energy, Newfoundland, for rock samples and discussions on the geology of the Subbasin.

Dr. G.S. Murthy of the Geophysics group in the Department of Earth Sciences for Steel Mountain and Indian Head samples.

Drs. R.S. Hyde of MUN Earth Sciences and S. Coleman-Saad of the Department of Mines and Energy, Newfoundland, for discussions on the geology of the Carboniferous sediments and the Pre-Carboniferous basement.

Mr. Tom E. Laidley for providing programming and invaluable assistance on the computer system.

Mr. John Read for help with the computer system.

Mr. Jim Everard for introducing me to gravity surveying and the rest of Newfoundland.

My fellow geophysics graduate students, C.L. Fang, C. Garrity, G.J. Kilfoil, P.R. Mohanty, B.K. Pal, and J.N. Prasad, and geology graduate students S. Solomon and D.I. Johnston, for their friendship, assistance, and discussions on geophysics and geology.

The Memorial University Computing Centre for use of their facilities, especially the plotter.

Mrs. G. Starkes of the Earth Sciences Department for word processing this thesis.

• The Department of Mines and Energy's Mineral Development Division for providing some evaporite samples from the study area.

The Memorial University of Newfoundland and the Department of Earth Sciences for financial assistance in the form of a University Fellowship and a departmental Bursary.

My Mom and Dad for their love and support throughout this project.

Customs and Immigration Canada for making my stay in Newfoundland more interesting than it should have been.

And, finally, all my new found friends for making my stay in Newfoundland all the more pleasant.

Bibliography

Al-Chalabi, M., "Some studies relating to nonuniqueness in gravity and magnetic inverse problems", Geophysics, vol. 36 (1971), pp. 835-855.

_____, "Interpretation of Gravity Anomalies by Non-Linear Optimization", Geoph. Prosp., vol. 20 (1971), pp. 1-16.

Baird, D.M., "Magnetite and gypsum deposits of the Sheep Brook -- Lookout Brook area", Geol. Surv. Can. Bull. #27, pp. 20-41, 1954.

Bott, M.H.P., "The Use of Rapid Digital Computing Methods for Direct Gravity Interpretations of Sedimentary Basins", Geoph. Jour. R. astr. Soc., vol. 3 (1967), pp. 63-67.

Corbato, C.E., "A Least-Squares Procedure for Gravity Interpretation", Geophysics, vol. 30 (1965), pp. 228-233.

Geological Survey of Canada, Aeromagnetic Series: Geophysical Paper 206, Map 206G (Revised) - "Dashwoods Pond", 1968.

_____, Aeromagnetic Series: Geophysical Paper 251, Map 251G (Revised) - "Main Gut", 1968.

_____, Aeromagnetic Series: Geophysical Paper
316, Map 316G (Revised) - "St. Fintans", 1968.

_____, Aeromagnetic Series: Geophysical Paper
318, Map 318G (Revised) - "Flat Bay", 1968.

Grant, F.S., and G.F. West, Interpretation Theory in Applied
Geophysics, McGraw-Hill, Inc., New York, 1965.

Handbook of Chemistry and Physics, 43 ed., Chemical Rubber Co., 1962.

Handbook of Chemistry and Physics, 50 ed., Chemical Rubber Co., 1969.

Heyl, A.V., and J.J. Ronan, "The iron deposits of Indian Head area",
Geol. Surv. Can. Bull. #27, pp. 42-62, 1954.

International Association of Geodesy, International Gravity Formula,
Geodetic Reference System (GRS67), Special Publication No. 3,
Paris, France (1967).

International Association of Geomagnetism and Aeronomy, Grid Values
for the IGRF 1965.0, Bulletin 29, 1971.

Jackson, D.D., "Interpretation of inaccurate, insufficient and
inconsistent data", Geoph. J. R. Astr. Soc., vol. 28 (1972),
pp. 97-109.

Knight, I., Geology of the Carboniferous Bay St. George Subbasin, Western Newfoundland, Memoir 1, Mineral Development Division, Newfoundland and Labrador Department of Mines and Energy, 1983.

Miller, H.G. "A Gravity Survey of Eastern Notre Dame Bay, Newfoundland", MSc. Thesis, Memorial University of Newfoundland, 1970.

_____, "Three statistical tests for 'goodness of fit', Can. J. Earth Sci., v. 15 (1978), pp. 171-173.

_____, and H.C. Weir, "The northwest Gander Zone -- a geophysical interpretation", Can. J. Earth Sci., vol. 19 (1982), pp. 1371-1381.

_____, and J.A. Wright, "Gravity and magnetic interpretation of the Deer Lake basin, Newfoundland", Can. J. Earth Sci., vol. 21 (1984), pp. 10-18.

Morelli, C., C. Gantar, T. Honkasalo, R.K. McConnell, B. Szabo, J.G. Tanner, U. Uotila, and C.T. Whelan, "The international standardization gravity net 1971 (IGSN71)", International Association of Geodesy, Paris, France (1971).

Murthy, G.S., and K.V. Rao, "Paleomagnetism of Steel Mountain and Indian Head anorthosites from Western Newfoundland", Can. J. Earth Sci., vol. 13 (1976), pp. 75-83.

Nettleton, L.L., Gravity and Magnetism in Oil Prospecting, McGraw-Hill, Inc., New York, 1976.

Patzold, R., "High Temperature Magnetic Susceptibility Bridge", MSc. Thesis, Memorial University of Newfoundland, 1972.

Qureshi, I.R. and H.G. Mula, "Two-Dimensional Distributions from Gravity Anomalies: A Computer Method", Geoph. Prosp., vol. 19 (1971), pp. 180-191.

Rasmussen, R. and L.B. Pedersen, "End Corrections in Potential Field Modeling", Geoph. Prosp., vol. 27 (1979), pp. 749-760.

Skeels, D.C., "Ambiguity in gravity interpretation", Geophysics, vol. 12 (1947), pp. 43-56.

SM-5 Users Manual, Scintrex (1980).

Solomon, S., Personal communication, 1984.

Talwani, M., "Program for Calculating the Gravity Anomaly Caused by Three-Dimensional Bodies of Arbitrary Shape", Lamont Geophysical Observatory, Cornell Univ., June 10, 1965.

_____, "Computation with the Help of a Digital Computer of Magnetic Anomalies Caused by Bodies of Arbitrary Shape", Geophysics, vol. 30 (1965), pp. 797-817.

Talwani, M., and M. Ewing, "Rapid Computation of the Gravitational Attraction of Three-Dimensional Bodies of Arbitrary Shape", Geophysics, vol. 25 (1960), pp. 203-225.

Telford, W.M., L.P. Gedhart, R.E. Sheriff, and D.A. Keys, Applied Geophysics, Cambridge University Press, New York, 1976.

Topping, J., Errors of Observation and Their Treatment, Chapman and Hall, Ltd., London, 1962.

Weaver, D.F. "A geological interpretation of the Bouguer anomaly field of Newfoundland", Publication of the Dominion Observatory, Ottawa, Ont., Vol. XXXV, No. 5 (1967), pp. 223-251.

Weir, H.C. "A Gravity Profile Across Newfoundland", MSc. Thesis, Memorial University of Newfoundland, 1971.

Whitten, E.T.H. "Orthogonal polynomial contoured trend surface maps for irregularly spaced data", Computer Applications, vol. 1 (1973), pp. 171-192.

Wilcox, R.E., T.P. Harding, and D.R. Seely, "Basic wrench tectonics", A.A.P.G. Bulliten, vol. 57 (1973), pp. 74-96.

Williams, H., Tectonic Lithofacies Map of the Appalachian Orogen, Memorial University of Newfoundland, Map 1, 1978.

List of Appendices

1.1	Gravity Data for Each Station (236 total)	153
2.1	RPGRAV.FOR (2.5-D forward modelling)	158
2.2	RP2.FOR (2.5-D inverse modelling)	163
2.3	QM2.FOR (2-D inverse modelling)	170
2.4	GRAV3D5.FOR (3-D forward gravity modelling)	176
2.5	MAG3D5.FOR (3-D forward magnetic modelling)	183
3.1	List of Inversion Parameters for the 2.5-D Gravity Inversion Models	189
3.2	2.5-D Gravity Inversion Models	190

Appendix 1.1: Gravity data for study area.

station numbers	UTM coordinates		elevation (feet)	Bouguer anomalies (mGal)
	easting	northing		
102	360.694	5325.553	570	-11.4
103	362.585	5342.189	75	-24.2
104	368.117	5324.266	850	-3.7
105	367.655	5336.508	250	-16.8
106	370.780	5343.109	255	-14.5
107	372.736	5330.833	370	-14.3
108	373.235	5319.703	1250	22.4
109	373.231	5353.062	5	-20.7
110	378.666	5329.593	925	0.9
111	381.061	5337.326	615	-15.7
112	384.305	5350.602	455	-23.8
113	387.729	5336.079	1025	1.0
115	389.065	5328.270	1550	13.0
116	389.324	5341.607	1150	-4.6
117	398.456	5353.668	1180	-0.7
118	390.895	5346.024	900	-9.4
121	395.327	5344.829	650	3.6
122	398.198	5339.218	1120	15.0
350	365.196	5326.858	649	-7.6
349	365.708	5327.402	599	-8.6
348	366.211	5327.868	475	-10.6
347	366.723	5328.434	364	-11.0
346	367.235	5328.979	317	-11.3
345	367.370	5329.654	256	-10.1
344	367.144	5330.516	264	-10.0
343	367.289	5331.313	251	-9.8
342	367.429	5332.199	333	-9.7
341	367.330	5333.091	374	-9.4
340	367.220	5333.816	470	-10.4
339	367.609	5334.530	495	-11.9
338	367.997	5335.222	419	-12.5
337	368.015	5336.000	329	-14.4
336	368.033	5336.778	172	-16.0
335	367.924	5337.536	154	-16.9
334	367.448	5338.159	255	-19.2
333	366.835	5338.663	207	-21.4
332	366.729	5339.221	160	-21.4
331	366.744	5339.866	223	-20.3
330	367.246	5340.377	291	-19.1
329	367.882	5340.840	230	-18.5
328	368.388	5341.551	273	-17.8
327	368.904	5342.318	218	-17.2
326	369.533	5342.860	141	-15.5
325	370.167	5343.257	171	-15.6
324	370.795	5343.798	132	-14.5
323	371.307	5344.398	137	-14.1

Appendix 1.1: Gravity data for study area.

station numbers	UTM coordinates		elevation (feet)	Bouguer anomalies(mGal)
	easting	northing		
322	372.052	5344.504	202	-13.3
321	372.794	5344.487	262	-13.1
320	373.545	5344.826	286	-13.1
319	374.171	5345.257	348	-12.5
318	374.800	5345.855	408	-12.1
317	375.310	5346.433	463	-11.9
316	375.822	5347.078	484	-11.2
315	376.324	5347.623	466	-11.3
314	377.077	5348.107	417	-12.3
313	377.711	5348.627	413	-13.0
312	378.338	5349.114	371	-14.2
311	378.847	5349.659	335	-14.8
310	378.864	5350.471	263	-13.9
309	379.365	5351.016	256	-14.4
308	379.874	5351.583	264	-15.7
307	380.738	5351.365	320	-16.6
306	381.472	5351.027	386	-17.9
305	382.331	5350.954	394	-18.4
304	383.198	5350.869	458	-21.0
303	383.945	5351.132	484	-24.0
302	384.695	5351.517	504	-22.6
301	385.319	5351.949	456	-20.8
300	385.952	5352.426	580	-18.3
299	386.577	5352.925	640	-18.3
298	387.085	5353.459	707	-17.0
297	387.835	5353.923	707	-15.7
296	388.460	5354.389	715	-15.8
295	388.970	5355.068	689	-14.9
294	389.103	5355.822	660	-15.4
293	389.243	5356.542	531	-15.7
500	374.500	5345.540	403	-12.5
501	375.375	5344.920	342	-13.3
502	376.390	5344.605	385	-14.6
503	377.400	5344.330	417	-16.3
504	378.330	5344.040	414	-16.4
505	379.060	5343.565	475	-15.8
506	379.930	5343.080	517	-15.6
507	380.840	5342.630	551	-15.9
508	381.710	5342.100	585	-17.3
509	382.470	5341.510	582	-18.1
510	383.300	5340.875	607	-17.0
511	384.375	5340.360	661	-15.4
512	385.490	5339.690	588	-14.4
513	386.505	5339.590	475	-13.6
514	387.490	5339.515	539	-12.0
515	388.510	5339.465	501	-11.5
516	389.510	5339.290	541	-9.2
517	390.975	5338.950	524	-7.5
518	383.480	5342.530	662	-20.2
519	382.750	5343.960	638	-20.4
520	366.740	5339.825	223	-20.2
521	367.505	5339.415	253	-19.6

Appendix I.1: Gravity data for study area.

station numbers	UTM coordinates		elevation (feet)	Bouguer anomalies(mGal)
	easting	northing		
522	368.400	5339.350	296	-18.4
523	369.865	5339.735	359	-16.9
524	370.640	5339.550	324	-17.6
525	371.900	5338.625	380	-15.4
526	373.030	5338.410	351	-15.0
527	374.025	5337.965	419	-14.4
528	374.900	5337.630	527	-14.2
529	376.000	5337.160	611	-14.1
530	376.855	5336.350	577	-13.8
531	377.860	5335.540	625	-15.8
532	378.275	5335.150	645	-17.8
533	379.250	5335.145	652	-18.7
534	380.980	5334.965	597	-19.0
535	380.980	5334.910	578	-17.4
536	368.135	5336.425	181	-17.0
537	365.365	5337.600	205	-22.3
538	363.135	5338.230	157	-27.0
539	362.175	5339.425	94	-29.5
540	361.010	5340.940	82	-26.4
541	360.510	5339.940	79	-27.2
542	361.575	5336.450	126	-25.2
543	359.875	5334.490	194	-21.9
544	357.010	5336.000	84	-26.5
545	355.400	5335.140	45	-23.9
546	353.485	5333.300	116	-19.6
547	356.975	5337.925	87	-26.1
548	359.275	5338.450	91	-25.9
549	379.250	5350.830	259	-14.2
550	382.000	5349.800	447	-16.4
551	382.500	5349.450	444	-20.3
552	383.000	5349.640	430	-21.6
553	386.530	5349.470	649	-20.7
554	388.920	5348.370	848	-15.4
555	387.710	5347.010	1010	-12.6
556	368.360	5345.220	134	-21.7
557	366.620	5345.960	139	-24.1
558	368.810	5348.210	70	-21.3
559	370.960	5350.090	34	-19.0
560	365.520	5343.100	111	-23.3
561	363.440	5343.470	74	-24.8
562	364.680	5340.530	164	-24.2
563	369.240	5336.380	251	-13.3
564	370.220	5335.590	235	-12.2
565	371.910	5334.640	317	-12.7
566	372.510	5332.330	381	-13.9
567	374.110	5330.330	410	-12.3
568	375.620	5328.810	351	-3.5
569	377.300	5330.830	801	-6.8
570	365.550	5333.570	181	-11.7
572	377.710	5357.000	186	-25.1

Appendix 1.1: Gravity data for study area.

station numbers	UTM coordinates		elevation (feet)	Bouguer anomalies(mGal)
	easting	northing		
575	386.510	5356.660	377	-10.6
577	395.490	5356.950	1113	-11.6
578	397.475	5356.800	799	-7.1
579	400.690	5356.735	1188	-1.0
580	403.995	5356.900	270	-1.2
581	406.340	5356.500	309	4.6
582	403.865	5354.150	1332	8.5
583	401.350	5354.360	768	0.3
584	395.075	5354.080	1234	-8.2
585	391.915	5353.660	825	-13.4
586	384.300	5354.100	496	-16.1
587	381.450	5354.300	354	-11.5
588	377.660	5354.560	166	-22.7
589	374.870	5354.970	13	-22.9
590	388.400	5350.950	551	-19.7
591	391.220	5350.810	637	-14.4
592	395.375	5351.350	1315	-5.9
593	397.990	5351.275	1428	0.2
594	401.560	5351.315	1430	6.1
595	399.875	5348.760	1473	5.8
596	396.950	5348.215	1085	1.1
597	397.610	5346.025	1545	5.2
598	392.830	5348.760	1126	-9.2
599	393.175	5347.330	1512	-8.3
600	391.620	5344.275	1438	-5.2
601	394.360	5342.150	1150	3.3
602	392.090	5339.905	1241	0.9
603	390.355	5336.805	1458	3.4
604	388.510	5334.935	1347	5.3
605	386.725	5332.700	963	5.7
606	384.650	5330.320	962	6.6
607	382.990	5328.050	1459	10.3
608	380.380	5325.540	1138	13.2
609	379.300	5323.635	1134	11.6
610	376.830	5320.900	1479	20.8
611	373.600	5322.240	1489	13.5
612	375.705	5323.640	1608	15.8
613	377.140	5325.850	326	8.4
614	378.645	5327.175	1004	8.4
615	381.190	5329.920	1133	4.6
616	383.190	5332.430	832	-3.6
617	385.255	5335.140	832	-5.0
618	387.525	5337.835	949	-5.4
619	384.675	5338.400	973	-10.1
620	384.160	5348.245	700	-20.3
621	380.640	5347.885	613	-17.0
622	378.950	5345.800	590	-14.8
623	381.160	5345.870	654	-17.3
624	383.550	5346.015	730	-19.1
625	386.655	5345.210	881	-16.4

Appendix 1.1: Gravity data for study area.

station numbers	UTM coordinates		elevation (feet)	Bouguer anomalies (mGal)
	easting	northing		
626	388.840	5344.010	1030	-9.1
627	386.550	5341.685	965	-10.9
628	381.190	5339.700	648	-15.9
629	378.580	5341.330	280	-17.6
630	376.000	5341.800	488	-14.9
631	373.740	5342.615	332	-14.4
632	370.930	5341.600	164	-16.3
633	373.035	5340.715	240	-16.3
634	374.900	5339.500	310	-15.9
635	377.625	5338.200	385	-16.4
636	379.845	5336.350	498	-16.2
637	383.180	5336.570	720	-13.7
638	381.860	5333.830	753	-13.3
639	379.690	5332.730	744	-15.5
640	378.130	5333.055	692	-18.1
641	375.450	5334.725	520	-15.3
642	374.850	5332.870	538	-14.6
643	372.950	5336.055	390	-12.9
644	370.400	5337.310	206	-14.7
645	369.800	5332.460	545	-11.1
646	370.420	5330.800	717	-15.0
647	372.090	5328.460	775	-5.4
648	374.070	5325.535	1077	3.3
649	372.090	5325.915	960	-1.5
650	371.330	5323.575	680	1.5
651	369.050	5327.890	381	-10.2
652	376.460	5351.530	186	-13.7
653	374.495	5349.710	181	-11.4
654	371.235	5347.270	166	-17.6
655	368.060	5343.045	121	-15.9
656	365.340	5335.745	351	-19.1
657	362.495	5335.005	119	-21.8
658	356.735	5333.895	175	-22.2
659	361.010	5332.765	248	-20.2
660	360.310	5330.750	1235	-12.7
661	357.280	5330.225	1009	-9.9
662	363.230	5331.010	928	-15.1
663	361.600	5328.155	1264	-7.9

Appendix 2.1: 2.5-D forward gravity modelling program.

```

C      2.5 DIMENSIONAL GRAVITY PROGRAM
C      RASMUSSEN AND PEDERSON FORMULATION
C      GEOPH. PROSP., VOL 27 (1979), PP.749-760
C
C      REQUIRED INPUTS
C      1. G1(I)----OBSERVED ANOMALIES
C      2. C(I)----COORDINATE ALONG PROFILE
C      3. N -----NUMBER OF STATIONS ON PROFILE
C      4. J-----NUMBER OF BLOCKS
C      5. P(J)----DENSITY BLOCK J
C      6. S(J)----NUMBER SIDES BLOCK J
C      7. Y1,Y2----STRIKE LENGTHS IN -Y AND +Y
C      ***BLOCK COORDINATES MUST BE ENTERED CLOCKWISE***
C      ***NO TWO SUCCESSIVE Z COORDINATES CAN BE EQUAL***
C      ***ALL DISTANCES IN KILOMETERS***
C      ***ALL DENSITIES IN GM/CM3***
C      ***MAXIMUM OF 19 SIDES PER BODY***
C      DIMENSION G1(50),C(50),W(50),P(50),IS(50),T(50)
C      DIMENSION X(20,20),Z(20,20),X2(20,20),Y1(20),Y2(20)
C      OPEN(1,NAME='RPGRAV.DAT',TYPE='OLD')
C      READ(1,900)N,J
C      TYPE 900,N,J
C      DO 1000 I=1,N
1000   READ(1,901) G1(I),C(I)
C      DO 1010 J1=1,J
1010   READ(1,902)P(J1),IS(J1),Y1(J1),Y2(J1)
C      DO 1025 L=1,J
C      ISS=IS(L)
C      DO 1020 I=1,ISS
C      READ(1,903)X(L,I),Z(L,I)
C      X2(L,I)=X(L,I)
1020   CONTINUE
1025   CONTINUE
C      DO 1130 L=1,J
C      I=IS(L)+1
C      X(L,I)=X(L,I)
C      Z(L,I)=Z(L,I)
C      X2(L,I)=X2(L,I)
1130   CONTINUE
C      TYPE 904
C      AK=6.67
1024   SUM1=0
C      SUM2=0
C      S=0
1027   DO 1029 L=1,J
C      TYPE 905,L,P(L),Y1(L),Y2(L)
C      ISS=IS(L)+1
C      DO 1028 I=1,ISS
1028   TYPE 906,L,I,X(L,I),Z(L,I)
1029   CONTINUE
C      CALCULATION OF GRAVITY EFFECT

```

Appendix 2.1: 2.5-D forward gravity modelling program.

```

c W(M) IS THE TOTAL ANOMALY AT EACH STATION
DO 1030 M=1,N
  W(M)=0
  DO 1032 L=1,J
    ISS=IS(L)
    DO 1031 I=1,ISS
      DX=X(L,I+1)-X(L,I)
      DZ=Z(L,I+1)-Z(L,I)
      ZN=-DX/SQRT(DX**2.0+DZ**2.0)
      PHI=ATAN2(DZ,DX)
      U1=X(L,I)*COS(PHI)+Z(L,I)*SIN(PHI)
      U2=X(L,I+1)*COS(PHI)+Z(L,I+1)*SIN(PHI)
      WX=Z(L,I)*COS(PHI)-X(L,I)*SIN(PHI)
      R1=SQRT(U1**2.0+WX**2.0)
      R2=SQRT(U2**2.0+WX**2.0)
      BR11=SQRT(R1**2.0+Y1(L)**2.0)
      BR21=SQRT(R2**2.0+Y1(L)**2.0)
      BR12=SQRT(R1**2.0+Y2(L)**2.0)
      BR22=SQRT(R2**2.0+Y2(L)**2.0)
      A=(X(L,I)*Z(L,I+1)-Z(L,I)*X(L,I+1))/
      &(DX**2.0+DZ**2.0)
      B1=A*LOG((U2+BR21)/(U1+BR11))
      B2=A*LOG((U2+BR22)/(U1+BR12))
      C1=Y1(L)+BR21
      IF(C1.EQ.0.00) THEN
        RATIO1=0.0
        D1=0.0
        GOTO 700
      END IF
      RATIO1=(Y1(L)+BR11)/C1
      IF(RATIO1.LE.0.00) THEN
        D1=0.0
        GOTO 700
      END IF
      D1=A*LOG(R2*RATIO1/R1)
      D2=A*LOG((R2*(Y2(L)+BR12))/(R1*(Y2(L)+BR22)))
      E1=ATAN((U2*Y1(L))/(WX*BR21))
      E2=ATAN((U2*Y2(L))/(WX*BR22))
      F1=ATAN((U1*Y1(L))/(WX*BR11))
      F2=ATAN((U1*Y2(L))/(WX*BR12))
      AR1=(Y1(L)*ZN*B1)-A*(DZ*D1+DX*(E1-F1))
      AR2=(Y2(L)*ZN*B2)-A*(DZ*D2+DX*(E2-F2))
      SUM1=SUM1+AR1
    1031 SUM2=SUM2+AR2
      S=(SUM2-SUM1)
      T(L)=-1.0*AK*P(L)*S
      TYPE 907,L,T(L)
      S=0
      SUM1=0
      SUM2=0
    1032 CONTINUE
  DO 1033 L=1,J

```

Appendix 2.1: 2.5-D forward gravity modelling program.

```

1033     W(M)=W(M)+T(L)
        DEL1=G1(M)-W(M)
        TYPE 908,M,C(M),G1(M),W(M),DEL1
        DO 1039 L=1,J
            ISS=IS(L)+1
            DO 1038 I=1,ISS
                M1=M+1
                IF(M1.GT.N)GO TO 1030
1038     X(L,I)=X(L,I)-(C(M1)-C(M))
1039     CONTINUE
1030 CONTINUE
C     GRAPHICS PACKAGE FOLLOWS
C     COORDINATE PACKAGE FOLLOWS HERE
TYPE 909
ACCEPT *,II
IF(II.LT.1)GO TO 1036
    CALL PR1PLOT(W,G1,C,N)
1036 TYPE 910
ACCEPT *,II
IF(II.LT.1)GO TO 1035
1034     CALL COORD(X2,Z,P,Y1,Y2)
        DO 1040 L=1,J
            ISS=IS(L)
            DO 1041 I=1,ISS
                X(L,I)=X2(L,I)
                I=IS(L)+1
1040 X(L,I)=X2(L,I)
        GO TO 1024
1035 OPEN(2,NAME='RPGRAV1.DAT',TYPE='OLD')
        WRITE(2,900)N,J
        DO 1090 I=1,N
1090     WRITE(2,901)G1(I),C(I),W(I)
        DO 1091 J1=1,J
1091     WRITE(2,902)P(J1),IS(J1),Y1(J1),Y2(J1)
        DO 1092 L=1,J
            ISS=IS(L)
            DO 1093 I=1,ISS
                WRITE(2,903)X2(L,I),Z(L,I)
1093     CONTINUE
1092 CONTINUE
900 FORMAT(2I5)
901 FORMAT(3F10.2)
902 FORMAT(F5.2,I5,2F8.3)
903 FORMAT(2F10.3)
904 FORMAT(2X,'PARAMETERS INPUT')
905 FORMAT(2X,'BLOCK NUMBER',I5,'DENSITY =',F5.3,'CM/CM3
&.',/,2X,'Y1=',F8.3,' AND Y2=',F8.3)
906 FORMAT(2X,'COORDINATES',2I3,2F9.3)
907     FORMAT(2X,'ANOMALY FROM BLOCK',I3,'=',F9.3,'MGAL')
908     FORMAT(2X,'STN NO -',I5,/,2X,'AT LOCATION',F9.3
1     ,2X,'OBSERVED ANOMALY-',F9.3,/,2X,'CALCULATED ANOMALY-',F9.3,
2     'DIFFERENCE-',F9.3,/)
909 FORMAT(2X,'DO YOU WANT A PRINTER PLOT 1=YES 0=NO')

```

Appendix 2.1: 2.5-D forward gravity modelling program.

```

910 FORMAT(2X,'TO CHANGE DENSITY OR COORDS 1=YES 0=NO')
1094 STOP
END
SUBROUTINE COORD(X,Z,P,YA,YB)
DIMENSION X(20,20),X2(20,20),P(20),Z(20,20),YA(20),
&YB(20)
113 TYPE 911
ACCEPT *,II
IF(II.LT.1)GO TO 10
TYPE 912
ACCEPT *,L,P(L)
GO TO 113
10 CONTINUE
TYPE 915
ACCEPT *,II
IF(II.LT.1)GOTO 2
TYPE 916
ACCEPT *,K,YA(K),YB(K)
GOTO 10
2 TYPE 913
ACCEPT *,II
IF(II.LT.1)GO TO 99
TYPE 914
ACCEPT *,L,I,X2(L,I),Z(L,I)
GO TO 2
911 FORMAT(2X,'DO YOU WISH TO CHANGE BLOCK DENSITIES 1=YES 0=NO')
912 FORMAT(2X,'ENTER BLOCK NUMBER AND NEW DENSITY')
913 FORMAT(2X,'DO YOU WISH TO CHANGE COORDS 1=YES 0=NO')
914 FORMAT(2X,'ENTER BLOCK NO,COORD NO,XCOORD,ZCOORD')
915 FORMAT(2X,'DO YOU WANT TO CHANGE THE STRIKE LENGTH?
& 1=YES,0=NO')
916 FORMAT(2X,'INPUT BLOCK #, Y1, Y2')
99 RETURN
END
C SUBROUTINE TO PRINTER PLOT
C Y AXIS ALONG LINE OF TYPE
SUBROUTINE PRI PLOT(Y,Y1,X,N)
DIMENSION Y(50),Y1(50),JY(20),X(50)
BYL=0
BY1L=0
BYM=0
BY1M=0
DO 910 K=1,N
JYL=IFIX(AMIN1(Y(K),BYL))
JY1L=IFIX(AMIN1(Y1(K),BY1L))
JYM=IFIX(AMAX1(Y(K),BYM))
JY1M=IFIX(AMAX1(Y1(K),BY1M))
BYL=FLOAT(JYL)
BY1L=FLOAT(JY1L)
BYM=FLOAT(JYM)
BY1M=FLOAT(JY1M)
910 CONTINUE
JM=AMAXO(JYM,JY1M)

```

Appendix 2.1: 2.5-D forward gravity modelling program.

```

JL=AMINO(JYL,JY1L)
J1L=JL/10-1
J1M=JM/10+1
J1=J1M-J1L+1
DO 930 K=1,J1
930   JY(K)=10*(J1L+K-1)
      TYPE 933 ,(JY(K),K=1,J1)
      TYPE 934
945   TYPE 935
      DO 940, KK=1, N
        LYC=Y(KK)+0.5-10*J1L
        LYO=Y1(KK)+.5-10*J1L
        IF(LYC.EQ.LYO)GO TO 917
        IF(LYC.GT.LYO)GO TO 918
        LY=LYO-LYC
        TYPE 936, KK
        GO TO 955
918   LY=LYC-LYO
        TYPE 937, KK
        GO TO 955
917   TYPE 938, KK
955   KK1=KK+1
        IF(KK1.GT.N)GO TO 921
        MX=IFIX(X(KK1)-X(KK))
        DO 950 M=1, MX
950     TYPE 939
940   CONTINUE
921   CONTINUE
933   FORMAT(8X, <J1>(I3, 7X))
934   FORMAT(10X, <J1>('X', 9X))
935   FORMAT(2X, '////')
936   FORMAT(2X, I7, '+', <LYC>X, 'C', <LY>X, 'O')
937   FORMAT(2X, I7, '+', <LYO>X, 'O', <LY>X, 'C')
938   FORMAT(2X, I7, '+', <LYC>X, 'B')
939   FORMAT(9X, '+', /)
      RETURN
      END

```

Appendix 2.2: 2.5-D gravity inversion program.

```

C 2.5 DIMENSIONAL GRAVITY PROGRAM
C RASMUSSEN AND PEDERSON FORMULATION
C PLUS A BOTT INVERSION
C AND CONSTRAINTS ON THE Z VARIABLE
C FORMULATION FROM: GEOPH. PROSP., VOL. 27 (1979), PP.749-760.
C 1. G1(I)----OBSERVED ANOMALIES
C 2. C(I)----COORDINATE ALONG PROFILE
C 3. N-----NUMBER OF STATIONS ON PROFILE
C 4. J-----NUMBER OF BLOCKS
C 5. P-----DENSITY OF THE BLOCK
C 6. S(J)----NUMBER SIDES BLOCK J
C 7. XL-----PROFILE LENGTH
C 8. W(J)----CALCULATED ANOMALIES
C 9. Y1,Y2---DISTANCE OF Y-EDGES IN -Y AND +Y
C DIRECTIONS, RESPECTIVELY
C 10. RZ1,RZ2--TOP AND BOTTOM DEPTH CONSTRAINTS,
C RESPECTIVELY
C 11. IZ-----CHECK FOR CONSTRAINTS:
C 0 = NONE; 3 = BETWEEN RZ1 AND RZ2;
C 5 = ON MINIMUM DEPTH ONLY (Z2)
C 12. ZD-----MINIMUM DEPTH FOR ENTIRE MODEL
C 13. ID-----STATION NUMBERS
C 14. SIGMA----NUMBER CHOSEN SUCH THAT THE MEAN IS 0.0 AND
C THE VARIANCE IS 0.500 (USUALLY 5.00 TO START)
C 15. NKOUNT---MAXIMUM NO. OF ITERATIONS ALLOWED (USUALLY 100)
C 16. WIDTH---HALF-WIDTH OF THE COS**2 BELL CURVE (USUALLY 5.0)
C 17. J2-----NO. OF STATIONS ON EITHER SIDE OF THE CENTER OF
C THE BELL CURVE CHECKED (USUALLY 5)
C 18. KOUNT---TOTAL NO. OF ITERATIONS
C **ALL DISTANCES IN KILOMETERS***
C ***ALL DENSITIES IN GM/CM3***
C ***MAXIMUM OF 49 SIDES PER BODY***
C DIMENSION G1(100),C(100),W(100),X2(50),Z(50),TH(100),
C &DLG(100),X(50),DLT(100),IZ(100),RZ1(100),RZ2(100),
C &Z2(100),ID(50),IM(100),IP(100),CXM1(100),CXP1(100),
C &DLT2(100)
C CHARACTER*72 TITLE
C CHARACTER*30 CFILE
C DATA ADJ/0.00/
C WRITE(6,950)

```

Appendix 2.2: 2.5-D gravity inversion program.

```

C   READ(6,951)CFILE
    ACCEPT 951,CFILE
    OPEN(1,NAME=CFILE,TYPE='OLD')
    OPEN(2,NAME='RPUNDIG1.DAT',TYPE='OLD')
    OPEN(3,NAME='RPLOT.DAT',STATUS='NEW')
    KOUNT=0
C   READ IN DATA
    READ(1,900)TITLE
    WRITE(2,901)TITLE
    WRITE(6,901)TITLE
    READ(1,902)N,P,XL,SIGMA,NKOUNT,WIDTH,J2,Y1,Y2,ZD
    TYPE 902,N,P,XL,SIGMA,NKOUNT,WIDTH,J2,Y1,Y2,ZD
    WRITE(2,902)N,P,XL,SIGMA,NKOUNT,WIDTH,J2,Y1,Y2,ZD
    DO 1000 I=1,N
        READ(1,903) G1(I),C(I),IZ(I),RZ1(I),RZ2(I),ID(I)
1000  Z2(I)=RZ1(I)
        GAMMA=0.00
        IF(C(I).NE.0.00)THEN
            GAMMA=C(I)
            DO 650 I=1,N
250          C(I)=C(I)-GAMMA
            END IF
            IF(GAMMA.LT.2.50)ADJ=-5.00
            IS=N+2
C   CALCULATE INITIAL BODY THICKNESS
            DO 20 I=1,N
                TH(I)=0.0
                DLG(I)=G1(I)
20          CONTINUE
            DO 21 I=1,N
                TH(I)=DLG(I)/(41.9*P)
21          CONTINUE
C   ASSIGN X,Z COORDINATES TO THE INITIAL BODY
            X(1)=0.0-GAMMA+ADJ
            X(2)=XL-GAMMA
            Z(1)=0.001+ZD
            Z(2)=0.002+ZD
            X(IS+1)=X(1)
            Z(IS+1)=Z(1)
            DO 22 I=3,IS
                J=N-I+3
                IF(IZ(J).EQ.0) THEN
                    Z(I)=ZD+TH(J)
                    GOTO 23
                END IF
                IF(IZ(J).EQ.5) THEN
                    Z(I)=Z2(J)
                    GOTO 23
                END IF
                Z(I)=ZD+TH(J)
                IF(Z(I).LT.RZ1(J)) THEN
                    Z(I)=RZ1(J)

```

Appendix 2.2: 2.5-D gravity inversion program.

```

      GOTO 23
    END IF
    IF(Z(I).GT.RZ2(J)) THEN
      Z(I)=RZ2(J)
    END IF
23   X(I)=C(J)
    IF(Z(I).NE.Z(I-1))GOTO 22
      Z(I)=Z(I)+.001
22   CONTINUE
      GK=6.67
1024 SUM1=0
      SUM2=0
      S=0
C   CALCULATION OF GRAVITY EFFECT
100 DO 1030 M=1,N
      S=0
      SUM1=0
      SUM2=0
      W(M)=0
      DO 1031 I=1,IS
        DX=X(I+1)-X(I)
        DZ=Z(I+1)-Z(I)
        ZN=-DX/SQRT(DX**2+DZ**2)
        PHI=ATAN2(DZ,DX)
        U1=X(I)*COS(PHI)+Z(I)*SIN(PHI)
        U2=X(I+1)*COS(PHI)+Z(I+1)*SIN(PHI)
        WX=Z(I)*COS(PHI)-X(I)*SIN(PHI)
        R1=SQRT(U1**2+WX**2)
        R2=SQRT(U2**2+WX**2)
        BR11=SQRT(R1**2+Y1**2)
        BR21=SQRT(R2**2+Y1**2)
        BR12=SQRT(R1**2+Y2**2)
        BR22=SQRT(R2**2+Y2**2)
        A=(X(I)*Z(I+1)-Z(I)*X(I+1))/
&(DX**2+DZ**2)
        B1=A*LOG((U2+BR21)/(U1+BR11))
        B2=A*LOG((U2+BR22)/(U1+BR12))
        C1=Y1+BR21
        IF(C1.EQ.0.00) THEN
          RATIO1=0.0
          D1=0.0
          GOTO 7000
        ENDIF
        RATIO1=(Y1+BR11)/C1
        IF(RATIO1.LE.0.00) THEN
          D1=0.0
          GOTO 7000
        END IF
        D1=A*LOG(R2*RATIO1/R1)
        D2=A*LOG((R2*(Y2+BR12))/(R1*(Y2+BR22)))
        E1=ATAN((U2*Y1)/(WX*BR21))
        E2=ATAN((U2*Y2)/(WX*BR22))
7000

```

Appendix 2.2: 2.5-D gravity inversion program.

```

F1=ATAN((U1*Y1)/(WX*BR11))
F2=ATAN((U1*Y2)/(WX*BR12))
AR1=(Y1*ZN*B1)-A*(DZ*D1+DX*(E1-F1))
AR2=(Y2*ZN*B2)-A*(DZ*D2+DX*(E2-F2))
SUM1=SUM1+AR1
1031 SUM2=SUM2+AR2
S=(SUM2-SUM1)
W(M)=-1*GK*P*S
ISS=IS+1
DO 1038 I=1,ISS
MI=M+1
IF(MI.GT.N)GO TO 1030
1038 X(I)=X(I)-(C(MI)-C(M))
1030 CONTINUE
C END OF GRAVITY CALCULATION.
C CALCULATE DLT FROM DIFFERENCE IN CALCULATED AND OBSERVED VALUES
DO 50 I=1,N
DLG(I)=G1(I)-W(I)
DLT(I)=DLG(I)/(41.9*P)
50 CONTINUE
C FIND AND CHECK SUM OF SQUARES OF RESIDUALS AND CHECK NKOUNT
TB=0.0
TTL=0.0
DO 51 I=1,N
TB=DLG(I)**2.0
TTL=TTL+TB
51 CONTINUE
WRITE(2,904)TTL
KOUNT=KOUNT+1
IF(TTL.LT.SIGMA)GOTO 56
IF(KOUNT.GE.NKOUNT)GOTO 56
C BEGIN COSINE BELL SMOOTHING
C IM-----STATION NO. I-J, WHERE I IS THE CENTER OF THE BELL
C XM,XP-----DISTANCE FROM BELL CENTER TO THE IMth STATION
C IP-----STATION NO. I+J, WHERE I IS THE CENTER OF THE BELL
C XM1,XP1---ANGLE (0-90) OF LOCATION XP FROM CENTER OF BELL (0)
C CXM1,CXP1-WEIGHTING FACTOR AT IMth/IPth STATION
C TWTM-----SUM OF WEIGHTS IN I-J DIRECTION
C TWTP-----SUM OF WEIGHTS IN I+J DIRECTION
C TWT-----TOTAL WEIGHTS AT A STATION
C DLT2-----THICKNESS CHANGE AT IMth or IPth STATION DUE TO CENTRAL
C POINT THICKNESS
PID2=3.1415927/2.0
DO 701 I=1,N
TWTM=0.0
TWTP=0.0
TWT=0.0
DO 702 J=1,J2
IM(J)=I-J
IF(IM(J).LT.1)GOTO 704
XM=C(I)-C(IM(J))
704 IP(J)=I+J

```

Appendix 2.2: 2.5-D gravity inversion program.

```

IF(IP(J).GT.N)GOTO 705
XP=C(IP(J))-C(I)
705 IF(IM(J).LT.1.AND.IP(J).LE.N)GOTO 703
IF(IM(J).LT.1.AND.IP(J).GT.N)GOTO 710
IF(IM(J).LT.1)GOTO 703
IF(XM.GE.WIDTH)GOTO 703
XMI=PID2*(XM/WIDTH)
CXMI(J)=(COS(XMI)**2.0)/2.0
TWTM=TWTM+CXMI(J)
703 IF(IP(J).GT.N)GOTO 702
IF(XP.GT.WIDTH)GOTO 702
XP1=PID2*(XP/WIDTH)
CXPI(J)=(COS(XP1)**2.0)/2.0
TWTP=TWTP+CXPI(J)
702 CONTINUE
710 TWT=TWTM+TWTP
DO 706 J=1,J2
IF(IM(J).GE.1.AND.TWT.GT.0.00) THEN
DLT2(IM(J))=DLT2(IM(J))+((CXMI(J)/TWT)*DLT(I))
END IF
IF(IP(J).LE.N.AND.TWT.GT.0.00) THEN
DLT2(IP(J))=DLT2(IP(J))+((CXPI(J)/TWT)*DLT(I))
END IF
IM(J)=0
IP(J)=0
CXMI(J)=0.00
CXPI(J)=0.00
706 CONTINUE
DLT(I)=DLT(I)/2.0
701 CONTINUE
DO 707 I=1,N
DLT(I)=(DLT(I)+DLT2(I))/2.0
TH(I)=TH(I)+DLT(I)
DLT2(I)=0.0
IF(TH(I).GT.0.01)GOTO 707
TH(I)=0.01
707 CONTINUE
C REASSIGN X,Z VALUES TO THE BODY
X(1)=0.0-GAMMA+ADJ
X(2)=XL-GAMMA
X(IS+1)=X(1)
Z(1)=0.001+ZD
Z(2)=0.002+ZD
Z(IS+1)=Z(1)
DO 54 I=3,IS
J=N-I+3
IF(IZ(J).EQ.0) THEN
Z(I)=ZD+TH(J)
GOTO 53
END IF
IF(IZ(J).EQ.5) THEN
Z(I)=Z2(J)

```

Appendix 2.2: 2.5-D gravity inversion program.

```

      GOTO 53
      END IF
      Z(I)=ZD+TH(J)
      IF(Z(I).LT.RZ1(J)) THEN
        Z(I)=RZ1(J)
        GOTO 53
      END IF
      IF(Z(I).GT.RZ2(J)) THEN
        Z(I)=RZ2(J)
      END IF
53   X(I)=C(J)
      IF(Z(I).NE.Z(I-1))GOTO 54
      Z(I)=Z(I)+.001
54   CONTINUE
      GOTO 100
C   CALCULATE MEAN AND STANDARD DEVIATION OF THE MODEL
56   WRITE(6,905)KOUNT
      XMEAN=0
      V1=0
      VAR=0
      DO 120 I=1,N
120  XMEAN=XMEAN+DLG(I)
      XMEAN=XMEAN/N
      DO 121 I=1,N
121  V1=V1+((DLG(I)-XMEAN)**2.0)
      VAR=SQRT(V1/(N-1))
      WRITE(6,906)XMEAN,VAR
      WRITE(2,906)XMEAN,VAR
C   RENUMBER BODY IN X AND OUTPUT FINAL MODEL
      DO 57 I=1,N
57   C(I)=C(I)+GAMMA
      X(1)=0.0+ADJ
      X(2)=X1
      DO 58 I=3,IS
        J=N-I+3
58   X(I)=C(J)
      DO 59 I=1,IS
        WRITE(6,907)X(I),Z(I)
59   CONTINUE
      DO 60 I=1,N
        WRITE(6,908)C(I),G1(I),DLG(I),W(I)
60   CONTINUE
1035 WRITE(2,909)N,P,XL,IS,SIGMA,TTL,KOUNT,ZD
      DO 1090 I=1,N
1090  WRITE(2,910)C(I),G1(I),DLG(I),W(I),ID(I)
      DO 1093 I=1,IS
        WRITE(2,911)X(I),Z(I)
1093 CONTINUE
      J=1
      WRITE(3,915)N,J
      DO 500 I=1,N
        WRITE(3,916)G1(I),C(I),W(I)

```

Appendix 2.2: 2.5-D gravity inversion program.

```
500 CONTINUE
    WRITE(3,917)IS
    DO 501 I=1,IS
        WRITE(3,918)X(I),Z(I)
501 CONTINUE
900 FORMAT(A72)
901 FORMAT(1X,A71)
902 FORMAT(15,2F6.2,F8.2,I5,F6.2,I3,3F8.3)
903 FORMAT(2F10.2,I5,2F10.2,I5)
904 FORMAT(F10.2)
905 FORMAT(2X,'THE TOTAL NUMBER OF INTERATIONS=',I5)
906 FORMAT(2X,'THE MEAN IS',F7.3,' AND THE STANDARD DEVIATION
        &IS',F7.3)
907 FORMAT(2F10.2)
908 FORMAT(4F10.2)
909 FORMAT(15,2F6.2,I5,F8.5,F10.2,I5,F8.3)
910 FORMAT(4F10.2,I10)
911 FORMAT(2F10.2)
915 FORMAT(2I5)
916 FORMAT(3F10.2)
917 FORMAT(5X,I5)
918 FORMAT(2F10.3)
950 FORMAT(2X,'WHAT IS THE NAME OF THE DATA FILE TO BE READ?',S)
951 FORMAT(A30)
999 STOP
    END
```

Appendix 2.3: 2-D gravity inversion program.

```

C   2 DIMENSIONAL GRAVITY PROGRAM
C   GRANT & WEST FORMULATION
C   PLUS A BOTT INVERSION
C   AND CONSTRAINTS ON THE Z VARIABLE
C   FORMULATION FROM: GEOPH. PROSP., VOL. 27 (1979), PP.749-760.
C   1. G1(I)----OBSERVED ANOMALIES
C   2. C(I)----COORDINATE ALONG PROFILE
C   3. N -----NUMBER OF STATIONS ON PROFILE
C   4. J-----NUMBER OF BLOCKS
C   5. P-----DENSITY OF THE BLOCK
C   6. S(J)----NUMBER SIDES BLOCK J
C   7. XL-----PROFILE LENGTH
C   8. W(J)----CALCULATED ANOMALIES
C   9. Y1,Y2---DISTANCE OF Y-EDGES IN -Y AND +Y
C               DIRECTIONS, RESPECTIVELY
C  10. RZ1,RZ2--TOP AND BOTTOM DEPTH CONSTRAINTS,
C               RESPECTIVELY
C  11. IZ-----CHECK FOR CONSTRAINTS:
C               0 = NONE; 3 = BETWEEN RZ1 AND RZ2;
C               5 = ON MINIMUM DEPTH ONLY (Z2)
C  12. ZD-----MINIMUM DEPTH FOR ENTIRE MODEL
C  13. ID-----STATION NUMBERS
C  14. SIGMA----NUMBER CHOSEN SUCH THAT THE MEAN IS 0.0 AND
C               THE VARIANCE IS 0.500 (USUALLY 5.00 TO START)
C  15. NKOUNT---MAXIMUM NO. OF ITERATIONS ALLOWED (USUALLY 100)
C  16. WIDTH---HALF-WIDTH OF THE COS**2 BELL CURVE (USUALLY 5.0)
C  17. J2-----NO. OF STATIONS ON EITHER SIDE OF THE CENTER OF
C               THE BELL CURVE CHECKED (USUALLY 5)
C  18. KOUNT---TOTAL NO. OF ITERATIONS
C   ***ALL DISTANCES IN KILOMETERS***
C   ***ALL DENSITIES IN GM/CM3***
C   ***MAXIMUM OF 49 SIDES PER BODY***
C   DIMENSION G1(100),C(100),W(100),X2(50),Z(50),TH(100),
C   &DLG(100),X(50),DLT(100),IZ(100),RZ1(100),RZ2(100),
C   &Z2(100),ID(50),IM(100),IP(100),CXM1(100),CXP1(100),
C   &DLT2(100)
C   CHARACTER*72 TITLE
C   CHARACTER*30 CFILE
C   DATA ADJ/0.00/
C   WRITE(6,950)
C   READ(6,951)CFILE
C   ACCEPT 951,CFILE
C   OPEN(1,NAME=CFILE,TYPE='OLD')
C   OPEN(2,NAME='UNDIG1.DAT',TYPE='NEW')
C   OPEN(3,NAME='QMPLOT.DAT',STATUS='NEW')
C   KOUNT=0
C READ IN DATA
C   READ(1,900)TITLE
C   WRITE(2,901)TITLE
C   WRITE(6,901)TITLE
C   READ(1,902)N,P,XL,SIGMA,NKOUNT,WIDTH,J2,ZD

```

Appendix 2.3: 2-D gravity inversion program.

```

TYPE 902,N,P,XL,SIGMA,NKOUNT,WIDTH,J2,ZD.
WRITE(2,902)N,P,XL,SIGMA,NKOUNT,WIDTH,J2,ZD
DO 1000 I=1,N
  READ(1,903) G1(I),C(I),IZ(I),RZ1(I),RZ2(I),ID(I)
1000 Z2(I)=RZ1(I)
  GAMMA=0.00
  IF(C(I).NE.0.00)THEN
    GAMMA=C(I)
    DO 650 I=1,N
650   C(I)=C(I)-GAMMA
  END IF
  IF(GAMMA.LT.2.50)ADJ=-5.00
  IS=N+2
C  CALCULATE INITIAL BODY THICKNESS
  DO 20 I=1,N
    TH(I)=0.0
    DLG(I)=G1(I)
20  CONTINUE
  DO 21 I=1,N
    TH(I)=DLG(I)/((41.9*P)
21  CONTINUE
C  ASSIGN X,Z COORDINATES TO THE INITIAL BODY
  X(1)=0.0-GAMMA+ADJ
  X(2)=XL-GAMMA
  Z(1)=0.001+ZD
  Z(2)=0.002+ZD
  X(IS+1)=X(1)
  Z(IS+1)=Z(1)
  DO 22 I=3,IS
    J=N-I+3
    IF(IZ(J).EQ.6) THEN
      Z(I)=ZD+TH(J)
      GOTO 23
    END IF
    IF(IZ(J).EQ.5) THEN
      Z(I)=Z2(J)
      GOTO 23
    END IF
    Z(I)=ZD+TH(J)
    IF(Z(I).LT.RZ1(J)) THEN
      Z(I)=RZ1(J)
      GOTO 23
    END IF
    IF(Z(I).GT.RZ2(J)) THEN
      Z(I)=RZ2(J)
    END IF
23   X(I)=C(J)
    IF(Z(I).NE.Z(I-1))GOTO 22
    Z(I)=Z(I)+.001
22  CONTINUE
  AK=6.67
1024 R1=0
  S=0

```

Appendix 2.3: 2-D gravity inversion program.

```

C   CALCULATION OF GRAVITY EFFECT
100 DO 1030 M=1,N
    S=0
    W(M)=0
    DO 1031 I=1,IS
        A=(X(I+1)-X(I))/(Z(I+1)-Z(I))
        B=(X(I)*Z(I+1)-X(I+1)*Z(I))/(Z(I+1)-Z(I))
        D=0.5*ALOG((X(I+1)**2+Z(I+1)**2)/(X(I)**2
&+Z(I)**2))
        E=A*(ATAN(X(I+1)/Z(I+1))-ATAN(X(I)/Z(I)))
        R1=B*(D+E)/(1+A**2)
1031   S=S+R1
        W(M)=2*AK*P*S
        ISS=IS+1
        DO 1038 I=1,ISS
            M1=M+1
            IF(M1.GT.N)GO TO 1030
1038   X(I)=X(I)-(C(M1)-C(M))
1030 CONTINUE
C   END OF GRAVITY CALCULATION
C   CALCULATE DLT FROM DIFFERENCE IN CALCULATED AND OBSERVED VALUES
    DO 50 I=1,N
        DLG(I)=G1(I)-W(I)
        DLT(I)=DLG(I)/(41.9*P)
50 CONTINUE
C   FIND AND CHECK SUM OF SQUARES OF RESIDUALS AND CHECK NKOUNT
    TB=0.0
    TTL=0.0
    DO 51 I=1,N
        TB=DLG(I)**2.0
        TTL=TTL+TB
51 CONTINUE
    WRITE(2,904)TTL
    KOUNT=KOUNT+1
    IF(TTL.LT.SIGMA)GOTO 56
    IF(KOUNT.GE.NKOUNT)GOTO 56
C   BEGIN COSINE BELL SMOOTHING
C   IM-----STATION NO. I-J, WHERE I IS THE CENTER OF THE BELL
C   XM,XP-----DISTANCE FROM BELL CENTER TO THE IMth STATION
C   IP-----STATION NO. I+J, WHERE I IS THE CENTER OF THE BELL
C   XM1,XP1----ANGLE (0-90) OF LOCATION XP FROM CENTER OF BELL (0)
C   CXM1,CXP1--WEIGHTING FACTOR AT IMth/IPth STATION
C   TWIM-----SUM OF WEIGHTS IN I-J DIRECTION
C   TWIP-----SUM OF WEIGHTS IN I+J DIRECTION
C   TWT-----TOTAL WEIGHTS AT A STATION
C   DLT2-----THICKNESS CHANGE AT IMth or IPth STATION DUE TO CENTRAL
C   POINT THICKNESS
    PID2=3.1415927/2.0
    DO 701 I=1,N
        TWIM=0.0
        TWIP=0.0
        TWT=0.0

```

Appendix 2.3: 2-D gravity inversion program.

```

DO 702 J=1,J2
  IM(J)=I-J
  IF(IM(J).LT.1)GOTO 704
  XM=C(I)-C(IM(J))
704  IP(J)=I+J
     IF(IP(J).GT.N)GOTO 705
     XP=C(IP(J))-C(I)
705  IF(IM(J).LT.1.AND.IP(J).LE.N)GOTO 703
     IF(IM(J).LT.1.AND.IP(J).GT.N)GOTO 710
     IF(IM(J).LT.1)GOTO 703
     IF(XM.GE.WIDTH)GOTO 703
     XM1=PID2*(XM/WIDTH)
     CXM1(J)=(COS(XM1)**2.0)/2.0
     TWTM=TWTM+CXM1(J)
703  IF(IP(J).GT.N)GOTO 702
     IF(XP.GE.WIDTH)GOTO 702
     XP1=PID2*(XP/WIDTH)
     CXP1(J)=(COS(XP1)**2.0)/2.0
     TWTP=TWTP+CXP1(J)
702  CONTINUE
710  TWT=TWTM+TWTP
     DO 706 J=1,J2
       IF(IM(J).GE.1.AND.TWT.GT.0.00) THEN
         DLT2(IM(J))=DLT2(IM(J))+((CXM1(J)/TWT)*DLT(I))
       END IF
       IF(IP(J).LE.N.AND.TWT.GT.0.00) THEN
         DLT2(IP(J))=DLT2(IP(J))+((CXP1(J)/TWT)*DLT(I))
       END IF
       IM(J)=0
       IP(J)=0
       CXM1(J)=0.00
       CXP1(J)=0.00
706  CONTINUE
     DLT(I)=DLT(I)/2.0
701 CONTINUE
     DO 707 I=1,N
       DLT(I)=(DLT(I)+DLT2(I))/2.0
       TH(I)=TH(I)+DLT(I)
       DLT2(I)=0.0
       IF(TH(I).GT.0.01)GOTO 707
       TH(I)=0.01
707 CONTINUE
C REASSIGN X,Z VALUES TO THE BODY
  X(1)=0.0-GAMMA+ADJ
  X(2)=XL-GAMMA
  X(IS+1)=X(1)
  Z(1)=0.001+ZD
  Z(2)=0.002+ZD
  Z(IS+1)=Z(1)
DO 54 I=3,IS
  J=N-I+3

```

Appendix 2.3: 2-D gravity inversion program.

```

IF(IZ(J).EQ.0) THEN
  Z(I)=ZD+TH(J)
  GOTO 53
END IF
IF(IZ(J).EQ.5) THEN
  Z(I)=Z2(J)
  GOTO 53
END IF
Z(I)=ZD+TH(J)
IF(Z(I).LT.RZ1(J)) THEN
  Z(I)=RZ1(J)
  GOTO 53
END IF
IF(Z(I).GT.RZ2(J)) THEN
  Z(I)=RZ2(J)
END IF
53  X(I)=C(J)
    IF(Z(I).NE.Z(I-1))GOTO 54
    Z(I)=Z(I)+.001
54  CONTINUE
    GOTO 100
C  CALCULATE MEAN AND STANDARD DEVIATION OF THE MODEL
56  WRITE(6,905)KOUNT
    XMEAN=0
    V1=0
    VAR=0
    DO 120 I=1,N
120  XMEAN=XMEAN+DLG(I)
    XMEAN=XMEAN/N
    DO 121 I=1,N
121  V1=V1+((DLG(I)-XMEAN)**2.0)
    VAR=SQRT(V1/(N-1))
    WRITE(6,906)XMEAN,VAR
    WRITE(2,906)XMEAN,VAR
C  RENUMBER BODY IN X AND OUTPUT FINAL MODEL
    DO 57 I=1,N
57  C(I)=C(I)+GAMMA
    X(1)=0.0+ADJ
    X(2)=XL
    DO 58 I=3,IS
      J=N-I+3
58  X(I)=C(J)
    DO 59 I=1,IS
      WRITE(6,907)X(I),Z(I)
59  CONTINUE
    DO 60 I=1,N
      WRITE(6,908)C(I),G1(I),DLG(I),W(I)
60  CONTINUE
1035 WRITE(2,909)N,P,XL,IS,SIGMA,TTL,KOUNT,ZD
    DO 1090 I=1,N
1090  WRITE(2,910)C(I),G1(I),DLG(I),W(I),ID(I)
    DO 1093 I=1,IS

```

Appendix 2.3: 2-D gravity inversion program.

```
      WRITE(2,911)X(I),Z(I)
1093 CONTINUE
      J=1
      WRITE(3,915)N,J
      DO 500 I=1,N
        WRITE(3,916)G1(I),C(I),W(I)
500 CONTINUE
      WRITE(3,917)IS
      DO 501 I=1,IS
        WRITE(3,918)X(I),Z(I)
501 CONTINUE
900 FORMAT(A72)
901 FORMAT(1X,A71)
902 FORMAT(15,2F6.2,F8.2,I5,F6.2,F3,16X,F8.3)
903 FORMAT(2F10.2,I5,2F10.2,I5)
904 FORMAT(F10.2)
905 FORMAT(2X,'THE TOTAL NUMBER OF INTERATIONS=',I5)
906 FORMAT(2X,'THE MEAN IS',F7.3,' AND THE STANDARD DEVIATION
      &IS',F7.3)
907 FORMAT(2F10.2)
908 FORMAT(4F10.2)
909 FORMAT(15,2F6.2,I5,F8.5,F10.2,I5,F8.3)
910 FORMAT(4F10.2,I10)
911 FORMAT(2F10.2)
915 FORMAT(2I5)
916 FORMAT(3F10.2)
917 FORMAT(5X,I5)
918 FORMAT(2F10.3)
950 FORMAT(2X,'WHAT IS THE NAME OF THE DATA FILE TO BE READ?',S)
951 FORMAT(A30)
999 STOP
      END
```

Appendix 2.4: 3-D gravity modelling program.

```

C          3-D GRAVITY PROGRAM BY M. TALWANI
C KK-----TOTAL NUMBER OF STATIONS
C MQ-----NUMBER OF CONTOURS FOR THIS BODY
C J-----IF J=0, THEN ANOTHER BODY FOLLOWS
C          IF J=9, THEN THIS IS THE LAST BODY
C AUX-----DEBUGGING STEP THAT OUTPUTS CONTRIBUTIONS
C          OF EACH SIDE, OF EACH POLYGON
C U-----IF U=0, THEN BODY TOP ENDS IN A CONTOUR
C          IF U NE 0, THEN BODY TOP ENDS IN A POINT
C ZU-----DEPTH TO TOP OF BODY WHEN U NE 0
C VU-----ZERO
C T-----IF T=0, THEN BODY BOTTOM ENDS IN A CONTOUR
C          IF T NE 0, THEN BODY BOTTOM ENDS IN A POINT
C ZT-----DEPTH TO THE BOTTOM OF BODY WHEN T NE 0
C VT-----ZERO
C GGG-----ANOTHER DEBUGGING STEP. IF G NE 0, OUTPUT OF
C          INTEGRATION CALCULATIONS OCCURS
C PUN-----ZERO
C FX-----X COORDINATE OF A STATION
C FY-----Y COORDINATE OF A STATION
C FZ-----Z COORDINATE OF A STATION
C GANOM----OBSERVED ANOMALY AT A STATION (FX,FY,FZ)
C ANOM----ANOMALY AT A STATION DUE TO ONE BODY
C TANOM----SUM OF ALL ANOM'S FOR A STATION
C RANOM----RANOM = TANOM - GANOM
C MID-----NUMERICAL ID OF A CONTOUR, i.e. FOR THE FIRST CONTOUR,
C          MID=1, etc.
C RHO-----DENSITY CONTRAST IN G/CM**3 AS A CONTOUR LEVEL.
C          THIS CAN CHANGE WITH DEPTH IN THIS MODEL.
C ZEE-----DEPTH OF THE CONTOUR
C III-----NUMBER OF CORNER POINTS FOR A CONTOUR
C DUM-----IF DUM NE 0, THEN THIS COUNTOUR IS IDENTICAL TO THE
C          PREVIOUS ONE
C X(I,J)----X COORDINATE OF A CONTOUR CORNER POINT
C Y(I,J)----Y COORDINATE OF A CONTOUR CORNER POINT
C V-----SUM OF CONTRIBUTIONS FOR A PARTICULAR CONTOUR
          DIMENSION FX(500),FY(500),FZ(500),III(100),RHO(100),ZEE(100),
          &MID(100),V(100),DEL(100),DELP(100),X(100,200),Y(100,200),
          &SIGMA(100),GG(100),TANOM(500),GANOM(500),RANOM(500)
          CHARACTER*72 TITLE
          CHARACTER*20 CFIN,CFOUT
          WRITE(6,950)
          ACCEPT 951,CFIN
          OPEN(10,NAME=CFIN,STATUS='OLD')
          WRITE(6,952)
          ACCEPT 951,CFOUT
          OPEN(11,NAME=CFOUT,STATUS='NEW')
          OPEN(12,NAME='S2GRAV.OUT',STATUS='NEW')
C INITIALIZE VARIABLES
          DATA JRK/0/,TANOM/500*0.0/,KRT/0/,FZ/500*0.0/
          50 KRT=KRT+1

```

Appendix 2.4: 3-D gravity modelling program.

```

DO 51 I4=1,100
  III(I4)=0.0
  RHO(I4)=0.0
  ZEE(I4)=0.0
  MID(I4)=0.0
  V(I4)=0.0
  DEL(I4)=0.0
  DELP(I4)=0.0
  SIGMA(I4)=0.0
  GG(I4)=0.0
DO 52 I5=1,200
  X(I4,I5)=0.0
  Y(I4,I5)=0.0
52 CONTINUE
51 CONTINUE
C READ IN DATA
  READ(10,900)TITLE
  WRITE(6,900)TITLE
55 READ(10,901)KK, MQ, J, AUX, U, ZU, VU, T, ZT, VT, GGG, PUN
  WRITE(6,902)KK, MQ, J, AUX, U, ZU, VU, T, ZT, VT, GGG, PUN
  IF(KRT.GT.1)GO TO 65
60 READ(10,903)(FX(K),FY(K),GANOM(K),K=1, KK)
  WRITE(6,904)(FX(K),FY(K),GANOM(K),K=1, KK)
65 MM=MQ+1
70 DO 75 M=2, MM
  READ(10,905)MID(M), RHO(M), ZEE(M), III(M), DUM
  WRITE(6,905)MID(M), RHO(M), ZEE(M), III(M), DUM
  II=III(M)
  MUM=M-1
  DO 20 I3=1,100
    DO 21 J3=1,200
      X(I, J)=0.0
      Y(I, J)=0.0
21 CONTINUE
20 CONTINUE
  IF(DUM)3,4,3
  3 IF(M-2)5,4,5
  5 DO 6 I=1, II
    X(M, I)=X(MUM, I)
  6 Y(M, I)=Y(MUM, I)
  GOTO 75
  4 READ(10,907)(X(M, I), Y(M, I), I=1, II)
  WRITE(6,907)(X(M, I), Y(M, I), I=1, II)
75 CONTINUE
80 WRITE(6,908)
85 WRITE(6,900)
  IF(PUN)100,200,100
C CHECK TO SEE IF BODY TOP OR BOTTOM ENDS IN A POINT
100 IF(U)105,110,105
105 MO=1
  ZEE(1)=ZU
  V(1)=VU
  GOTO 115

```

Appendix 2.4: 3-D gravity modelling program.

```

110 MO=2
115 IF(T)120,125,120
120 MP=MM+1
    ZEE(MP)=ZT
    V(MP)=VT
    GOTO 130
125 MP=MM
130 NGC=MP-MO+1
    MRS=MO+2
    NGG=NGC-2
200 DO 500 K=1, KK
    IF(JRK.EQ.0)THEN
C   WRITE X, Y, Z COORDINATES OF THE STATIONS
        WRITE(6,916)
        WRITE(6,917)
205    WRITE(6,918)K, FX(K), FY(K), FZ(K)
    END IF
C   BEGIN CALCULATION OF CONTRIBUTIONS OF EACH CONTOUR
210 DO 420 M=2, MM
    SIGA=0
    SFELZ=0
    Z=ZEE(M)-FZ(K)
215  ALPH1=X(M,1)-FX(K)
    BETA1=Y(M,1)-FY(K)
    R1=SQRT(ALPH1**2+BETA1**2)
    IF(R1)220,225,220
220  GAMM1=ALPH1/R1
    DELT1=BETA1/R1
225  IF(AUX)230,235,230
230  WRITE(6,909)MID(M), III(M), ZEE(M), RHO(M)
235  II=III(M)
    DO 395 I=2, II
    ALPH2=X(M,I)-FX(K)
    BETA2=Y(M,I)-FY(K)
    R2=SQRT(ALPH2**2+BETA2**2)
    IF(R2)240,365,240
240  GAMM2=ALPH2/R2
    DELT2=BETA2/R2
245  IF(R1)250,365,250
250  DEATH=ALPH1-ALPH2
    TAXES=BETA1-BETA2
    IF(DEATH.EQ.0.0.AND.TAXES.EQ.0.0)GOTO 365
    SS=SQRT(DEATH**2+TAXES**2)
    EGA=DEATH/SS
    TAU=TAXES/SS
    P=TAU*ALPH1-EGA*BETA1
    IF(ABS(P)-.00001)365,365,255
255  IF(P)260,365,265
260  S=-1.0
    GOTO 270
265  S=1.0
270  EMM=BETA1*ALPH2-BETA2*ALPH1

```

Appendix 2.4: 3-D gravity modelling program.

```

275 IF(EMM)280,365,285
280 W=-1.0
      GOTO 290
285 W=1.0
290 IF(Z)291,292,291
291 PSI=S*(Z/SQRT(P**2+Z**2))
292 AA=GAMM1*GAMM2+DELT1*DELT2
      IF((1.-AA**2.0).LT.0.00)THEN
          A=0.0
          GOTO 310
      END IF
      IF(AA)300,295,305
295 A=W*1.570796327
      GOTO 310
300 A=W*(ATAN((SQRT(1.-AA**2))/AA)+3.141592654)
      GOTO 310
305 A=W*ATAN((SQRT(1.-AA**2))/AA)
310 IF(Z)312,311,312
311 B=0
      C=0
      GOTO 360
312 BB=(PSI*(EGA*GAMM1+TAU*DELT1))
      IF(BB-1.)320,315,320
315 B=1.570796327
      GOTO 335
320 IF(BB+1.)330,325,330
325 B=-1.570796327
      GOTO 335
330 IF(ABS(BB).LT.1.00) THEN
      B=ATAN(BB/(SQRT(1.-BB**2)))
      ELSE
      B=0
      END IF
335 CC=(PSI*(EGA*GAMM2+TAU*DELT2))
      IF(CC-1.)345,340,345
340 C=1.570796327
      GOTO 360
345 IF(CC+1.)355,350,355
350 C=-1.570796327
      GOTO 360
355 IF(ABS(CC).LT.1.0) THEN
      C=ATAN(CC/(SQRT(1.-CC**2)))
      ELSE
      C=0.0
      END IF
360 D=C-B
      FELZ=A+D
      GOTO 370
365 FELZ=0
      A=0
      B=0
      C=0
      D=0

```

Appendix 2.4: 3-D gravity modelling program.

```
370 IF(AUX)375,385,375
375 PARFE=6.67*RHO(M)*FELZ
380 CCG=ALPH1+FX(K)
    CCGS=BETA1+FY(K)
    CCGG=ALPH2+FX(K)
    COGGS=BETA2+FY(K)
    IRMA=I-1
    WRITE(6,910)IRMA,CCG,CCGS,CCGG,COGGS,A,B,C,D,PARFE
    WRITE(6,911)SS,TAU,EGA,P
385 SFELZ=SFELZ+FELZ
    SIGA=SIGA+A
390 ALPH1=ALPH2
    BETA1=BETA2
    GAMM1=GAMM2
    DELT1=DELT2
    R1=R2
395 CONTINUE
400 IF(SIGA)401,414,403
401 IF(SIGA+.00001)404,402,402
402 SFELZ=SFELZ-SIGA
    GOTO 414
403 IF(SIGA-.00001)402,402,409
404 IF(SIGA+6.2831754)408,408,405
405 IF(SIGA+3.1416027)414,407,406
406 IF(SIGA+3.1415827)407,407,414
407 SFELZ=SFELZ-SIGA-3.1415927
    GOTO 414
408 SFELZ=SFELZ-SIGA-6.2831854
    GOTO 414
409 IF(SIGA-6.2831754)410,413,413
410 IF(SIGA-3.1415827)414,412,411
411 IF(SIGA-3.1416027)412,412,414
412 SFELZ=SFELZ-SIGA+3.1415927
    GOTO 414
413 SFELZ=SFELZ-SIGA+6.2831854
414 V(M)=6.67*RHO(M)*SFELZ
    SIGMA(M)=SIGA
420 CONTINUE
C END CALCULATION OF GRAVITY DUE TO EACH CONTOUR
C CHECK TO SEE IF BODY TOP OR BOTTOM END IN POINT
  IF(Y)425,430,425
425 MO=1
    MID(1)=0
    III(1)=1
    ZEE(1)=ZU
    RHO(1)=RHO(2)
    SIGMA(1)=0.0
    V(1)=VU
    GOTO 435
430 MO=2
435 IF(T)440,445,440
440 MP=MM+1
```

Appendix 2.4: 3-D gravity modelling program.

```

MID(MP)=MID(MM)+1
III(MP)=1
ZEE(MP)=ZT
RHO(MP)=RHO(MM)
SIGMA(MP)=0.0
V(MP)=VT
GOTO 450
445 MP=MM
C BEGIN NUMERICAL INTERGRATION TO GET GRAVITY ANOMALIES
450 DEL(MO)=0.0
DELP(MO)=0.0
DELP(MO+1)=0.0
DEL(MP)=0.0
ANOM=0.0
MN=MP-2
455 DO 460 M=MO,MN
XA1=(ZEE(M)-ZEE(M+1))/(ZEE(M)-ZEE(M+2))
XB1=3.0*ZEE(M+2)-2.0*ZEE(M)-ZEE(M+1)
XC1=V(M)*XA1*XB1
XA2=(ZEE(M)-ZEE(M+1))/(ZEE(M+1)-ZEE(M+2))
XB2=3.0*ZEE(M+2)-2.0*ZEE(M+1)-ZEE(M)
XC2=V(M+1)*XA2*XB2
XA3=(ZEE(M)-ZEE(M+1))*(ZEE(M)-ZEE(M+1))*(ZEE(M)-ZEE(M+1))
XB3=(ZEE(M+1)-ZEE(M+2))*(ZEE(M)-ZEE(M+2))
XC3=V(M+2)*(XA3/XB3)
DEL(M+1)=(XC1+XC2+XC3)/6.0
YA1=(ZEE(M+1)-ZEE(M+2))*(ZEE(M+1)-ZEE(M+2))*(ZEE(M+1)-ZEE(M+2))
YB1=(ZEE(M)-ZEE(M+2))*(ZEE(M)-ZEE(M+1))
YC1=V(M)*(YA1/YB1)
YA2=(ZEE(M+1)-ZEE(M+2))/(ZEE(M)-ZEE(M+1))
YB2=ZEE(M+2)+2.0*ZEE(M+1)-3.0*ZEE(M)
YC2=V(M+1)*YA2*YB2
YA3=(ZEE(M+1)-ZEE(M+2))/(ZEE(M)-ZEE(M+2))
YB3=ZEE(M+1)+2.0*ZEE(M+2)-3.0*ZEE(M)
YC3=V(M+2)*YA3*YB3
DELP(M+2)=(YC1+YC2+YC3)/6.0
460 CONTINUE
ANOM=0.5*(DEL(MO+1)+DELP(MP))
DO 465 M=MO,MP
ANOM=ANOM+0.5*(DEL(M)+DELP(M))
GG(M)=ANOM-0.5*DELP(MP)
465 CONTINUE
GG(MO)=0.0
GG(MO+1)=0.0
GG(MP)=GG(MP)+0.5*DELP(MP)
C WRITE DATA INTO CPOUT AND S2GRAV.OUT
WRITE(11,930)FX(K),FY(K),ANOM,
TANOM(K)-TANOM(K)+ANOM
JRK=JRK+1
IF(PUN)470,475,470
470 WRITE(11,914)(V(M),M=MO,MP)
475 IF(GGG)476,500,476

```

Appendix 2.4: 3-D gravity modelling program.

```

476 WRITE(6,915)(GG(M),M=MO,MP)
    IF(:JN)480,500,480
480 WRITE(11,914)(GG(M),M=MRS,MP)
500 CONTINUE
    WRITE(11,931)
510 IF(J.NE.9)GOTO 50
    DO 511 K=1,KK
        RANOM(K)=GANOM(K)-TANOM(K)
C        WRITE(6,919)K,FX(K),FY(K),TANOM(K)
        WRITE(12,920)K,FX(K),FY(K),GANOM(K),TANOM(K),RANOM(K)
511 CONTINUE
900 FORMAT(A72)
901 FORMAT(1X,2I3,1I,2F2.1,2F12.6,F2.1,2F12.6,2F2.1)
902 FORMAT(1X,2I5,1I,2F4.1,2F12.6,F4.1,2F12.6,2F4.1)
903 FORMAT(6F12.3)
904 FORMAT(1X,6F12.3)
905 FORMAT(1X,12,F10.4,F16.3,18,F6.2)
907 FORMAT(6F12.3)
908 FORMAT(10X,'3-D GRAVITY PROGRAM')
909 FORMAT(1X,///,12,3X,'VERTICES-',12,3X,'DEPTH-',F7.2,3X,F5.2)
910 FORMAT(1X,12,3F9.2,F10.2,4F12.7,F12.6)
911 FORMAT(4E18.7)
912 FORMAT(1X,12,15,E10.3,F8.2,F12.7,F12.6,2E12.4)
913 FORMAT(1X,///,10X,'TOTAL ANOMALY-',1X,E12.4)
914 FORMAT(6E12.6)
915 FORMAT(1X,9E12.4)
916 FORMAT(15X,'FIELD POINT COORDINATES',//,20X'CONTOUR DATA')
917 FORMAT(11X,'K',4X,'X',9X,'Y',11X,'Z')
918 FORMAT(1X,12,F8.2,F12.2,F12.2)
919 FORMAT(10X,'THE ANOMALY FOR FIELD POINT #',15,'',/,12X,
&'COORDINATES -',F10.3,'',F10.3,/,14X,'IS ',F10.2,/)
920 FORMAT(15,5F10.3)
930 FORMAT(2X,3F10.3)
931 FORMAT(//)
950 FORMAT(2X,'WHAT IS THE NAME OF THE INPUT FILE? ',S)
951 FORMAT(A20)
952 FORMAT(2X,'WHAT IS THE NAME OF THE OUTPUT FILE? ',S)
    STOP
    END

```

Appendix 2.5: 3-D magnetics modelling program

```

C          3-D MAGNETICS PROGRAM
C    BASED ON EQUATIONS GIVEN IN TALWANI, GEOPHYSICS 30,
C          PP. 797-817,1965.
C    KK-----TOTAL NUMBER OF STATIONS
C    MQ-----NUMBER OF CONTOURS FOR THIS BODY
C    AUX-----DEBUGGING STEP THAT OUTPUTS CONTRIBUTIONS
C              OF EACH SIDE OF EACH POLYGON
C    U-----IF U=0, THEN BODY TOP ENDS IN A CONTOUR
C             IF U NE 0, THEN BODY TOP ENDS IN A POINT
C    ZU-----DEPTH TO TOP OF BODY WHEN U NE 0
C    VU-----ZERO
C    T-----IF T=0, THEN BODY BOTTOM ENDS IN A CONTOUR
C             IF T NE 0, THEN BODY BOTTOM ENDS IN A POINT
C    ZT-----DEPTH TO THE BOTTOM OF BODY WHEN T NE 0
C    VU-----ZERO
C    GGG-----ANOTHER DEBUGGING STEP. IF G NE 0, OUTPUT OF
C              INTEGRATION CALCULATIONS OCCURS
C    PUN-----ZERO
C    FX-----X COORDINATE OF A STATION
C    FY-----Y COORDINATE OF A STATION
C    AI-----MAGNETIC INCLINATION IN DEGREES
C    AD-----MAGNETIC DECLINATION IN DEGREES
C    F-----TOTAL BACKGROUND FIELD
C    NBOD-----NUMBER OF BODIES
C    FZ-----OBSERVED ANOMALY AT A STATION (FX,FY)
C    ANOM-----ONE OF THE 6 NUMBERS CALCULATED FOR EACH CONTOUR THAT
C              ARE USED TO CALCULATE THE DX,DY, AND DZ VECTORS
C    DX,DY-----CALCULATED MAGNETIC VECTOR AT A STATION DUE TO A BODY,
C              IN THE X AND Y DIRECTIONS, RESPECTIVELY.
C    DZ,DH-----CALCULATED MAGNETIC VECTOR AT A STATION DUE TO A BODY,
C              VERTICAL AND HORIZONTAL COMPONENTS, RESPECTIVELY
C    DT-----TOTAL ANOMALY AT A STATION DUE TO A BODY
C    TDX,TDY-----TOTAL CALCULATED MAGNETIC VECTOR AT A STATION IN THE
C              X AND Y DIRECTIONS, RESPECTIVELY
C    TDZ,TDH-----TOTAL CALCULATED MAGNETIC VECTOR AT A STATION IN THE
C              VERTICAL AND HORIZONTAL DIRECTIONS, RESPECTIVELY
C    TDT-----TOTAL CALCULATED MAGNETIC ANOMALY AT A STATION
C    MID-----NUMERICAL ID OF A CONTOUR, I.E. FOR THE FIRST CONTOUR,
C              MID=1, etc.
C    RHO-----DENSITY CONTRAST IN G/CM**3 AS A CONTOUR LEVEL.
C              THIS CAN CHANGE WITH DEPTH IN THIS MODEL.
C    ZEE-----DEPTH OF THE CONTOUR
C    III-----NUMBER OF CORNER POINTS FOR A CONTOUR
C    DUM-----IF DUM NE 0, THEN THIS CONTOUR IS IDENTICAL TO THE
C              PREVIOUS ONE
C    X(I,J)-----X COORDINATE OF A CONTOUR CORNER POINT
C    Y(I,J)-----Y COORDINATE OF A CONTOUR CORNER POINT
C    V-----SUM OF CONTRIBUTIONS FOR A PARTICULAR CONTOUR
C
C    DIMENSION FX(100),FY(100),FZ(100),Z(50),MID(50),
C    &BN(50),G(50),PSQ(50),Z2P2(50),BNSQ(50),BM(50),BC(50),
C    &BP(50),ANOM(6),DX(100),DY(100),DZ(100),TDH(100),

```

Appendix 2.5: 3-D magnetics modelling program

```

&DH(100),DT(100),TDX(100),TDY(100),TDZ(100),BMSQ(50),
&TDT(100),III(50),X(50),Y(50)
  DIMENSION X2(50,50),Y2(50,50),GC(50,6),DEL(50,6),
&DELP(50,6),S(50,6)
  CHARACTER*20,CFILE
  CHARACTER*72,TITLE
  WRITE(6,925)
  ACCEPT 926,CFILE
  OPEN(1,NAME=CFILE,STATUS='OLD')
  OPEN(2,NAME='MAGDAT.OUT',STATUS='NEW')
  OPEN(3,NAME='MAGPLT.DAT',STATUS='NEW')
  READ(1,900)TITLE
  WRITE(2,900)TITLE
  WRITE(6,900)TITLE
  READ(1,901)AI,AD,F,NBOD,KK
  AI=(3.1415927/180.0)*AI
  ACI=COS(AI)
  ASI=SIN(AI)
  AD=(3.1415927/180.0)*AD
  ACD=COS(AD)
  ASD=SIN(AD)
  READ(1,903)(FX(K),FY(K),FZ(K),K-1,KK)
  DO 300 IJK=1,NBOD
  READ(1,902)MQ,J,AUX,U,ZU,VU,T,ZT,GGG,PUN
  READ(1,920)AK
  AJX=AK*F*ACI*ACD
  AJY=AK*F*ACI*ASD
  AJZ=AK*F*ASI
  MM=MQ+1
  DO 30 M=2,MM
  READ(1,904)MID(M),Z(M),III(M),DUM
  II=III(M)
  MUM=M-1
  IF(DUM.EQ.0.0)GOTO 4
  IF((M-2).EQ.0.0)GOTO 4
  DO 6 I=1,II
    X2(M,I)=X2(MUM,I)
    Y2(M,I)=Y2(MUM,I)
  6   GOTO 30
  4   READ(1,905)(X2(M,I),Y2(M,I),I-1,II)
  30  CONTINUE
  IF(PUN.EQ.0.0)GOTO 100
  IF(U.EQ.0.0)GOTO 50
    MO=1
    Z(1)=ZU
    DO 45 J=1,6
      S(1,J)=VU
    45  GOTO 55
  50  MO=2
  55  IF(T.EQ.0.0)GOTO 70
    MP=MM+1
    Z(MP)=ZT

```

Appendix 2.5: 3-D magnetics modelling program

```

        DO 65 J=1,6
65      S(MP,J)=VT
        GOTO 75
70      MP=MM
75      NGC=MP-MO+1
        MRS=MO+2
        NGC=NGC-2
100 DO 250 I=1, KK
        DO 110 L1=2, MM
        DO 105 L2=1, 6
        S(L1, L2)=0.0
105      CONTINUE
110      CONTINUE
        DO 125 J=2, MM
        DO 115 L=1, III(J)
        X(L)=X2(J, L)-FX(I)
        Y(L)=Y2(J, L)-FY(I)
        IF(L.GT.1) THEN
            IF(X(L).NE.X(L-1))GOTO 114
            X(L)=X(L)+0.001
114          IF(Y(L).NE.Y(L-1))GOTO 115
            Y(L)=Y(L)+0.001
        END IF
115      CONTINUE
        K2=III(J)-1
        DO 120 K=1, K2
C      THE CALCULATIONS OF C1, C2, & C3 AND NECESSARY PARAMETERS
        BN(K)=(X(K+1)-X(K))/(Y(K+1)-Y(K))
        G(K)=X(K)-Y(K)*BN(K)
        BNSQ(K)=1.0+BN(K)**2.0
        PSQ(K)=(G(K)**2.0)/BNSQ(K)
        BR1=SQRT(X(K)**2.0+Y(K)**2.0+Z(J)**2.0)
        BR2=SQRT(X(K+1)**2.0+Y(K+1)**2.0+Z(J)**2.0)
        ZSQ=Z(J)**2.0
        Z2P2(K)=ZSQ+PSQ(K)
        C1=((1.0/BNSQ(K))/Z2P2(K))*(((G(K)*Y(K+1)-BN(K)*ZSQ)
&/BR2)-((G(K)*Y(K)-BN(K)*ZSQ)/BR1))
        C2=((1.0/BNSQ(K))/Z2P2(K))*(((G(K)**2.0+ZSQ+G(K)*
&Y(K+1)*BN(K))/BR2)-((G(K)**2.0+ZSQ+G(K)*Y(K)*BN(K))/BR1))
        C3=Z(J)*((1.0/BNSQ(K))/Z2P2(K))*(((Y(K+1)*BNSQ(K)+
&G(K)*BN(K))/BR2)-((Y(K)*BNSQ(K)+G(K)*BN(K))/BR1))
C      THE CALCULATIONS OF C4 AND C5 AND NECESSARY PARAMETERS
        BM(K)=1.0/BN(K)
        BC(K)=Y(K)-X(K)*BM(K)
        BMSQ(K)=1.0+BM(K)**2.0
        C4=((1.0/BMSQ(K))/Z2P2(K))*(((BC(K)*X(K+1)-BM(K)*ZSQ)/BR2)-
&((BC(K)*X(K)-BM(K)*ZSQ)/BR1))
        C5=Z(J)*((1.0/BMSQ(K))/Z2P2(K))*(((X(K+1)*BMSQ(K)+
&BC(K)*BM(K))/BR2)-((X(K)*BMSQ(K)+BC(K)*BM(K))/BR1))
C      THE CALCULATION OF C6 AND NECESSARY PARAMETERS
        R1=SQRT(X(K)**2.0+Y(K)**2.0)
        R2=SQRT(X(K+1)**2.0+Y(K+1)**2.0)

```

Appendix 2.5: 3-D magnetics modelling program

```

R12=SQRT((X(K)-X(K+1))**2.0+(Y(K)-Y(K+1))**2.0)
DELXR=(X(K)-X(K+1))/R12
DELYR=(Y(K)-Y(K+1))/R12
BP(K)=SQRT(PSQ(K))
CSBETA=DELXR*(X(K)/R1)+DELYR*(Y(K)/R1)
CSGAMM=DELXR*(X(K+1)/R2)+DELYR*(Y(K+1)/R2)
C6=(BP(K)/Z2P2(K))*(((R2*CSGAMM)/BR2)-((R1*CSBETA)/BR1))
C TOTALS OF @ C# FOR EACH BODY
S(J,1)=S(J,1)+C1
S(J,2)=S(J,2)+C2
S(J,3)=S(J,3)+C3
S(J,4)=S(J,4)+C4
S(J,5)=S(J,5)+C5
S(J,6)=S(J,6)+C6
120 CONTINUE
S(J,1)=-1.0*S(J,1)
S(J,3)=-1.0*S(J,3)
S(J,6)=-1.0*S(J,6)
125 CONTINUE
IF(U.EQ.0.0)GOTO 160
MO=1
MID(1)=0
III(1)=1
Z(1)=ZU
DO 155 J=1,6
155 S(1,J)=VU
GOTO 165
160 MO=2
165 IF(T.EQ.0.0)GOTO 180
MP=MM+1
MID(MP)=MID(MM)+1
III(MP)=1
Z(MP)=ZT
DO 175 J=1,6
175 S(1,J)=VT
GOTO 185
180 MP=MM
185 DO 190 J=1,6
DEL(MO,J)=0.0
DELP(MO,J)=0.0
DELP(MO+1,J)=0.0
DEL(MP,J)=0.0
190 ANOM(J)=0.0
MN=MP-2
C INTEGRATION TO GET DEL(I,J) AND DELP(I,J)
DO 210 J=1,6
DO 200 M=MO,MN
XA1=(Z(M)-Z(M+1))/(Z(M)-Z(M+2))
XB1=3.0*Z(M+2)-2.0*Z(M)-Z(M+1)
XC1=S(M,J)*XA1*XB1
XA2=(Z(M)-Z(M+1))/(Z(M+1)-Z(M+2))
XB2=3.0*Z(M+2)-2.0*Z(M+1)-Z(M)

```

Appendix 2.5: 3-D magnetics modelling program

```

XC2=S(M+1,J)*XA2*XB2
XA3=(Z(M)-Z(M+1))*(Z(M)-Z(M+1))*(Z(M)-Z(M+1))
XB3=(Z(M+1)-Z(M+2))*(Z(M)-Z(M+2))
XC3=S(M+2,J)*(XA3/XB3)
DEL(M+1,J)=(XC1+XC2+XC3)/6.0
YA1=(Z(M+1)-Z(M+2))*(Z(M+1)-Z(M+2))*(Z(M+1)-Z(M+2))
YB1=(Z(M)-Z(M+2))*(Z(M)-Z(M+1))
YC1=S(M,J)*(YA1/YB1)
YA2=(Z(M+1)-Z(M+2))/(Z(M)-Z(M+1))
YB2=Z(M+2)+2.0*Z(M+1)-3.0*Z(M)
YC2=S(M+1,J)*YA2*YB2
YA3=(Z(M+1)-Z(M+2))/(Z(M)-Z(M+2))
YB3=Z(M+1)+2.0*Z(M+2)-3.0*Z(M)
YC3=S(M+2,J)*YA3*YB3
DELP(M+2,J)=(YC1+YC2+YC3)/6.0
200 CONTINUE
C CALCULATION OF THE TOTAL ANOM(J)
ANOM(J)=0.5*(DEL(MO+1,J)+DELP(MP,J))
DO 205 M=MO,MP
ANOM(J)=ANOM(J)+0.5*(DEL(M,J)+DELP(M,J))
GG(M,J)=ANOM(J)-0.5*DELP(MP,J)
205 CONTINUE
GG(MO,J)=0.0
GG(MO+1,J)=0.0
GG(MP,J)=GG(MP,J)+0.5*DELP(MP,J)
210 CONTINUE
CHECK=-1.0*(ANOM(1)+ANOM(4))
IF(CHECK.NE.ANOM(6)) THEN
ANOM(6)=CHECK
END IF
WRITE(2,906)
WRITE(2,907)(ANOM(L),L=1,6)
C CALCULATION OF MAGNETIC VECTORS FOR A PARTICULAR BODY
DX(I)=AJX*ANOM(1)+AJY*ANOM(2)+AJZ*ANOM(3)
DY(I)=AJX*ANOM(2)+AJY*ANOM(4)+AJZ*ANOM(5)
DZ(I)=AJX*ANOM(3)+AJY*ANOM(5)+AJZ*ANOM(6)
DH(I)=DX(I)*ACD+DY(I)*ASD
DT(I)=DH(I)*ACI+DZ(I)*ASI
WRITE(2,908)
WRITE(2,909)IJK,I,DX(I),DY(I),DZ(I),DH(I),DT(I)
WRITE(2,910)
250 CONTINUE
C CALCULATION OF THE TOTAL ANOMALY AT A STATION
DO 260 L=1,KK
TDX(L)=TDX(L)+DX(L)
TDY(L)=TDY(L)+DY(L)
TDZ(L)=TDZ(L)+DZ(L)
TDH(L)=TDH(L)+DH(L)
TDT(L)=TDT(L)+DT(L)
260 CONTINUE
300 CONTINUE
WRITE(2,911)

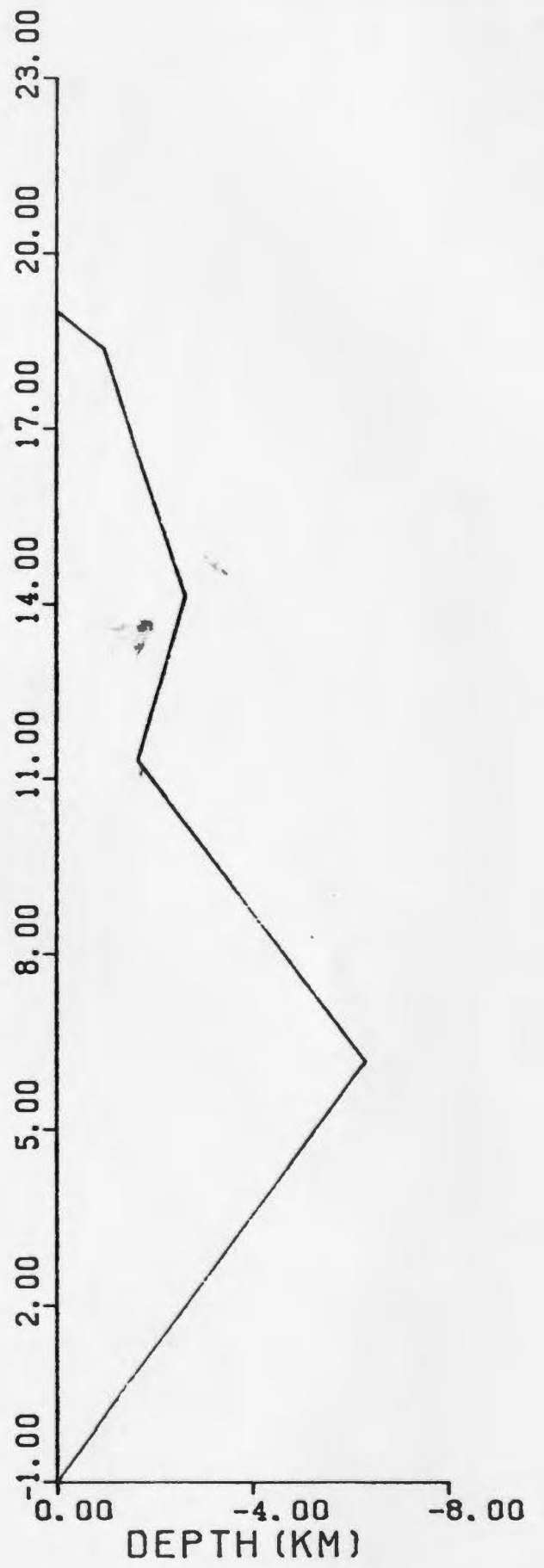
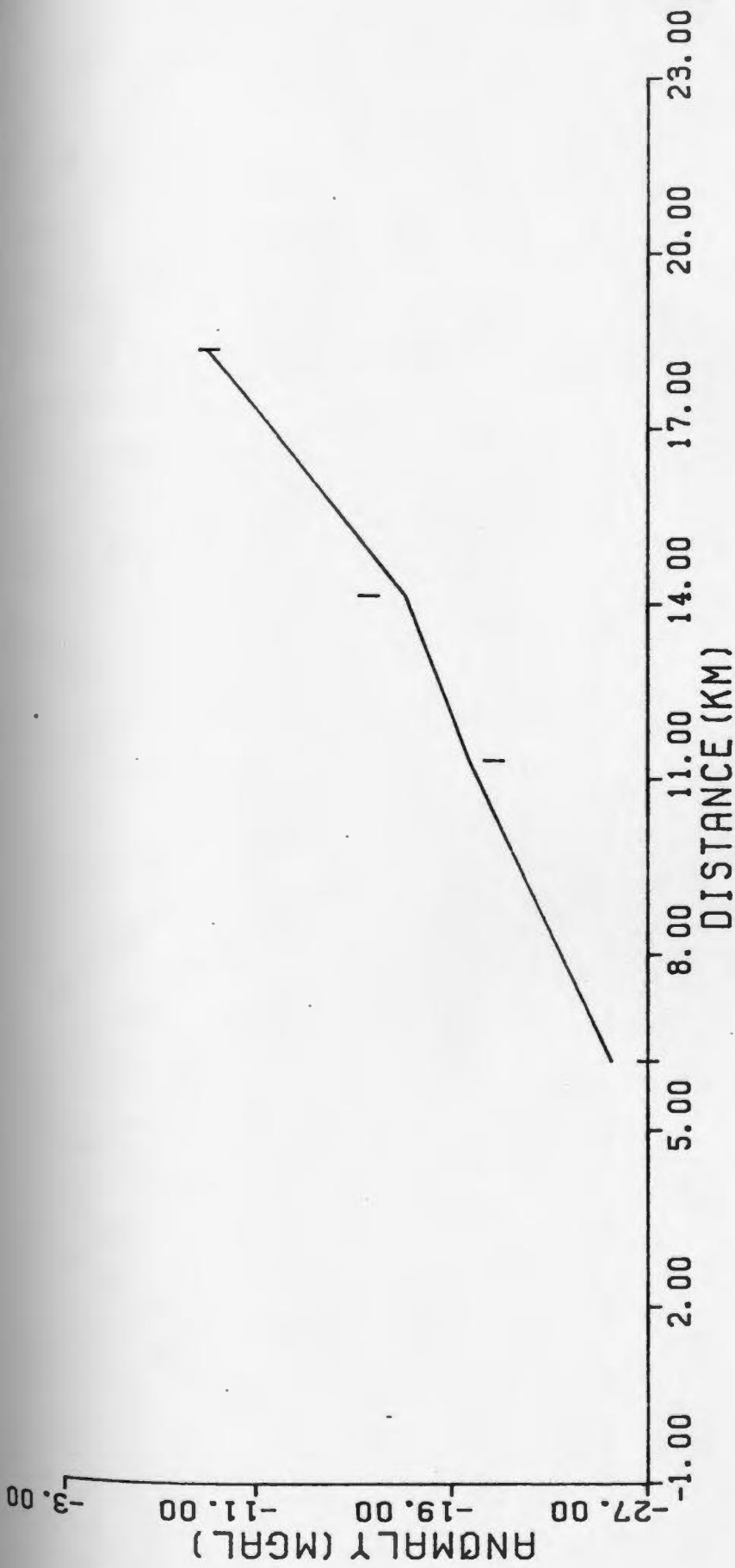
```

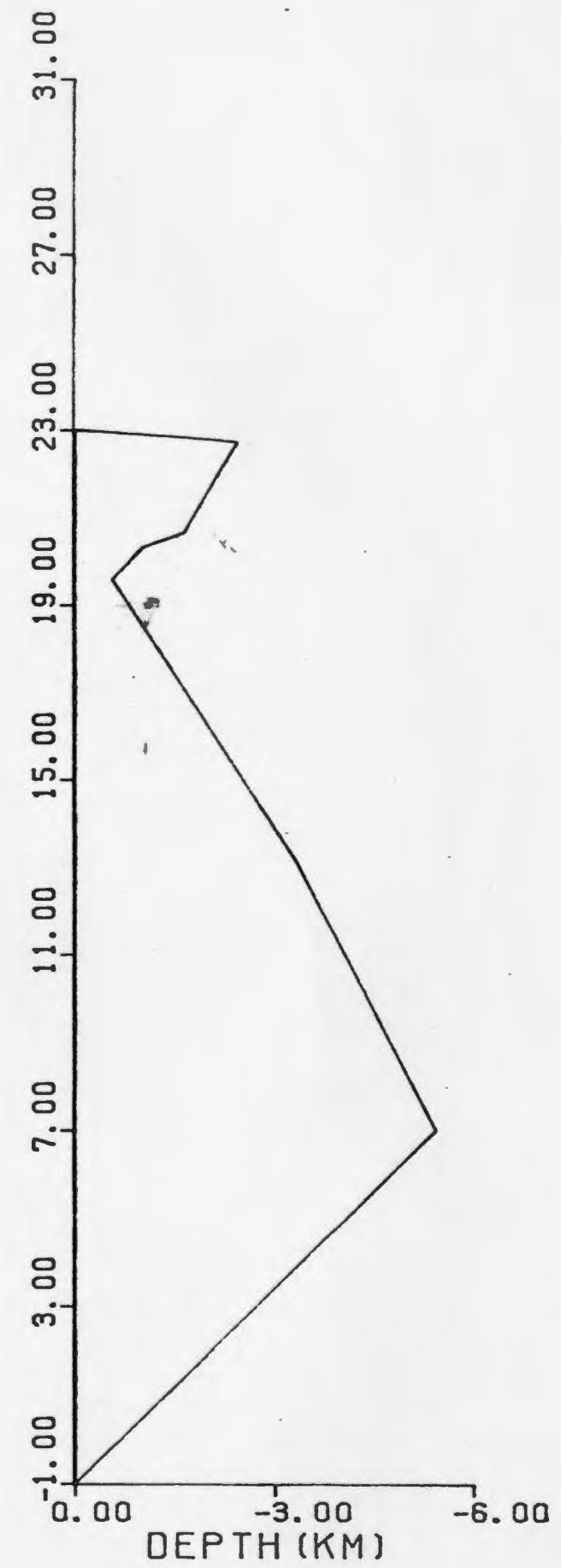
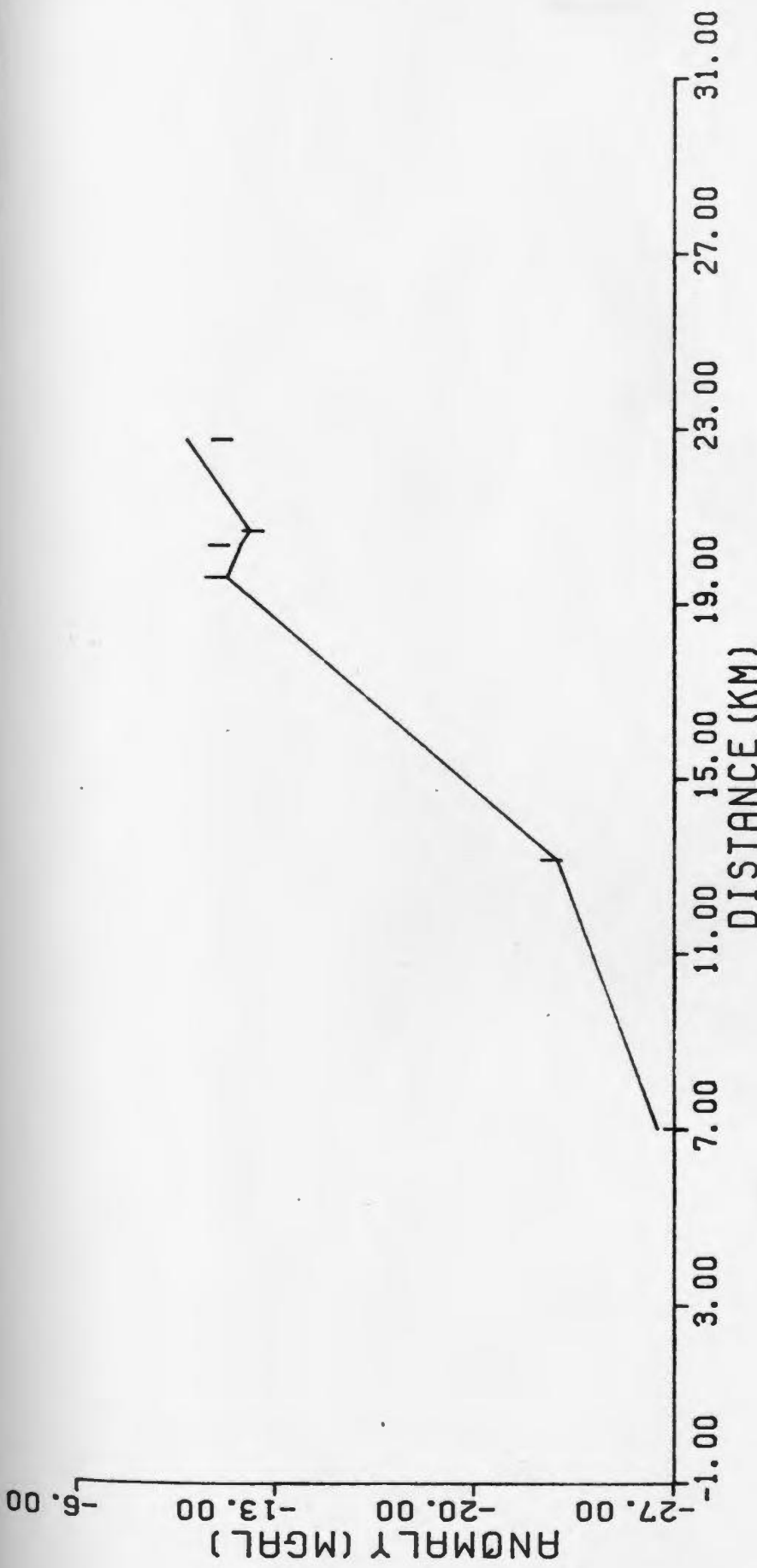
Appendix 2.5: 3-D magnetics modelling program

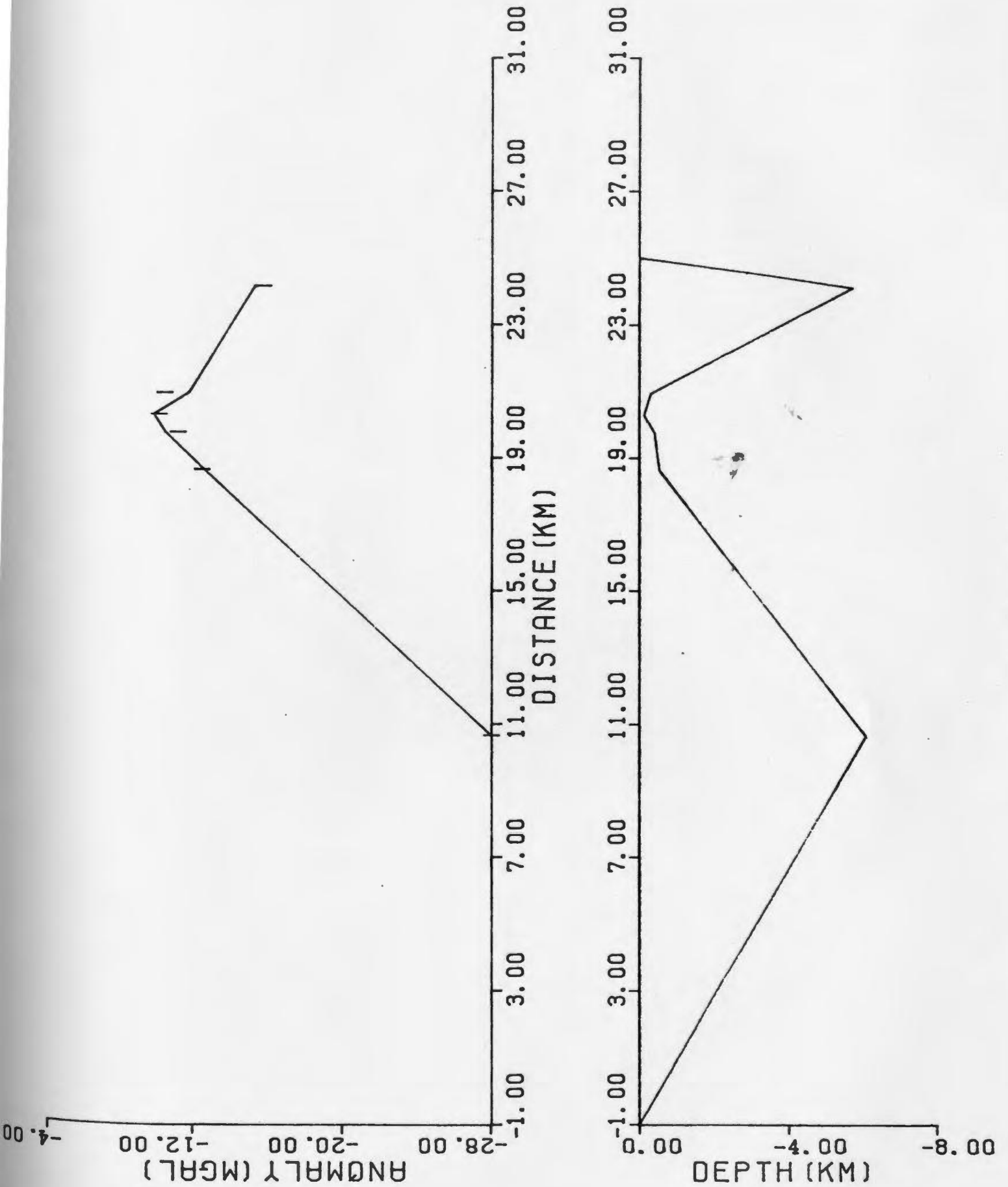
```
DO 310 L=1, KK
  STN=FLOAT(L)
  WRITE(3,915)STN, FX(L), FY(L), TDX(L), TDY(L), TDZ(L)
  &, TDH(L), TDT(L)
  WRITE(2,912)L, TDX(L), TDY(L), TDZ(L), TDH(L), TDT(L)
310 CONTINUE
900 FORMAT(A72)
901 FORMAT(2F6.2, F10.3, 2I5)
902 FORMAT(I3, I2, 2F4.1, 2F9.6, F4.1, 2F9.6, 2F4.1, F9.6)
903 FORMAT(6F10.3)
904 FORMAT(I2, F10.3, I5, F6.2)
905 FORMAT(6F10.3)
906 FORMAT(7X, 'V1', 10X, 'V2', 10X, 'V3', 10X, 'V4', 10X, 'V5', 10X,
  &'V6')
907 FORMAT(2X, 6F12.3)
908 FORMAT(2X, 'BODY# STN#', 4X, 'DX', 8X, 'DY', 8X, 'DZ', 8X, 'DH',
  &8X, 'DT')
909r FORMAT(2X, 2I5, 5F10.3)
910 FORMAT(/)
911 FORMAT(3X, 'STN#', 2X, 'TOTAL DX', 4X, 'TOTAL DY', 4X, 'TOTAL
  &DZ', 4X, 'TOTAL DH', 4X, 'TOTAL DT', /)
912 FORMAT(2X, I5, 5F12.3)
915 FORMAT(2X, F5.0, 7F10.3)
920 FORMAT(F10.6)
925 FORMAT(2X, 'WHAT IS THE NAME OF THE INPUT FILE? ', S)
926r FORMAT(A20)
  STOP
  END
```

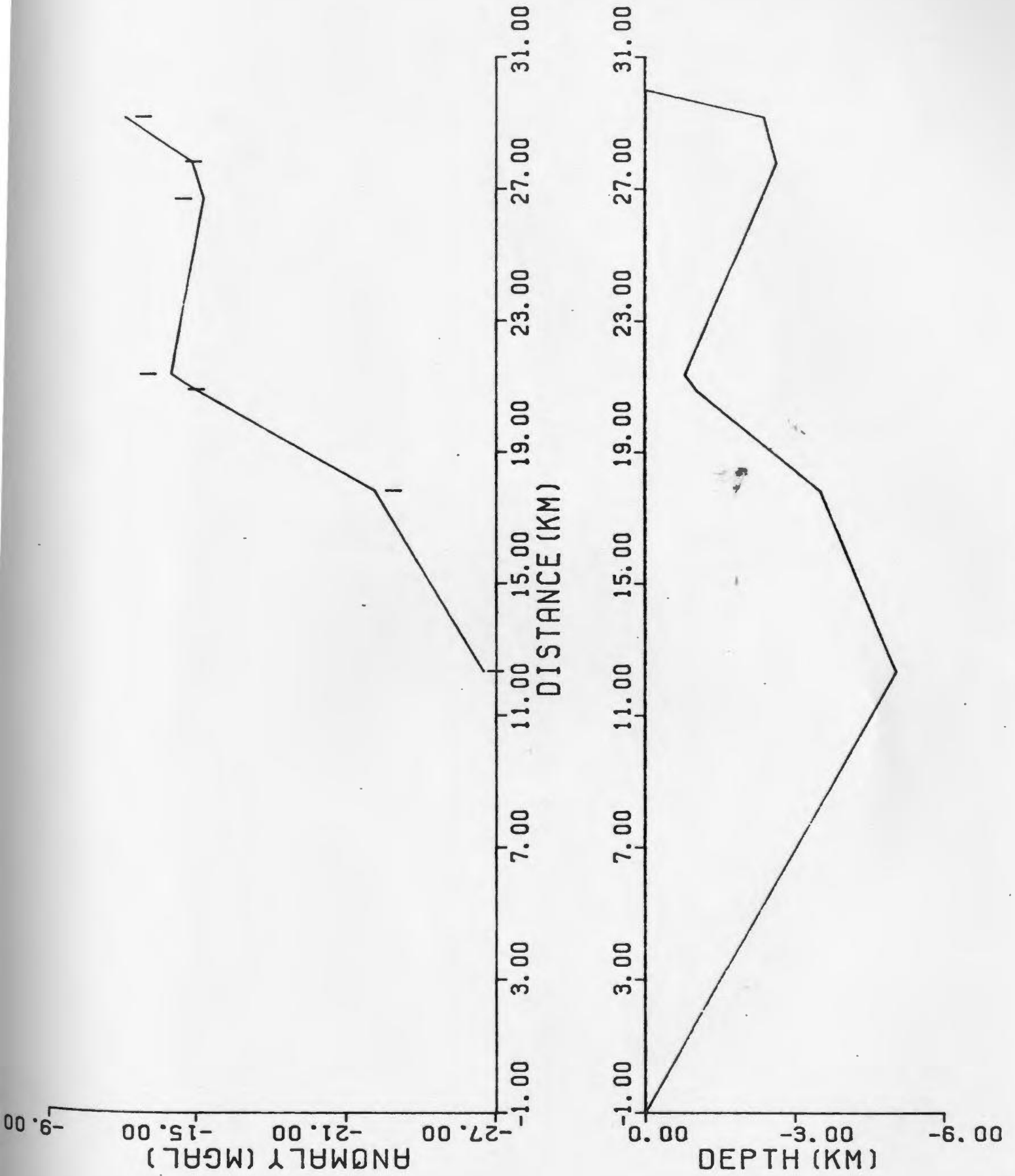
Appendix 3.1: Inversion parameters for 2.5-D gravity inversion models

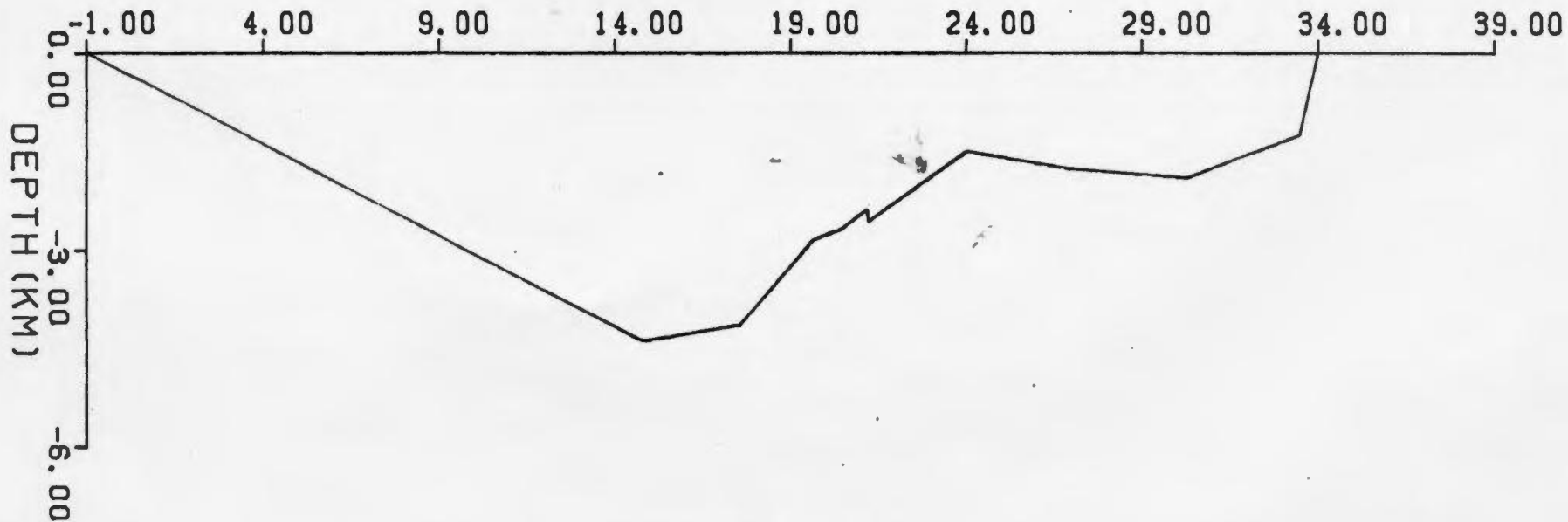
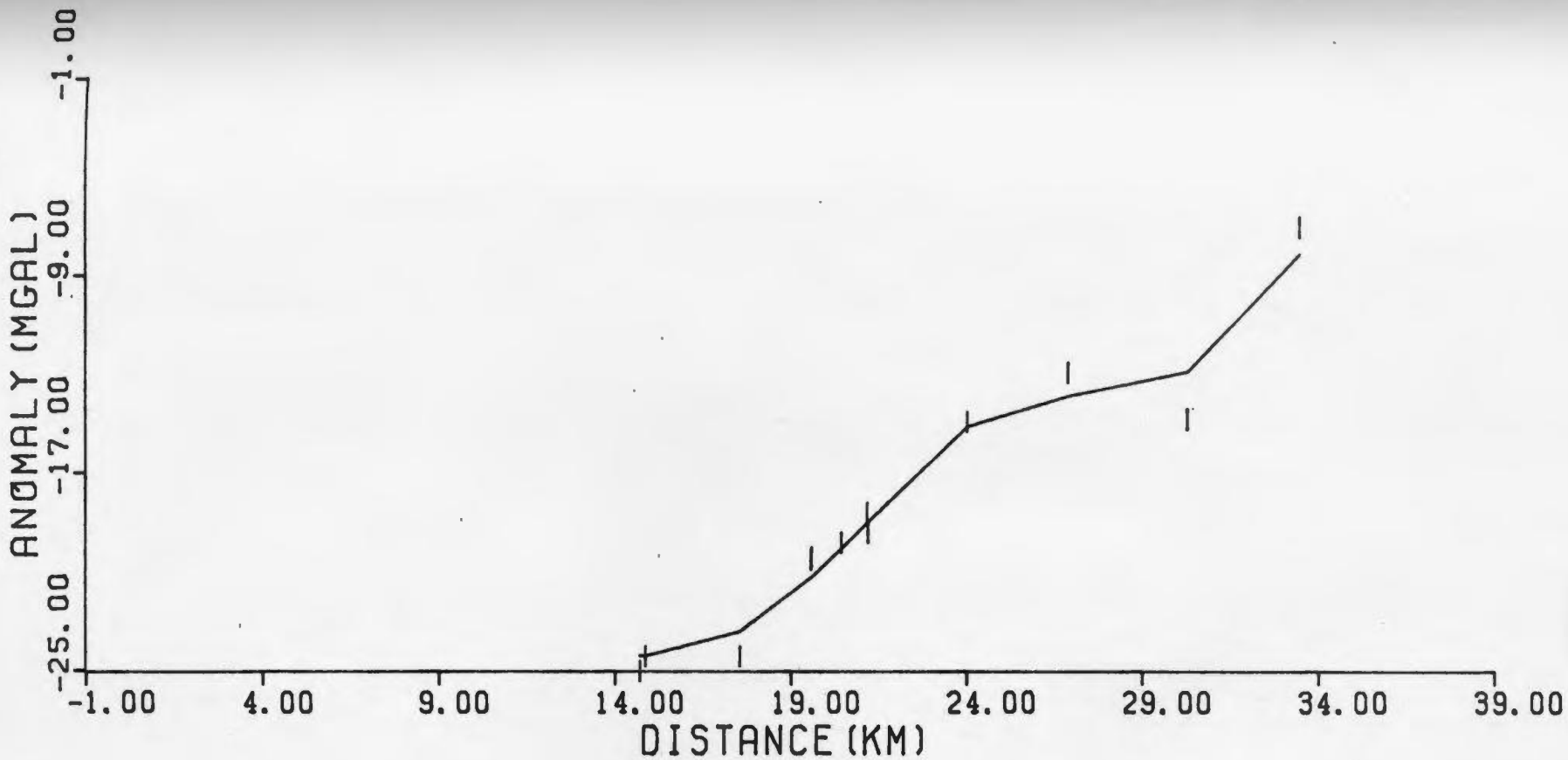
Profile	-Y(km)	+Y(km)	ϵ	Number of iterations	Mean	Standard Deviation
01	-16.00	44.00	5.36	25	-0.294	1.293
02	-18.50	41.50	1.40	39	-0.039	0.522
03	-21.00	39.00	1.25	203	-0.006	0.495
04	-23.44	36.66	1.50	40	-0.001	0.499
05	-25.90	34.10	8.76	8	0.021	0.891
06	-28.40	31.60	2.50	12	-0.028	0.493
07	-30.90	29.10	2.50	24	-0.018	0.492
08	-33.30	26.70	3.95	15	0.022	0.702
09	-35.80	24.20	3.00	15	-0.052	0.500
10	-38.20	21.80	2.25	49	-0.014	0.499
11	-40.70	19.30	1.25	19	0.011	0.496
12	-43.10	16.90	3.79	38	-0.032	0.648
13	-45.60	14.40	2.79	44	-0.037	0.963
14	-48.10	11.90	6.65	6	-0.004	1.289
1S	-28.00	32.00	5.22	62	0.001	0.590
2S	-35.00	25.00	13.13	17	0.007	0.791
1B	-6.00	25.50	1.50	18	-0.187	0.498
2B	-15.10	17.40	11.11	45	-0.016	0.710
3B	-22.40	10.10	6.83	4	-0.029	0.986
4B	-18.50	14.00	6.60	5	-0.001	0.676



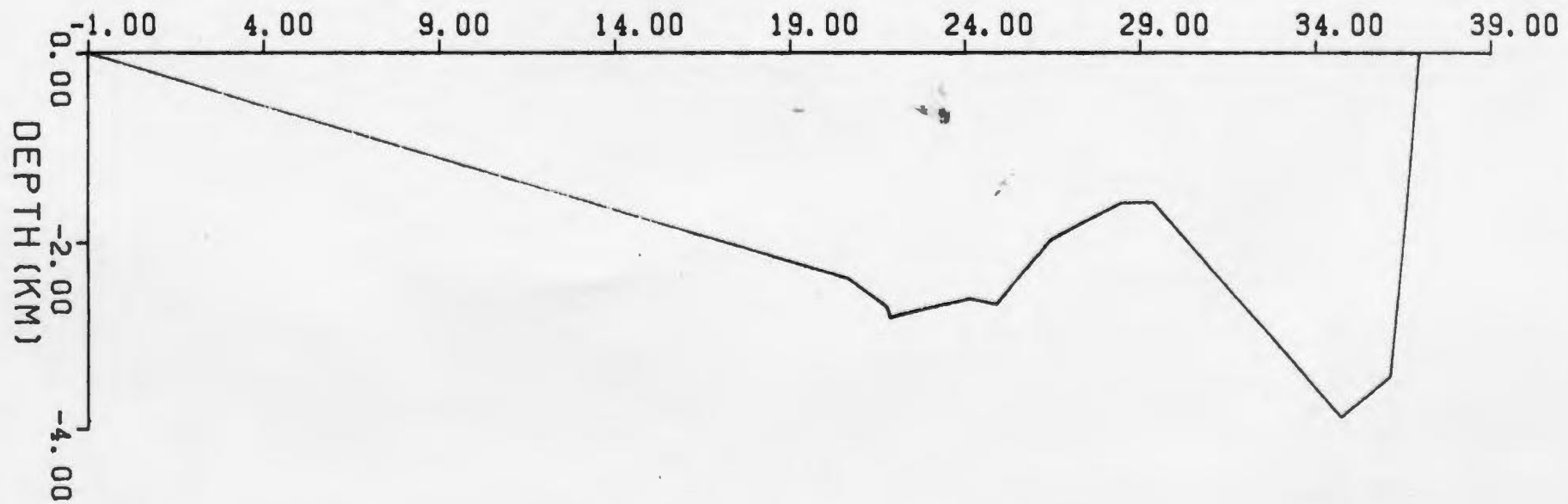
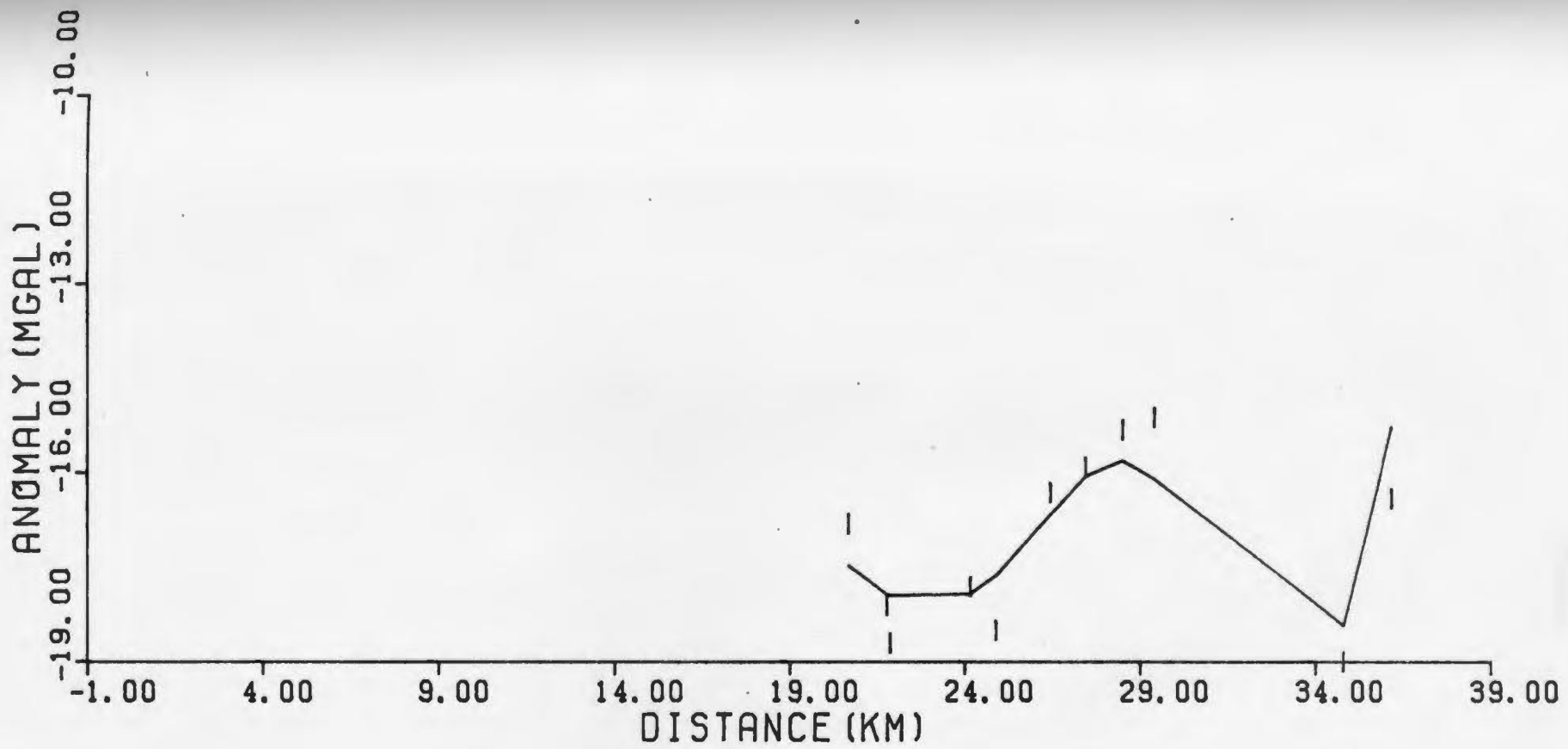




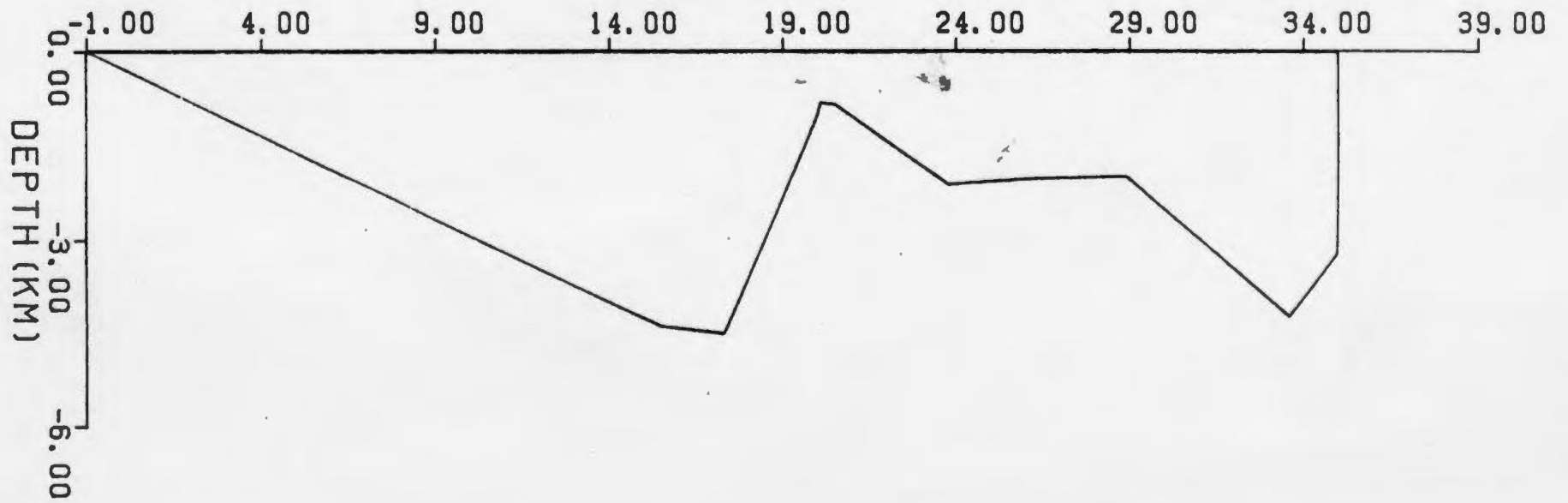
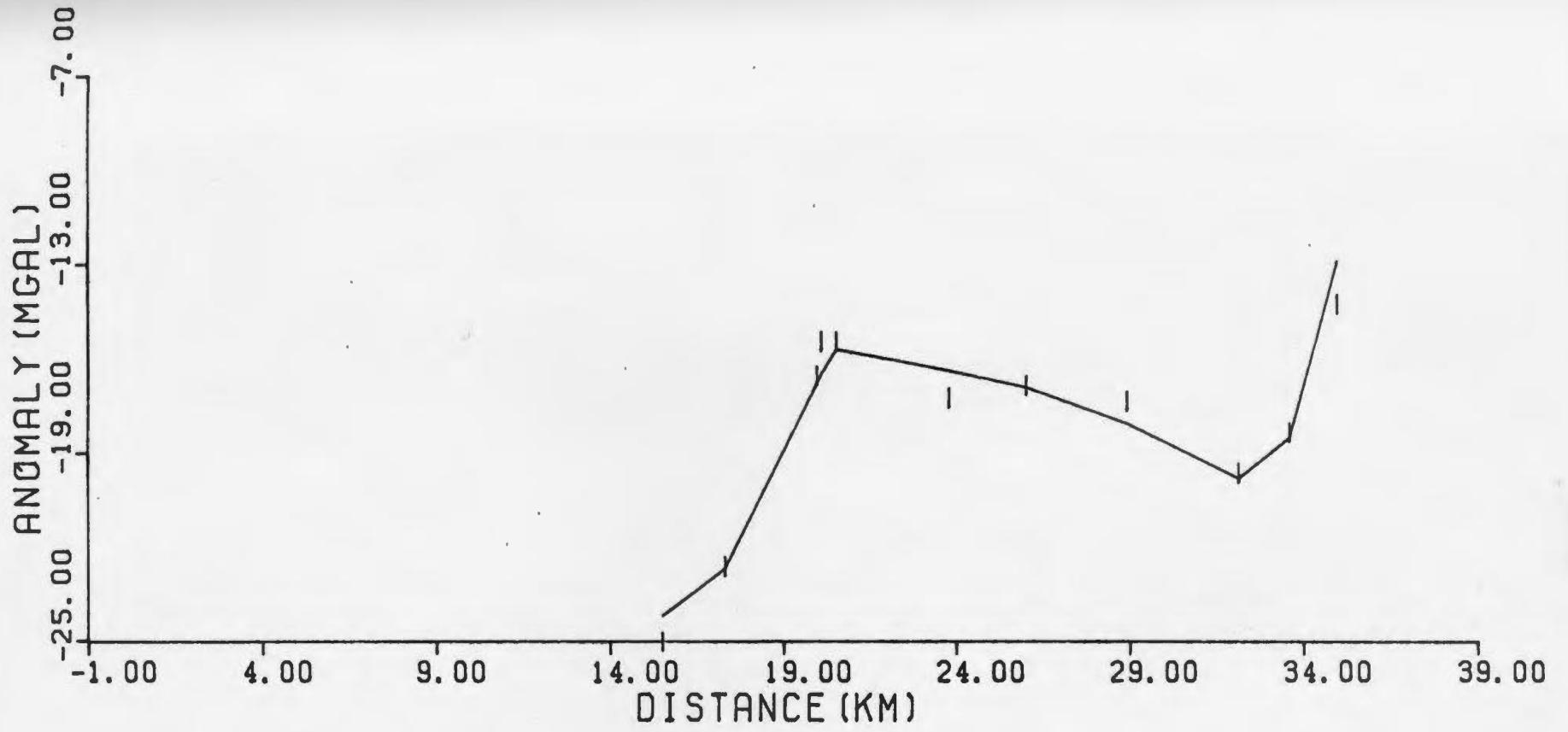


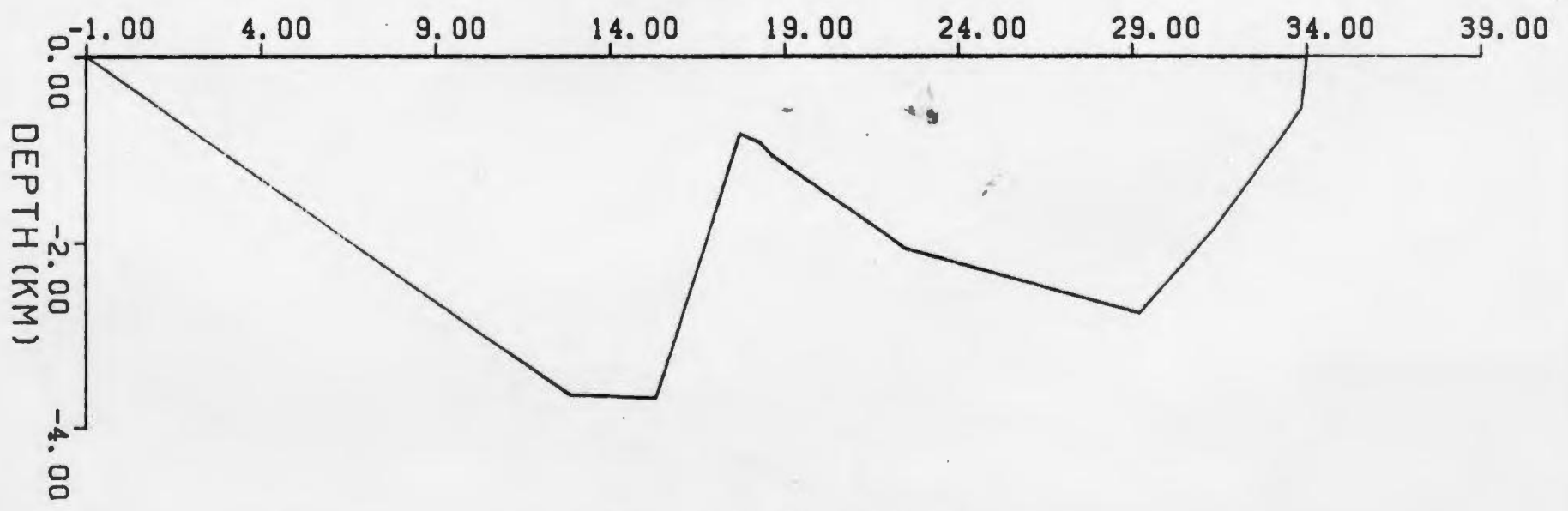
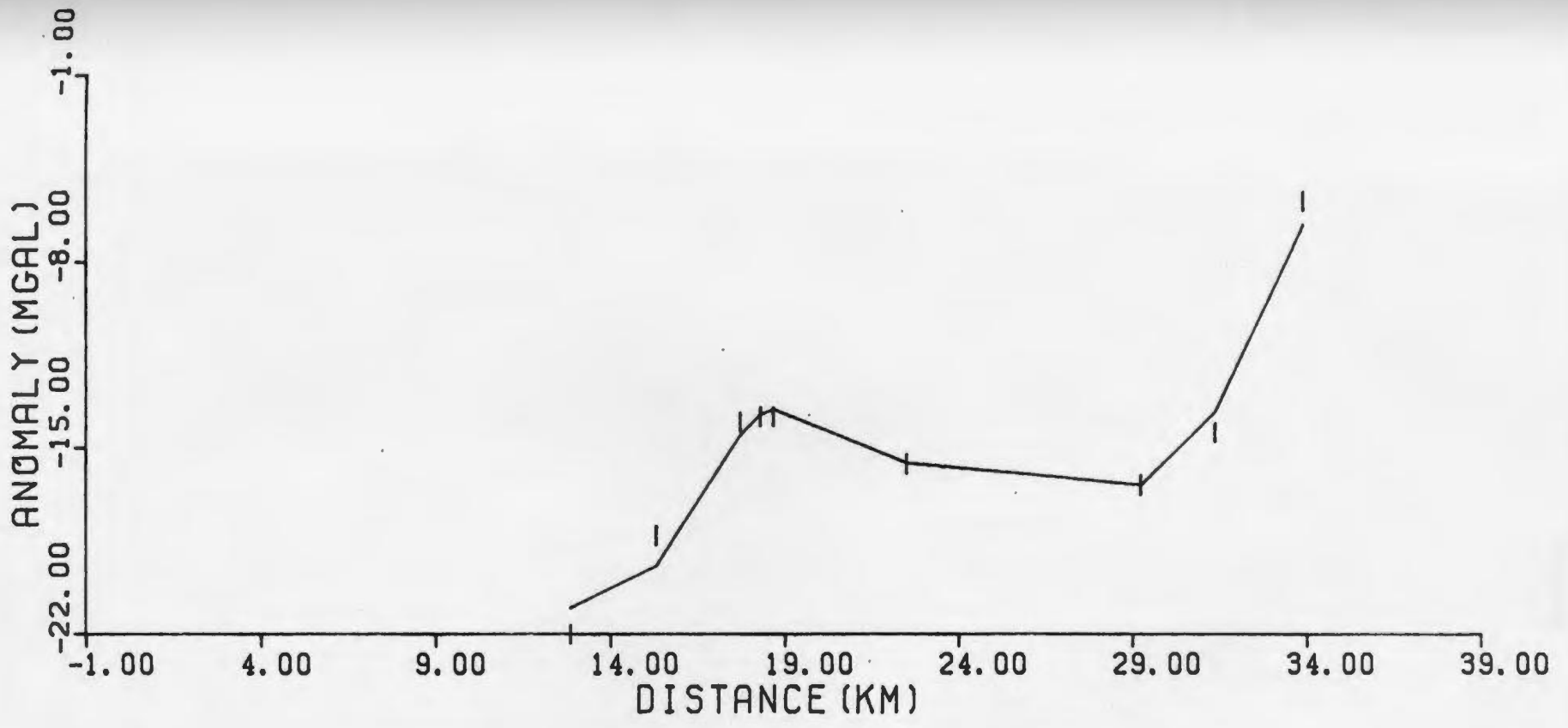


Appendix 3.2e Profile 5

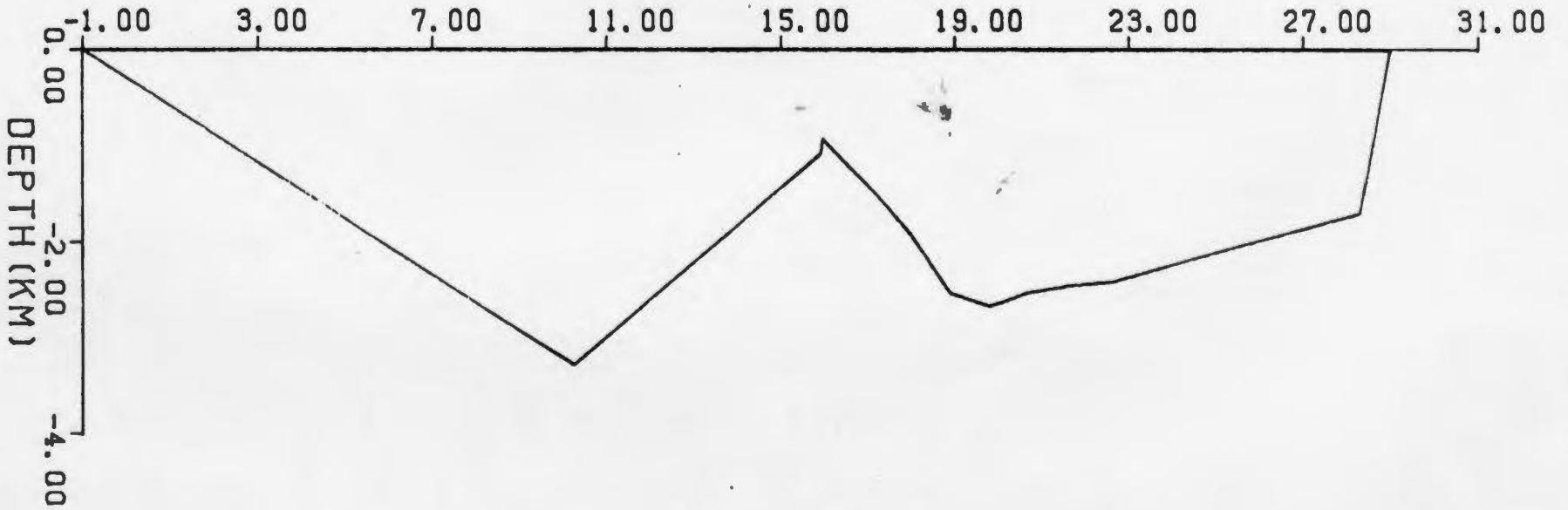
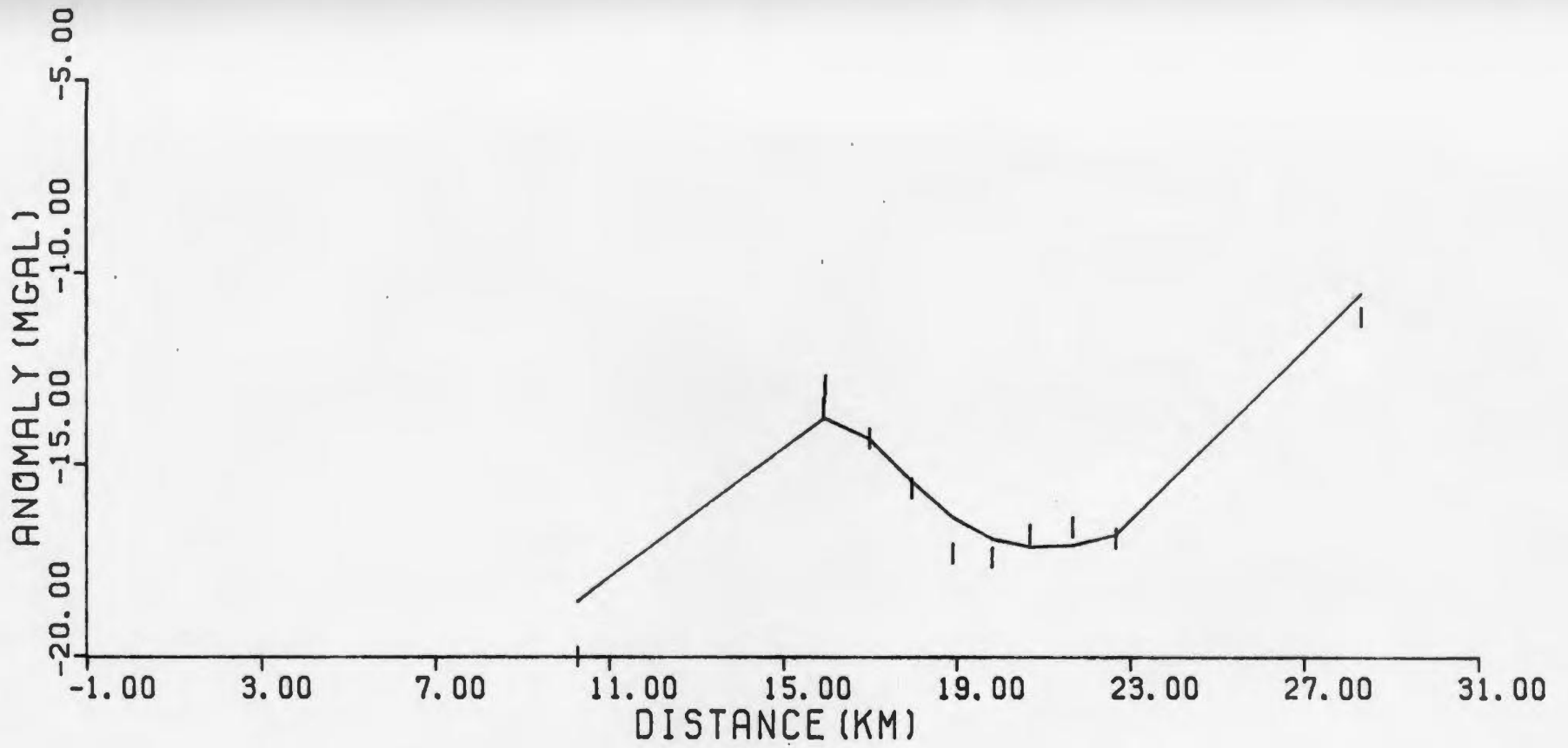


Appendix 2.3f Profile 6

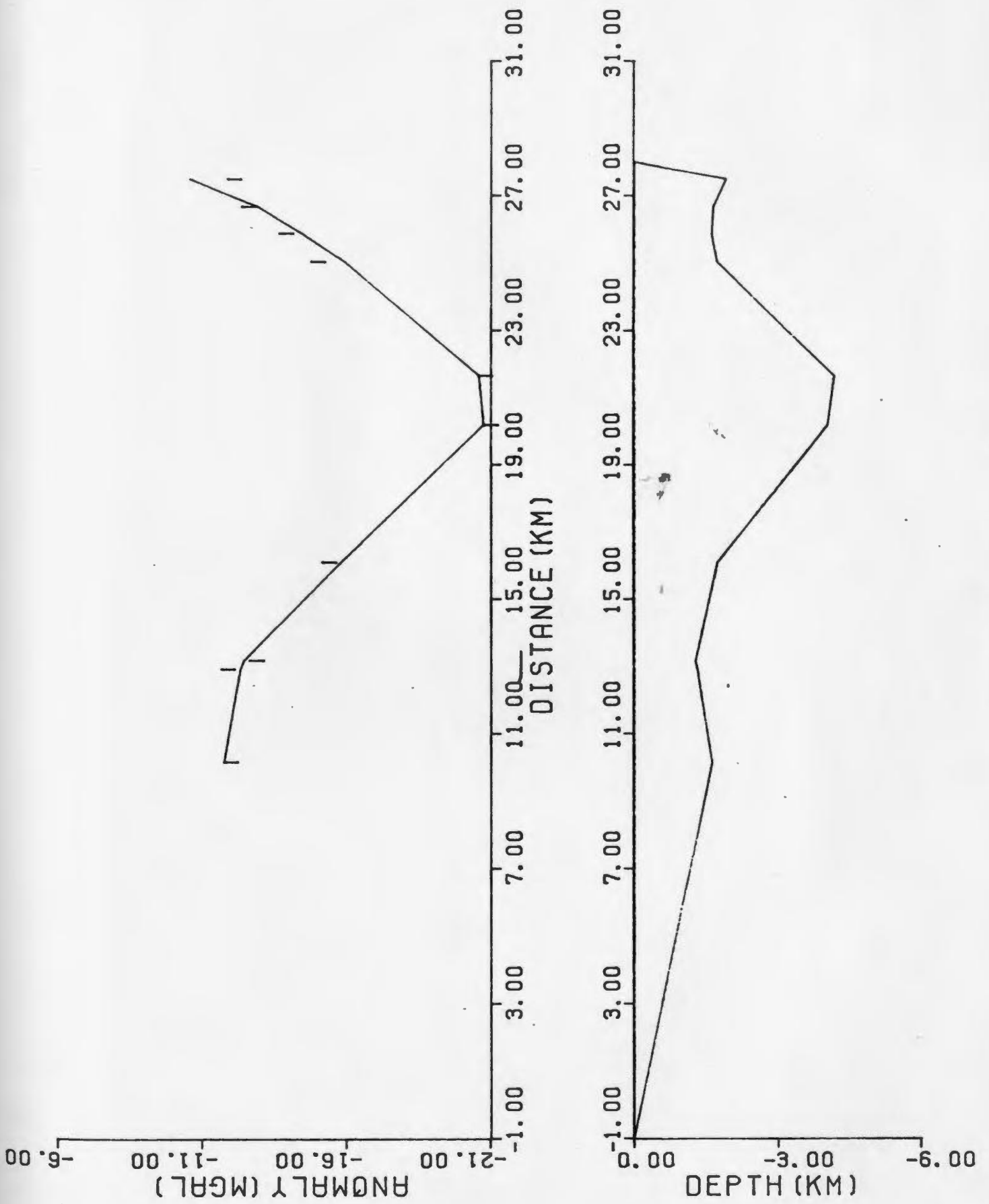


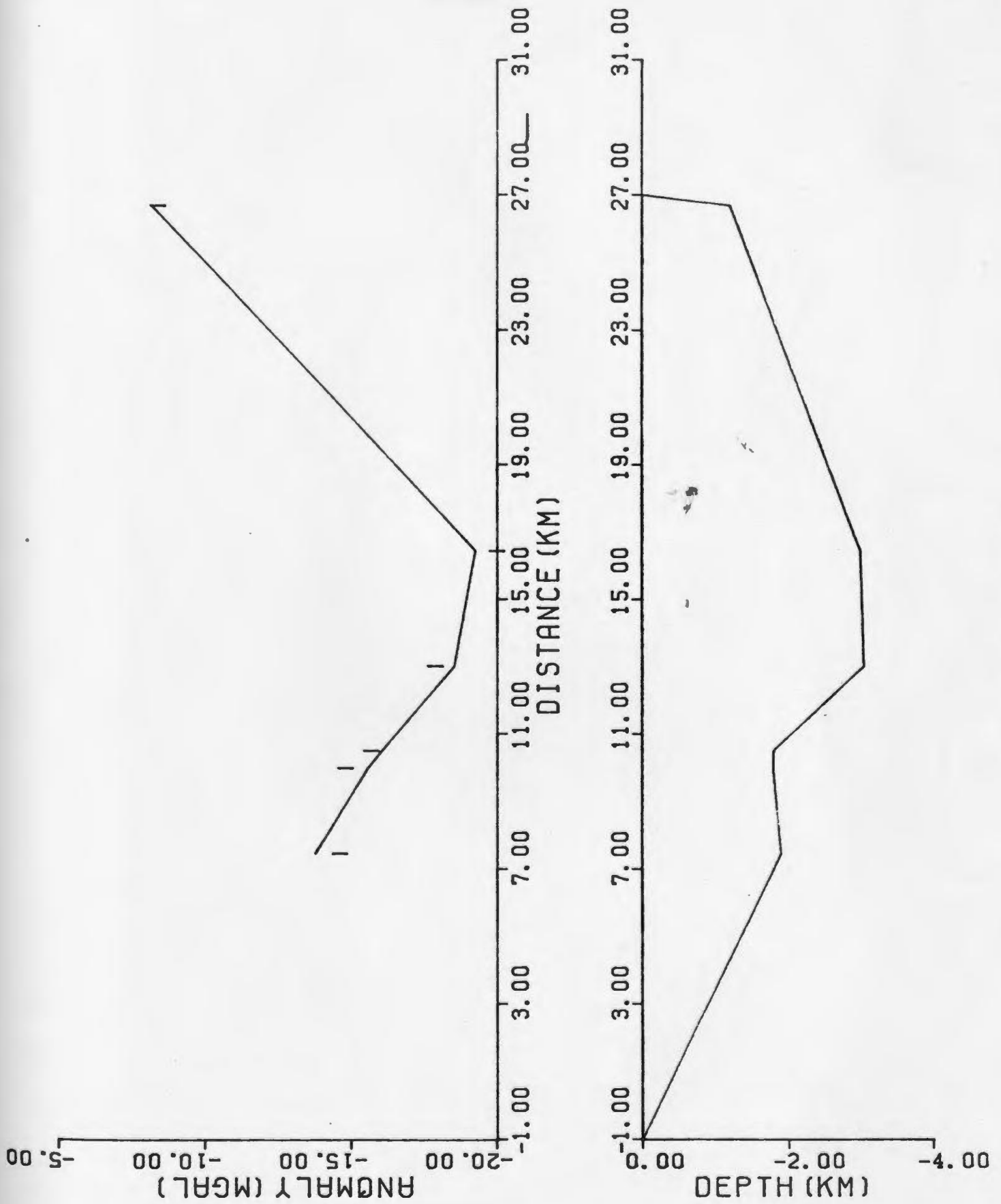


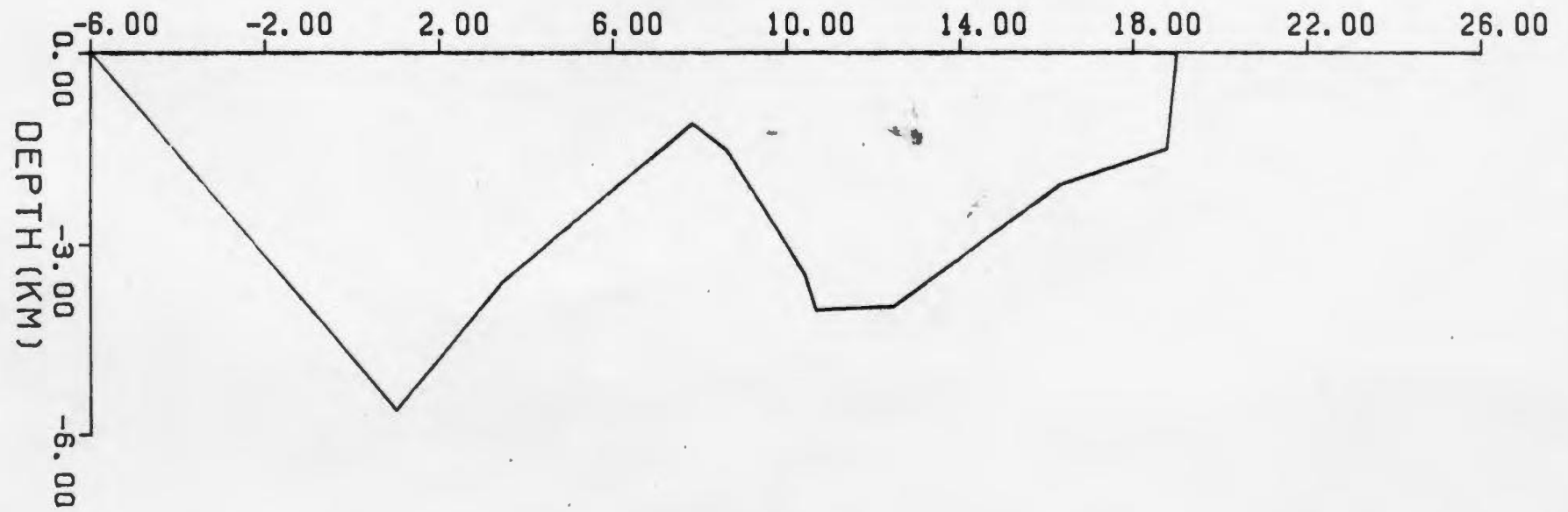
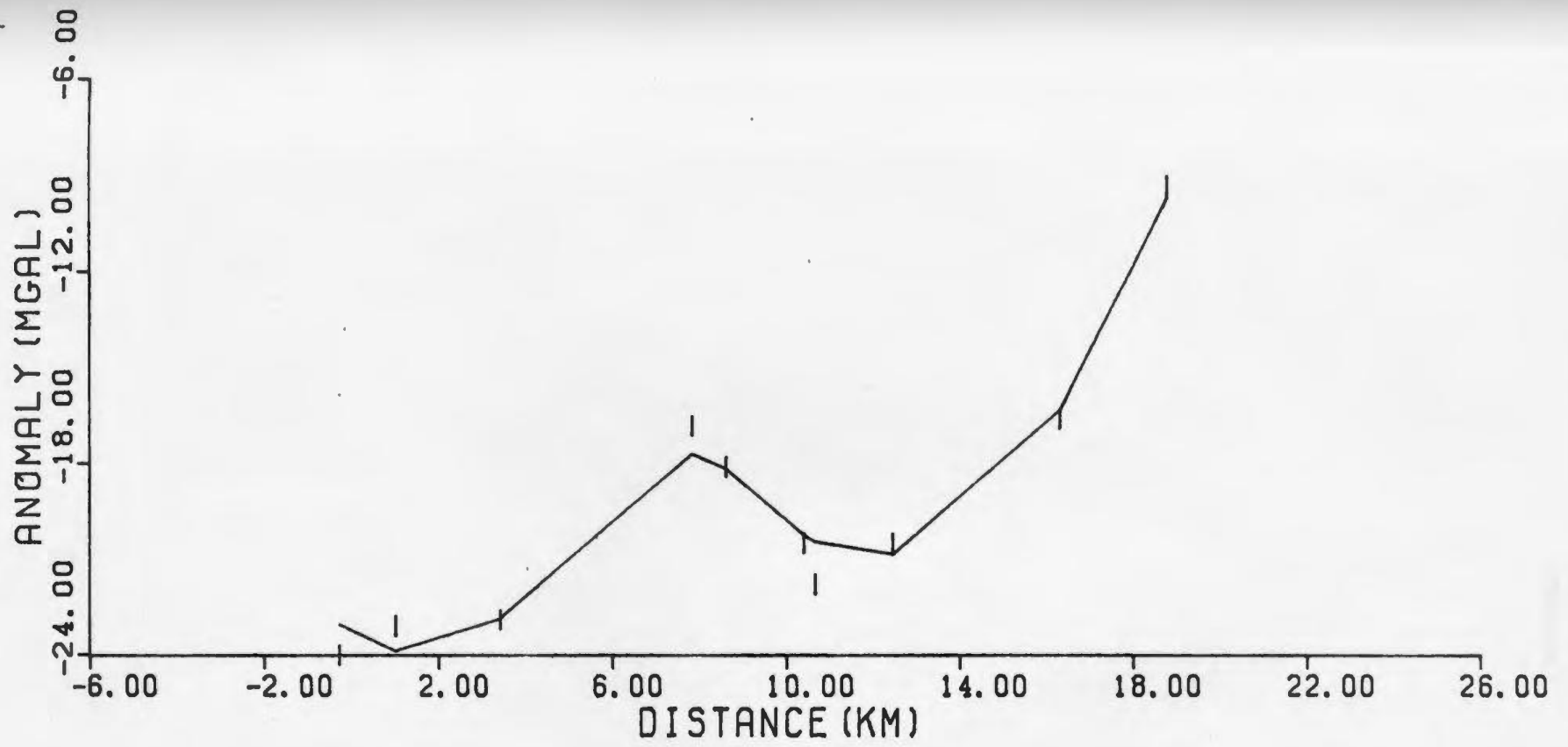
Appendix 2.3h Profile 8



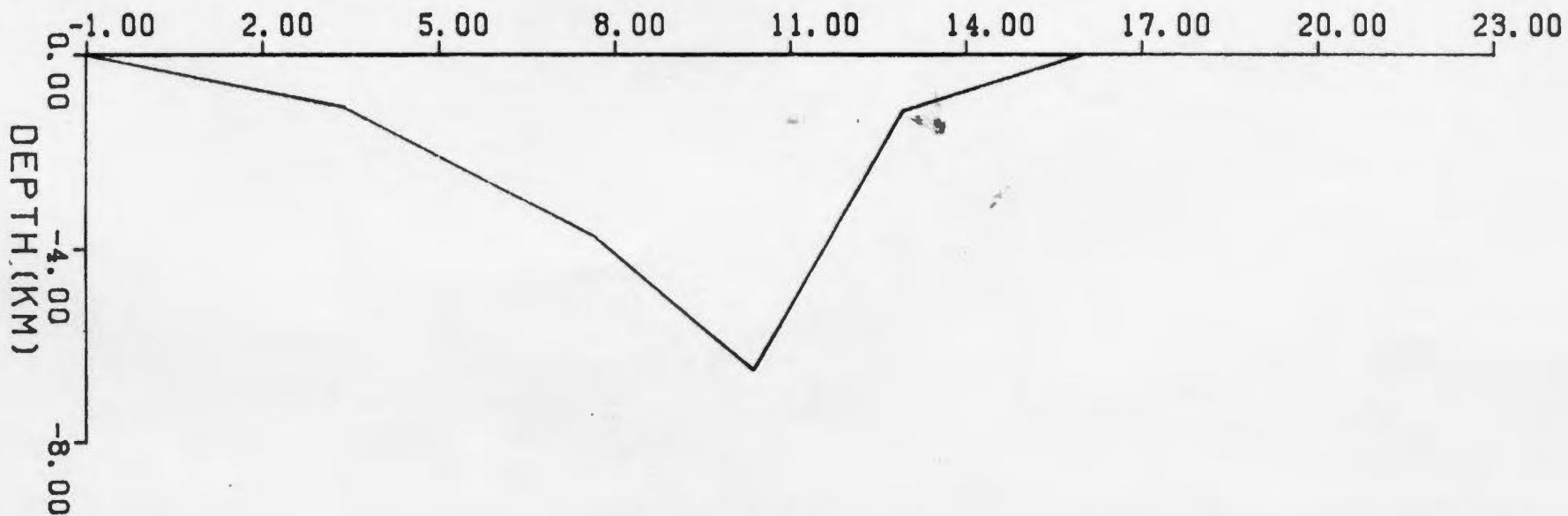
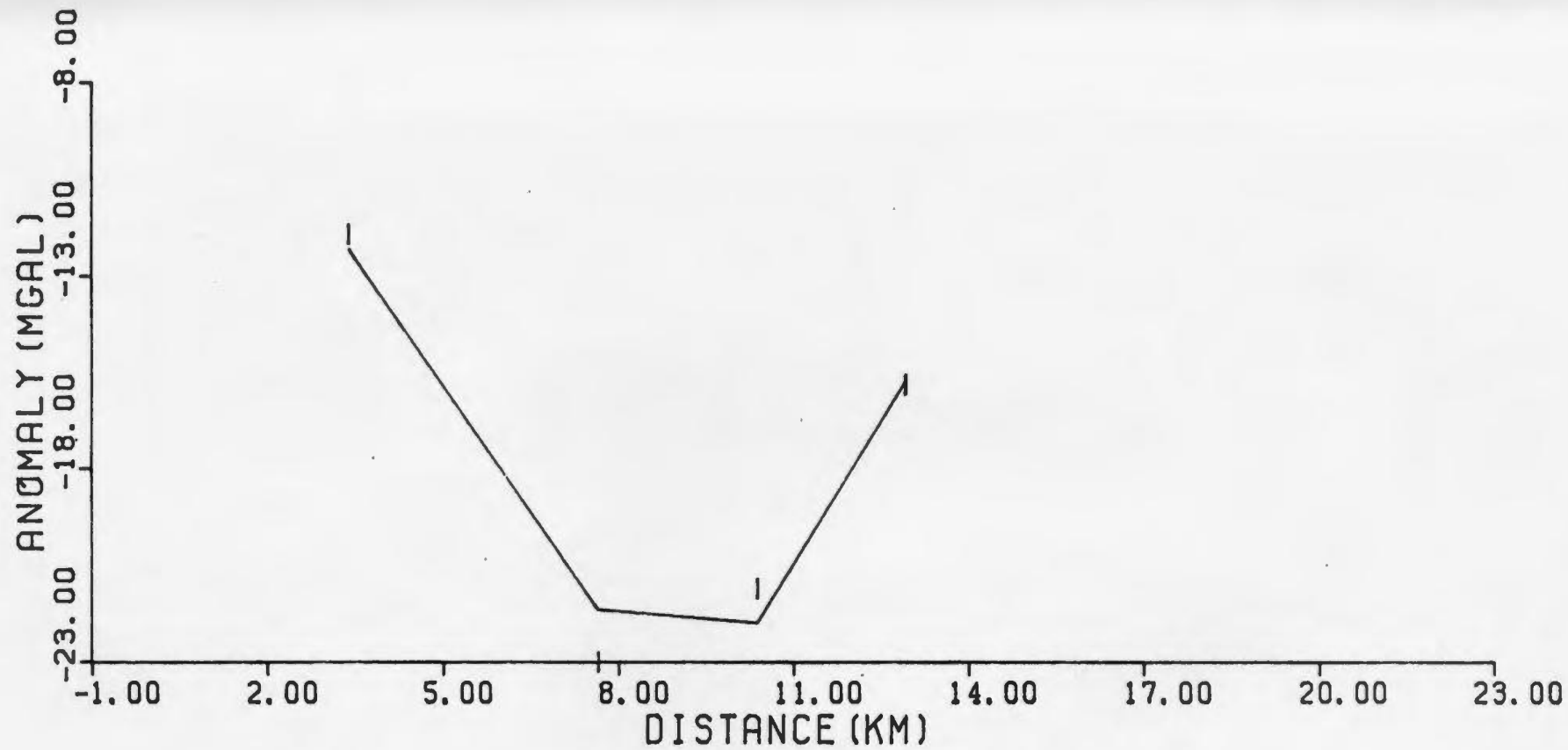
Appendix 3.21 Profile 9



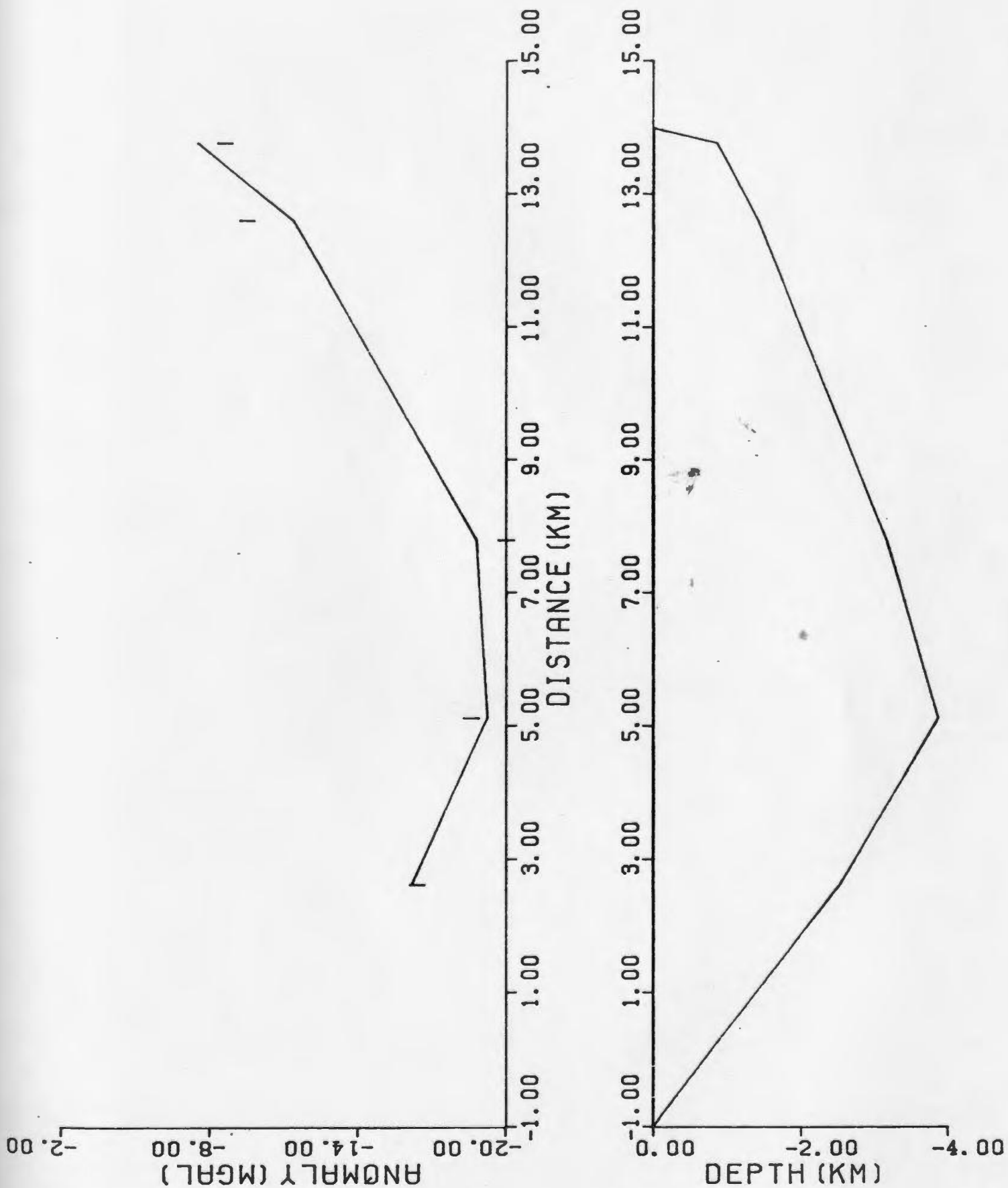


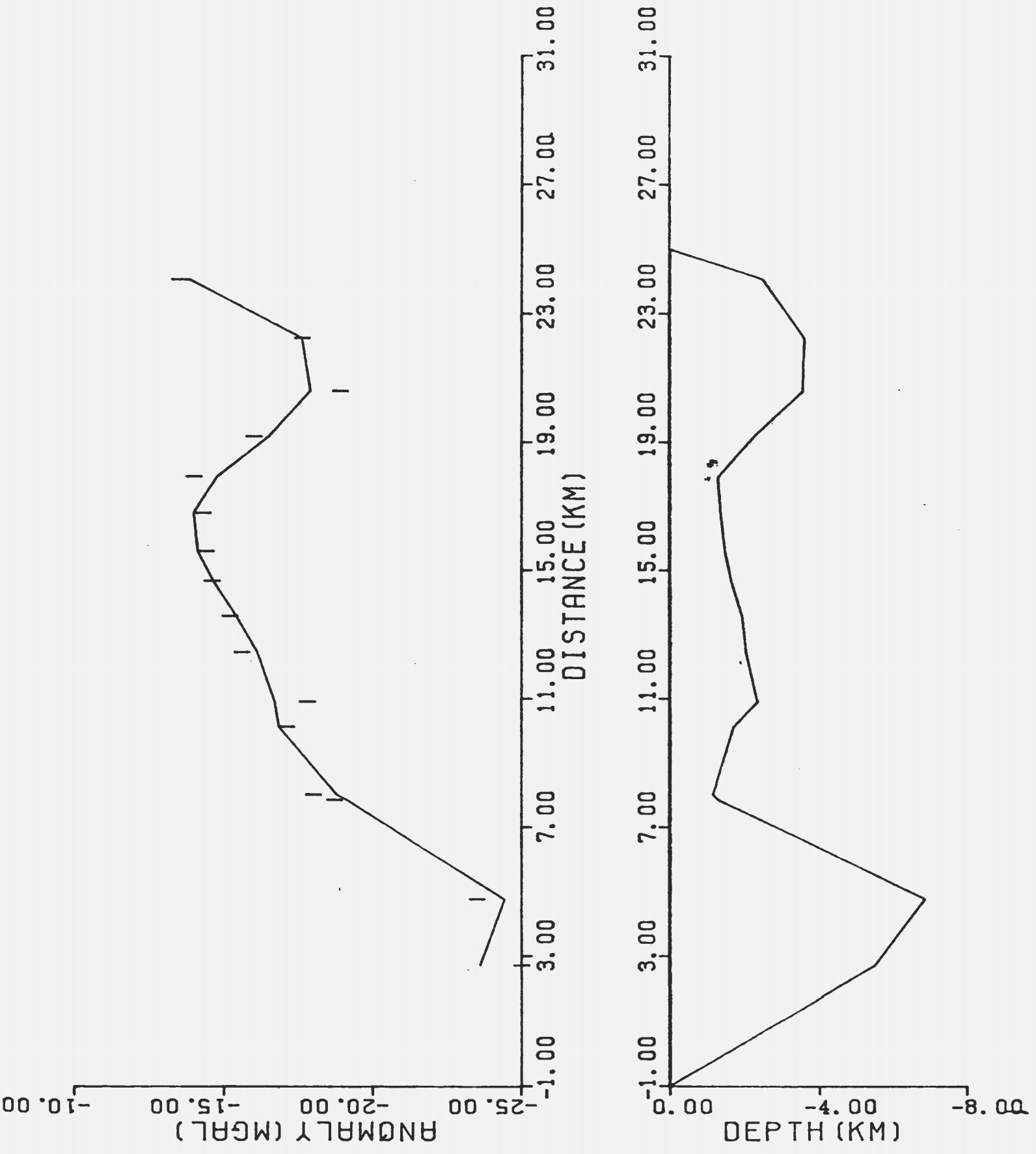


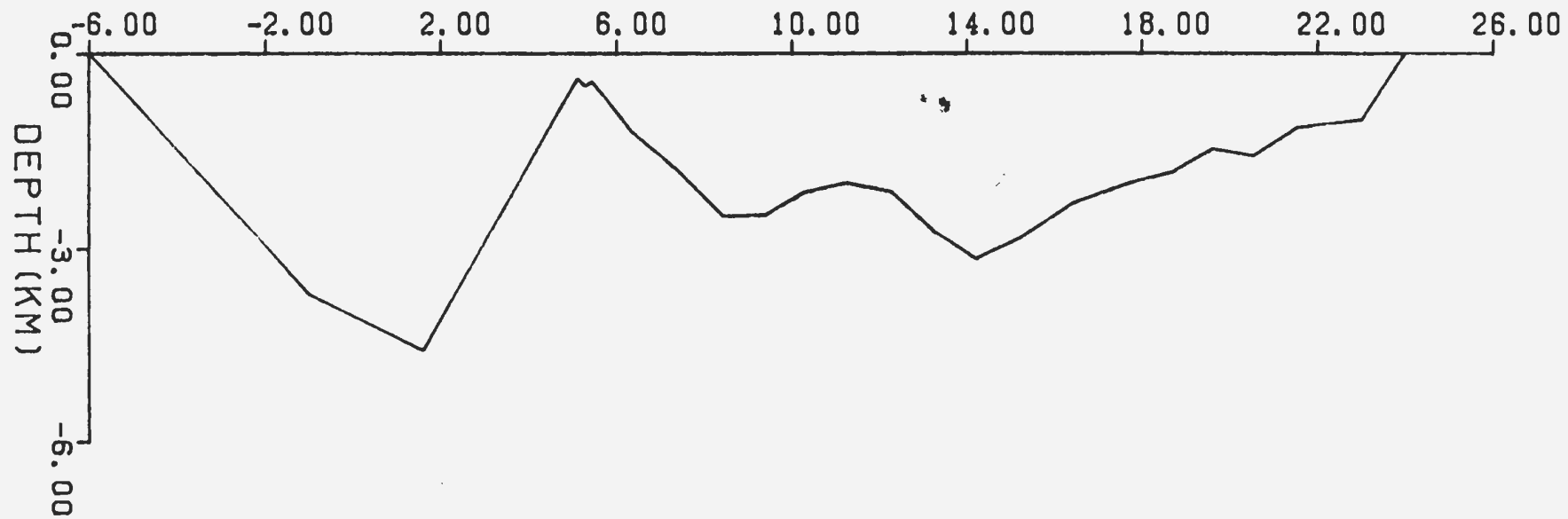
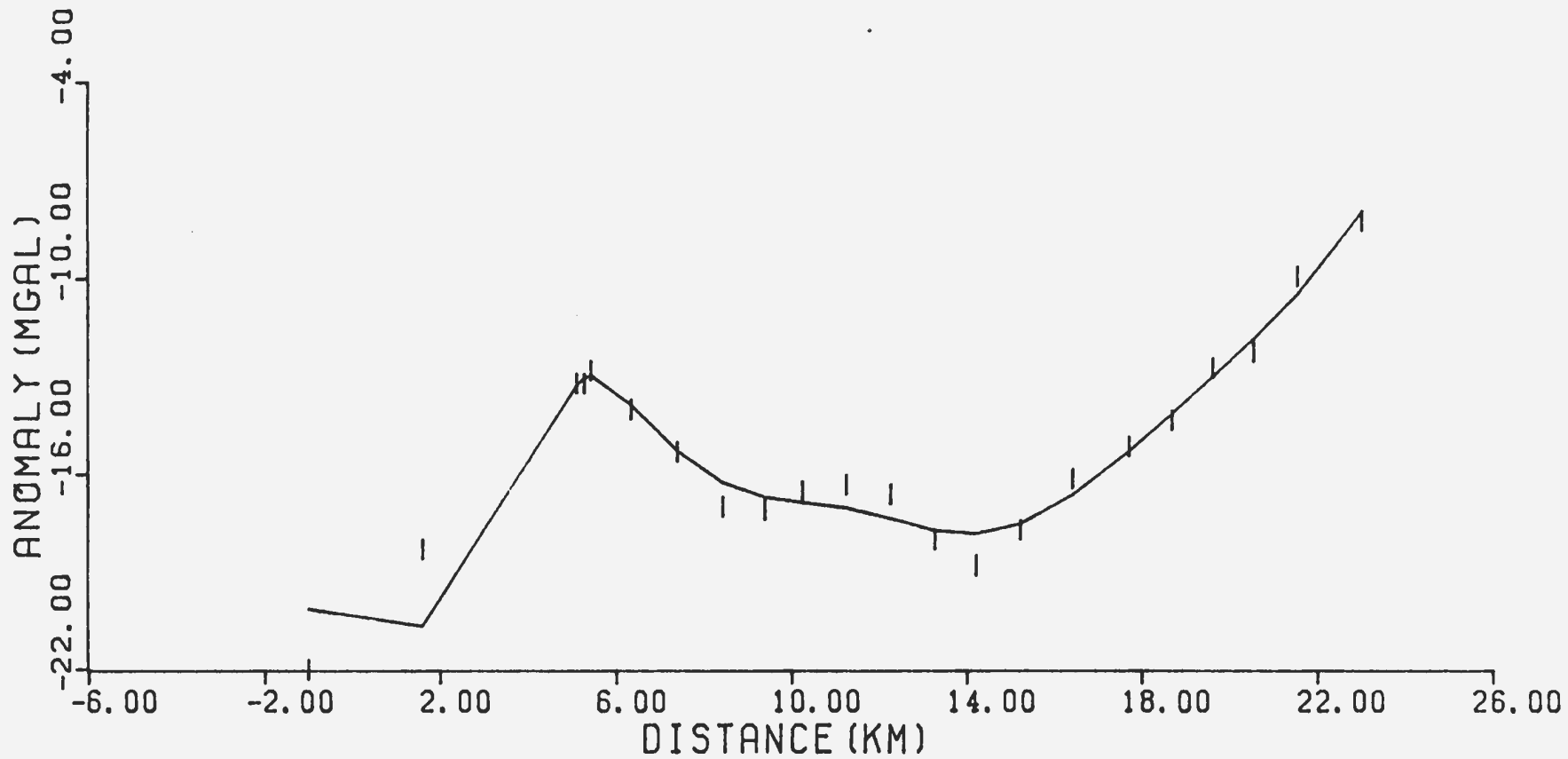
Appendix 2.31 Profile 12



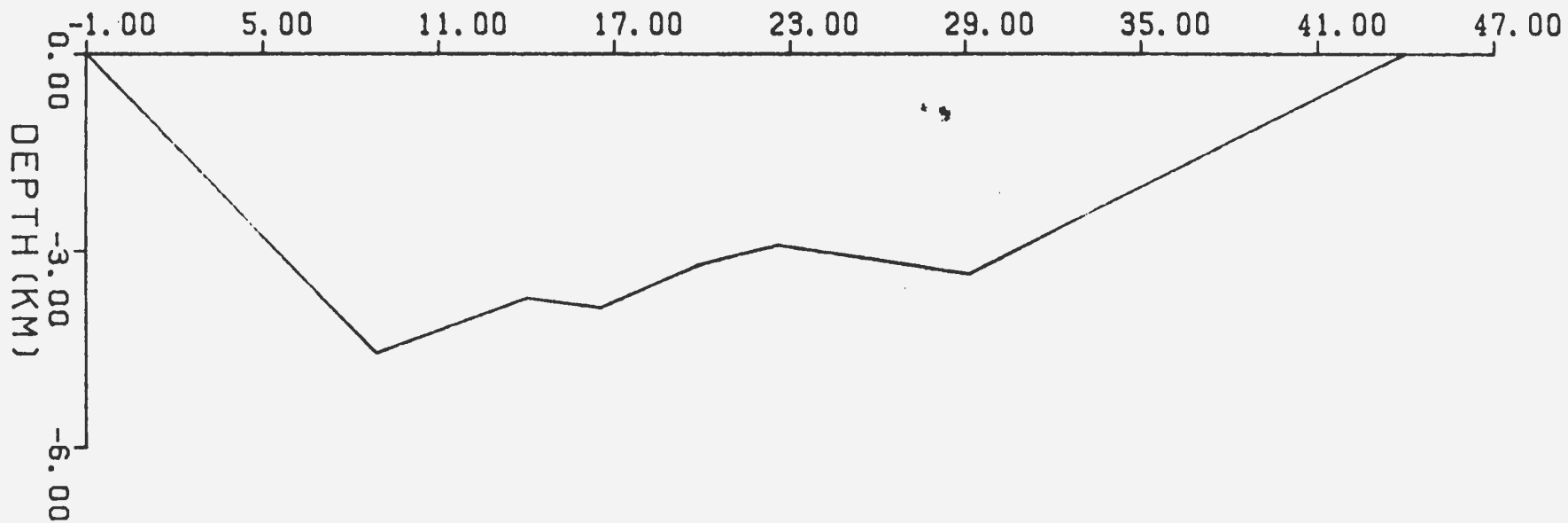
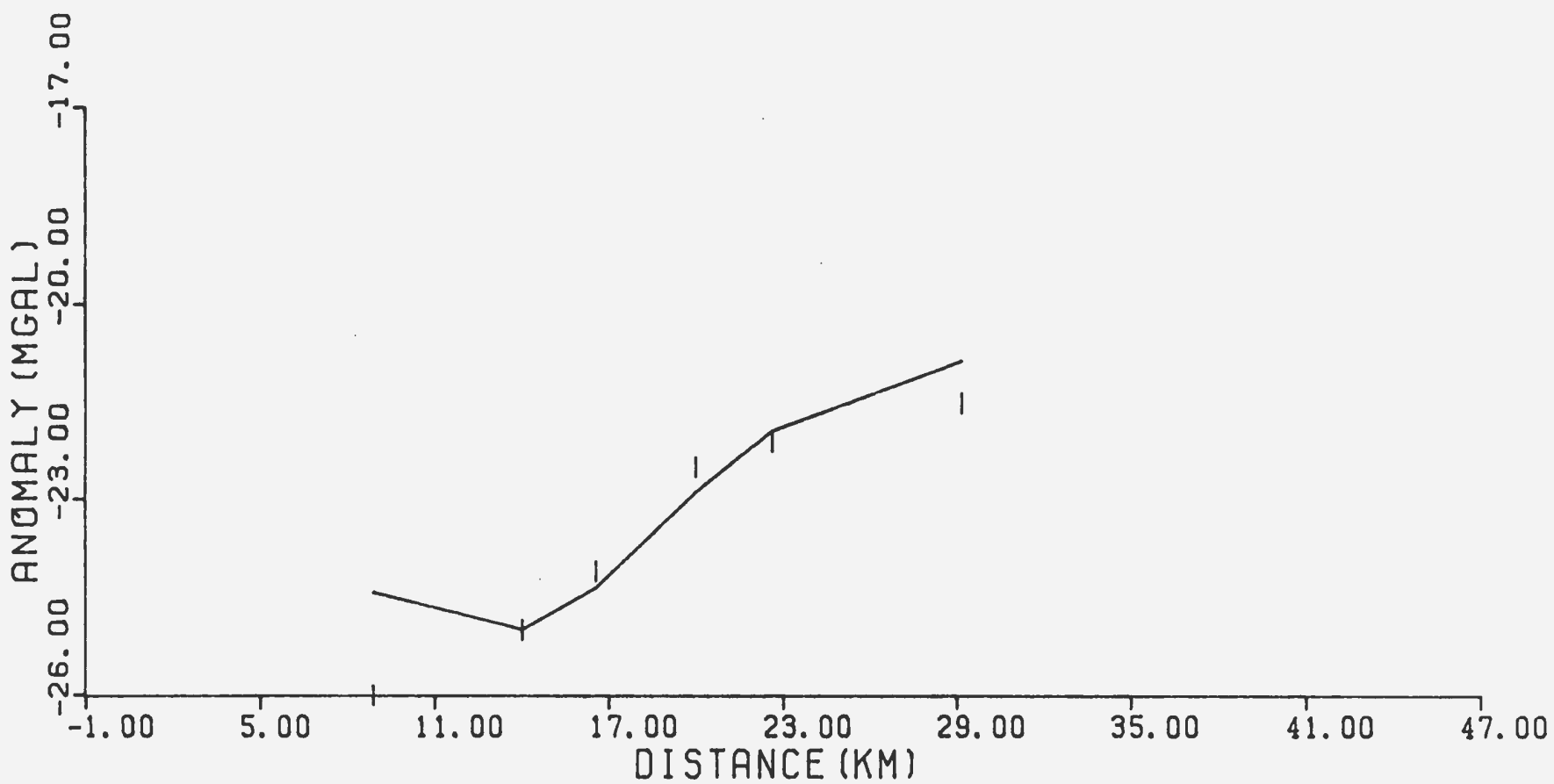
Appendix 3.2m Profile 13



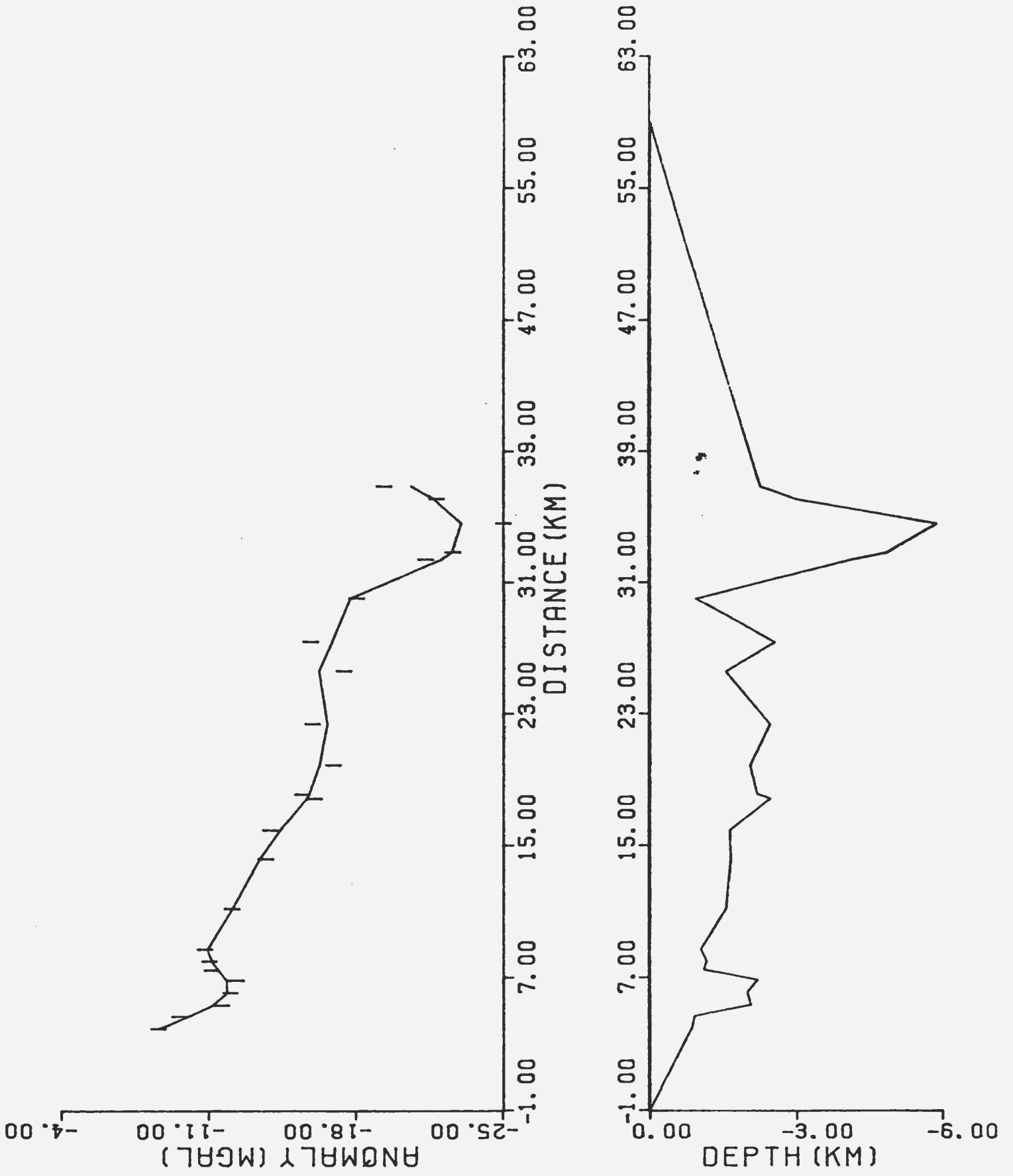


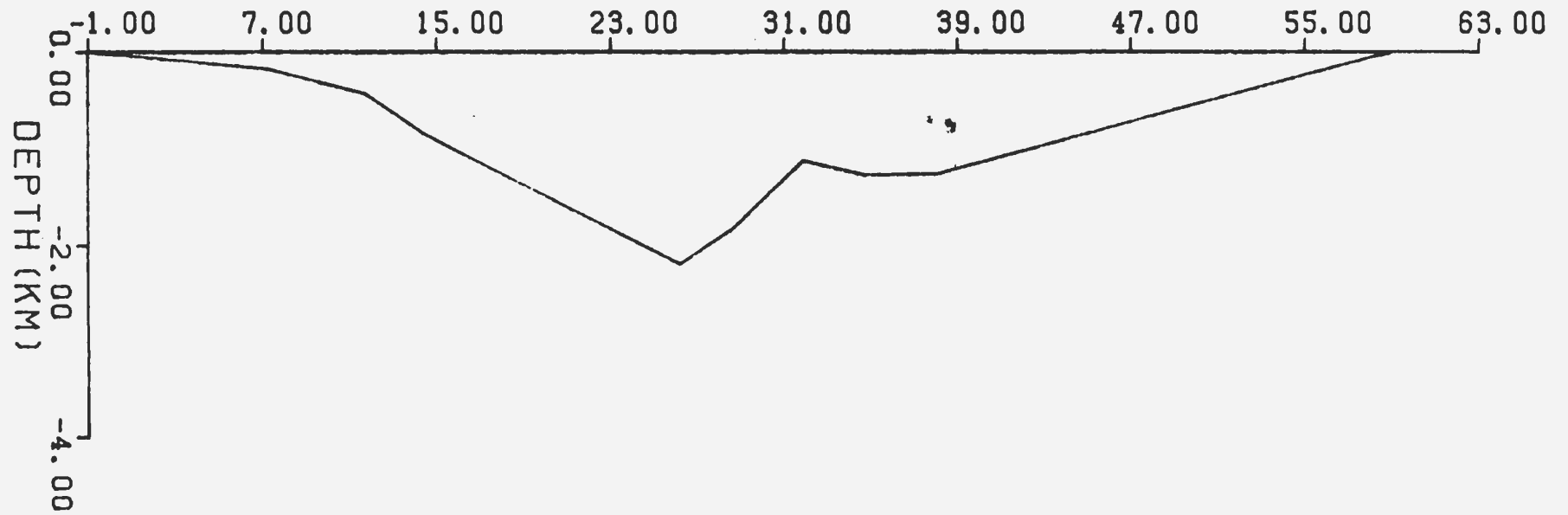
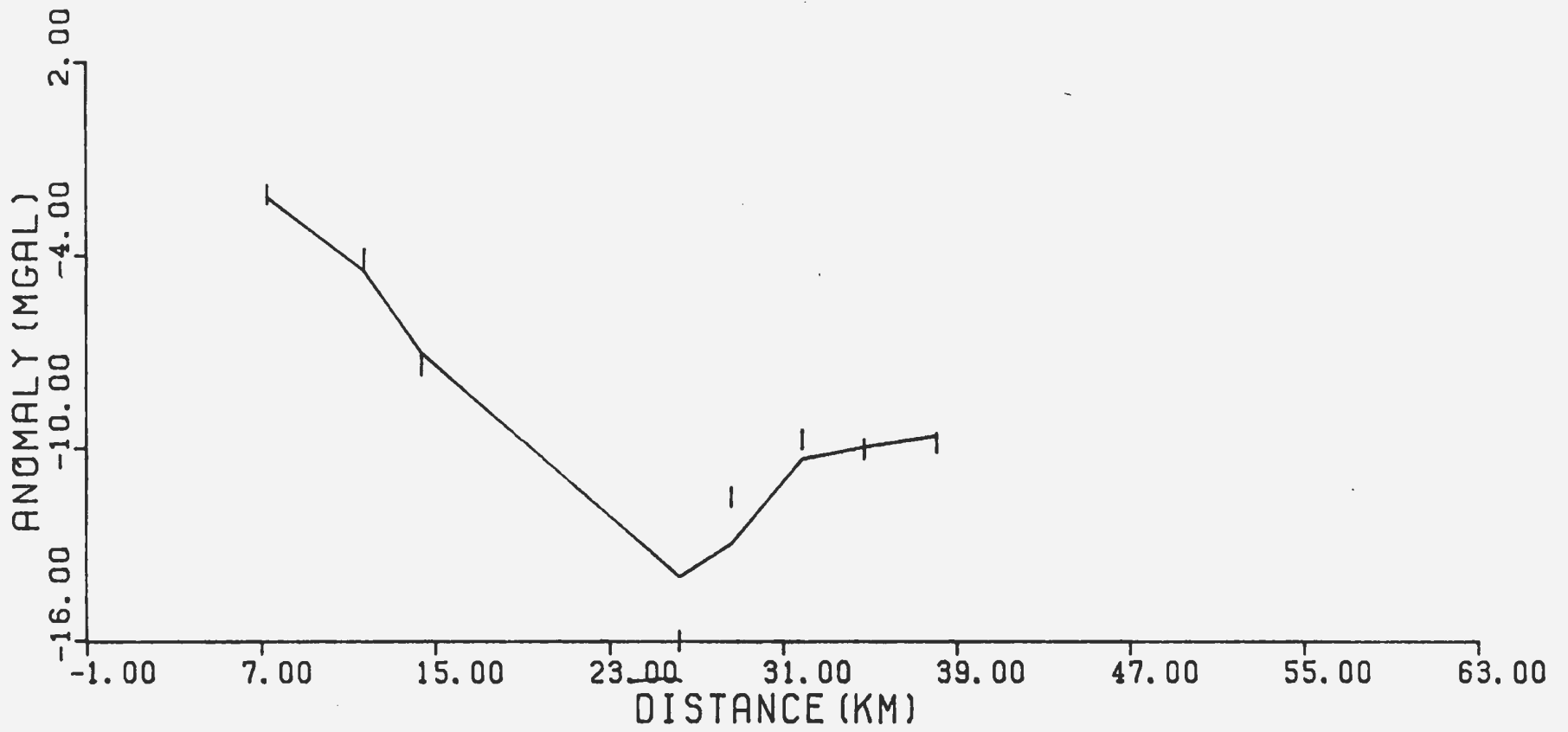


Appendix 2.3p Profile 2S

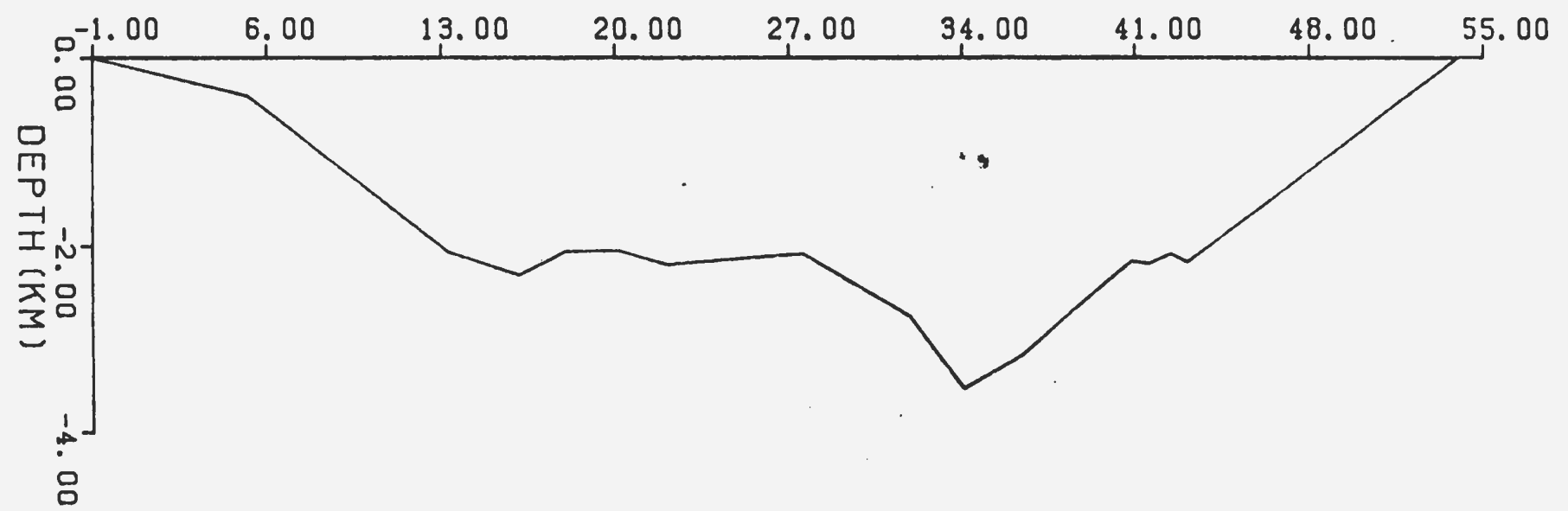
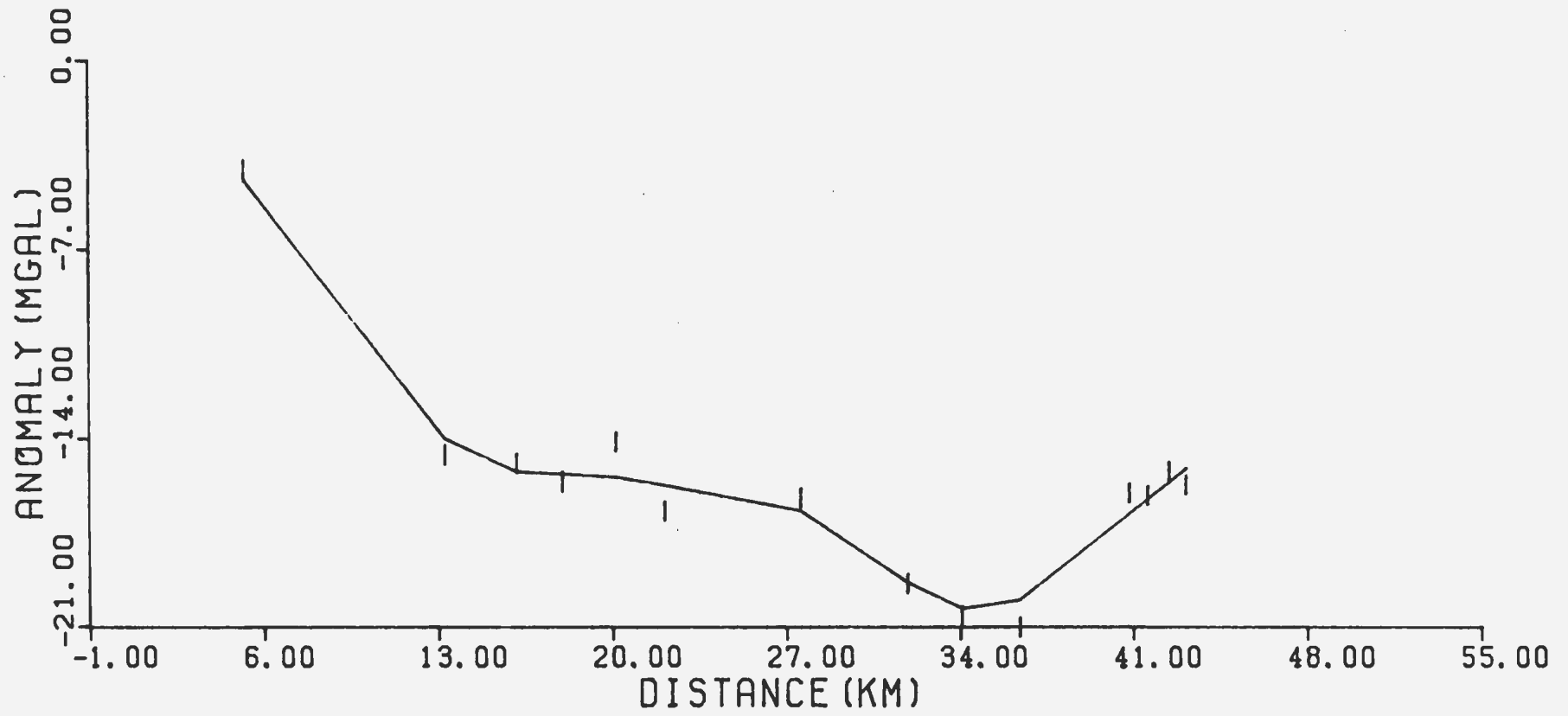


Appendix 3.2q Profile 1B





Appendix 3.2a Profile 3B



Appendix 2.3t Profile 4B

C37726

